Controllability in finite and infinite dimension and applications to bio-inspired nonlinear systems

Clément Moreau

▶ **To cite this version:**

Clément Moreau. Controllability in finite and infinite dimension and applications to bio-inspired nonlinear systems. Optimization and Control [math.OC]. Université Côte d'Azur, 2020. English. NNT : 2020COAZ4020 . tel-03106682v2

HAL Id: tel-03106682
https://hal.science/tel-03106682v2

Submitted on 8 Feb 2021

HAL is a multi-disciplinary open access archive for the deposit and dissemination of scientific research documents, whether they are published or not. The documents may come from teaching and research institutions in France or abroad, or from public or private research centers.

L'archive ouverte pluridisciplinaire **HAL**, est destinée au dépôt et à la diffusion de documents scientifiques de niveau recherche, publiés ou non, émanant des établissements d'enseignement et de recherche français ou étrangers, des laboratoires publics ou privés.

UNIVERSITÉ CÔTE D'AZUR

ÉCOLE DOCTORALE
SCIENCES FONDAMENTALES ET APPLIQUÉES

THÈSE DE DOCTORAT

Contrôlabilité en dimension finie et infinie et applications à des systèmes non linéaires issus du vivant

Présentée et soutenue par :

Clément MOREAU

En vue de l'obtention du grade de

Docteur en Sciences

de l'Université Côte d'Azur

Discipline : Mathématiques

Equipe MCTAO – Inria Sophia Antipolis-Méditerranée

CEREMADE – Université Paris-Dauphine-PSL

Thèse dirigée par Jean-Baptiste POMET

et co-encadrée par Laetitia GIRALDI et Pierre LISSY

Soutenue le 17 juin 2020

Devant le jury, composé de :

Karine Beauchard	Professeure	ENS Rennes	Examinatrice
Jean-Baptiste Caillau	Professeur	Université Côte d'Azur	Examinateur
Antonio DeSimone	Professeur	SISSA	Examinateur
Eamonn Gaffney	Professeur	University of Oxford	Rapporteur
Laetitia Giraldi	Chargée de recherche	Inria Sophia Antipolis-Méditerranée	Encadrante
Pierre Lissy	Maître de conférences	Université Paris-Dauphine-PSL	Encadrant
Jean-Baptiste Pomet	Directeur de recherche	Inria Sophia Antipolis-Méditérranée	Directeur
Emmanuel Trélat	Professeur	Sorbonne Université	Rapporteur

Contrôlabilité en dimension finie et infinie et applications à des systèmes non linéaires issus du vivant

Cette thèse traite des aspects mathématiques de la contrôlabilité de micro-robots nageurs et de la mobilité de micro-filaments, avec des ramifications en théorie du contrôle et en modélisation.

La première partie présente les résultats de théorie du contrôle obtenus. On énonce d'une part une condition nécessaire de contrôlabilité locale pour une classe particulière de systèmes à deux contrôles en dimension finie, grâce à l'étude de la série de Chen-Fliess associée à ces systèmes. D'autre part, on établit la contrôlabilité avec contrainte de positivité sur l'état pour des systèmes d'équations aux dérivées partielles linéaires paraboliques couplées. On démontre qu'il est possible de contrôler ce type de systèmes en conservant l'état approximativement positif lorsque la matrice de diffusion est diagonalisable, et en conservant l'état positif dans le cas particulier ou celle-ci est égale à la matrice identité.

La deuxième partie aborde les applications au domaine de la micro-natation, et constitue une illustration des résultats de la première partie. On s'intéresse plus précisément à des robots nageurs magnétiques planaires constitués de deux et trois segments, reliés entre eux par des liaisons élastiques, et contrôlés par un champ magnétique. On démontre que ces robots ne sont en général pas contrôlables au voisinage de leur équilibre pour lequel les segments sont alignés, et on explicite les cas particuliers dans lesquels on peut obtenir la contrôlabilité. Les résultats sont appuyés par des simulations numériques.

Dans la troisième partie, on présente des travaux de modélisation et de simulation numérique autour du mouvement de micro-filaments élastiques à bas nombre de Reynolds. On décrit un modèle à N segments performant, robuste et polyvalent. On le valide en comparaison à un autre modèle, puis on l'utilise pour réaliser une étude numérique du phénomène de *buckling* (flambage) d'un filament.

Mots-clés : théorie du contrôle, contrôlabilité, micro-natation, modélisation de micro-filaments, *buckling* dynamique

Controllability in finite and infinite dimension and applications to bio-inspired nonlinear systems

This thesis deals with mathematical aspects of controllability of micro-swimming robots and of motility of micro-filaments, with ramifications in control theory and modeling.

The first part presents our control theory results. On the one hand, we state a necessary condition of local controllability for a particular class of systems with two controls, based on the study of the Chen-Fliess series associated to these systems. On the other hand, we establish controllability for linear coupled parabolic systems of partial differential equations with nonnegative state constraint. We show that it is possible to control these systems while making sure that the state remains approximately nonnegative when the diffusion matrix is diagonalizable, and that it remains nonnegative in the particular case where it is equal to the identity matrix.

The second part addresses applications to micro-swimming, and illustrates the results of the first part. More precisely, we study planar magnetic micro-swimmer robots made of two or three segments, connected by elastic joints, and controlled by a magnetic field. We show that these robots are not controllable in general around their equilibrium position, and describe explicitly the cases for which local controllability can be obtained. The results are illustrated by numerical simulations.

In the third part are featured works of modeling and numerical simulation around elastic micro-filaments motility at low Reynolds number. We describe an efficient, robust and versatile N-link model. We numerically validate it by comparing it to another model, and use it to conduct a numerical study of filament buckling.

Keywords : control theory, controllability, micro-swimming, low Reynolds number propulsion, micro-filament modeling, dynamic buckling

Université Côte d'Azur, Equipe McTAO, Inria, CNRS, LJAD
2004 route des Lucioles, 06902 Valbonne

*

Université Paris-Dauphine PSL, CEREMADE
Place du Maréchal de Lattre de Tassigny, 75016 Paris

Remerciements

Il y a plus de quatre ans, lorsque j'ai commencé mon stage de master 2, j'ai commencé à travailler avec Laetitia, Pierre et Jean-Baptiste. Tout au long de ces années, pendant mon stage, mon année passée à York puis ma thèse qui s'achève aujourd'hui, j'ai pu mesurer la chance immense que j'ai eue de les avoir pour encadrant·e·s. Ils m'ont accompagné et soutenu à chaque instant, sachant toujours se rendre disponible lorsque j'en avais besoin, toujours avec bienveillance et dynamisme. Chacun·e, à travers ses admirables qualités scientifiques et humaines, m'a appris à sa manière à devenir jour après jour un jeune chercheur. Je souhaite leur exprimer ici une profonde gratitude pour l'intérêt qu'ils m'ont porté et les efforts qu'ils m'ont consacré. Laetitia, Pierre, Jean-Baptiste, merci du fond du cœur pour votre aide inestimable, et pour tous ces moments passés ensemble, lors de discussions, déjeuners, cafés, conférences et j'en passe !

Je voudrais remercier Eamonn Gaffney et Emmanuel Trélat pour avoir accepté de rapporter cette thèse. J'admire beaucoup leur travail, et suis touché et honoré par l'intérêt qu'ils portent au mien.

Merci à Karine Beauchard, Jean-Baptiste Caillau et Antonio DeSimone de me faire l'honneur de bien vouloir faire partie de mon jury.

Je remercie en outre tou·te·s les membres du jury ainsi que le personnel de l'école doctorale et de l'Inria pour les efforts qu'ils ont fait ou feront pour que ma soutenance se déroule de la meilleure façon possible en cette période pour le moins troublée.

I would like to address a very special and warm thanks to Hermes Gadelha, my first and best collaborator. Working with him has been a true pleasure and led to productive research and promising results. Hermes, thank you for your help, your enthusiasm and your friendship.

I also want to thank Kenta Ishimoto for welcoming me for a postdoc next year at University of Kyoto. I am very excited to work with him and start my new life in Japan.

Revenons à la langue de Molière pour adresser mes remerciements à tous mes collègues de l'Inria. Les membres de l'équipe McTAO d'abord : Lamberto, Sofya, et mes co-bureaux Sébastien et Yacine qui devraient également soutenir leur thèse sous peu et à qui je souhaite beaucoup de réussite. Je remercie particulièrement Jean-Baptiste Caillau pour ses conseils,

sa bienveillance et sa présence tout au long de ma thèse, notamment en tant que membre de mon comité de suivi. Je remercie les autres membres de ce comité, Jean-Luc Gouzé et Mireille Bossy. Un chaleureux merci à Claire pour son efficacité et son aide précieuse au quotidien. Merci à toutes et tous les membres des équipes FACTAS et BIOCORE, nos voisins d'étage, et en particulier les « jeunes » : Agustin, Carlos, Claudia, Israël, Lucie, Marjorie, Nicolas, Pierre-Olivier, Walid, Wassim, Yves... pour tous ces bons moments à la cantine, au café, au bar ou à la plage. Merci également à Martine pour m'avoir permis de m'impliquer dans des projets de médiation scientifique ; j'y ai pris grand plaisir. Merci enfin à toutes celles et tous ceux, trop nombreux pour les nommer, qui ont œuvré d'une façon ou d'un autre pour que les dix-huit mois que j'ai passés à l'Inria Sophia soient aussi agréables.

J'ai reçu un accueil tout aussi chaleureux de la part du CEREMADE, où j'ai passé l'année écoulée. Merci à Vincent et à toutes celles et ceux qui ont veillé à ce que je m'y sente bien. Merci infiniment à César, Isabelle et Marie pour leur travail et leur aide, si précieux. Merci à mes (nombreux !) co-bureaux : Clément, Enguerrand, Frank, Ivailo, puis Jeanne B. et Giovanni, pour leur présence et leur bonne humeur. De même, je remercie tou·te·s les jeunes du labo pour les déjeuners au CROUS normal ou au CROUS club, les prêts de jetons pour la machine à café, et les verres au Cottage après le séminaire : Adrien, Amirali, Claudia, Donato, Fabio, mon cher co-représentant Grégoire, Hugo, Jean, qui m'a généreusement offert un exemplaire de [Cor07], Jeanne N., Laetitia, Louis, Peng, Quentin, Ruihua, Samuel, Théo, Thomas, Tristan... J'adresse un remerciement spécial à Armand, qui me suit partout (ou l'inverse ?) depuis la prépa, pour son investissement dans les TD que nous avons donnés ensemble à Nice et son aide pour la mise en forme de ce manuscrit.

Je souhaite remercier les personnes aux côtés de qui j'ai eu la chance de donner des TD durant ma thèse : Armand, Claire, Mohammed, Pascal et Roland à Nice ; Emeric, Gabriele, Jacques, Nicolas et Paul à Dauphine. L'expérience de l'enseignement m'a beaucoup apporté, notamment grâce à eux. Merci également à l'équipe de Ma thèse en 180 secondes pour m'avoir permis de participer à cette super expérience au cours de ma première année.

Merci à Anouk pour les cafés à Jussieu, les potins du LJLL et nos nombreuses discussions depuis le master 2. Merci au reste de la team du master : Alexandre, Marc et Nicolas, et enfin à tou·te·s les membres de la communauté mathématique dont j'ai eu le plaisir de faire la rencontre lors de séminaires, conférences et autres événements conviviaux.

Je remercie ma grande et belle famille pour avoir été à mes côtés depuis toujours : les Coussot, les Jourdas, les Moreau, les Servais et les autres, et puis les Thil depuis peu ! Merci plus particulièrement à mes frères, soeur et belle-soeur, et à mes parents, sans qui je ne serais pas là.

Je voudrais adresser des remerciements émus à tou·te·s mes ami·e·s qui ont été un soutien précieux durant ces trois années de thèse. Merci aux « suricates » : Margo, en compagnie de qui j'ai écrit le gros de ce manuscrit lors de studieuses journées à la BNF ; Quentin et Sarah,

pour leur aide inestimable dans la traduction en anglais du premier chapitre ; Valentin, mon « jumeau » en traitement d'images, avec qui j'ai pu partager comme avec personne d'autre les joies et les peines de la recherche, et à qui je souhaite la belle carrière de chercheur qu'il mérite ; Antoine, Camille, Corentin, Jeanne et Manon, pour tout ce fun et tous ces bons moments partagés. Merci à l'« OMZ » : Augustin, qui m'a toujours ouvert sa porte avant et après mon déménagement à Paris pour un tourbillon de slunchs et de culture ; Clémence et les petits verres et discussions que j'aime tant partager avec elle ; Timothée, coloc pour quelques mois et ami pour la vie ; Nicolas et Solweig, membres du trouple, pour tout ce qu'ils m'apportent depuis si longtemps. Merci à Doriane, première amie niçoise puis coloc idéale, qui a assisté à mes premiers pas dans la thèse, et rendu ensoleillé mon séjour sous le ciel bleu de la Côte d'Az ; merci à Arne, pour notre rencontre lors des formations de l'école doctorale et pour tout le reste. Merci à la « team culture » : Camille, Camille, Florent et Julie, aux Cachanais·e·s : Bertrand, dernier coloc en date, Célestine, Constance, Laure, Mathilde, Perrine, Théis, aux ancien·ne·s de l'ENTPE, Elodie, Flavien, à tou·te·s mes fêtard·e·s préféré·e·s : Adèle, Anne-Fleur, Astrid, Cassandre, David, Dominic, Gaspard, Guillaume, Jill, Lisa, Marcelline, Maxime, Olivier, Richard, Sinh, Victoria, et, comme on dit, j'en passe et des meilleur·e·s, qui se reconnaîtront, je l'espère.

Enfin, merci à Paul pour son soutien immense et indéfectible au cours des derniers mois et pour le bonheur qu'il m'offre chaque jour.

Table des matières

Notations

$\mathbb{N}, \mathbb{N}^*$	sets of nonnegative and positive integers
$\mathbb{R}, \mathbb{C}$	sets of real and complex numbers
$\mathrm{Re}(x)$	real part of complex number x
$\mathcal{M}_{n,m}(\mathbb{R})$	set of matrices of size $n \times m$
$\mathcal{M}_n(\mathbb{R})$	set of square matrices of size n
I_n	identity matrix of size n
$\mathrm{rank}(A)$	rank of matrix A
A^T	transpose of matrix A
$\mathrm{L}^2(I, X)$	space of square integrable measurable functions from an interval I of $\mathbb{R}$ to a Banach space X
$\mathrm{L}^\infty(I, X)$	space of essentially bounded measurable functions from an interval I of $\mathbb{R}$ to a Banach space X
$\|\cdot\|_X$	norm on a Banach space X
$B_\eta(x)$	open ball centered at x with radius η
$\langle \cdot, \cdot \rangle$	usual scalar product on $\mathbb{R}^n$
$\mathbf{1}_\Omega$	characteristic function of set A
$\partial\Omega$	boundary of set Ω
$\overset{\circ}{\Omega}$	interior of set Ω
$\lvert\Omega\rvert$	volume of set Ω

Chapitre 1

Synthèse des contributions

Note au lecteur : ce chapitre est la version en français du Chapitre 2.

1.1 Introduction

Contrôler un système consiste à agir dessus afin de maîtriser l'évolution de son état. La théorie du contrôle se divise en trois sous-domaines que l'on peut chacun résumer en une question :

— *contrôlabilité* : peut-on, à l'aide du contrôle, guider l'état un système d'un point de départ donné à un point d'arrivée donné ? Dans ce cas, le contrôle recherché est dit en « boucle ouverte », c'est-à-dire qu'il dépend seulement du temps et pas de l'état ;

— *stabilisation* : peut-on, à l'aide du contrôle, rendre stable un point d'équilibre instable du système, et si oui, comment faire ? Dans ce cas, le contrôle du système fonctionne en « boucle fermée » avec un contrôle dépendant de l'état ;

— *contrôle optimal* : s'il est possible d'atteindre une cible donnée, comment faire pour y parvenir en minimisant un certain coût (le temps passé à l'atteindre, l'énergie consommée, la distance parcourue...) ?

Citons quelques exemples : une voiture dont on actionne les roues pour la diriger vers un point et la faire arriver avec une certaine orientation, un satellite que l'on change d'orbite à l'aide de réacteurs, de l'eau dans un récipient que l'on bouge pour en rendre lisse la surface, une réaction chimique dont on gère la vitesse par l'ajout d'un réactif au cours du temps, ou encore une tumeur cancéreuse dont on essaie de limiter la croissance par l'injection d'un médicament. On trouvera de nombreux autres exemples d'applications de la théorie du contrôle dans [Isi95].

On peut distinguer deux familles de systèmes de contrôle : les cas où l'état à contrôler comporte un nombre *fini* de paramètres (*e.g.* la position et l'orientation d'un robot) et ceux où la grandeur à contrôler vit dans un espace de dimension *infinie* (*e.g.* un profil de

température ou la concentration d'un composé variant sur une région de l'espace Ω). Dans le premier cas, l'état à un instant donné est un élément de $\mathbf{R}^n$ et son évolution est décrite par une équation différentielle ordinaire (EDO) ; dans le deuxième cas, l'état vit dans un espace fonctionnel (typiquement $\mathrm{L}^2(\Omega)$) et son évolution est décrite par une équation aux dérivées partielles (EDP).

Dans ma thèse, je me suis intéressé à des questions de contrôlabilité. Les résultats abstraits que j'ai obtenus sont regroupés dans la Partie I. Le Chapitre 3, consacré au contrôle en dimension finie, présente une nouvelle condition nécessaire de contrôlabilité locale pour des systèmes contrôle-affines à deux contrôles. Dans le Chapitre 4, on s'intéresse à la contrôlabilité de systèmes paraboliques en dimension infinie avec une contrainte de positivité sur l'état. Cette forme de contrôlabilité contrainte a été récemment démontrée pour l'équation de la chaleur [LTZ18], puis pour des équations paraboliques semilinéaires [PZ17]. Ma contribution établit la contrôlabilité avec contrainte de positivité dans un nouveau cas : celui de systèmes d'EDP paraboliques linéaires couplées.

Dans la Partie II sont présentées des applications de ces résultats à l'étude de *micro-nageurs* magnétiques en deux dimensions. Il s'agit de robots filiformes microscopiques, immergés dans un fluide, dont on souhaite contrôler le déplacement à l'aide d'un champ magnétique. Ce type de robot nageur a des applications prometteuses dans le domaine biomédical (délivrance de médicaments, micro-chirurgie, mesure de données dans les organes). Les chapitres 5 et 6 présentent un modèle de ces nageurs et explorent leurs propriétés de contrôlabilité. Grâce au résultat du Chapitre 3, j'ai démontré que les nageurs étudiés ne sont en général pas localement contrôlables au voisinage de leur position d'équilibre, et j'ai explicité les cas particuliers dans lequels on peut obtenir la contrôlabilité locale.

Enfin, je me suis intéressé à des filaments microscopiques associés à la biologie (comme les micro-robots étudiés en Partie II, mais aussi les flagelles des cellules et des bactéries, ou encore les microtubules qui constituent la structure des cellules) à travers des travaux de modélisation et de simulation numérique de micro-filaments élastiques. Ces travaux sont rassemblés dans la Partie III. Le Chapitre 7 présente le modèle mis au point, sa validation numérique et des exemples d'applications. Dans le Chapitre 8, on effectue une étude numérique d'une de ces applications : le phénomène de *buckling* (flambage) d'un micro-filament.

Les chapitres 3 à 8 reproduisent, avec d'éventuelles modifications mineures, des articles publiés, soumis ou en préparation. Le présent chapitre introductif expose pour chacun de ces chapitres un contexte général, un tour d'horizon des résultats existants, les contributions de la thèse, et les perspectives futures.

Les sections 1.2 et 1.3 regroupent les résultats de la Partie I ; l'étude du contrôle de micro-nageurs magnétiques à deux et trois segments est présentée en section 1.4 et la section 1.5 décrit le travail effectué sur la modélisation de micro-filaments élastiques.

1.2 Contrôlabilité de systèmes en dimension finie

1.2.1 Généralités

Soit $n, m \in \mathbb{N}^*$. Le cadre abstrait dans lequel on se place en théorie du contrôle est le suivant : soit une équation de la forme

$$\dot{y}(t) = f(t, y, u). \tag{1.1}$$

Dans cette équation, $y \in \mathbb{R}^n$ est appelé l'état, $\dot{y}$ désigne la dérivée de y par rapport à t et $u \in \mathbb{R}^m$ est appelé le *contrôle*, que l'on s'autorise à choisir afin d'influer sur le système et guider l'état y.

Définition 1.1. Le système (1.1) est *globalement contrôlable en temps T* si, pour tous $y_0, y_1 \in \mathbb{R}^n$, il existe $u \in \mathrm{L}^\infty([0,T], \mathbb{R}^m)$ tel que la solution de (1.1) avec $y(0) = y_0$ vérifie $y(T) = y_1$.

Remarque 1.2. En toute généralité, on pourrait seulement supposer que l'état y et le contrôle u vivent dans des espaces métriques $\mathcal{Y}$ et $\mathcal{U}$ (voir [Son13, Section 2.7]). En particulier, dans le cas d'EDP, $\mathcal{Y}$ est un espace fonctionnel.

On considère souvent que l'état y évolue sur une variété différentiable. Puisqu'on effectue dans cette section des études locales, les résultats que l'on présente sont indépendants du choix de coordonnées sur $\mathbb{R}^n$. On choisit donc, sans perte de généralité, de prendre $\mathbb{R}^n$ pour espace d'état dans toute la suite.

Quand le système 1.1 est contrôlable, il est également intéressant de se demander s'il est possible de faire en sorte que l'état y reste dans une région définie de l'espace d'état (typiquement $\{y \geqslant 0\}$) tout au long de l'intervalle $[0,T]$: c'est la question de la contrôlabilité *avec contrainte sur l'état*. On aborde cette question pour un système de contrôle en dimension infinie dans la section 1.3.

Je donnerai dans la suite de cette section un bref tour d'horizon des concepts et résultats autour de mon travail effectué sur les systèmes d'EDO.

Quelques propriétés de contrôlabilité pour les systèmes linéaires et non linéaires

Les systèmes de contrôle les plus simples sont les systèmes de contrôle linéaires autonomes, s'écrivant sous la forme

$$\dot{y} = Ay + Bu, \tag{1.2}$$

avec $y \in \mathbb{R}^n$, $u \in \mathbb{R}^m$, $A \in \mathcal{M}_n(\mathbb{R})$ et $B \in \mathcal{M}_{n,m}(\mathbb{R})$.

La contrôlabilité globale du système (1.2) en tout temps est résolue depuis les années 1960 ([KHN63] entre autres) et le théorème suivant, qui fournit une condition nécessaire et suffisante algébrique sur les matrices A et B :

Théorème 1.3. *On définit la matrice de Kalman K comme suit :*

$$K = \begin{pmatrix} B & AB & A^2B & \dots & A^{n-1}B \end{pmatrix} \in \mathcal{M}_{n,mn}(\mathbb{R}). \tag{1.3}$$

Alors, pour tout $T > 0$, le système (1.2) est contrôlable en temps T si et seulement si le rang de K est égal à n.

Considérons maintenant un système non-linéaire général de la forme

$$\dot{y} = f(y, u). \tag{1.4}$$

Dans ce cas, on distingue contrôlabilité globale (Définition 1.1) et contrôlabilité locale. Parmi les résultats de contrôlabilité globale, on peut citer entre autres le théorème de Rashevskii-Chow, énoncé plus bas, qui donne une condition de contrôlabilité globale pour des systèmes contrôle-affines sans dérive.

On définit maintenant deux notions de contrôlabilité *locale* du système au voisinage d'un de ses points d'équilibre.

Définition 1.4. Un point d'équilibre du système (1.4) est un couple $(y_{\text{eq}}, u_{\text{eq}}) \in \mathbb{R}^n \times \mathbb{R}^m$ tel que

$$f(y_{\text{eq}}, u_{\text{eq}}) = 0.$$

Soit $(y_{\text{eq}}, u_{\text{eq}})$ un point d'équilibre de (1.4).

Définition 1.5. Le système (1.4) est dit localement contrôlable en temps petit (*small-time locally controllable* en anglais, ou STLC) en $(y_{\text{eq}}, u_{\text{eq}})$ si, pour tout $\varepsilon > 0$, il existe $\eta > 0$ tel que pour tout y_0 et y_1 dans $B_\eta(y_{\text{eq}})$, il existe une fonction $u \in \mathrm{L}^\infty([0, \varepsilon], \mathbb{R}^m)$ telle que la solution $y(\cdot) : [0, \varepsilon] \to \mathbb{R}^n$ de (1.4) avec $y(0) = y_0$ vérifie $y(\varepsilon) = y_1$ et

$$\|u - u_{\text{eq}}\|_{\mathrm{L}^\infty([0,\varepsilon])} \leqslant \varepsilon. \tag{1.5}$$

Définition 1.6. Soit $\alpha \geqslant 0$. Le système (1.4) est dit α-STLC en $(y_{\text{eq}}, u_{\text{eq}})$ si, pour tout $\varepsilon > 0$, il existe $\eta > 0$ tel que pour tout y_0 et y_1 dans $B_\eta(y_{\text{eq}})$, il existe une fonction $u \in \mathrm{L}^\infty([0, \varepsilon], \mathbb{R}^m)$ telle que la solution $y(\cdot) : [0, \varepsilon] \to \mathbb{R}^n$ de (1.4) avec $y(0) = y_0$ vérifie $y(\varepsilon) = y_1$ et

$$\|u - u_{\text{eq}}\|_{\mathrm{L}^\infty([0,\varepsilon])} \leqslant \alpha. \tag{1.6}$$

Remarque 1.7. On peut facilement voir que la « 0-STLC » est alors identique à la STLC telle que définie dans la Définition 1.5. En revanche, si $\alpha > 0$, être α-STLC est plus faible que d'être STLC, car le contrôle peut rester « grand » même si le voisinage de y_{eq} devient « petit ».

La notion de STLC de la Définition 1.5, reproduite de [Cor07, Def. 3.2, p. 125], requiert que le contrôle u soit « très » proche du contrôle d'équilibre quand on va « très » près de la position d'équilibre y_{eq}. On la trouve également par exemple dans les travaux de M. Kawski [Kaw86, Kaw87]. Historiquement, le terme « STLC » a été d'abord utilisé par H. Hermes [Her82] et H. Sussmann [Sus83] entre autres, pour décrire ce que nous appelons ici α-STLC. Dans ce formalisme, la notion décrite dans la Définition 1.5 est appelée « contrôlabilité locale en temps petit avec contrôles petits ».

La STLC apparaît de façon naturelle dans le théorème suivant.

Définition 1.8. Soit $(y_{\text{eq}}, u_{\text{eq}})$ un point d'équilibre de (1.4). Le système linéarisé en $(y_{\text{eq}}, u_{\text{eq}})$ est le système de contrôle linéaire suivant :

$$\dot{y} = \frac{\partial f}{\partial y}(y_{\text{eq}}, u_{\text{eq}})y + \frac{\partial f}{\partial u}(y_{\text{eq}}, u_{\text{eq}})u. \tag{1.7}$$

Théorème 1.9. *Si le système linéarisé* (1.7) *en* $(y_{\text{eq}}, u_{\text{eq}})$ *est contrôlable, alors le système* (1.4) *est STLC en* $(y_{\text{eq}}, u_{\text{eq}})$.

Ce théorème fournit une condition suffisante simple de STLC, qui n'est cependant pas nécessaire : le système (1.4) peut être STLC alors que le linéarisé associé n'est pas contrôlable. Dans ce cas, on dispose d'outils plus fins pour établir ou non la STLC, en particulier dans le cas contrôle-affine présenté dans le suite.

Systèmes contrôle-affines

Notons $\mathcal{X}$ l'espace des champs de vecteurs analytiques sur $\mathbb{R}^n$. On assimile un élément f de $\mathcal{X}$ à une application de $\mathbb{R}^n$ dans $\mathbb{R}^n$ et, pour x dans $\mathbb{R}^n$, $f(x)$ est considéré comme un vecteur colonne et $f'(x)$ désigne la matrice jacobienne en x de l'application f.

Un cas particulier de système non linéaire est le cas dit *contrôle-affine*. Un système contrôle-affine prend la forme suivante :

$$\dot{y} = f_0(y) + \sum_{i=1}^{m} f_i(y) u_i, \tag{1.8}$$

avec $f_0, \dots, f_m \in \mathcal{X}$ [1].

Le champ f_0, appelé *dérive*, correspond comme son nom l'indique à la partie non maîtrisable de l'équation, contre laquelle il faudra possiblement lutter grâce aux contrôles pour atteindre la cible.

On connaît pour les systèmes de la forme (1.8) un certain nombre de conditions nécessaires et de conditions suffisantes de STLC au voisinage d'un point d'équilibre, que l'on détaille dans la suite de cette section. L'amélioration de ces conditions nécessaires et conditions suffisantes a fait l'objet de recherches productives dans de la fin des années 1970 à la fin des années 1990, portées d'abord par H. Hermes [Her76, Her78, Her82], puis par H. Sussmann [Sus83, Sus87], M. Kawski [Kaw87, Kaw90], G. Stefani [Ste86], A. Tret'yak [Tre90], A. Agrachev [AG93a, AG93b], M. Krastanov [Kra98]... Le sujet a connu récemment un regain d'intérêt, illustré notamment par une condition nécessaire pour une nouvelle notion de STLC, démontrée par K. Beauchard et F. Marbach dans le cas $m = 1$ [BM18] (voir Théorème 1.25 ci-dessous).

Toutefois, aucune condition nécessaire et suffisante de contrôlabilité pour les systèmes contrôle-affines avec dérive n'existe à ce jour. Ma contribution, synthétisée dans la section suivante et développée dans le Chapitre 3, apporte une modeste avancée du côté des conditions nécessaires dans le cas où $m = 2$.

Commençons par quelques rappels sur les crochets de Lie de deux champs de vecteurs. Etant donnés deux champs de vecteurs $f = (f^1, \dots, f^n)$ et $g = (g^1, \dots, g^n)$ dans $\mathcal{X}$, le crochet de Lie $[f, g]$ est défini par la formule suivante :

$$\forall x \in \mathbb{R}^n, [f, g](x) = g'(x)f(x) - f'(x)g(x). \tag{1.9}$$

Ainsi, pour j dans $\{1, \dots, n\}$, la j-ième composante de $[f, g]$ est donnée par

$$\forall x \in \mathbb{R}^n, [f, g]^j(x) = \sum_{k=1}^{n} f^k(x) \frac{\partial g^j}{\partial x_k}(x) - g^k(x) \frac{\partial f^j}{\partial x_k}(x). \tag{1.10}$$

1. L'hypothèse d'analyticité n'est pas indispensable ; certains résultats supposent les champs f_i seulement C^∞. Pour une discussion sur la nécessité de les supposer analytiques, voir [Son13, chap.4] ou encore [Sus85]

On utilisera également la notation suivante pour les crochets de Lie itérés, définie par récurrence : $\mathrm{ad}_f^0 g = g$ et pour tout k entier supérieur à 1,

$$\mathrm{ad}_f^k g = [f, \mathrm{ad}_f^{k-1} g].$$

Enfin, pour une famille de champs de vecteurs $\mathcal{F}$, on définit :

— $\mathrm{Br}(\mathcal{F})$ l'ensemble des crochets de Lie itérés [2] de $\mathcal{F}$;

— $\mathrm{Lie}(\mathcal{F})$ l'algèbre de Lie engendrée par $\mathcal{F}$, c'est-à-dire le plus petit sous-espace vectoriel $\mathcal{G}$ de $\mathcal{X}$ tel que $\mathcal{F} \subset \mathcal{G}$ et pour tout f, g dans $\mathcal{G}$, $[f, g] \in G$.

On dira qu'un crochet itéré est d'ordre k lorsqu'il contient exactement k champs (*e.g.* $[f_0, f_1]$ est d'ordre 2, $[f_0, [f_0, [f_0, [f_0, f_1]]]]$ et $[[f_2, f_1], [f_0, [f_2, f_1]]]$ sont d'ordre 5).

L'étude de la contrôlabilité des systèmes contrôle-affines fait naturellement apparaître les crochets de Lie générés par les champs f_i. Pour s'en convaincre, examinons un cas simple sans dérive avec $m = 2$, tiré de [Cor07, p.130] :

$$\dot{y} = f_1(y)u_1 + f_2(y)u_2. \tag{1.11}$$

Supposons que l'état se trouve en un point y_0 tel que $f_1(y_0) \neq 0$ et $f_2(y_0) \neq 0$. Pour $\eta \in \mathbb{R}$, les contrôles $(\eta, 0)$ et $(0, \eta)$ permettent de déplacer le système respectivement dans les directions $\pm f_1(y_0)$ et $\pm f_2(y_0)$, en fonction du signe de η.

Soit $\varepsilon > 0$ et η_1, η_2 dans $\mathbb{R}$. On définit les contrôles suivants sur l'intervalle $[0, 4\varepsilon]$:

$$(u_1(t), u_2(t)) = \begin{cases} (\eta_1, 0) & \text{si } t \in [0, \varepsilon], \\ (0, \eta_2) & \text{si } t \in]\varepsilon, 2\varepsilon], \\ (-\eta_1, 0) & \text{si } t \in]2\varepsilon, 3\varepsilon], \\ (0, -\eta_2) & \text{si } t \in]3\varepsilon, 4\varepsilon]. \end{cases}$$

On peut alors montrer que

$$y(4\varepsilon) = y_0 + \eta_1\eta_2\varepsilon^2[f_1, f_2](y_0) + o(\varepsilon^2).$$

Autrement dit, en jouant sur le signe de η_1 et η_2, on peut déplacer le système dans les directions $\pm[f_1, f_2]$.

On peut ainsi pressentir que les directions accessibles pour le système (1.8) autour d'un point d'équilibre sont données par les crochets de Lie générés par les champs f_i. Le Théorème 1.15 qui suit formalise cette idée en énonçant une condition nécessaire de contrôlabilité locale.

Remarque 1.10. Étant donné un point d'équilibre $(y_{\mathrm{eq}}, u_{\mathrm{eq}})$ du système (1.8) , on peut se ramener au point $(0, 0)$ en effectuant la translation $(y, u) \mapsto (y - y_{\mathrm{eq}}, u - u_{\mathrm{eq}})$. Sans perte de généralité, on suppose donc dans toute la suite que $(0, 0)$ est un point d'équilibre de (1.8).

Cas sans dérive. Dans le cas sans dérive, on connaît des conditions nécessaires et suffisantes de STLC et de contrôlabilité globale, données par le Théorème 1.12 ci-dessous, dit de Rashevskii-Chow.

Définition 1.11. Le système (1.8) vérifie la *Lie algebra rank condition (LARC)* en un point $(x, 0)$ si

$$\{g(x), g \in \mathrm{Lie}(f_0, f_1, \ldots, f_m)\} = \mathbb{R}^n. \tag{1.12}$$

2. Une construction détaillée de $\mathrm{Br}(\mathcal{F})$ est effectuée dans [Sus87].

Théorème 1.12 ([Ras38, Cho39])**.** *Supposons que* $f_0 = 0$.

1. *Si* (1.8) *vérifie la LARC en* $(0,0)$*, alors il est STLC en* $(0,0)$.
2. *Si* (1.8) *vérifie la LARC en* $(x,0)$ *pour tout* $x \in \mathbb{R}$*, alors il est globalement contrôlable en tout temps.*

Dans le cas où $f_0 \neq 0$, on ne connaît pas de condition nécessaire et suffisante de STLC. On dispose toutefois d'un résultat portant sur l'*ensemble accessible* en temps inférieur à T :

Définition 1.13. Soit $T > 0$. On appelle ensemble accessible en temps T, et on note $\mathcal{A}^T$, l'ensemble

$$\mathcal{A}^T = \{y_0 \in \mathbb{R}^n | \exists u \in \mathrm{L}^\infty(0,T,\mathbb{R}^m), y_u(T) = y_0\},$$

où $y_u(T)$ désigne la solution de (1.8) avec $y(0) = 0$ et contrôle u. On note également

$$\mathcal{A}^{\leqslant T} = \bigcup_{t\in[0,T]} \mathcal{A}^t.$$

Théorème 1.14 ([Son13, Theorem 9, p. 156])**.** *Si le système* (1.8) *vérifie la LARC en 0, alors pour tout* $T > 0$,

$$\overset{\circ}{A}{}^{\leqslant T} \neq \emptyset.$$

Répondre à la question de la contrôlabilité pour le système (1.8) revient donc à déterminer si l'intérieur de l'ensemble accessible $A^{\leqslant T}$ contient l'équilibre 0 pour tout T.

Conditions nécessaires de STLC.

Théorème 1.15 ([Sus73])**.** *S'il existe* $\alpha \geqslant 0$ *tel que le système* (1.8) *est* α*-STLC en* $(0,0)$*, alors il vérifie la LARC en ce point.*

La réciproque n'est pas vraie ; par exemple le système

$$\begin{cases} \dot{y}_1 &= y_2^2, \\ \dot{y}_2 &= u, \end{cases} \tag{1.13}$$

vérifie la LARC en l'équilibre $((0,0),0)$ mais n'est pas contrôlable, car on a nécessairement $y_2 \geqslant 0$.

Cet exemple assez trivial suggère que la LARC n'est pas une condition nécessaire très optimale : elle englobe beaucoup trop de cas non contrôlables. Malheureusement, il n'en existe pas de meilleure à ma connaissance dans le cas général. Des résultats plus fins existent dans le cas scalaire ($m = 1$) ; on en cite quelques-uns dans la suite. Voyons d'abord de quelles conditions suffisantes de STLC on dispose dans le cas général.

Conditions suffisantes de STLC. Commençons par quelques notations, prises dans [Cor07, Section 3.4]. Soit $\mathfrak{S}_m$ l'ensemble des permutations de $\{1,\dots,m\}$. Pour $\pi \in \mathfrak{S}_m$, on note $\tilde{\pi}$ l'application qui envoie $(f_0, f_1, \dots, f_m)$ sur $(f_0, f_{\pi(1)}, \dots, f_{\pi(m)})$ dans un crochet donné. On peut ainsi définir, pour g un élément de $\mathrm{Br}(f_0,\dots,f_m)$,

$$\sigma(g) = \sum_{\pi\in\mathfrak{S}_m} \tilde{\pi}(g).$$

Par exemple, si $m = 2$ et $g = [f_1, [f_2, [f_1, f_0], f_0]]$, alors

$$\sigma(g) = [f_1, [f_2, [f_1, f_0], f_0]] + [f_2, [f_1, [f_2, f_0], f_0]].$$

Enfin, étant donné un crochet g dans $\mathrm{Br}(f_0, \dots, f_m)$, et $i \in \{0, \dots, m\}$, on note :

— $\delta_i(g)$ le nombre de fois que f_i apparaît dans g. Dans l'exemple ci-dessus, $\delta_0(g) = 2$, $\delta_1(g) = 2$, et $\delta_2(g) = 1$;

— pour $\theta \in [0, 1]$, $\rho_\theta(g) = \theta\delta_0(g) + \sum_{i=1}^m \delta_i(g)$;

— pour $\eta > 0$, H_η le sous espace de $\mathbb{R}^n$ engendré par l'évaluation en 0 des crochets g de $\mathrm{Br}(f_0, \dots, f_m)$ tels que $\rho_\theta(g) < \eta$.

On introduit maintenant la célèbre condition de Sussmann [Sus87].

Définition 1.16 (Condition de Sussmann)**.** Soit $\theta \in [0, 1]$. On dit que le système (1.8) satisfait $S(\theta)$ en $(0, 0)$ si

— il satisfait la LARC en $(0, 0)$;

— pour tout g dans $\mathrm{Br}(f_1, \dots, f_m)$ tel que $\delta_0(g)$ est impair et $\delta_i(g)$ est pair pour tout $i \in \{1, \dots, m\}$,

$$\sigma(g)(0) \in H_{\rho_\theta(g)}.$$

On a alors le résultat suivant :

Théorème 1.17 ([Sus87, Theorem 7.3])**.** *S'il existe $\theta \in [0, 1]$ tel que le système (1.8) satisfasse $S(\theta)$ en $(0, 0)$, alors le système (1.8) est STLC en $(0, 0)$.*

Le Théorème 1.17 établit que la STLC du système (1.8) est conditionnée par le comportement des crochets comportant un nombre impair de fois f_0 et un nombre pair de fois les autres champs. Ces crochets ont souvent été appelés *mauvais* crochets au sens où ce sont leurs directions en 0 qui semblent constituer une obstruction à la contrôlabilité dans le cas où la condition de Sussmann ne serait pas vérifiée. Par opposition, pour un crochet h et $\theta \in [0, 1]$ donné, les crochets de $H_{\rho_\theta(g)}$ sont appelés *bons* crochets : le système sera contrôlable si ces crochets englobent suffisamment de directions en 0 et peuvent ainsi « neutraliser » les directions prises par les mauvais crochets.

Toutefois, comme Kawski l'a remarqué dans [Kaw86, Example 2.5.1], le caractère bon ou mauvais des crochets d'ordre élevé n'est pas intrinsèque et dépend de la base choisie pour les espaces de crochets de Lie générés par les champs de vecteurs du système. Par commodité, et parce que ce phénomène n'a pas d'importance pour les crochets d'ordre bas que l'on considère essentiellement ici, on qualifiera parfois certains crochets dans la suite de « bons » ou « mauvais » ; il convient toutefois de garder à l'esprit qu'il s'agit d'une terminologie imprécise.

Conditions de STLC pour les systèmes mono-entrée. On se restreint désormais au cas $m = 1$, dit *à contrôle scalaire* ou encore *mono-entrée* :

$$\dot{y} = f_0(y) + f_1(y)u_1. \tag{1.14}$$

Pour $k \in \mathbb{N}$, notons S_k l'ensemble généré par les crochets de Lie itérés de $f_0, \dots, f_m$ contenant au plus k fois f_0 ; et, pour $y \in \mathbb{R}^n$, $S_k(0)$ le sous-espace de $\mathbb{R}^n$ généré par les éléments de S_k évalués en 0.

Remarque 1.18. On a bien entendu $S_k \subset S_{k+1}$ pour tout k.

Théorème 1.19 ([Sus83])**.** *Supposons que, en un point d'équilibre* $(0,0)$ *:*

— *le système* (1.14) *satisfasse la LARC en* $(0,0)$ *;*

— *pour tout* k *entier supérieur ou égal à 1, on ait*

$$S_{2k}(0) \subset S_{2k-1}(0). \tag{1.15}$$

Alors le système (1.14) *est STLC en* $(0,0)$*.*

Le Théorème 1.19 améliore et simplifie légèrement la condition de Sussmann (Définition 1.16) dans le cas scalaire. Il stipule que le système (1.14) est STLC à condition que les « mauvais » crochets g comportant f_1 un nombre pair de fois ne créent pas de nouvelles directions en 0 par rapport aux « bons » crochets qui comportent au maximum $(\delta_1(g)-1)$ fois f_1.

On cherche à présent à comprendre ce qu'il se passe quand la condition (1.15) n'est pas vérifiée. À l'ordre le plus bas, elle ne l'est pas quand $[f_1,[f_0,f_1]](0) \notin S_1(0)$; c'est l'objet du théorème suivant. On note

$$B_1 = [f_1,[f_0,f_1]], \tag{1.16}$$

et on appelle B_1 le « premier mauvais crochet ».

Théorème 1.20 ([Sus83, Proposition 6.3])**.** *Supposons que* $B_1(0)$ *n'appartienne pas à* $S_1(0)$*. Alors, pour tout* $\alpha \geqslant 0$*, le système* (1.14) *n'est pas* α*-STLC en* $(0,0)$*.*

Ce théorème établit que le crochet B_1 constitue une véritable obstruction à la STLC quand sa direction en 0 est en dehors de $S_1(0)$. On aimerait alors pouvoir, de façon analogue, établir que la présence dans $S_1(0)$ des autres éléments de $S_2(0)$ est nécessaire à la STLC. Hélas, ce n'est pas le cas : les choses se compliquent dès que l'on s'intéresse au « deuxième mauvais crochet »

$$B_2 = [[f_0,f_1],[f_0,[f_0,f_1]]]. \tag{1.17}$$

En effet, si $B_1(0) \in S_1(0)$ et $B_2(0) \notin S_1(0)$, alors (1.14) *peut ou peut ne pas* être STLC. Par exemple, le système suivant (tiré de [Sus83, p.711]) :

$$\begin{cases} \dot{y}_1 &= u, \\ \dot{y}_2 &= y_1, \\ \dot{y}_3 &= y_1^3 + y_2^2, \end{cases} \tag{1.18}$$

est STLC en 0 alors même qu'il vérifie $B_2(0) \notin S_1(0)$.

En ajoutant de nouvelles directions à S_1, on obtient la nouvelle condition nécessaire suivante :

Théorème 1.21 ([Kaw87])**.** *Soit* $S' = \mathrm{Vect}\{\mathrm{ad}_{f_0}^k(\mathrm{ad}_{f_1}^3 f_0), k \in \mathbb{N}\}$*. Si* $B_2(0) \notin S_1(0) + S'(0)$*, alors* (1.14) *n'est pas STLC en* $(0,0)$*.*

Ce théorème n'exclut pas que le système puisse être α-STLC pour $\alpha > 0$. Dans [Kra98, Théorème 1.2], M. Krastanov établit des conditions nécessaires de α-STLC, où α dépend notamment de la valeur prise en 0 par des crochets d'ordre 5. Ces conditions sont toutefois extrêmement techniques (c'est pourquoi on ne les reproduit pas ici). Elle tendent à confirmer

qu'il est illusoire de pouvoir établir des conditions nécessaires aussi agréables que le Théorème 1.20 pour tous les autres cas où la condition (1.15) n'est pas vérifiée.

G. Stefani a établi dans [Ste86] une condition nécessaire qui englobe celle du Théorème 1.20 et constitue à ma connaissance la condition la plus complète à ce jour :

Théorème 1.22 ([Ste86])**.** *S'il existe k dans $\mathbb{N}$ tel que*

$$\mathrm{ad}_{f_1}^{2k} f_0(0) \notin S_{2k-1}(0),$$

alors, pour tout $\alpha \geqslant 0$, le système (1.14) n'est pas α-STLC en $(0,0)$.

Pour finir, citons un nouveau résultat obtenu par K. Beauchard et F. Marbach dans [BM18] en faisant appel à une notion différente de contrôlabilité locale, qui exige que le contrôle soit petit pour une norme différente.

On définit l'espace de Sobolev $\mathrm{W}^{k,\infty}(I)$ comme suit : étant donné un intervalle I de $\mathbb{R}$, une fonction f appartient à $\mathrm{W}^{k,\infty}(I)$ si pour tout p dans $\{0,\dots,k\}$, $f^{(p)} \in \mathrm{L}^\infty(I)$. La norme de f sur cet espace est alors donnée par

$$\|f\|_{\mathrm{W}^{k,\infty}} = \max_{p\in\{0,\dots k\}} \|f^{(p)}\|_{\mathrm{L}^\infty(I)}.$$

Définition 1.23. Soit $k \in \mathbb{N}$. Le système (1.14) est dit $\mathrm{W}^{k,\infty}$-STLC en $(y_{\mathrm{eq}}, u_{\mathrm{eq}})$ si, pour tout $\varepsilon > 0$, il existe $\eta > 0$ tel que pour tout y_0 et y_1 dans $B_\eta(y_{\mathrm{eq}})$, il existe une fonction $u \in \mathrm{L}^\infty([0,\varepsilon],\mathbb{R})^m$ telle que la solution de (1.14) avec $y(0) = y_0$ vérifie $y(\varepsilon) = y_1$ et

$$\|u - u_{\mathrm{eq}}\|_{\mathrm{W}^{k,\infty}[0,\varepsilon]} \leqslant \varepsilon. \tag{1.19}$$

Remarque 1.24. Pour $k = 0$, la notion est bien sûr identique à la STLC. D'autre part, on peut ordonner les différentes notions de STLC des définitions 1.5, 1.6 et 1.23 selon une chaîne d'implications. Soit k et k' dans $\mathbb{N}$ tels que $k \geqslant k'$ et α et α' dans $\mathbb{R}$ tels que $\alpha \geqslant \alpha'$. On a alors

$$\mathrm{W}^{k,\infty}\text{-STLC} \Rightarrow \mathrm{W}^{k',\infty}\text{-STLC} \Rightarrow \text{STLC} \Rightarrow \alpha'\text{-STLC} \Rightarrow \alpha\text{-STLC}. \tag{1.20}$$

Soit $d = \dim S_1(0)$ et $k \in \{1,\dots,d\}$. Par analogie avec (1.16) et (1.17), notons

$$B_k = [\mathrm{ad}_{f_0}^{k-1} f_1, \mathrm{ad}_{f_0}^{k} f_1]. \tag{1.21}$$

Théorème 1.25 ([BM18, Theorem 3])**.** *Soit $k \in \{2,\dots,d\}$. Si $B_k(0) \notin S_1(0)$, alors (1.14) n'est pas $\mathrm{W}^{2k-3,\infty}$-STLC en $(0,0)$.*

Remarque 1.26. Ce résultat, tel qu'énoncé dans [BM18], est également vrai pour $k = 1$, en convenant qu'une fonction $u : [0,\epsilon] \to \mathbb{R}$ est dans $\mathrm{W}^{-1,\infty}([0,\epsilon])$ si $t \mapsto \int_0^t u(s)\mathrm{d}s$ est dans $\mathrm{L}^\infty([0,\epsilon])$.

Pour illustrer ce théorème, reprenons l'exemple (1.18), que l'on sait être STLC en 0. Le Théorème 1.25 pour $k = 2$ stipule qu'il n'est en revanche pas $\mathrm{W}^{1,\infty}$-STLC, ce qui signifie que les contrôles utilisés ne peuvent pas être trop réguliers : on devra par exemple utiliser des contrôles fortement oscillants.

Ce résultat suggère en un sens que plus k est grand, moins le mauvais crochet B_k constitue une obstruction forte à la contrôlabilité quand sa direction en 0 est en dehors de $S_1(0)$.

1.2.2 Contributions de la thèse : condition nécessaire de contrôlabilité locale pour une classe particulière de systèmes à deux contrôles

Le travail réalisé pendant ma thèse, qui est l'objet de cette section, propose une extension du théorème 1.20 dans le cas de systèmes contrôle-affines comportant cette fois-ci deux contrôles. Ce travail a fait l'objet d'un article soumis à la revue *ESAIM :COCV*, reproduit dans le Chapitre 3.

On s'intéresse ici à un système contrôle-affine de la forme (1.8) avec $m = 2$:

$$\dot{y} = f_0(y) + f_1(y)u_1 + f_2(y)u_2. \tag{1.22}$$

On suppose que

$$f_0(0) = 0, f_2(0) = 0, \tag{1.23}$$

c'est-à-dire que, pour tout $u_2^{\text{eq}} \in \mathbb{R}$, $(0, (0, u_2^{\text{eq}}))$ est un point d'équilibre : le contrôle u_2 ne peut pas agir sur le système lorsque celui-ci est en sa position d'équilibre $y = 0$. Mon travail a consisté à étudier le rôle de ce contrôle supplémentaire, par rapport au cas scalaire, dans la contrôlabilité du système.

La volonté d'étudier les systèmes de la forme (1.22) est née de l'étude des modèles de micro-nageurs contrôlés par un champ magnétique, dont on parle en section 1.4 de cette introduction et dans la Partie II. Le système d'équations qui régit la dynamique de ces nageurs est en effet de la forme (1.22). J'ai démontré pour ce système plusieurs résultats de contrôlabilité (voir Théorèmes 1.55 et 1.60 et l'ensemble des Chapitres 5 et 6). L'esprit du résultat présenté ici est de généraliser les résultats obtenus sur les nageurs, en traitant le problème abstrait de contrôlabilité associé au système (1.22).

De façon analogue à la section précédente, on note :

— R_1 l'espace engendré par les crochets de Lie de f_0, f_1, f_2 contenant au plus une fois f_1 ;

— $R_1(0)$ le sous-espace vectoriel de $\mathbb{R}^n$ engendré par les éléments de R_1 évalués en 0.

Rappelons également que le « mauvais » crochet B_1 est défini par $B_1 = [f_1, [f_0, f_1]]$.

Mon résultat principal est la condition nécessaire de contrôlabilité suivante :

Théorème 1.27 ([GLMP19] et Chapitre 3, Théorème 3.16)**.** *Supposons que* $B_1(0) \notin R_1(0)$.

1. *Si* $B_1(0) \in R_1(0) + \text{Vect}([f_1, [f_2, f_1]](0))$, *soit* $\beta \in \mathbb{R}$ *tel que*

$$B_1(0) + \beta[f_1, [f_2, f_1]](0) \in R_1(0).$$

   Alors, pour tout $u_2^{eq} \in \mathbb{R}$ *tel que* $u_2^{eq} \neq \beta$, *le système* (1.22) *n'est pas STLC en* $(0, (0, u_2^{eq}))$.

2. *Si* $B_1(0) \notin R_1(0) + \text{Vect}([f_1, [f_2, f_1]](0))$, *alors, pour tout* $u_2^{eq} \in \mathbb{R}$ *et tout* $\alpha \geqslant 0$, *le système* (1.22) *n'est pas* α*-STLC en* $(0, (0, u_2^{eq}))$.

On sait d'après le Théorème 1.20 que le « mauvais » crochet B_1 constitue une obstruction à la contrôlabilité quand sa valeur en 0 est en dehors de $R_1(0)$. Le Théorème 1.27 ci-dessus vient compléter ce résultat en indiquant que, pour le système (1.22) à deux contrôles, le crochet $[f_1, [f_2, f_1]]$ peut *neutraliser* le crochet B_1, c'est-à-dire contribuer à rétablir la STLC

même si $B_1(0) \not\subseteq R_1(0)$. Cela est possible seulement dans le cas 1., *i.e.* quand les valeurs de ces deux crochets en 0 partagent une direction commune en dehors de $R_1(0)$, qui est matérialisée par la constante β. La valeur β est alors la *seule valeur* de u_2 pour laquelle le système (1.22) peut être STLC.

On trouvera une illustration frappante de ce phénomène dans les simulations numériques du déplacement d'un micro-nageur magnétique présentées sur les Figures 1.4 et 1.5 dans la section 1.4.3. Comme on le verra dans la suite, les trajectoires dessinées sur ces figures sont celles d'un système de la forme (1.22), et sont choisies de telle sorte à recouvrir approximativement l'espace accessible par le système au voisinage de $(0, (0, u_2^{\mathrm{eq}}))$ pour une certaine valeur de u_2^{eq}. Comme le prévoit le Théorème 1.27, seule la valeur « critique » β permet à l'ensemble accessible de recouvrir un voisinage de l'origine. Dans les autres cas, on observe qu'il reste localement à gauche ou à droite de l'origine, ce que l'on peut interpréter comme l'effet de la dérive engendrée par le mauvais crochet $[f_1, [f_0, f_1]]$.

Éléments de preuve du Théorème 1.27. La démonstration du résultat ci-dessus est inspirée de celle du Théorème 1.20 réalisée dans [Sus83]. Elle repose sur l'étude d'une forme de développement asymptotique de (1.22) au voisinage de l'état d'équilibre, appelé *série de Chen-Fliess* – voir la Définition 1.28 ci-dessous.

Commençons par quelques notations. Soit $k \in \mathbb{N}$ et $I = (i_1, \dots, i_k)$ un multi-indice dans $\{0, 1, 2\}^k$. On note $f_{i_1} f_{i_2} \dots f_{i_k}$ la composition successive des champs $f_{i_1}, \dots, f_{i_k}$ vus comme des opérateurs différentiels.

Étant donné un contrôle $u = (u_1, u_2)$ dans $\mathrm{L}^\infty([0,T], \mathbb{R})^2$, on définit l'intégrale itérée $\int_0^T u_I$ par

$$\int_0^T u_{i_k}(\tau_k) \int_0^{\tau_k} u_{i_{k-1}}(\tau_{k-1}) \int_0^{\tau_{k-1}} \dots u_{i_2}(\tau_2) \int_0^{\tau_2} u_{i_1}(\tau_1) \mathrm{d}\tau_1 \mathrm{d}\tau_2 \dots \mathrm{d}\tau_k,$$

avec la convention $u_0 = 1$.

Enfin, on note y_u la solution de (1.22) avec $y(0) = 0$ et le contrôle u.

Définition 1.28. Soit $\Phi : \mathbb{R}^n \to \mathbb{R}$ une fonction analytique réelle définie sur un voisinage de 0, et $u = (u_1, u_2)$ un contrôle dans $\mathrm{L}^\infty([0,T], \mathbb{R})^2$. La série de Chen-Fliess [Fli78, Fli75, Che57] associée à (1.22), Φ, u et T est définie par

$$\Sigma(u, f, \Phi, T) = \sum_I \left(\int_0^T u_I \right) (f_I \Phi)(0), \tag{1.24}$$

la somme étant effectuée sur tous les multi-indices $I = (i_1, \dots, i_k)$ dans $\{0, 1, 2\}^k$ avec $k \in \mathbb{N}$.

Proposition 1.29 ([Sus83, Proposition 4.3, p. 698])**.** *Pour tout $A > 0$, il existe $T_0(A) > 0$ tel que la série (1.24) converge pour tout $T \leqslant T_0$ et u tel que $\|u\|_{\mathrm{L}^\infty([0,T],\mathbb{R})^2} \leqslant A$, uniformément en u et T, vers $\Phi(y_u(T))$, i.e.*

$$\Phi(y_u(T)) = \Sigma(u, f, \Phi, T). \tag{1.25}$$

Le schéma de preuve du Théorème 1.27 est le suivant :

1. on définit des coordonnées locales pour l'état y, et une fonction Φ analytique réelle bien choisie qui associe à y l'une de ces coordonnées.
2. on démontre qu'il existe $T_0 > 0$ tel que pour tout $T \in [0, T_0]$ et tout contrôle $u = (u_1, u_2)$ satisfaisant les hypothèses de petitesse de la notion de STLC appropriée (STLC ou α-STLC selon les cas), on a
$$\Phi(y_u(T)) \geqslant 0. \tag{1.26}$$
3. on en déduit que l'ensemble $\{x \in \mathbb{R}^n | \Phi(x) < 0\}$ n'est pas localement accessible pour le système (1.22), et donc que ce dernier n'est pas localement contrôlable selon la définition choisie.

Notons p_1 le terme de la série de Chen-Fliess $\Sigma(u, f, \Phi, T)$ associé à $I_2 = (1, 1, 0)$, qui se trouve être celui associé au mauvais crochet B_1. Pour démontrer (1.26), on montre que l'on a, pour un bon choix de Φ et sous les bonnes hypothèses sur u et T énoncées au point 2 ci-dessus,
$$p_1 > 0 \quad \text{et} \quad |\Sigma(u, f, \Phi, T) - p_1| \leqslant p_1; \tag{1.27}$$
ce qui permet de déduire (1.26) en utilisant (1.25).

Les calculs permettant d'obtenir (1.27) sont développés en section 3.5 du Chapitre 3.

1.2.3 Perspectives

Extensions du Théorème 1.27

Le Théorème 1.27 traite le cas pour lequel $B_1(0)$ n'appartient pas à $R_1(0)$. Par analogie avec le cas scalaire, il est alors naturel de se demander quelles sont les propriétés de contrôlabilité du système (1.22) quand $B_1(0)$ appartient à $R_1(0)$, mais que d'autres crochets d'ordre plus élevé sont en dehors de $R_1(0)$ en 0. Dans le cas scalaire, on a vu avec le Théorème 1.21 que l'on dispose d'un résultat quand le crochet d'ordre 5 $B_2(0)$ n'appartient pas à $R_1(0)$. Je travaille à énoncer un résultat similaire pour le cas à deux contrôles.

Dans le cas du Théorème 1.27, qui porte sur des crochets d'ordre 3, seul le « bon » crochet $[f_1, [f_2, f_1]]$ peut « neutraliser » le « mauvais » crochet $[f_1, [f_0, f_1]]$, à condition que ceux-ci partagent la même direction en dehors de $R_1(0)$.

À l'ordre 5, j'ai établi que les mauvais crochets à neutraliser sont au nombre de deux : le crochet $B_2 = [[f_0, f_1], [f_0, [f_0, f_1]]]$ ainsi que le crochet $C_2 = [[f_2, f_1], [f_0, [f_2, f_1]]]$. On peut ensuite distinguer deux cas : celui où les bons crochets capables de neutraliser B_2 et C_2 sont d'un ordre inférieur, et celui où ils sont également d'ordre 5.

Neutralisation par $[f_1, [f_2, f_1]]$

Par analogie avec le Théorème 1.25 et nos résultats, on peut conjecturer que le crochet $[f_1, [f_2, f_1]]$ (et possiblement d'autres d'ordre plus élevé) pourrait neutraliser les mauvais crochets tels que B_2, C_2 ou encore B_k avec $k > 2$, à condition de partager avec eux une direction en dehors de $R_1(0)$. Cela autoriserait ainsi le système (1.22) à être $\mathrm{W}^{2k-3,\infty}$-STLC quand $B_k(0) \notin R_1(0)$, ce qu'il ne saurait être dans le cas scalaire d'après le Théorème 1.25. L'exemple 3.27 dans le Chapitre 3 va dans le sens de cette conjecture, en donnant un exemple de système $\mathrm{W}^{1,\infty}$-STLC pour lequel :

— $B_1(0) \in R_1(0)$;
— $B_2(0) \notin R_1(0)$;

— $[f_1, [f_2, f_1]](0) = B_2(0)$.

Neutralisation par des crochets du même ordre

Si aucun crochet d'ordre inférieur ne peut neutraliser les mauvais crochets B_2 et C_2, six crochets d'ordre 5 peuvent alors jouer un rôle de neutralisation, analogue à celui de $[f_1, [f_2, f_1]]$ dans le Théorème 1.27. Ces crochets sont donnés par

$$[[f_2, f_1], [f_0, [f_0, f_1]]], [[f_0, f_1], [f_0, [f_2, f_1]]], [[f_0, f_1], [f_2, [f_0, f_1]]],$$
$$[[f_2, f_1], [f_2, [f_0, f_1]]], [[f_0, f_1], [f_2, [f_2, f_1]]], [[f_2, f_1], [f_2, [f_2, f_1]]].$$

La question qui reste à élucider est la suivante : quelles conditions, portant sur les directions de ces crochets en 0, permettent de conclure que le système (1.22) est localement contrôlable ou non, et pour quelle notion de contrôlabilité (STLC, α-STLC ou autre) ? Mes recherches à ce sujet sont en cours.

1.3 Contrôlabilité d'équations paraboliques en dimension infinie avec contrainte de positivité sur l'état

1.3.1 Généralités ; résultats existants

Les résultats standard de contrôlabilité assurent que l'on peut atteindre une cible à partir d'un point de départ, sans pour autant présager du comportement de la solution entre ces deux états. Or, de nombreux systèmes d'équations décrivent des phénomènes physiques avec des variables positives (température, concentration...). Il est donc naturel d'exiger de pouvoir les contrôler tout en conservant la positivité de l'état tout au long de la trajectoire – ou, plus généralement, d'exiger que la trajectoire reste dans une région déterminée de l'espace d'état. Ce problème connaît ces dernières années un intérêt croissant avec de nombreuses avancées prometteuses : citons [LTZ18] pour les EDO et [LTZ17, PZ17] pour les EDP.

La contrainte de positivité sur l'état engendre des phénomènes intéressants : la contrôlabilité avec état positif n'est pas toujours possible, même si le système étudié est contrôlable sans contrainte [PZ17]. Dans les cas où il est possible de contrôler avec état positif, on peut avoir existence d'un temps minimal de contrôlabilité [LTZ17].

Je m'intéresserai dans cette section à des équations aux dérivées partielles paraboliques faisant intervenir un opérateur elliptique en espace ainsi que la dérivée première temporelle de l'état. L'évolution de ce type d'équations est notamment caractérisée par des phénomènes de diffusion, de régularisation et de dissipation de l'énergie dans le cas linéaire, et de possible explosion en temps fini dans le cas non linéaire. Dans le cas le plus simple qui est celui de l'équation de la chaleur linéaire, la contrôlabilité [LR95, FI96] et la contrôlabilité avec état positif [LTZ17] sont connues.

La contribution de ma thèse consiste en des résultats similaires pour des systèmes d'équations paraboliques linéaires couplées. J'ai établi que, sous de bonnes hypothèses :

— si la matrice de couplage du terme de diffusion est égale à la matrice identité, alors on peut contrôler vers une trajectoire en conservant la positivité de l'état (Théorème 1.38) ;

— si la matrice de couplage est diagonalisable, on peut contrôler vers une trajectoire globalement bornée en conservant approximativement la positivité de l'état (Théorème

1.41).

La présente section 1.3.1 décrit brièvement l'état de l'art. Mes résultats sont présentés dans la section 1.3.2 et la section 1.3.3 est consacrée aux perspectives futures de mon travail, notamment à une extension possible à des équations paraboliques semilinéaires avec un contrôle interne.

Dans toute la section 1.3, d est un entier naturel non nul, Ω désigne un ouvert borné connexe non vide de $\mathbb{R}^d$, au bord régulier et ω un ouvert non vide inclus dans Ω. L'opérateur laplacien sur Ω est noté Δ.

Contrôle de l'équation de la chaleur

Soit $T > 0$. On considère l'équation de la chaleur linéaire avec contrôle interne et condition au bord de Neumann

$$\begin{cases} \partial_t y - \Delta y &= \mathbf{1}_\omega u & \text{sur } (0,T)\times\Omega, \\ \frac{\partial y}{\partial n} &= 0 & \text{sur } (0,T)\times\partial\Omega, \\ y(0,\cdot) &= y_0 & \text{sur } \Omega. \end{cases} \tag{1.28}$$

Étant donné $y_0 \in \mathrm{L}^\infty(\Omega)$, on appelle *trajectoire libre issue de* y_0 la solution de (1.28) avec condition initiale y_0 et contrôle $u = 0$.

Commençons par définir la notion de contrôlabilité que l'on utilisera dans la suite.

Définition 1.30 (Contrôlabilité aux trajectoires)**.** Soit $T > 0$. Le système (1.28) est dit *contrôlable aux trajectoires* en temps T si, pour tout $y_0, \bar{y}_0 \in \mathrm{L}^\infty(\Omega)$, il existe un contrôle u dans $\mathrm{L}^\infty((0,T)\times\omega)$ tel que la solution y de (1.28) avec condition initiale y_0 et contrôle u vérifie

$$y(T,\cdot) = \bar{y}(T,\cdot), \tag{1.29}$$

où $\bar{y}$ est la trajectoire libre issue de $\bar{y}_0$.

Le résultat suivant a été démontré pour $d = 1$ dans [FR71] et en dimension quelconque dans [LR95, FI96].

Théorème 1.31. *Le système* (1.28) *est contrôlable aux trajectoires en tout temps.*

Plus récemment, dans [LTZ17], J. Lohéac, E. Trélat et E. Zuazua ont montré que l'équation est également contrôlable vers un état d'équilibre positif en conservant la positivité de la solution. Toutefois, dans ce cas, la contrôlabilité en temps quelconque n'est pas préservée : il existe un temps minimal strictement positif dépendant de la condition initiale et de la cible.

Théorème 1.32 ([LTZ17, Theorem 4.1])**.** *Soit* $y_0 \in \mathrm{L}^\infty(\Omega)$ *non identiquement nul tel que* $y_0 \geqslant 0$*, et* y_1 *un état d'équilibre du système* (1.28)*. Supposons qu'il existe* $\zeta > 0$ *tel que* $y_1 \geqslant \zeta$ *sur* Ω*. Alors, il existe* $T > 0$ *et un contrôle* $u \in \mathrm{L}^2((0,T)\times\omega)$ *tels que la solution* y *de* (1.28) *avec condition initiale* y_0 *et contrôle* u *vérifie* $y(T) = y_1$ *et qu'on aie de plus*

$$\forall (t,x) \in (0,T)\times\Omega, y(t,x) \geqslant 0.$$

Remarque 1.33. Un résultat analogue avec contrôle au bord est également énoncé dans [LTZ17].

Les démonstrations de mes résultats (Théorèmes 1.38 et 1.41 ci-dessous) sont inspirées de celle de ce théorème dont on présente les principaux arguments ici. La preuve repose en grande partie sur le lemme suivant :

Lemme 1.34 ([LTZ17, Lemma 4.1])**.** *Soit $y_0, y_1 \in \mathrm{L}^\infty(\Omega)$ et $\tau > 0$. Il existe $C(\tau) > 0$ et un contrôle $u \in \mathrm{L}^2((0,\tau)\times\omega)$ tels que la solution y de (1.28) avec condition initiale y_0 et contrôle u vérifie $y(\tau) = y_1$ et qu'on aie de plus*

$$\forall t \in (0,T), \|y(t) - \tilde{y}(t)\|_{\mathrm{L}^\infty(\Omega)} \leqslant C(\tau)\|y_0 - y_1\|_{\mathrm{L}^2(\Omega)},$$

où $\tilde{y}$ est la trajectoire libre de (1.28) issue de y_0.

Soit $\tau > 0$, $\varepsilon > 0$ et y_0 et y_1 définis comme dans le théorème. La construction de la trajectoire contrôlée s'effectue en plusieurs étapes :

1. partant de y_0, on laisse évoluer l'équation sans contrôle. L'état converge alors en norme L^2 vers l'état d'équilibre constant $\bar{y}_0 = \frac{1}{|\Omega|}\int_\Omega y_0$ (qui est strictement positif car y_0 n'est pas identiquement nul). On attend suffisamment longtemps pour atteindre un état y^0 très proche (*i.e.* à ε près en norme L^2) de $\bar{y}_0$.

2. on contrôle de y^0 vers $\bar{y}_0$ en temps τ. Comme ces deux états sont proches, on s'assure grâce au Lemme 1.34 que la trajectoire contrôlée reste proche en norme L^∞ de la trajectoire libre issue de y^0, et donc positive pourvu que ε soit pris suffisamment petit.

3. on prend N dans $\mathbb{N}$ tel que $N \geqslant \frac{|y_1 - \bar{y}_0|}{\varepsilon}$ et on définit N états d'équilibre intermédiaires par
$$\forall k \in \{1,\dots,N\}, y^k = (1 - \frac{k}{N})\bar{y}_0 + \frac{k}{N}y_1. \tag{1.30}$$
On définit ensuite N contrôles conduisant de $\bar{y}_0$ vers y^1 puis, pour $k \in \{1,\dots,N\}$, de y^k vers y^{k+1} en temps τ, et on utilise à chaque étape le Lemme 1.34 pour s'assurer que la trajectoire contrôlée entre y^k et y^{k+1} reste proche en norme L^∞ de la trajectoire libre issue de y^k, et donc positive pourvu que ε, défini à l'étape précédente, soit pris suffisamment petit.

Enfin, on concatène les contrôles définis aux points 1, 2 et 3 et on a bien construit un contrôle qui guide le système de y_0 à y_1 en gardant l'état positif.

Remarque 1.35. La technique utilisée par les auteurs de [LTZ17] au point 3 de cette preuve, qui consiste à se diriger vers la trajectoire cible en passant par une succession d'états d'équilibre constants proches les uns des autres, est dite « en escalier ». On s'assure, en combinant la proximité de ces états successifs avec un lemme de type Lemme 1.34, que la trajectoire contrôlée reste donc proche des états d'équilibre constants, ce qui permet de conclure sur la positivité de l'état.

J'exploite cette technique dans la suite pour démontrer des résultats similaires dans le cas d'un système parabolique couplé. Pour le Théorème 1.38, l'« escalier » est constitué de trajectoires et non plus d'états d'équilibre (voir Figure 1.1), mais l'esprit de la preuve reste le même.

Contrôle de systèmes paraboliques linéaires

Étudions maintenant les propriétés de contrôlabilité de plusieurs équations paraboliques couplées. Soit R un opérateur elliptique auto-adjoint du second ordre donné par

$$R = \sum_{i,j=1}^{d} \partial_i(r_{ij}(x)\partial_j) + c(x), \tag{1.31}$$

avec $c \in \mathrm{L}^\infty(\Omega)$, et $r_{ij} \in \mathrm{W}^{1,\infty}(\Omega)$ pour $i, j \in \{1, \dots, d\}$ vérifiant

$$r_{ij}(x) = r_{ji}(x) \tag{1.32}$$

et la condition d'ellipticité

$$\exists \alpha > 0, \forall \xi \in \mathbb{R}^d, \sum_{i,j=1}^{d} r_{ij}(x)\xi_i\xi_j \geqslant a_0|\xi|^2 \tag{1.33}$$

presque partout sur Ω.

Soient n, m des entiers naturels non nuls. On considère le système linéaire avec condition au bord de Neumann

$$\begin{cases} \partial_t Y - DRY &= AY + Bu\mathbf{1}_\omega & \text{sur } (0,T)\times\Omega; \\ \frac{\partial Y}{\partial n} &= 0 & \text{sur } (0,T)\times\partial\Omega; \\ Y(0,\cdot) &= Y_0(\cdot) & \text{sur } \Omega. \end{cases} \tag{1.34}$$

avec $A \in \mathcal{M}_n(\mathbb{R})$, $B \in \mathcal{M}_{n,m}(\mathbb{R})$, et $D \in \mathcal{M}_n(\mathbb{R})$ diagonalisable.

En tant qu'opérateur auto-adjoint, $-R$ admet une suite $(\lambda_p)_{p\in\mathbb{N}}$ de valeurs propres vérifiant

$$0 = \lambda_0 < \lambda_1 \leqslant \lambda_2 \leqslant \dots, \quad \lim_{p\to+\infty} \lambda_p + \infty,$$

associées à des fonctions propres $(\phi_p)_{p\in\mathbb{N}}$ formant une base orthonormée de $\mathrm{L}^2(\Omega)$.

Étant données deux matrices A dans $\mathcal{M}_n(\mathbb{R})$ et B dans $\mathcal{M}_{n,m}(\mathbb{R})$, on note

$$[A|B] = \left(B \mid AB \mid \dots \mid A^{n-1}B\right). \tag{1.35}$$

la matrice de Kalman associée à A et B.

La contrôlabilité du système (1.34) est donnée par une condition de type Kalman (voir Théorème 1.3 :

Théorème 1.36 ([AKBDGB09b])**.** *Le système (1.34) est contrôlable aux trajectoires en tout temps si et seulement si, pour tout p dans $\mathbb{N}$,*

$$\operatorname{rank}\left[(-\lambda_p D + A)|B\right] = n. \tag{1.36}$$

Remarque 1.37. Dans le cas où $D = I_n$, la condition (1.36) devient simplement

$$\operatorname{rank}\left[A|B\right] = n. \tag{1.37}$$

1.3.2 Contributions de la thèse

Dans ma thèse, je me suis intéressé à la question de la contrôlabilité du système (1.34) entre deux états positifs en s'assurant que l'état reste positif en tout temps.

Comme on l'a vu, le Théorème 1.32 énoncé plus haut donne un résultat de ce type pour l'équation de la chaleur. Ma contribution consiste en deux résultats analogues pour le système (1.34) : les Théorèmes 1.38 et 1.41 ci-dessous.

Cas général (D diagonalisable)

Ici, le système (1.34) n'est pas forcément dissipatif (en particulier, le couplage entre les différentes composantes de Y peut engendrer des comportements oscillants) et on ne peut donc pas attendre qu'il converge vers un état d'équilibre constant comme dans la preuve du Théorème 1.32.

Sous certaines hypothèses raisonnables, on peut cependant retrouver la contrôlabilité avec état (presque) positif. Dans la suite, pour $r \geqslant 0$, $\mathrm{H}^r(\Omega)$ désigne l'espace de Sobolev $W^{r,2}(\Omega)$.

Théorème 1.38 (Chapitre 4, Théorème 4.10)**.** *Suposons que les conditions suivantes sont vérifiées :*

1. *la matrice A est quasipositive, i.e.*

$$\forall i, j \in \{1, \dots, n\}, i \neq j \Rightarrow a_{i,j} \geqslant 0; \tag{1.38}$$

2. *la matrice A est telle que*

$$\forall \xi \in \mathbb{R}^n, \langle A\xi, \xi \rangle \leqslant 0, \tag{1.39}$$

3. *les valeurs propres de $-R$ sont telles qu'on a (1.36).*

Soient $\tilde{Y}$ et Y^{f} dans $\mathrm{L}^\infty(\mathbb{R}_+ \times \Omega)^n$ des trajectoires de (1.34), issues respectivement de Y_0 et $Y_0^{\mathrm{f}} \in \mathrm{L}^\infty(\Omega)^n$ et telles que $Y_0 \geqslant 0$ et $Y_0^{\mathrm{f}} \geqslant 0$. Notons

$$\zeta = \min\left(\inf_{(\mathbb{R}_+ \times \Omega)^n} Y(x,t), \inf_{(\mathbb{R}_+ \times \Omega)^n} Y^{\mathrm{f}}(x,t) \right).$$

(on a $\zeta \geqslant 0$ grâce à l'hypothèse de quasipositivité). Alors, pour tout $\varepsilon > 0$, il existe $T > 0$ et $u \in (\mathrm{L}^2((0,T), \mathrm{H}^r(\omega)) \cap \mathrm{H}^s((0,T), \mathrm{L}^2(\omega)))^m$ avec r, s suffisamment grands (en un sens précisé au Chapitre 4) tels que la solution Y de (1.34) avec condition initiale Y_0 et contrôle u vérifie

$$Y(T, \cdot) = Y^{\mathrm{f}}(T, \cdot),$$

et, pour tout t dans $[0,T]$,

$$Y(t, \cdot) \geqslant \zeta - \varepsilon. \tag{1.40}$$

Remarque 1.39. En particulier, si $\zeta > 0$, on peut contrôler vers Y^{f} en gardant l'état positif.

Remarque 1.40. La condition de quasipositivité (1.38) assure que les trajectoires libres issues d'une condition initiale positive restent positives [Pie10, Lemma 1.1]. La condition (1.39) assure quand à elle que les trajectoires libres restent globalement bornées.

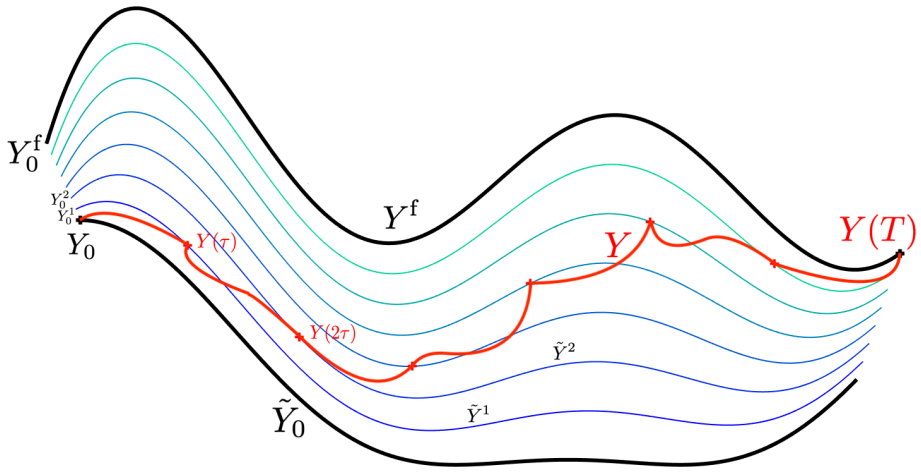

FIGURE 1.1 – Représentation schématique de la méthode de construction de la trajectoire contrôlée dans la preuve du Théorème 1.38.

La preuve de ce résultat est détaillée dans le Chapitre 4. Elle est basée sur la méthode en escalier décrite plus haut pour le Théorème 1.32. Partant de la trajectoire libre $\tilde{Y}_0$ issue de Y_0, on se dirige vers Y^{f} en passant par un chemin constitué de trajectoires libres, positives et proches les unes des autres (voir Figure 1.1). Pour s'assurer que la trajectoire contrôlée reste proche de ces trajectoires libres, et donc approximativement positive, on utilise un lemme similaire au Lemme 1.34 : voir Chapitre 4, Lemme 4.13.

Cas où $D = I_n$

Dans ce cas particulier, on peut améliorer légèrement la conclusion du Théorème 1.38.

Théorème 1.41 (Chapitre 4, Théorème 4.12)**.** *Suposons que les conditions suivantes sont vérifiées :*

1. $D = I_n$;
2. *la matrice A est quasipositive (voir (1.38)) ;*
3. *A et B vérifient le condition de Kalman (1.37).*

Soient Y_0, Y_0^{f} dans $\mathrm{L}^\infty(\Omega)^n$ et Y^{f} la trajectoire associée à Y_0^{f}. On suppose que $Y_0 \geqslant 0$, $Y_0^{\mathrm{f}} \geqslant 0$ et qu'aucune des composantes de Y_0 et Y_0^{f} n'est identiquement nulle. Alors, il existe $T > 0$ et $u \in (\mathrm{L}^2((0,T), \mathrm{H}^r(\omega)) \cap \mathrm{H}^s((0,T), \mathrm{L}^2(\omega)))^m$ avec r, s suffisamment grands (en un sens précisé au Chapitre 4) tels que la solution Y de (1.34) avec condition initiale Y_0 et contrôle u vérifie

$$Y(T, \cdot) = Y^{\mathrm{f}}(T, \cdot), \tag{1.41}$$

et, pour tout t dans $[0,T]$,

$$Y(t, \cdot) \geqslant 0. \tag{1.42}$$

La preuve de ce théorème est détaillée au Chapitre 4. On en présente les principaux éléments ici. La première étape consiste à effectuer un changement de variable qui découple

les équations de (1.34). Posons en effet, pour $t \geqslant 0$,

$$Z = e^{-tA}Y. \tag{1.43}$$

On remarque que si Y est solution du système (1.34), alors Z est solution du système

$$\begin{cases} \partial_t Z - RZ &= e^{-tA}Bu\mathbf{1}_\omega & \text{sur } (0,T)\times\Omega; \\ \frac{\partial Z}{\partial n} &= 0 & \text{sur } (0,T)\times\partial\Omega; \\ Z(0,\cdot) &= Y(0,\cdot) & \text{sur } \Omega. \end{cases} \tag{1.44}$$

On cherche à montrer qu'il existe $T > 0$ et $u \in (\mathrm{L}^2((0,T),\mathrm{H}^r(\omega)) \cap \mathrm{H}^s((0,T),\mathrm{L}^2(\omega)))^m$ tel que la solution Z de (1.44) avec condition initiale Y_0 et contrôle u vérifie

$$Z(T,\cdot) = Z^{\mathrm{f}}(T,\cdot), \tag{1.45}$$

et, pour tout t dans $[0,T]$,

$$Z(t,\cdot) \geqslant 0. \tag{1.46}$$

Par (1.43) et (1.44), un tel contrôle u est tel que la solution Y de (1.34) avec condition initiale Y_0 vérifie (1.41) et (1.42).

En l'absence de contrôle, le système (1.44) est simplement constitué de n équations paraboliques découplées. On déduit alors, en exprimant les solutions dans la base des valeurs propres de R, que les trajectoires $\tilde{Z}_0$ et Z^{f} issues respectivement de Y_0 et Y_0^{f}, convergent respectivement en norme L^2 (et toute autre norme) vers

$$\bar{Z}_0 = \frac{1}{|\Omega|}\int_\Omega Y_0 \quad \text{et} \quad \bar{Z}_0^{\mathrm{f}} = \frac{1}{|\Omega|}\int_\Omega Y_0^{\mathrm{f}}.$$

Par hypothèse, Y_0 et Y_0^{f} sont positifs et aucune de leurs composantes n'est identiquement nulle. On en déduit que toutes les composantes de $\bar{Z}_0$ et $\bar{Z}_0^{\mathrm{f}}$ sont strictement positives. On dispose donc de $\zeta > 0$ tel que $\bar{Z}_0 \geqslant \zeta$ et $\bar{Z}_0^{\mathrm{f}} \geqslant \zeta$.

Soit $\tau > 0$ et $\delta > 0$. On construit le contrôle u en plusieurs étapes (qui sont sensiblement les mêmes que dans la preuve du Théorème 1.32) :

1. On définit un temps T_0 tel que, pour tout $t \geqslant T_0$,

$$\|\tilde{Z}_0(t) - \bar{Z}_0\|_{\mathrm{L}^2(\Omega)^n} \leqslant \delta \quad \text{et} \quad \|Z^{\mathrm{f}}(t) - \bar{Z}^{\mathrm{f}}\|_{\mathrm{L}^2(\Omega)^n} \leqslant \delta,$$

   et on prend le contrôle $u = 0$ sur $[0,T_0]$.
2. On contrôle de $\tilde{Z}_0(T_0)$ vers $\bar{Z}_0$ en temps τ.
3. On contrôle de $\bar{Z}_0$ à $\bar{Z}_0^{\mathrm{f}}$ en utilisant la méthode en escalier, *i.e.* en passant par N états constants proches les uns des autres. Chaque étape est effectuée en temps τ.
4. On contrôle de $\bar{Z}_0^{\mathrm{f}}$ à la trajectoire Z^{f} en temps τ.

À chaque étape, on s'assure que la trajectoire contrôlée Z reste positive grâce à un lemme similaire au Lemme 1.34 (voir Chapitre 4, Lemme 4.15).

On définit alors $T = T_0 + (N+2)\tau$ et $u \in (\mathrm{L}^2((0,T),\mathrm{H}^r(\omega)) \cap \mathrm{H}^s((0,T),\mathrm{L}^2(\omega)))^m$ en juxtaposant les contrôles définis aux points 1, 2, 3 et 4.

Ce contrôle u est tel que Z vérifie (1.45) et (1.46), donc finalement Y vérifie bien (1.41) et (1.42).

1.3.3 Perspectives

Contrôle avec état positif

Il serait souhaitable de pouvoir remplacer ε par 0 dans l'équation (1.40) du Théorème 1.38, ce qui semble intuitivement possible, en particulier si la trajectoire cible Z reste strictement positive en tout temps. Mes recherches à ce sujet sont en cours.

Contrôle d'équations paraboliques semi-linéaires avec contrainte de positivité

On s'est aussi intéressé au cas d'une équation parabolique semi-linéaire, c'est-à-dire l'équation de la chaleur (1.28) à laquelle on rajoute un terme non-linéaire $f : \mathbb{R} \to \mathbb{R}$ dépendant de l'état :

$$\begin{cases} \partial_t y - \Delta y + f(y) &= \mathbf{1}_\omega u & \text{sur } (0,T)\times\Omega, \\ y &= 0 & \text{sur } (0,T)\times\partial\Omega, \\ y(0,\cdot) &= y_0 & \text{sur } \Omega. \end{cases} \tag{1.47}$$

Le comportement de ce type de systèmes est moins sympathique que celui de l'équation de la chaleur linéaire. En effet, si la fonction f croît trop rapidement, la solution peut exploser en temps fini. Dans ce cas, on peut d'abord se demander s'il est possible de contrôler l'équation de sorte que la solution soit globalement définie en tout temps [LB20].

Dans des cas plus favorables où les solutions sans contrôle sont globalement définies en tout temps, pour la contrôlabilité aux trajectoires, cela se complique tout de même puisqu'alors, contrairement au cas linéaire, contrôler en un temps plus long ne signifie pas forcément que le contrôle coûtera moins cher.

On définit deux autres notions de contrôlabilité :

Définition 1.42 (Contrôlabilité à zéro)**.** Soit $T > 0$. Le système (1.28) est dit *contrôlable à zéro* en temps T si, pour tout $y_0 \in \mathrm{L}^2(\Omega)$, il existe un contrôle u dans $\mathrm{L}^\infty((0,T)\times\omega)$ tel que la solution y de (1.28) avec condition initiale y_0 et contrôle u vérifie

$$y(T,\cdot) = 0. \tag{1.48}$$

Définition 1.43 (Contrôlabilité approchée)**.** Soit $T > 0$. Le système (1.28) est dit *contrôlable de façon approchée* en temps T si, pour tout $\varepsilon > 0$, et $y_0, y_1 \in \mathrm{L}^2(\Omega)$, il existe un contrôle u dans $\mathrm{L}^\infty((0,T)\times\omega)$ tel que la solution y de (1.28) avec condition initiale y_0 et contrôle u vérifie

$$\|y(T,\cdot) - y_1\|_{\mathrm{L}^2(\Omega)} \leqslant \varepsilon. \tag{1.49}$$

Remarque 1.44. La contrôlabilité aux trajectoires implique la contrôlabilité à zéro. L'inverse n'est en général pas vrai, sauf dans le cas où l'équation est linéaire. En effet, il suffit alors de poser $y^* = y - \bar{y}$ pour se ramener à la contrôlabilité à zéro.

De plus, dans le cas linéaire, si on a la propriété d'unicité rétrograde suivante :

$$\left.\begin{cases} \partial_t y - \Delta y &= \mathbf{1}_\omega u & \text{on } (0,T)\times\Omega, \\ \frac{\partial y}{\partial n} &= 0 & \text{on } (0,T)\times\partial\Omega, \\ y(T,\cdot) &= 0 & \text{on } \Omega. \end{cases}\right\} \Rightarrow y \equiv 0,$$

alors on peut en déduire que l'ensemble des extrémités de trajectoires au temps T est dense dans $\mathrm{L}^2(\Omega)$, et donc que la contrôlabilité à zéro implique la contrôlabilité approchée.

E. Fernández-Cara et E. Zuazua ont démontré dans [FCZ00] des conditions sur f pour avoir contrôlabilité à zéro du système (1.47) :

Théorème 1.45 ([FCZ00, Theorems 1.2, 1.4])**.** *Soit $q = 1+\frac{4}{d}$. Supposons que la non-linéarité f satisfasse les trois conditions suivantes :*

1. *f est localement lipschitzienne ;*
2. *$\exists C > 0, \forall s \in \mathbb{R}, |f'(s)| \leqslant C(1 + |s|^q)$ p.p. ;*
3. *$\frac{f(s)}{|s| \ln^{\frac{3}{2}}(1+|s|)} \to 0$ quand $|s| \to +\infty$.*

Supposons de plus l'existence de (au moins) une solution globalement définie et bornée à (1.47). Alors (1.47) est contrôlable aux trajectoires en tout temps et contrôlable aux trajectoires de façon approchée.

Remarque 1.46. La condition 3 est cruciale pour assurer la contrôlabilité. En fait, s'il existe $p > 2$ tel que

$$|f(s)| \sim |s| \ln^p(1 + |s|) \quad \text{quand} \quad |s| \to +\infty, \tag{1.50}$$

alors le système (1.47) peut ne pas être contrôlable à zéro en temps quelconque ([FCZ00, Theorem 1.1]).

Dans le cas intermédiaire $p \in]\frac{3}{2}, 2]$ traité tout récemment par K. Le Balc'h [LB20], on a une forme de contrôlabilité locale à zéro (*i.e.* contrôlabilité à zéro pour les conditions initiales proches de 0 en un certain sens) en temps grand, et contrôlabilité de l'explosion des solutions (*i.e.* on peut faire en sorte que la solution soit globalement définie en tout temps).

Comme pour l'équation de la chaleur, on s'est plus récemment demandé s'il était possible de contrôler ces équations avec contrainte de positivité sur l'état. Des résultats en ce sens ont été donnés pour une équation *avec contrôle au bord* par D. Pighin et E. Zuazua dans [PZ17] : considérons donc le système

$$\begin{cases} \partial_t y - \Delta y + f(y) &= 0 & \text{sur } (0,T) \times \Omega, \\ y &= \mathbf{1}_\Gamma u & \text{sur } (0,T) \times \partial\Omega, \\ y(0,\cdot) &= y_0 & \text{sur } \Omega, \end{cases} \tag{1.51}$$

où Γ est un sous ensemble de $\partial\Omega$, non vide et relativement ouvert par rapport à $\partial\Omega$. On a alors :

Théorème 1.47 ([PZ17, Theorems 1.2 et 1.3])**.**

1. *(Contrôlabilité entre états d'équilibre). Soit y_0 et y_1 dans L^Ω deux états d'équilibre strictement positifs de (1.51). Supposons que y_0 et y_1 soient connectés, i.e. qu'il existe $\gamma : [0,1] \to \mathrm{L}^\infty(\Omega)$ continue et telle que $\gamma(0) = y_0$ et $\gamma(1) = 1$. Supposons de plus que pour tout $s \in [0,1]$, $\gamma(s) > 0$.*
   Alors, il existe un temps $T > 0$ et un contrôle $u \in \mathrm{L}^\infty((0,T) \times \Gamma)$ tels que la solution y de (1.51) avec condition initiale y_0 vérifie $y(T) = y_1$ et pour tout t dans $(0,T)$, $y(t) \geqslant 0$.
2. *(Contrôlabilité dans le cas dissipatif). Dans le cas dissipatif ($sf(s) \geqslant 0$ pour tout $s \in \mathbb{R}$), le système (1.51) est contrôlable aux trajectoires en temps grand avec état positif.*

La preuve du premier point de ce théorème est basée sur la méthode en escalier : on va de y_0 à y_1 en passant par une succession d'états d'équilibre proches les uns des autres le long de γ. Cela explique la nécessité de supposer que les états y_0 et y_1 soient connectés

par γ (car une simple combinaison linéaire de y_0 et y_1, comme utilisé plus haut, n'est pas nécessairement un état d'équilibre du système (1.51)).

Le Théorème 1.47 établit des résultats de contrôlabilité avec contrainte de positivité sur l'état dans des cas très particuliers du système (1.51) : états stationnaires connectés et cas dissipatif. Par ailleurs, il est également présenté dans [PZ17, Proposition 1] un exemple dans lequel le système n'est pas contrôlable avec état positif dans le cas général (*i.e.* si y_0 n'est pas un état d'équilibre et f n'est pas dissipative).

Ces travaux sont valables dans le cas d'un contrôle au bord. L'un de mes objectifs est d'étudier ce qu'il se passe dans le cas d'un contrôle interne, afin de pouvoir énoncer un résultat similaire au Théorème 1.47 pour le système (1.47).

Cependant, même dans un cas sympathique où la non-linéarité f est globalement lipschitzienne, voire de type potentiel linéaire ($f(y) = ay, a \in \mathbb{R}$), la méthode « en escalier » ne fonctionne plus, car les trajectoires libres sont susceptibles de s'éloigner très rapidement les unes des autres (exponentiellement en temps). On ne peut alors pas s'assurer que l'on finira par arriver à la trajectoire cible en réalisant des « pas » de taille ϵ fixée.

Au stade actuel de ma réflexion, je conjecture ainsi que le système (1.47) avec une nonlinéarité f globalement lipschitzienne n'est pas contrôlable avec état positif en toute généralité, et travaille à la construction d'un contre-exemple.

1.4 Micro-natation

1.4.1 Contexte

Propulsion à bas nombre de Reynolds

Nager, c'est l'action de se déplacer à l'intérieur d'un fluide en se déformant. À notre échelle, les stratégies de natation font en général appel à l'*inertie* du fluide. Un exemple classique est celui de la coquille Saint-Jacques qui s'ouvre lentement et se ferme rapidement, utilisant ainsi l'inertie pour produire un déplacement net dans le sens opposé à son ouverture. La situation est très différente pour un organisme ou un robot microscopique. Le nombre de Reynolds, qui mesure le rapport entre les effets inertiels et les effets visqueux, est proportionnel à la longueur caractéristique de l'objet considéré, et vaut environ 10^3 à 10^4 pour un humain nageant dans l'eau. Pour un micro-organisme tel qu'un spermatozoïde, qui mesure seulement quelques dizaines à quelques centaines de micromètres, ce nombre est bien inférieur à 1 (10^{-4} à 10^{-5}) ; on est alors dans un régime appelé *écoulement de Stokes* où les effets inertiels sont négligeables face aux effets visqueux. Dans une présentation [Pur77] considérée comme fondatrice du domaine de la micro-natation, Purcell appelle ce phénomène le *théorème de la coquille Saint-Jacques* : à bas nombre de Reynolds, faire des mouvements réversibles conduit à faire du sur-place. Ce régime de Stokes, bien particulier, justifie que la micro-natation constitue un domaine à part entière.

Micro-robots nageurs

L'étude de la micro-natation a notamment pour but de concevoir de robots capables de se déplacer efficacement à cette petite échelle. De tels robots offriraient de nombreuses applications dans le domaine biomédical : robots livreurs [CHS+17] qui délivrent des médicaments à des endroits précis du corps humain en se déplaçant dans les vaisseaux sanguins ou à travers les tissus ; robots capteurs [BKJH+11] capables de collecter des informations

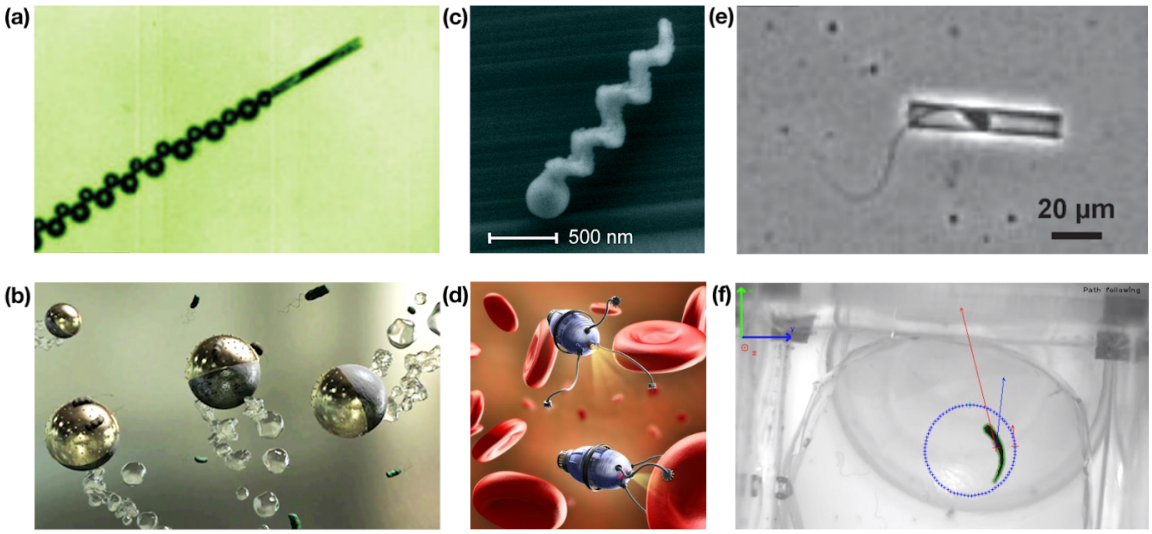

FIGURE 1.2 – Quelques exemples et illustrations de micro-robots nageurs. (a) Robot chimique propulsé par production de bulles de gaz [SMBU+09]. (b) Vue d'artiste de robots chimiques appelés « sphères de Janus » [GLA05]. (c) Robot magnétique en forme de tire-bouchon [PZN13]. (d) Vue d'artiste de micro-robots chirurgiens. (e) Robot biologique propulsé par un spermatozoïde capturé dans un tube magnétique permettant de fixer la direction souhaitée [MMSC+15]. (f) Robot magnétique de la forme étudiée dans la thèse, astreint ici à nager le long d'un cercle [AFPRG19].

dans des endroits inaccessibles aux capteurs ordinaires ; robots nettoyeurs [WLdÁ+15] qui attrapent une substance indésirable (par exemple toxique pour l'organisme) et la capturent pour la déplacer ailleurs ou la faire disparaître ; robots chirurgiens [LRB+09] qui pourraient réaliser des actes chirurgicaux peu intrusifs.

Dans tous les cas, ces micro-nageurs doivent être capable se déplacer efficacement, rapidement et avec précision. Différentes stratégies peuvent être envisagées pour les propulser : propulsion à l'aide d'une réaction chimique [SMBU+09], d'un champ magnétique [PZN13, GSM+10, GF09], d'un micro-nageur biologique [MMSC+15], d'un champ de pression acoustique [GGOS+13], d'un gradient de température, *etc.* La Figure 1.2 présente quelques exemples.

On renvoie à [Wan13, LdÁG+17, PF18] pour des revues plus complètes sur l'état de l'art en matière de micro-robots nageurs et de leurs applications.

Contrôlabilité

À bas nombre de Reynolds, la dynamique d'un nageur quelconque s'exprime comme un système d'équations différentielles ordinaires, linéaires en les dérivées des paramètres de position. On peut alors voir ce type de système comme un système de contrôle et étudier sa contrôlabilité.

Les premiers travaux dans ce domaine [SW89] supposent que le contrôle est donné par la déformation du nageur : c'est en changeant sa forme qu'on produit un déplacement. Citons par exemple le nageur de Purcell constitué de trois segments reliés par des liai-

sons élastiques, dont on étudie une version magnétisée dans la suite. D'autres études sur la contrôlabilité de nageurs par déformation sont effectuées dans [MTT07, Loh12, LM14, LST13, ADGZ13, GMZ13, LST13]. Dans ce cas, la dynamique est régie par un système contrôle-affine sans dérive. On a vu qu'on dispose alors de résultats puissants de contrôlabilité dûs à la géométrie sous-riemannienne, comme le théorème de Rashevskii-Chow. De nombreux résultats de contrôle optimal ont également été obtenus dans ce cadre : citons [TH07, ADL08, ADH$^+$13, CGM14]

Quand on agit indirectement sur la déformation du nageur *via* un champ magnétique comme dans la suite, la commandabilité est plus délicate à obtenir. On peut le comprendre intuitivement : on n'a alors plus que deux ou trois contrôles (les composantes du champ magnétique dans le plan ou l'espace) pour agir sur l'ensemble des paramètres de position et de forme du nageur. Le système de contrôle associé présente quant à lui une dérive. Comme on l'a vu en section 1.2, les résultats de contrôlabilité pour les systèmes avec dérive sont moins généraux et l'on ne connaît pas de condition nécessaire et suffisante de contrôlabilité locale.

Pour ma part, je me suis intéressé à la contrôlabilité d'un modèle de robot à liens élastique planaire, contrôlé à l'aide d'un champ magnétique extérieur [GO14, ADGZ15]. La contrôlabilité du nageur magnétique à deux liens a été d'abord étudiée dans [GP17]. Les auteurs montrent que les techniques standard (étude du linéarisé, condition de Sussmann) échouent à démontrer sa contrôlabilité locale au voisinage de la position d'équilibre. Ils obtiennent un résultat de contrôlabilité locale « faible » (α-STLC, voir Définition 1.6) en adaptant la méthode du retour de Jean-Michel Coron [Cor07, Chapter 6], conçue à l'origine pour établir la contrôlabilité locale de certaines EDP.

Dans ma thèse, j'ai introduit une nouvelle approche, inspirée des travaux de Sussmann [Sus83], qui consiste en quelques mots à construire un développement judicieux de la solution contrôlée au voisinage de la position d'équilibre. J'ai pu grâce à cela montrer la non-contrôlabilité à l'équilibre du nageur magnétique à deux liens [GLMP18]. J'ai ensuite généralisé cette approche pour déduire une condition nécessaire générale de contrôlabilité locale, présentée en section 1.2 (Théorème 1.27), et résoudre plus largement la question de la contrôlabilité locale des nageurs à deux et trois liens au voisinage de leur équilibre. Ainsi, les Théorèmes 1.55 et 1.60 montrent que la contrôlabilité locale en temps petit de ces nageurs n'est possible que si le champ magnétique appliqué au robot reste proche d'une valeur constante bien particulière, qui dépend des paramètres de magnétisation du robot.

Dans la section 1.4.2, on décrit succinctement le modèle, puis on présente dans la section 1.4.3 les résultats de contrôlabilité obtenus pour les nageurs, illustrés par des simulations numériques. Enfin, la section 2.4.4 est consacrée aux perspectives futures.

Les résultats de cette section ont été publiés dans [GLMP18] et [Mor19], reproduits aux Chapitres 5 et 6.

1.4.2 Modélisation de micro-nageurs magnétiques

Dans cette section, on s'intéresse à un robot micro-nageur magnétique constitué de deux ou trois segments rigides connectés les uns aux autres par des ressorts de torsion. Le mouvement des nageurs est supposé planaire. La Figure 1.3 présente un schéma de ces robots.

Quand cela n'impliquera aucune ambiguïté, certaines notations seront choisies communes aux nageurs à deux et trois segments.

Les segments sont notés S_1 et S_2 pour le nageur à deux segments et S_1, S_2, S_3 pour le

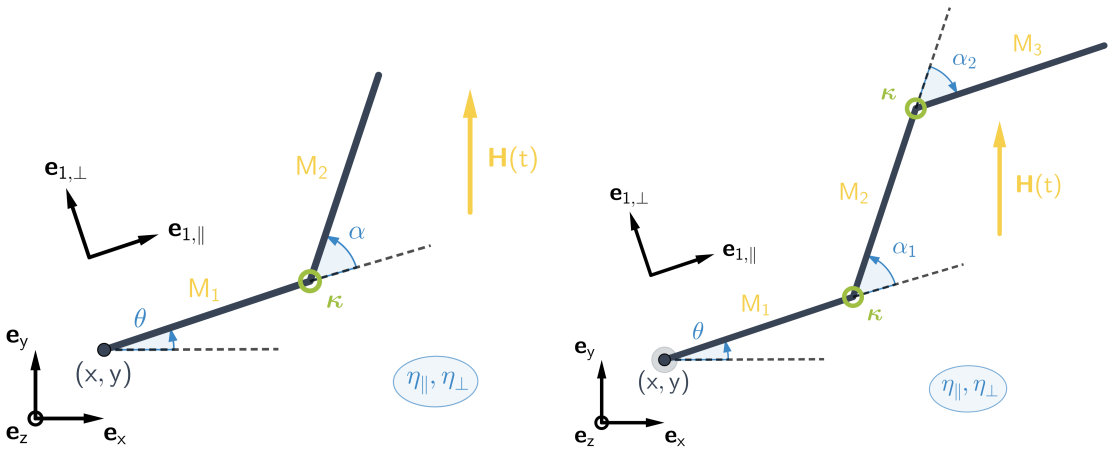

FIGURE 1.3 – Paramétrisation des micro-nageurs magnétiques étudiés

nageur à trois segments. Chaque segments a pour longueur ℓ et pour coefficients hydrodynamiques $\eta_\parallel$ et $\eta_\perp$, avec $\eta_\perp > \eta_\parallel > 0$. De plus, chaque segment S_i est considéré comme un dipôle magnétique dans sa direction, de moment M_i. Les segments sont reliés entre eux par des liaisons élastiques, modélisées par des ressorts de torsion de raideur κ.

Les nageurs se déplacent dans le plan de référence noté $(O, \mathbf{e}_x, \mathbf{e}_y)$. On pose $\mathbf{e}_z = \mathbf{e}_x \times \mathbf{e}_y$. On repère le premier segment S_1 grâce à la position de son extrémité $\mathbf{x} = (x, y)$ et son orientation θ par rapport à $\mathbf{e}_x$. Pour le nageur à deux segments, on note α l'angle entre S_1 et S_2. Pour le nageur à trois segments, on note respectivement α_1 et α_2 l'angle entre S_1 et S_2 et l'angle entre S_2 et S_3. Enfin, on note $(\mathbf{e}_{i,\parallel}, \mathbf{e}_{i,\perp})$ la base orthonormée associée au segment S_i.

Ainsi, le nageur à deux liens est entièrement décrit par les quatre variables $\mathbf{z}_2 = (x, y, \theta, \alpha)^T$ et celui à trois liens par les cinq variables $\mathbf{z}_3 = (x, y, \theta, \alpha_1, \alpha_2)^T$. En complément, on notera occasionnellement $\mathbf{x}_i$ la position de l'extrémité du segment S_i pour $i = 1, 2, 3$.

Le nageur est soumis à un champ magnétique uniforme en espace et variable en temps, noté $\mathbf{H}(t)$; on le décompose selon la base associée au premier segment S_1 : $\mathbf{H}(t) = (H_\parallel(t), H_\perp(t))$.

Lors de son mouvement, le nageur subit trois types d'interactions : des couples de rappel élastique exercés aux jonctions entre les segments, des couples magnétiques dûs au champ magnétique extérieur et l'interaction hydrodynamique exercée par le fluide environnant. On détaille ci-après l'expression de chacune de ces interactions.

1. **Élasticité** : le couple de rappel exercé sur le segment S_i est proportionnel à la raideur κ et à l'angle entre les segments S_{i-1} et S_i. Ainsi, pour le nageur à deux segments, le couple exercé sur S_2 est égal à $\mathbf{T}^{\text{el}} = \kappa\alpha\mathbf{e}_z$ et, pour le nageur à trois segments, les couples exercés sur S_2 et sur S_3 sont respectivement égaux à $\mathbf{T}_2^{\text{el}} = \kappa\alpha_1\mathbf{e}_z$ et $\mathbf{T}_3^{\text{el}} = \kappa\alpha_2\mathbf{e}_z$. En l'absence de champ magnétique, les segments constituant le nageur auront donc tendance à s'aligner entre eux.
2. **Magnétisme** : le champ magnétique exerce sur le segment S_i un couple proportionnel à la magnétisation M_i, donné par $\mathbf{T}_i^{\text{m}} = M_i\mathbf{e}_{i,\parallel} \times \mathbf{H}$.
3. **Hydrodynamique** : on modélise la traînée hydrodynamique exercée sur le nageur à l'aide de la *Resistive Force Theory* introduite dans [GH55], qui suppose que la force

exercée par unité de longueur sur chaque segment est proportionnelle à sa vitesse et aux coefficients hydrodynamiques $\eta_{\parallel}$ et $\eta_{\perp}$. La force hydrodynamique exercée sur le segment S_i est notée $\mathbf{F}_i^h$, et le couple hydrodynamique par rapport à un point $\mathbf{x}_0$ est noté $\mathbf{T}_{i,\mathbf{x}_0}^h$. Les expressions détaillées de $\mathbf{F}_i^h$ et $\mathbf{T}_{i,\mathbf{x}_0}^h$ sont développées au Chapitre 6, section 6.2.

Comme le nombre de Reynolds du fluide environnant est supposé suffisamment petit, on néglige les effets inertiels face aux effets visqueux. On peut donc écrire l'équilibre des forces et des moments en tout temps [LP09]. Pour le nageur à deux liens, on obtient quatre équations en écrivant :

— l'équilibre des forces sur le nageur, projeté sur (Ox) et (Oy) ;

— l'équilibre des moments sur le nageur au point $\mathbf{x}$;

— l'équilibre des moments sur le segment S_2 au point $\mathbf{x}_2$,

ce qui donne le système suivant :

$$\left\{\begin{array}{lll} \mathbf{F}_1^h + \mathbf{F}_2^h & & = 0, \\ \mathbf{T}_{1,\mathbf{x}}^h + \mathbf{T}_{2,\mathbf{x}}^h & + \mathbf{T}_1^m + \mathbf{T}_2^m & = 0, \\ \underbrace{\mathbf{T}_{2,\mathbf{x}_2}^h}_{\text{hydrodynamique}} & + \underbrace{\mathbf{T}_2^m}_{\text{magnétisme}} + \underbrace{\mathbf{T}^{\text{el}}}_{\text{élasticité}} & = 0. \end{array}\right. \tag{1.52}$$

Pour le nageur à trois liens, on obtient cinq équations en écrivant :

— l'équilibre des forces sur le nageur, projeté sur (Ox) et (Oy) ;

— l'équilibre des moments sur le nageur au point $\mathbf{x}$;

— l'équilibre des moments sur l'ensemble $\{S_2 + S_3\}$ au point $\mathbf{x}_2$,

— l'équilibre des moments sur le segment S_3 au point $\mathbf{x}_3$,

ce qui donne le système suivant :

$$\left\{\begin{array}{lll} \mathbf{F}_1^h + \mathbf{F}_2^h + \mathbf{F}_3^h & & = 0, \\ \mathbf{T}_{1,\mathbf{x}}^h + \mathbf{T}_{2,\mathbf{x}}^h + \mathbf{T}_{3,\mathbf{x}}^h & + \mathbf{T}_1^m + \mathbf{T}_2^m + \mathbf{T}_3^m & = 0, \\ \mathbf{T}_{2,\mathbf{x}_2}^h + \mathbf{T}_{3,\mathbf{x}_2}^h & + \mathbf{T}_2^m + \mathbf{T}_3^m + \mathbf{T}_2^{\text{el}} & = 0, \\ \underbrace{\mathbf{T}_{3,\mathbf{x}_3}^h}_{\text{hydrodynamique}} & + \underbrace{\mathbf{T}_3^m}_{\text{magnétisme}} + \underbrace{\mathbf{T}_3^{\text{el}}}_{\text{élasticité}} & = 0. \end{array}\right. \tag{1.53}$$

Notons $R_{\theta,2} = \left(\begin{array}{cc|c} \cos\theta & \sin\theta & 0 \\ -\sin\theta & \cos\theta & 0 \\ \hline 0 & 0 & I_2 \end{array}\right)$ et $R_{\theta,3} = \left(\begin{array}{cc|c} \cos\theta & \sin\theta & 0 \\ -\sin\theta & \cos\theta & 0 \\ \hline 0 & 0 & I_3 \end{array}\right)$.

En exprimant chaque contribution des systèmes (1.52) et (1.53) en fonction des paramètres de position, de leurs dérivées temporelles et des grandeurs du système, on obtient les systèmes différentiels suivants :

— pour le nageur à deux segments :

$$A_2(\alpha)R_{-\theta,2}\dot{\mathbf{z}}_2 = \begin{pmatrix} 0 \\ 0 \\ 0 \\ -\kappa\alpha \end{pmatrix} + H_{\parallel}\begin{pmatrix} 0 \\ 0 \\ M_2\sin\alpha \\ M_2\sin\alpha \end{pmatrix} - H_{\perp}\begin{pmatrix} 0 \\ 0 \\ M_1 + M_2\cos\alpha \\ M_2\cos\alpha \end{pmatrix}; \tag{1.54}$$

— pour le nageur à trois segments :

$$\begin{aligned} A_3(\alpha_1,\alpha_2)R_{-\theta,3}\dot{\mathbf{z}}_3 &= \begin{pmatrix} 0 \\ 0 \\ 0 \\ -\kappa\alpha_1 \\ -\kappa\alpha_2 \end{pmatrix} + H_{\parallel} \begin{pmatrix} 0 \\ 0 \\ M_2\sin\alpha_1 + M_3\sin(\alpha_1+\alpha_2) \\ M_2\sin\alpha_1 + M_3\sin(\alpha_1+\alpha_2) \\ M_3\sin(\alpha_1+\alpha_2) \end{pmatrix} \\ &\quad - H_{\perp} \begin{pmatrix} 0 \\ 0 \\ M_1 + M_2\cos\alpha_1 + M_3\cos(\alpha_1+\alpha_2) \\ M_2\cos\alpha_1 + M_3\cos(\alpha_1+\alpha_2) \\ M_3\cos(\alpha_1+\alpha_2) \end{pmatrix}. \end{aligned} \tag{1.55}$$

Lex expressions détaillées de A_2 et A_3 sont données dans l'Appendice, section A.1.

On montre par des calculs, détaillés dans la section A.2 de l'Appendice, que A_2 et A_3 sont toujours inversibles. On peut donc finalement exprimer la dynamique des nageurs sous la forme de systèmes contrôle-affines, dans lesquels le champ magnétique est vu comme le contrôle, et notés

$$\dot{\mathbf{z}}_2 = \mathbf{G}_0 + H_{\parallel}(t)\mathbf{G}_1 + H_{\perp}(t)\mathbf{G}_2 \tag{1.56}$$

pour le nageur à deux liens, et

$$\dot{\mathbf{z}}_3 = \mathbf{F}_0 + H_{\parallel}(t)\mathbf{F}_1 + H_{\perp}(t)\mathbf{F}_2 \tag{1.57}$$

pour le nageur à trois liens.

Il suit immédiatement de la forme du membre de droite de (1.54) et (1.55) la proposition suivante :

Proposition 1.48. *Soient $x, y, \theta, \beta \in \mathbb{R}$.*

1. *Pour le nageur à deux segments, les états de la forme $((x, y, \theta, 0), (\beta, 0))$ sont des états d'équilibre du système (1.56).*
2. *Pour le nageur à trois segments, les états de la forme $((x, y, \theta, 0, 0), (\beta, 0))$ sont des états d'équilibre du système (1.57).*

Remarque 1.49. En fait, x et y n'apparaissent pas dans la dynamique et θ n'apparaît qu'à travers une matrice de rotation. Par conséquent, les systèmes (1.56) et (1.57) sont invariants par translation et rotation. Dans la suite, on étudiera donc sans perte de généralité les systèmes (1.56) et (1.57) au voisinage des équilibres $((0, 0, 0, 0), (\beta, 0))$ et $((0, 0, 0, 0, 0), (\beta, 0))$, que l'on notera indifféremment $(0, (\beta, 0))$ dans un souci de lisibilité.

Remarque 1.50. Les champs $\mathbf{G}_0$, $\mathbf{G}_1$, $\mathbf{F}_0$, $\mathbf{F}_1$ s'annulent en les états d'équilibre susnommés. Les systèmes (1.56) et (1.57) sont donc de la forme des systèmes contrôle-affines à deux contrôles (1.22) étudiés dans la section 1.2 de cette introduction. C'est d'ailleurs d'une volonté de généraliser cette étude de la contrôlabilité des nageurs qu'est né le théorème 1.27 énoncé plus haut.

Le théorème suivant donne un résultat partiel de contrôlabilité du nageur à deux segments, tiré de [GP17].

Théorème 1.51 ([GP17, Theorem 5]). *Pour tout $\varepsilon > 0$, le nageur à deux segments est $(2|\gamma_2| + \epsilon)$-STLC en $(0,(0,0))$ avec*

$$\gamma_2 = \kappa\left(\frac{1}{M_1} + \frac{1}{M_2}\right).$$

Remarque 1.52. Le résultat présenté dans [GP17] est plus général, puisqu'il ne suppose pas que les longueurs et coefficients hydrodynamiques de S_1 et S_2 sont égaux.

Durant ma thèse, j'ai contribué à améliorer ce résultat et à énoncer son équivalent pour le nageur à trois segments.

1.4.3 Contributions de la thèse : contrôlabilité de nageurs à deux et trois segments

Cette section présente les résultats publiés dans [GLMP18] avec Laetitia Giraldi, Pierre Lissy et Jean-Baptiste Pomet et dans [Mor19].

Ces résultats décrivent les propriétés de contrôlabilité des nageurs à deux et trois segments au voisinage de leur position d'équilibre. Pour chacun des nageurs, on traite quelques cas particuliers dans les propositions 1.53 et 1.57 avant d'énoncer le résultat général dans les Théorèmes 1.55 et 1.60.

On utilise dans les propositions qui suivent la notion de STLC, introduite dans la Définition 1.5.

Proposition 1.53. *Le nageur à deux segments est :*

- *STLC en $(0,(0,0))$ si $M_1 + M_2 = 0$;*
- *non-STLC en $(0,(\beta,0))$ pour tout $\beta \in \mathbb{R}$ si $M_1 = 0$, $M_2 = 0$ ou $M_1 - M_2 = 0$.*

La démonstration de cette proposition est effectuée dans le Chapitre 6 (Proposition 6.17).

Hypothèse 1.54. Pour le nageur à deux segments, on suppose que les magnétisations M_1 et M_2 vérifient $M_1 \neq 0$, $M_2 \neq 0$, $M_1 - M_2 \neq 0$ et $M_1 + M_2 \neq 0$.

Mon résultat principal sur le nageur à deux segments est le suivant :

Théorème 1.55 ([Mor19] et Chapitre 6, Théorème 6.21). *Sous l'hypothèse 1.54, le nageur à deux segments est STLC en $(0,(\gamma_2,0))$ avec*

$$\gamma_2 = \kappa\left(\frac{1}{M_1} + \frac{1}{M_2}\right).$$

De plus, il n'est pas STLC en $(0,(\beta,0))$ si $\beta \neq \gamma_2$.

Éléments de preuve. On démontre le théorème ci-dessus en deux temps :

Preuve de la non-STLC. Soit $\beta \neq \gamma_2$. On utilise la condition nécessaire fournie par le Théorème 1.27. En effet, on peut vérifier que le système (1.56) satisfait :

- $\mathbf{G}_0(0) = \mathbf{G}_1(0) = 0$
- $[\mathbf{G}_2,[\mathbf{G}_0,\mathbf{G}_2]](0) \notin R_1(0)$;

— $[\mathbf{G}_2, [\mathbf{G}_0, \mathbf{G}_2]](0) = \gamma_2 [\mathbf{G}_2, [\mathbf{G}_1, \mathbf{G}_2]](0)$.

(on rappelle que $R_1(0)$ désigne ici le sous-espace de $\mathbb{R}^4$ engendré par les crochets de Lie itérés de $\mathbf{G}_0, \mathbf{G}_1, \mathbf{G}_2$ contenant au plus une fois $\mathbf{G}_2$ et évalués en 0.)

On peut donc conclure, en appliquant le Théorème 1.27, que le nageur n'est pas STLC en $(0, (\beta, 0))$.

Preuve de la STLC en $(0, (\gamma_2, 0))$. On définit $\widetilde{H}_{\|} = H_{\|} + \gamma_2$ pour obtenir le nouveau système

$$\dot{z} = \widetilde{\mathbf{G}}_0 + \widetilde{H}_{\|} \widetilde{\mathbf{G}}_1 + H_{\perp} \widetilde{\mathbf{G}}_2. \tag{1.58}$$

avec $\widetilde{\mathbf{G}}_0 = \mathbf{G}_0 - \gamma_2 \mathbf{G}_1$, $\widetilde{\mathbf{G}}_1 = \mathbf{G}_1$ et $\widetilde{\mathbf{G}}_2 = \mathbf{G}_2$. On vérifie alors que

— (1.58) satisfait la LARC en $(0, (0, 0))$ (voir Définition 1.11),

— (1.58) satisfait la condition de Sussmann $S(1)$ (voir Définition 1.16).

D'après le Théorème 1.17, ces conditions impliquent la STLC en $(0, (0, 0))$ du système (1.58), et donc la STLC en $(0, (\gamma_2, 0))$ de (1.56). □

Une version détaillée de cette preuve est présentée dans le Chapitre 6.

Remarque 1.56. Le Théorème 1.55, publié dans [Mor19], s'inscrit dans le prolongement d'un premier résultat sur le nageur à deux segments, publié dans [GLMP18] qui affirme que le nageur à deux segments n'est pas STLC en $(0, (0, 0))$. Ce résultat est donc contenu dans le Théorème 1.55. Cependant, la preuve présentée dans [GLMP18], plus constructive, apporte un intéressant complément aux arguments développés dans [Mor19]. Voir à ce sujet la remarque 3.19 dans le Chapitre 3 et le Chapitre 4 qui reprend [GLMP18].

On étudie maintenant le cas du nageur à trois segments.

Proposition 1.57. *Supposons que l'une de ces conditions soit vérifiée :*

— $M_1 - M_3 = 0$;

— $(M_1 + M_3 = 0 \ \text{ et } \ M_2 = 0)$;

— $9M_2(M_1 + M_3) - 5M_1M_3 - 7M_2^2 = 0$;

Alors, le nageur à trois segments n'est pas STLC en $(0, (\beta, 0))$ avec $\beta \in \mathbb{R}$.

La démonstration de cette proposition est effectuée dans le Chapitre 5 (Assumption 6.8).

Hypothèse 1.58. Pour le nageur à trois segments, on suppose que les magnétisations M_1, M_2 et M_3 vérifient

$$\begin{aligned} M_1 - M_3 &\neq 0; \\ (M_1 + M_3 \neq 0 \ \text{ ou } \ M_2 &\neq 0); \\ 9M_2(M_1 + M_3) - 5M_1M_3 - 7M_2^2 &\neq 0; \\ P(M_1, M_2, M_3) &\neq 0, \end{aligned} \tag{1.59}$$

avec

$$P(x, y, z) = 49y^3 - 91y^2(x + z) + 36y(x + z)^2 - (45y + 65(x + z))xz.$$

Remarque 1.59. La dernière de ces quatre conditions, non traitée dans la proposition 1.57, correspond à une expression apparaissant dans les calculs de la preuve du Théorème 1.60. La question de la contrôlabilité du nageur quand $P(M_1, M_2, M_3) = 0$ reste ouverte. Les simulations numériques montrent que, dans ce cas et avec un contrôle $H_{\|}$ au voisinage de γ_3, on a approximativement $\alpha_1 = \alpha_2$ en tout temps (voir la Figure 1.5). Cela peut suggérer que le mouvement du nageur est alors limité et que le système n'est pas contrôlable.

Mon résultat principal sur le nageur à trois segments est le suivant :

Théorème 1.60 ([Mor19] et Chapitre 6, Théorème 6.10)**.** *Sous l'hypothèse 1.58, le nageur à trois liens est STLC en* $(0, (\gamma_3, 0))$ *avec*

$$\gamma_3 = \kappa \frac{17(M_1 + M_3) - 16M_2}{9M_2(M_1 + M_3) - 5M_1M_3 - 7M_2^2}.$$

De plus, il n'est pas STLC en $(0, (\beta, 0))$ *si* $\beta \neq \gamma_3$.

La démonstration de ce théorème suit la même structure que celle du Théorème 1.55 et est détaillée dans le Chapitre 6.

Remarque 1.61. Les théorèmes 1.55 et 1.60 démontrent en particulier que les nageurs étudiés ne sont en général pas localement contrôlables en $(0, (0, 0))$, c'est-à-dire avec des « petits » champs magnétiques. Ce manque de contrôlabilité est la traduction du fait que les champs $\mathbf{G}_1$ et $\mathbf{F}_1$ s'annulent en 0 : la composante parallèle du champ magnétique ne peut pas agir sur le nageur lorsque celui-ci est aligné.

Ces résultats présentent un intérêt théorique du point de vue de la contrôlabilité des systèmes, mais fournissent aussi des informations importantes pour les applications en micro-natation. L'expression explicite des contrôles à fournir pour obtenir la STLC, et l'aspect des simulations numériques, contribuent à mieux comprendre la façon dont ce type de nageur se déplace.

Simulations numériques

Pour visualiser numériquement les résultats des Théorèmes 1.55 et 1.60, on calcule des trajectoires à partir de l'équilibre 0 avec des contrôles restant « proches » du contrôle d'équilibre. Soit $\beta \in \mathbb{R}$ et $\varepsilon > 0$. On définit les contrôles

$$\begin{aligned} H_{\|}(t) &= \beta + \varepsilon(h_1 + h_2 \cos(10t) + h_3 \cos(100t)), \\ H_{\perp}(t) &= \varepsilon(h_4 + h_5 \cos(10t) + h_3 \cos(100t)), \end{aligned} \tag{1.60}$$

avec h_1 à h_6 des constantes prises aléatoirement dans $[-1, 1]$. En calculant et dessinant un certain nombre de ces trajectoires sur un petit intervalle de temps, on peut s'attendre à ce qu'elles recouvrent « à peu près » l'espace atteignable, permettant ainsi d'observer d'éventuelles régions inatteignables.

Les figures 1.4 pour le nageur à 2 liens et 1.5 pour le nageur à 3 liens présentent les résultats de ces simulations. On peut effectivement observer que seules les valeurs γ_2 et γ_3 permettent aux nageurs de couvrir un voisinage de l'origine dans le plan (x, y).

Pour le nageur à trois liens, on observe également sur la Figure 1.5 (graphique en bas au centre) le phénomène décrit dans la remarque 1.59, qui se produit pour les angles α_1 et

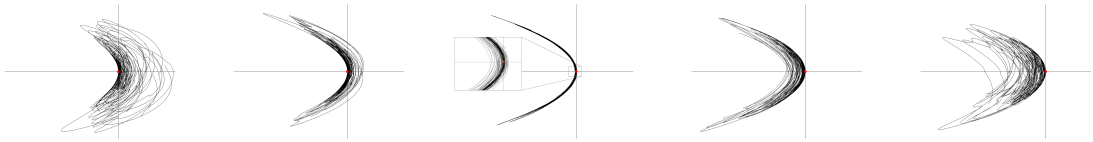

(a) $\beta = 0.5\gamma_2$ (b) $\beta = 0.9\gamma_2$ (c) $\beta = \gamma_2$ (d) $\beta = 1.1\gamma_2$ (e) $\beta = 1.25\gamma_2$

FIGURE 1.4 – Illustration de la contrôlabilité locale du nageur à deux liens. Sur chaque graphique, l'évolution de (x, y) pour 30 trajectoires a été dessinée avec des réalisations des contrôles (1.60) pris autour de $(\beta, 0)$. Quand β est différent de la valeur critique γ_2, les trajectoires restent systématiquement à gauche ou à droite de l'origine. Seul le contrôle de référence $(\gamma_2, 0)$ permet aux trajectoires de couvrir un voisinage de l'origine (graphique central). Valeurs numériques utilisées : $\eta = 4$, $\xi = 2$, $\ell = 1$, $M_1 = 1$, $M_2 = 3$, $k = 1$, $\varepsilon = 10^{-2}$, $T = 1$.

α_2 lorsque le polynôme $P(M_1, M_2, M_3)$ défini en (1.59) s'annule. Les simulations semblent montrer que dans ce cas, on a appproximativement $\alpha_1 = \alpha_2$ en tout temps au voisinage du contrôle de référence $(\gamma_3, 0)$, ce qui n'est pas le cas si $P(M_1, M_2, M_3) \neq 0$. Le nageur semble ainsi « moins » contrôlable dans cette situation, sans que je puisse à ce stade démontrer qu'il est ou non STLC.

1.4.4 Perspectives

Extension à N segments

On peut généraliser par analogie le modèle des nageurs à deux et trois segments à une formulation à N segments avec $N \geqslant 4$. Les nageurs magnétiques à N liens sont étudiés dans [ADGZ15], où il est montré qu'ils peuvent avancer dans certaines directions en étant soumis à un champ magnétique oscillant. Les expériences réalisées notamment dans [AFPRG19] (voir la Figure 1.3-(f)) valident une version 3D de ce modèle et résolvent un problème de contrôle optimal pour maximiser le déplacement du nageur sur une période.

Comme pour les nageurs à deux et trois liens, on se ramène à un système du type

$$\dot{\mathbf{z}}_N = \mathbf{F}_0 + H_{\parallel}(t)\mathbf{F}_1 + H_{\perp}(t)\mathbf{F}_2. \tag{1.61}$$

et on étudie la contrôlabilité en $(0, (\beta, 0))$ avec $\beta \in \mathbb{R}$.

La complexité des expressions mises en jeu devient néanmoins trop grande pour pouvoir calculer explicitement les champs de vecteurs, les crochets de Lie d'intérêt, et *a fortiori* des valeurs critiques analogues à γ_2 et γ_3, même à l'aide d'un logiciel de calcul formel. J'ai en revanche démontré le résultat suivant :

Proposition 1.62. *Pour le nageur à N segments, $[\mathbf{F}_2, [\mathbf{F}_0, \mathbf{F}_2]](0)$ et $[\mathbf{F}_2, [\mathbf{F}_1, \mathbf{F}_2]](0)$ sont colinéaires.*

La démonstration de cette proposition est effectuée dans l'Appendice A, section A.3.

On en déduit que :

— s'il existe une valeur γ_N tel que $[\mathbf{F}_2, [\mathbf{F}_0, \mathbf{F}_2]](0) = \gamma_N [\mathbf{F}_2, [\mathbf{F}_1, \mathbf{F}_2]](0)$, alors cette valeur est la seule en laquelle le nageur *pourrait* être STLC, *i.e.* le système (1.61) n'est pas

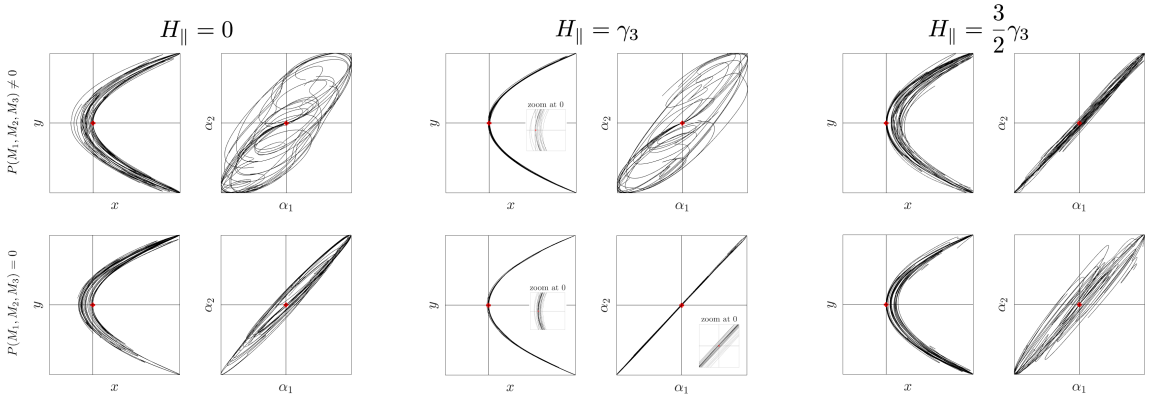

FIGURE 1.5 – Illustration de la contrôlabilité locale du nageur à trois liens. Sur chaque couple de graphiques, l'évolution de (x, y) et de (α_1, α_2) pour 15 trajectoires a été dessinée avec des réalisations des contrôles (1.60) pris autour de $(\beta, 0)$. Quand β est différent de la valeur critique γ_3, les trajectoires dans le plan (x, y) restent systématiquement à gauche ou à droite de l'origine. Seul le contrôle de référence $(\gamma_3, 0)$ permet aux trajectoires de couvrir un voisinage de l'origine. La deuxième rangée de graphiques montre le changement de comportement du système dans le plan (α_1, α_2) quand $\beta = \gamma_3$ et $P(M_1, M_2, M_3) = 0$. Valeurs numériques utilisées : $\eta = 4$, $\xi = 2$, $\ell = 1$, $M_1 = 8$ (première rangée), $M_1 = 7.069$ (deuxième rangée), $M_2 = 10$, $M_3 = 4$, $k = 1$, $\varepsilon = 10^{-2}$, $T = 1$.

STLC en $(0, (\beta, 0))$ pour $\beta \neq \gamma_N$.

— γ_N existe en général, c'est-à-dire à l'exclusion uniquement de conditions génériques sur les magnétisations analogues à celles des hypothèses 1.54 et 1.58.

Par ailleurs, dans la section 1.5 et les Chapitres 7 et 8, on utilise également un modèle de type N liens pour étudier des filaments élastiques non magnétisés à bas nombre de Reynolds.

Nageur coudé à l'équilibre

Suivant la remarque 1.61, on peut se demander s'il n'est pas préférable de considérer un nageur « coudé » qui ne serait pas rectiligne à l'équilibre, de façon à ce que le contrôle $H_\parallel$ puisse agir dessus. Dans [GLMP16], j'ai étudié un exemple de tel nageur à 3 liens coudé, dans lequel on remplace le couple élastique $\mathbf{T}_3^{\text{el}} = \kappa\alpha_2$ par

$$\mathbf{T}_3^{\text{el}} = \kappa(\alpha_2 - \alpha_0), \tag{1.62}$$

avec $\alpha_0 \neq 0$. L'état $((0, 0, 0, 0, \alpha_0), (0, 0))$, noté $(\mathbf{z}_0, (0, 0))$, devient alors un état d'équilibre. On présente brièvement les résultats développés dans [GLMP16]. Définissons la *STLC partielle pour les variables x et y* :

Définition 1.63. Le système de contrôle associé au nageur coudé est dit *partiellement STLC en $(\mathbf{z}_0, (0, 0))$ pour les variables x et y* si, pour tout $\varepsilon > 0$, il existe des voisinages $\mathcal{V}$ de $\mathbf{z}_0$ et $\mathcal{W}$ de $(0, 0)$ tel que pour tout $\mathbf{z}_\text{i}$ dans $\mathcal{V}$ et (x_1, y_1) dans $\mathcal{W}$, il existe un contrôle $(H_\parallel, H_\perp)$ défini sur $[0, \epsilon]$ tel que la trajectoire du nageur partant de $\mathbf{z}_\text{i}$ vérifie :

— $x(\varepsilon) = x_1$ et $y(\varepsilon) = y_1$;

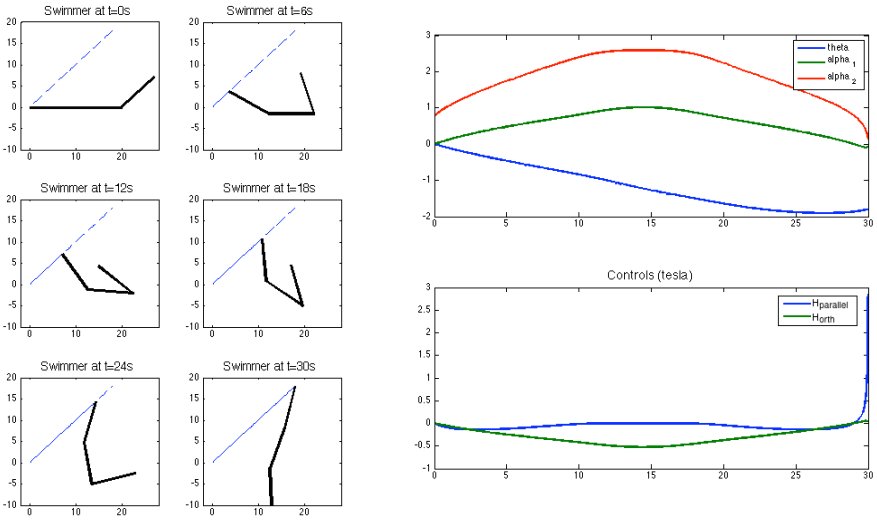

FIGURE 1.6 – Suivi de trajectoire le long d'une ligne droite pour le nageur à 3 liens coudé. Sur le dernier graphique représentant le nageur à $t = 30s$, on peut observer qu'il s'approche de la forme rectiligne $\alpha_1 = \alpha_2 = 0$ (c'est également visible sur le graphique en haut à gauche, qui représente l'évolution de α_1 (en vert) et α_2 (en rouge) en fonction du temps. Le graphique en bas à droite montre l'évolution des contrôles au cours du temps : le contrôle $H_{\|}$ (en bleu) nécessaire pour poursuivre le suivi de trajectoire explose en fin de simulation.

— pour tout t dans $[0, \varepsilon]$, $|H_{\|}| \leqslant \varepsilon$ et $|H_{\perp}| \leqslant \varepsilon$.

Remarque 1.64. Pour un tour d'horizon plus complet de la notion de contrôlabilité partielle, voir par exemple [Dup15, Chapitres I et IV].

En linéarisant le système associé au nageur coudé autour de son état d'équilibre $(\mathbf{z}_0, (0,0))$ et en calculant la matrice de Kalman, j'ai montré le résultat suivant :

Proposition 1.65. *Le nageur coudé à 3 segments est partiellement STLC en* $(\mathbf{z}_0, (0,0))$ *pour les variables* x *et* y*.*

En fait, puisqu'on a deux contrôles et qu'on cherche à contrôler deux paramètres, on peut même inverser un système pour faire directement suivre à l'extrémité du nageur une trajectoire $(x(t), y(t))$ prescrite... jusqu'à ce que les trois segments s'alignent entre eux, c'est-à-dire que $\alpha_1 = \alpha_2 = 0$ à un certain instant. Quand cela arrive, cette méthode (naïve) de suivi de trajectoires échoue (voir Figure 1.6). La question de savoir si on peut contrôler le nageur coudé en évitant de passer par un état où $\alpha_1 = \alpha_2 = 0$ reste ouverte.

Extension à un modèle 3D

Tous les résultats de cette section portent sur des nageurs en deux dimensions. Dans le cas en trois dimensions, la contrôlabilité quand on contrôle la déformation a été étudiée dans [LM14, GMZ13]. Il serait intéressant de savoir dans quelle mesure les propriétés de contrôlabilité en 2D sont conservées ou modifiées en 3D dans le cas avec contrôle par champ magnétique.

1.5 Modélisation de micro-filaments et applications

Cette section synthétise mon travail effectué en collaboration avec H. Gadêlha et L. Giraldi, développé ensuite dans la Partie III.

1.5.1 Contexte

La nature comporte une immense variété de « micro-nageurs » développant toutes sortes de stratégies pour se déplacer dans le fluide qui les entoure. Bien souvent, ils font appel, comme les spermatozoïdes ou certaines bactéries, à un ou plusieurs flagelles [GL95, TS04, GGSKB10, SK18] ; d'autres, comme certaines cellules ou micro-algues, font battre des cils de façon synchronisée [GGS+11]. Dans chaque cas, c'est l'interaction de filaments flexibles avec le fluide qui génère le mouvement. C'est ce qui constitue le cadre et la motivation de cette section.

Les micro-filaments élastiques n'apparaissent d'ailleurs pas uniquement comme instruments de locomotion des micro-organismes. Par exemple, le cytosquelette est un ensemble de microtubules et microfilaments d'actine donnant sa structure et ses propriétés mécaniques à une cellule. Comprendre comment ces filaments constituant le cytosquelette réagissent aux contraintes qui leurs sont appliquées est un problème essentiel en biologie cellulaire [How01, CSRB08].

Pour décrire et simuler la dynamique de micro-filaments inextensibles, de nombreux modèles ont été proposés, parmi lesquels des formulations discrètes [HSF10, SZ11, ADGZ13, GMZ13, Bro14, SK18] et continues [HB79, WROG98, TS04, Ant05, LP09, GGSKB10]. La détermination des forces de contact inconnues le long du filament [Ant05] passe le plus souvent par le calcul de multiplicateurs de Lagrange [BW77, LP09, SZ11] pour conserver une longueur constante. Cela peut conduire à une instabilité numérique, qui nécessite l'ajout de termes correctifs [TS04, GGSKB10, MJGS15].

Le premier objectif de cette partie de ma thèse a été de décrire un modèle efficace, numériquement robuste et polyvalent pour permettre d'étudier numériquement une grande variété de phénomènes autour des micro-filaments. J'ai validé le modèle en le comparant aux résultats d'un modèle continu validé expérimentalement [TS04, GGSKB10, MJGS15]. Enfin, j'ai conçu et mis en ligne un code Matlab prêt à l'emploi, facilement adaptable à diverses situations, disponible ici :

`https://github.com/Clementmoreau/Filament`

Ce modèle a notamment été repris et adapté en 3D dans [WIG19], pour prendre en compte les interactions avec un mur dans [WIGG19], et pour prendre en compte des interactions hydrodynamiques non locales dans [HMMJG+19].

Je me suis par la suite intéressé à l'une des applications possibles de ce modèle : la dynamique du phénomène de *buckling* (flambage) de micro-filaments [BS01, TS04, BT09, Gad18], dont j'ai réalisé une étude numérique précise. On observe notamment l'apparition de trois formes finales différentes en fonction du paramètre caractéristique de *buckling*, ainsi que d'autres phénomènes développés dans le Chapitre 8.

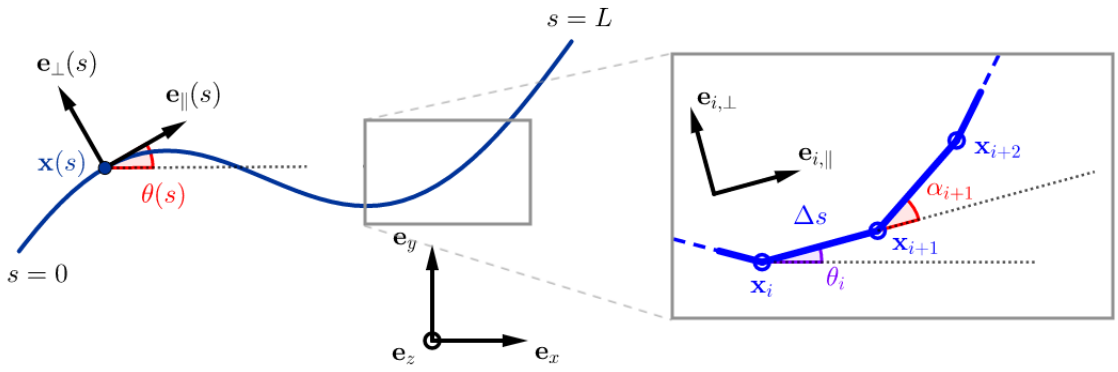

FIGURE 1.7 – Du filament continu au modèle à N segments

1.5.2 Contributions de la thèse

Modélisation de micro-filaments à bas nombre de Reynolds

Cette section reprend succinctement les résultats publiés dans [MGG18], reproduit dans le Chapitre 7.

Le modèle que j'ai étudié est basé sur la discrétisation d'un filament élastique inextensible de longueur L en N éléments notés $S_1, \dots, S_N$, comme sur la Figure 1.7. La mise en équations du modèle présente bien sûr de nombreuses similarités avec le nageur magnétique de la section précédente, aussi bien au niveau des notations que de l'expression des forces et moments.

Chaque élément a pour longueur $\Delta s = L/N$, pour coefficients hydrodynamiques $\eta_\parallel$ et $\eta_\perp$, et deux segments consécutifs sont reliés entre eux par une liaison élastique de torsion de raideur κ. Le filament est repéré dans le plan $(O, \mathbf{e}_x, \mathbf{e}_y)$ par le vecteur

$$\mathbf{x}_N = (x, y, \theta, \alpha_2, \dots, \alpha_N)^T \in \mathbb{R}^{N+2},$$

soit : les coordonnées $\mathbf{x} = (x, y)$ de l'extrémité de S_1, l'angle θ entre $\mathbf{e}_x$ et S_1 et les angles entre deux segments consécutifs, notés $\alpha_2, \dots, \alpha_N$, qui indiquent la forme du filament (voir la Figure 1.7).

Pour le segment S_i, la force hydrodynamique, notée $\mathbf{F}_i^{\mathrm{h}}$, et le couple hydrodynamique par rapport à un point $\mathbf{x}_0$, noté $\mathbf{T}_i^{\mathrm{h},\mathbf{x}_0}$, sont modélisés par la Resistive Force Theory (voir [GH55] et la section 1.4.2). L'interaction élastique $\mathbf{T}_i^{\mathrm{el}}$ entre les segments S_i et S_{i-1} est proportionnelle à la raideur κ et à l'angle α_i.

Comme dans la section 1.4, on suppose que le nombre de Reynolds est suffisamment petit pour que les effets inertiels soient négligeables (régime de Stokes). On a donc équilibre des forces et des moments à tout instant. On obtient $N + 2$ équations en écrivant :

— deux équations pour l'équilibre des forces sur le filament projeté sur les axes (Ox) et (Oy) ;

— une équation pour l'équilibre des moments sur le filament par rapport au point $\mathbf{x}$;

— $N - 1$ équations pour l'équilibre des moments sur l'ensemble $\{S_k + \dots + S_N\}$ pour tout k dans $\{2, \dots, N\}$, par rapport au point $\mathbf{x}_k$,

ce qui donne

$$\begin{cases} \sum_{i=1}^{N} \mathbf{F}_i^h & = & 0, \\ \sum_{i=1}^{N} \mathbf{T}_i^{h,\mathbf{x}_1} & = & 0, \\ \sum_{i=2}^{N} \mathbf{T}_i^{h,\mathbf{x}_2} & = & -\mathbf{T}_2^{\mathrm{el}}, \\ \vdots & \vdots & \vdots \\ \mathbf{T}_N^{h,\mathbf{x}_N} & = & -\mathbf{T}_N^{\mathrm{el}}, \end{cases} \tag{1.63}$$

que l'on récrit sous forme matricielle

$$AQ\dot{\mathbf{x}}_N = B. \tag{1.64}$$

Les expressions détaillées de A, Q et B sont présentées en section 7.7.1 du Chapitre 7.

La résolution numérique de (1.64) peut s'effectuer avec un solveur d'EDO standard (*e.g.* le solveur `ode45` de Matlab). Pour confirmer la validité numérique du modèle, je l'ai comparé aux résultats d'un modèle EDP basé sur la formulation continue [TS04, GGSKB10, MJGS15] associé à un schéma numérique *ad hoc* et validé expérimentalement. Le test consiste à considérer deux formes initiales (un demi-cercle et un arc de parabole) pour le filament et les laisser évoluer jusqu'à l'équilibre rectiligne. Même pour un faible nombre de segments, le modèle discret reproduit le comportement du modèle EDP avec une très bonne précision (voir Figure 7.3 dans le Chapitre 7).

Le modèle EDP utilisé pour la validation utilise un terme correctif pour s'assurer que la longueur totale du filament reste constante. Le système d'équations (1.64) n'en a pas besoin puisque l'inextensibilité du filament apparaît directement dans la géométrie du modèle. Cela rend le modèle discret notablement plus robuste en particulier dans les cas « raides » où la courbure du filament est localement élevée (comme dans le cas de l'arc de parabole). Ainsi, à précision équivalente sur la longueur totale du filament, le modèle discret nécessite un temps de calcul considérablement plus faible que le modèle EDP testé en comparaison (voir la Table 1.1).

Le cadre numérique de notre modèle permet une adaptation facile et rapide à de nombreux cas. En voici quelques exemples, dont certains sont détaillés dans la section 7.5 du Chapitre 7 :

- l'ajout d'un couple interne le long du filament, modélisant la résistance au glissement, qui peut engendrer un phénomène pour lequel une courbure appliquée à une extrémité du filament entraîne l'apparition d'une courbure opposée à l'extrémité opposée. Ce phénomène, observé sur des bio-flagelles tels que les spermatozoïdes [CG17, IGG+18], est appelé *counterbend* [LML05, GGG13]. Voir section 7.5.3 ;
- l'ajout de forces de contact aux extrémités du filament pour modéliser le phénomène de *buckling* (« flambage » en français) [Ant05, BS01, TS04, BT09, Gad18], qui traduit le comportement d'un filament soumis à des forces de compression. Voir la section suivante et le Chapitre 8 ;
- l'ajout de termes modélisant des effets extérieurs comme un champ magnétique (voir section 7.5.2), un effet inertiel, un courant dans le fluide... ;
- l'ajout de termes modélisant les interactions hydrodynamique non locales qui ne sont pas prises en compte par la Resistive Force Theory [HMMJG+19] ;
- l'adaptation du modèle en 3D [WIG19] ;
- *etc.*

Filament flexible			
Test	Modèle discret N=70	Tolérance	Modèle EDP
Demi-cercle 	2	1% 0.1% 0.01%	1.3 249 3750
Parabole 	1.5	1% 0.1% 0.01%	90 1820 $>$ 1h
Filament rigide			
Test	Modèle discret N=70	Tolérance	Modèle EDP
Demi-cercle 	3	1% 0.1% 0.01%	97 850 $>$ 1h
Parabole 	1.7	1% 0.1% 0.01%	$>$ 1h $>$ 1h $>$ 1h

TABLE 1.1 – Temps de calcul en secondes pour deux conditions initiales et deux rigidités différentes.

L'étude numérique et analytique de problèmes dans cette liste, en s'appuyant sur le cadre donné par le modèle à N segments, constitue un éventail de perspectives futures pour mes recherches, en collaboration avec H. Gadêlha.

Etude numérique du phénomène de *buckling*

Cette section reprend succinctement un article en préparation, reproduit dans le Chapitre 8.

Le *buckling*, appelé « flambage » en français, correspond au comportement particulier d'un matériau soumis à des forces de compression ou de cisaillement. Les micro-filaments expérimentent largement ce phénomène, sous l'action d'un fluide en mouvement [GG06] ou de forces internes [BT09].

Je me suis intéressé plus précisément à un filament élastique initialement rectiligne, dont on pousse les extrémités l'une vers l'autre. Pour ce problème, étudié tout d'abord par Euler au XVIII^{e} siècle [Eul44], on connaît des solutions analytiques à l'équilibre statique.

Ces solutions classiques ne tiennent pas compte de l'aspect dynamique : la compétition entre le temps caractéristique de relaxation nécessaire à l'établissement de l'équilibre statique et la vitesse à laquelle les extrémités se déplacent. Cette compétition conduit à des comportements dynamiques plus complexes, qui diffèrent grandement en fonction des paramètres.

J'ai réalisé dans ma thèse une étude numérique de ce problème de *buckling* dynamique. L'originalité de mon travail réside entre autres dans le fait qu'on choisit de poursuive le mouvement des extrémités du filament jusqu'au-delà de l'instant où elles se croisent. Les simulations effectuées permettent alors de distinguer différents régimes conduisant à l'apparition de différentes formes pour le filament, en fonction des paramètres du système. Mes

résultats sont présentés succinctement ici et développés dans le Chapitre 8.

Équations du modèle. On utilise le modèle de filament développé dans la section précédente. On part d'une condition initiale où le filament est rectiligne et « presque » horizontal, c'est-à-dire qu'on introduit un bruit gaussien d'amplitude très faible dans la courbure (les angles α_i) pour modéliser numériquement l'asymétrie infinitésimale qui déclenche le phénomène de *buckling*. On pousse ensuite les extrémités du filament l'une vers l'autre selon les contraintes cinématiques suivantes :

$$\begin{array}{ll} \dot{y}_1(t) = 0, & \dot{y}_{N+1}(t) = 0, \\ \dot{x}_1(t) = (1-a)V_p, & \dot{x}_N(t) = -(1+a)V_p, \end{array} \tag{1.65}$$

où V_p est la vitesse de poussée et $a \in [0,1]$ un paramètre d'asymétrie. Quand $a = 0$, les deux extrémités se déplacent l'une vers l'autre à la même vitesse ; à l'inverse, quand $a = 1$, seule l'une des extrémités se déplace tandis que l'autre est fixe. Ces deux paramètres n'existent pas dans le cas statique. Ils caractérisent la manière dont les extrémités se rapprochent en fonction du temps, et représentent donc l'aspect dynamique du système.

On adimensionnalise le système d'équations régissant la dynamique du filament (donné par le système (1.63) auquel on a ajouté les équations (1.65)) pour obtenir un paramètre caractéristique de *buckling* que l'on appelle le nombre de *buckling* et que l'on note Bu :

$$\mathrm{Bu} = \frac{\eta_{\|} \mathrm{L}^3 V_p}{E_b}.$$

Dans cette expression, $\eta_{\|}$ correspond au coefficient de traînée hydrodynamique, L à la longueur du filament et E_b à sa rigidité (voir Chapitre 7). Le nombre de *buckling* traduit le rapport entre le temps caractéristique de relaxation du filament et la vitesse à laquelle les extrémités se déplacent. Quand Bu est très faible, on retrouve le comportement observé dans le cas statique.

Apparition de trois différentes formes. La Figure 1.8 présente les différents comportements adoptés par le filament en fonction de Bu. On peut observer trois régimes distincts :

— pour $\mathrm{Bu} = 10^{-1}$ à $\mathrm{Bu} = 1$, le filament se retourne (*flip*) peu après que les extrémités se soient croisées.

— pour $\mathrm{Bu} = 10^{1}$ à $\mathrm{Bu} = 10^{2}$, on observe l'apparition d'une boucle (*loop*) qui persiste jusqu'à la fin de la simulation.

— pour $\mathrm{Bu} = 10^{3}$ et plus, le filament prend dans certains cas une forme qui évoque celle d'un noeud (*knot*).

Pour certaines valeurs de Bu, deux formes différentes peuvent coexister. La Figure 1.8-(b) montre la prédominance de chacune des formes en fonction de Bu. On voit notamment que les « boucles » et les « noeuds » semblent apparaître de façon équiprobable pour les grandes valeurs de Bu.

La Figure 1.8-(c) montre l'influence du paramètre d'asymétrie a sur l'apparition des différentes formes. Quand a augmente, les boucles et les noeuds apparaissent à partir de valeurs de plus en plus grandes de Bu. L'apparition de la boucle et du noeud est donc favorisée par les valeurs de a proches de 0, c'est-à-dire par des situations plutôt symétriques.

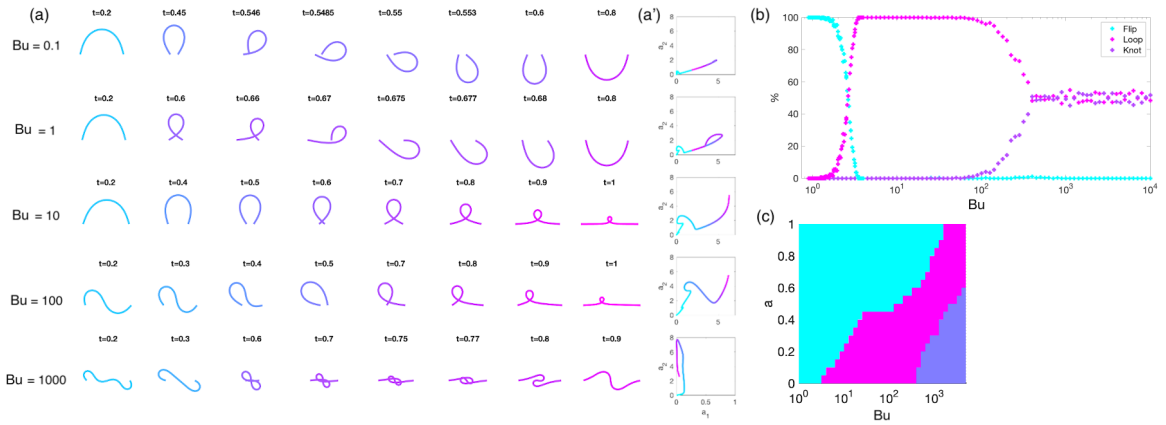

FIGURE 1.8 – Visualisation de l'apparition de différentes formes au cours du *buckling* (a). Évolution de la forme du filament au cours du temps pour différentes valeurs de Bu. On peut observer les trois formes (*flip*, *loop* et *knot*) correspondant aux trois régimes de *buckling*. (a'). Évolution de l'amplitude des deux premiers modes de Fourier de la courbure du filament pour chacune des simulations présentées en (a). L'intérêt de ces graphiques est développé dans le Chapitre 8. (b). Prédominance de chaque forme en fonction de Bu, exprimée en pourcentage d'apparition sur 500 simulations. (c). Prédominance de chaque forme en fonction de Bu et a.

.

Évolution de l'amplitude des modes de Fourier. J'ai complété cette analyse des formes en temps long par une étude du comportement du filament en temps court. Au cours des premiers instants, on observe que le filament présente plusieurs « bosses » (voir par exemple le filament en bas à gauche de la Figure 1.8-(a) qui disparaissent rapidement. Ces bosses correspondent à des modes de Fourier d'ordre élevé de la courbure du filament. La Figure 1.9 montre l'évolution de l'amplitude de ces modes de Fourier au cours du temps pour différentes valeurs de Bu. Dans chaque cas, chaque mode apparaît, atteint un maximum d'amplitude, puis décroît. Ces maxima ont lieu successivement, dans l'ordre décroissant des modes. En notant $T^k_{\max}$ le temps auquel le mode k atteint son maximum, on a établi numériquement que cette décroissance suivait une loi de la forme

$$T^k_{\max} = T_0 \exp(-\alpha k^{1/4}), \tag{1.66}$$

avec $T_0 > 0$ et $\alpha > 0$ quasiment indépendants de Bu (voir le graphique de droite sur la Figure 1.9).

Perspectives. Ces observations numériques mettent en lumière des phénomènes intéressants, en comparaison à des études numériques et expérimentales [CDK17] mais aussi du point de vue du comportement mathématique du système. En particulier, j'ai constaté que, pour certaines valeurs de Bu, la forme finale du filament semblait très imprédictible, même à un stade avancé de la simulation. D'autre part, les amplitudes des trois premiers modes de Fourier de la courbure, qui semblent jouer un rôle majeur dans le comportement du filament au cours du *buckling*, suivent des trajectoires complexes comportant des bifurcations (voir

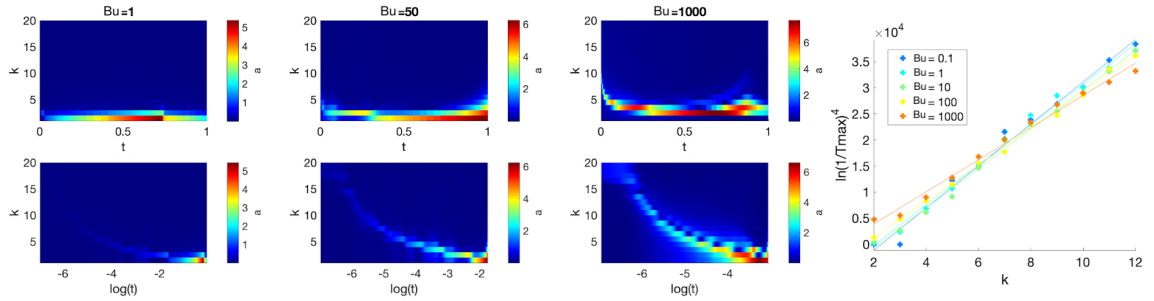

FIGURE 1.9 – Résultats obtenus sur la décroissance des modes de Fourier de la courbure du filament. Pour trois valeurs différentes de Bu, on a représenté l'amplitude des 20 premiers modes de Fourier (en ordonnée) en fonction du temps (en abscisse). L'échelle de temps est linéaire sur la rangée du haut, permettant de constater que seuls les deux ou trois premiers modes apparaissent l'essentiel du temps. L'échelle de temps sur la rangée du bas est logarithmique : on peut alors observer l'apparition et la décroissance de l'amplitude des modes élevés en temps court, qui suit une loi modélisée par (1.66), représentée sur le graphique de droite.

Figure 8.5 au Chapitre 8). L'étude analytique de ce système pour mieux comprendre ces comportements constitue une perspective future prometteuse.

Chapter 2

Review of the contributions

Note to the reader: this chapter is the English version of Chapter 1.

2.1 Introduction

To control a system means to act on it in order to monitor its state evolution. Control theory is divided into three subdomains, each of which summarised in a question:

— *controllability* : using the control, is it possible to steer the system's state from a given start point to a given point of arrival? In this case, the control is said to be "open-loop", *i.e.* it depends only on time and not on the state;

— *stabilisation* : using the control, is it possible to make an unstable equilibrium of the system stable, and if so, how? In this case, the control runs in a "closed loop", with a state-dependent control;

— *optimal control* : assuming it is possible to reach a given target, how to reach it while minimising some cost function (total time, energy, distance, *etc.*)?

Let us mention a few examples: a car whose wheels are operated to make it arrive at a given place with a given orientation, a satellite changing orbits with reactors, a water container moving to make the surface of the water flat, a chemical reaction monitored by adding a reagent, a tumor whose growth is controlled by drug injection. Numerous other examples are given in [Isi95].

We can split control systems into two families: the case where the state comprises a *finite* number of parameters – *e.g.* position and orientation of a robot – and those where the state lives in a space of *infinite* dimension – *e.g.* temperature profile or chemical concentration on a space region Ω. In the first case, the state at a given instant belongs to $\mathbb{R}^n$ and its evolution is described by an ordinary differential equation (ODE). In the second case, the state belongs to a functional space (typically $\mathrm{L}^2(\Omega)$) and its evolution is described by a partial differential equation (PDE).

In my thesis, I have studied matters of controllability. My abstract controllability results are gathered in Part I. Chapter 3, dedicated to finite-dimensional control, displays a new necessary condition for local controllability of control-affine systems with two controls. In Chapter 4, we study controllability with nonnegative state constraint of infinite dimensional parabolic systems. This type of controllability has recently been proven for the heat equation [LTZ18] as well as for semilinear parabolic equations [PZ17]. My contribution establishes controllability with nonnegative state constraint in the case of linear coupled parabolic PDE systems.

Part II features applications of these results to controllability of planar magnetic micro-swimmers – microscopic slender robots immersed in a fluid and brought into movement through a magnetic field. Such micro-swimming robots have promising applications in the biomedical domain (targeted drug delivery, micro-surgery, sensing). Chapters 5 and 6 present a model of these swimmers and their controllability properties. Thanks to the result from Chapter 3, I could prove that the considered swimmers are not locally controllable around their equilibrium position in general, and elucidated the cases for which controllability can be obtained.

Finally, I studied biology-related microfilaments – such as micro-robots from Part II but also cells and bacteria flagella or microtubular structures, by conducting works of modeling and numerical simulation of elastic micro-filaments. The results are gathered in Part III. Chapter 7 displays the model, its numerical validation and examples of applications. In Chapter 8, we undertake a numerical study of one of these applications: the buckling phenomenon.

Chapters 3 to 8 reproduce, with few minor changes, articles that are either published, submitted or under preparation. The present introductory chapter discloses, for each of these chapters, general context, state of the art, contributions of this thesis and future perspectives.

Sections 2.2 and 2.3 pool results from Part I. The study of two- and three-link magnetic micro-swimmers is displayed in section 2.4. Section 2.5 describes the work realised on elastic microfilaments modeling.

2.2 Controllability in finite dimension

2.2.1 Generalities

Let n, m be positive integers. The abstract framework in control theory is the following: consider the equation

$$\dot{y} = f(t, y, u). \tag{2.1}$$

In this equation, $y \in \mathbb{R}^n$ is called the state, function of time t, $\dot{y}$ is the derivative of y with respect to t, and $u \in \mathbb{R}^m$ is called the *control*, that we can choose in order to influence the system and steer the state y.

Definition 2.1. System (2.2) is *globally controllable in time* T if, for all $y_0, y_1 \in \mathbb{R}^n$, there

exists $u \in \mathrm{L}^\infty([0,T],\mathbb{R}^m)$ such that the solution of (2.1) with $y(0) = y_0$ satisfies $y(T) = y_1$.

Remark 2.2. In a broader framework, one could only assume that the state y and control u live in metric spaces $\mathcal{Y}$ and $\mathcal{U}$ (see [Son13, Section 2.7]). In particular, in the case of PDEs, $\mathcal{Y}$ is a functional space.

One usually considers that the state y evolves on a differentiable manifold. Our results in this section are local, therefore independent from the coordinate choice on $\mathbb{R}^n$. Without loss of generality, we choose to take $\mathbb{R}^n$ as state space in all the following.

For a controllable system, it is also interesting to determine whether it is possible to make sure that the state y remains in a given region of the state space (typically $\{y \geqslant 0\}$) all along the interval $[0,T]$: this is called *state constrained* controllability. This question is addressed for a control system in infinite dimension in section 2.3.

The following section is dedicated to a short review of the notions and previous results around my work in control of ODEs.

Some controllability properties of linear and nonlinear systems

The most simple control systems are the linear autonomous systems, that read

$$\dot{y} = Ay + Bu, \tag{2.2}$$

with $y \in \mathbb{R}^n$, $u \in \mathbb{R}^m$, $A \in \mathcal{M}_n(\mathbb{R})$ and $B \in \mathcal{M}_{n,m}(\mathbb{R})$.

Global controllability of System (2.2) for all time is known since the 1960s ([KHN63] among others) with the following theorem that provides an algebraic necessary sufficient condition on matrices A and B:

Theorem 2.3. *Define the Kalman matrix K as*

$$K = \begin{pmatrix} B & AB & A^2B & \dots & A^{n-1}B \end{pmatrix} \in \mathcal{M}_{n,mn}(\mathbb{R}). \tag{2.3}$$

Then, for all $T > 0$, System (2.2) is controllable in time T if and only if $\mathrm{rank}K = n$.

Now, let us consider a general nonlinear control system like the following:

$$\dot{y} = f(y,u). \tag{2.4}$$

In this case, distinction is made between global controllability, as defined in Definition 2.1, and local controllability. Global controllability results include the Rashevskii-Chow theorem, stated below, that provides a condition of global controllability for a driftless control-affine systems.

Let us define two notions of *local* controllability around an equilibrium point.

Definition 2.4. An equilibrium point of System (2.4) is a couple $(y_{\mathrm{eq}}, u_{\mathrm{eq}}) \in \mathbb{R}^n \times \mathbb{R}^m$ such that

$$f(y_{\mathrm{eq}}, u_{\mathrm{eq}}) = 0.$$

Let $(y_{\mathrm{eq}}, u_{\mathrm{eq}})$ an equilibrium of (2.4).

Definition 2.5. System (2.4) is small-time locally controllable (STLC) at $(y_{\mathrm{eq}}, u_{\mathrm{eq}})$ if, for all $\varepsilon > 0$, there exists $\eta > 0$ such that, for all y_0 and y_1 in $B_\eta(y_{\mathrm{eq}})$, there exists a function

$u \in \mathrm{L}^\infty([0,\varepsilon],\mathbb{R}^m)$ such that the solution $y(\cdot) : [0,\varepsilon] \to \mathbb{R}^n$ of (2.4) with $y(0) = y_0$ satisfies $y(\varepsilon) = y_1$ and

$$\|u - u_{\mathrm{eq}}\|_{\mathrm{L}^\infty([0,\varepsilon])} \leqslant \varepsilon. \tag{2.5}$$

Definition 2.6. Let $\alpha \geqslant 0$. System (2.4) is α-STLC at $(y_{\mathrm{eq}}, u_{\mathrm{eq}})$ if, for all $\varepsilon > 0$, there exists $\eta > 0$ such that, for all y_0 and y_1 in $B_\eta(y_{\mathrm{eq}})$, there exists a function $u \in \mathrm{L}^\infty([0,\varepsilon],\mathbb{R}^m)$ such that the solution $y(\cdot) : [0,\varepsilon] \to \mathbb{R}^n$ of (2.4) with $y(0) = y_0$ satisfies $y(\varepsilon) = y_1$ and

$$\|u - u_{\mathrm{eq}}\|_{\mathrm{L}^\infty([0,\varepsilon])} \leqslant \alpha. \tag{2.6}$$

Remark 2.7. One easily sees that "0-STLC" is identical to STLC as defined in Definition 2.5. However, if $\alpha > 0$, α-STLC is weaker than STLC, because the control might remain "large" as the neighbourhood of y_{eq} becomes "smaller".

STLC as defined in 2.5, following [Cor07, Def. 3.2, p. 125], requires the control u to be "very" close to the equilibrium control when going "very" close to the equilibrium position y_{eq}. This notion can be found, for example, in the works of M. Kawski as well [Kaw86, Kaw87]. Historically, the term "STLC" has first been used by H. Hermes [Her82] and H. Sussmann [Sus83] among others, to describe what we call α-STLC. In this formalism, the notion described in Definition 2.5 is called "small-time local controllability with small controls".

STLC appears naturally in the following result.

Definition 2.8. Let $(y_{\mathrm{eq}}, u_{\mathrm{eq}})$ an equilibrium of (2.4). The linearised system at $(y_{\mathrm{eq}}, u_{\mathrm{eq}})$ is given by the following linear control system :

$$\dot{y} = \frac{\partial f}{\partial y}(y_{\mathrm{eq}}, u_{\mathrm{eq}})y + \frac{\partial f}{\partial u}(y_{\mathrm{eq}}, u_{\mathrm{eq}})u. \tag{2.7}$$

Theorem 2.9. *If the linearised system (2.7) at $(y_{\mathrm{eq}}, u_{\mathrm{eq}})$ is controllable, then System (2.4) is STLC at $(y_{\mathrm{eq}}, u_{\mathrm{eq}})$.*

This theorem provides a simple sufficient condition for STLC, yet this condition is not necessary: System (1.4) can be STLC even if the linearised system is not controllable. In that case, there exists sharper tools to establish STLC or non-STLC, especially in the control-affine case, dealt with in the following.

Control-affine systems

Let $\mathcal{X}$ be the space of real analytic vector fields on $\mathbb{R}^n$. We identify an element f of $\mathcal{X}$ to a map from $\mathbb{R}^n$ to $\mathbb{R}^n$. For x in $\mathbb{R}^n$, $f(x)$ is considered as a column vector and $f'(x)$ designates the Jacobian matrix of the map f at x.

A particular case of nonlinear system is the *control-affine* case. A control-affine system takes the following form:

$$\dot{y} = f_0(y) + \sum_{i=1}^{m} f_i(y)u_i, \tag{2.8}$$

with $f_0, \dots, f_m \in \mathcal{X}$ [1].

The field f_0 is called the *drift*. As its name suggests, it corresponds to the uncontrollable part of the equation, against which one might have to fight through the controls to reach the target successfully.

Numerous necessary and sufficient conditions of STLC at an equilibrium are known for systems of type (2.8). We present them in detail in what follows. The improvement of these conditions has been subject to productive research from the late 1970s to the late 1990s, carried out, among others, by H. Hermes [Her76, Her78, Her82], then H. Sussmann [Sus83, Sus87], M. Kawski [Kaw87, Kaw90], G. Stefani [Ste86], A. Tret'yak [Tre90], A. Agrachev [AG93a, AG93b], M. Krastanov [Kra98]... This subject has recently drawn some new interest, as shows a necessary condition for a new notion of STLC, proven by K. Beauchard and F. Marbach in the case $m = 1$ [BM18] (see Theorem 2.25 below).

Nevertheless, no necessary and sufficient condition of local controllability for control-affine systems with drift has been found to this day. My contribution, synthesised in the next section and developed in Chapter 3, makes a modest step forward on the side of necessary conditions in the case $m = 2$.

Let us start with a few reminders of Lie brackets. Given two vector fields $f = (f^1, \dots, f^n)$ and $g = (g^1, \dots, g^n)$ in $\mathcal{X}$, their Lie brackets $[f, g]$ is given by:

$$\forall x \in \mathbb{R}^n, [f, g](x) = g'(x)f(x) - f'(x)g(x). \tag{2.9}$$

Hence, for j in $\{1, \dots, n\}$, the j-th component of $[f, g]$ reads

$$\forall x \in \mathbb{R}^n, [f, g]^j(x) = \sum_{k=1}^{n} f^k(x)\frac{\partial g^j}{\partial x_k}(x) - g^k(x)\frac{\partial f^j}{\partial x_k}(x). \tag{2.10}$$

We will also use the following notation for iterated Lie brackets, defined recursively: $\mathrm{ad}_f^0 g = g$ and for all positive integer k,

$$\mathrm{ad}_f^k g = [f, \mathrm{ad}_f^{k-1} g].$$

Lastly, for $\mathcal{F}$ a collection of vector fields, define

— $\mathrm{Br}(\mathcal{F})$ the set of formal iterated Lie brackets [2] of $\mathcal{F}$;

— $\mathrm{Lie}(\mathcal{F})$ the Lie algebra generated by $\mathcal{F}$, *i.e.* the smallest linear subspace $\mathcal{G}$ of $\mathcal{X}$ such that $\mathcal{F} \subset \mathcal{G}$ and for all f, g in $\mathcal{G}$, $[f, g] \in G$.

We say that an iterated Lie bracket is of order k is it contains exactly k fields (*e.g.* $[f_0, f_1]$ is of order 2, $[f_0, [f_0, [f_0, [f_0, f_1]]]]$ and $[[f_2, f_1], [f_0, [f_2, f_1]]]$ are of order 5).

Lie brackets generated by the f_i fields naturally appear in the study of control-affine systems. In order to understand why, let us look at a simple driftless case with $m = 2$, taken from [Cor07, p.130]:

$$\dot{y} = f_1(y)u_1 + f_2(y)u_2. \tag{2.11}$$

Assume the state is at a point y_0 such that $f_1(y_0) \neq 0$ and $f_2(y_0) \neq 0$. For $\eta \in \mathbb{R}$, controls $(\eta, 0)$ and $(0, \eta)$ allow to steer the system respectively in directions $\pm f_1(y_0)$ and

1. The analyticity of the fields f_i is not necessary. Some results only assume that they are C^∞. For further discussion on this matter, see [Son13, chap.4] or [Sus85]

2. Detailed construction of $\mathrm{Br}(\mathcal{F})$ is made in [Sus87].

$\pm f_2(y_0)$, depending on the sign of η.

Let $\varepsilon > 0$ and η_1, η_2 in $\mathbb{R}$. Define the following controls on $[0, 4\varepsilon]$:

$$(u_1(t), u_2(t)) = \begin{cases} (\eta_1, 0) & \text{si } t \in [0, \varepsilon], \\ (0, \eta_2) & \text{si } t \in]\varepsilon, 2\varepsilon], \\ (-\eta_1, 0) & \text{si } t \in]2\varepsilon, 3\varepsilon], \\ (0, -\eta_2) & \text{si } t \in]3\varepsilon, 4\varepsilon]. \end{cases}$$

Then, one can check that

$$y(4\varepsilon) = y_0 + \eta_1\eta_2\varepsilon^2[f_1, f_2](y_0) + o(\varepsilon^2).$$

In other words, by tuning η_1 and η_2, one can steer the system in the directions $\pm[f_1, f_2]$.

Hence, one can sense that the reachable directions for System (2.8) around an equilibrium are given by the Lie brackets generated by the fields f_i. Theorem 2.15 below states a necessary condition of local controllability that formalises.

Remark 2.10. Given an equilibrium $(y_{\text{eq}}, u_{\text{eq}})$ of System (2.8), we can always assume it is $(0, 0)$ by performing the translation $(y, u) \mapsto (y - y_{\text{eq}}, u - u_{\text{eq}})$. Therefore, without loss of generality, we assume in all the following that $(0, 0)$ is an equilibrium point of (2.8).

Driftless case. In the driftless case, we know necessary sufficient conditions of STLC and of global controllability, given by Theorem 2.12 hereafter, called the Rashevskii-Chow theorem.

Definition 2.11. System (2.8) satisfies the *Lie algebra rank condition (LARC)* at $(x, 0)$ if

$$\{g(x), g \in \text{Lie}(f_0, f_1, \ldots, f_m)\} = \mathbb{R}^n. \tag{2.12}$$

Theorem 2.12 ([Ras38, Cho39])**.** *Assume $f_0 = 0$.*

1. *If (2.8) satisfies the LARC at $(0, 0)$, then it is STLC at $(0, 0)$.*
2. *If (2.8) satisfies the LARC at $(x, 0)$ for all $x \in \mathbb{R}$, then it is globally controllable for all time.*

When $f_0 \neq 0$, we do not know any necessary sufficient condition. There is however a result about the *accessible space* in time smaller than T:

Definition 2.13. Let $T > 0$. The accessible space in time T, noted $\mathcal{A}^T$, is the set

$$\mathcal{A}^T = \{y_0 \in \mathbb{R}^n | \exists u \in \mathrm{L}^\infty(0, T, \mathbb{R}^m), y_u(T) = y_0\},$$

where $y_u(T)$ is the solution of (2.8) with $y(0) = 0$ and control u. Let us also define

$$\mathcal{A}^{\leqslant T} = \bigcup_{t \in [0,T]} \mathcal{A}^t.$$

Theorem 2.14 ([Son13, Theorem 9, p. 156])**.** *If System (2.8) satisfies the LARC at 0, then for all $T > 0$,*

$$\overset{\circ}{A}{}^{\leqslant T} \neq \emptyset.$$

Determining whether (2.8) is controllable of not is therefore equivalent to determining if the interior of $A^{\leqslant T}$ contains the equilibrium 0 for all T.

Necessary conditions.

Theorem 2.15 ([Sus73])**.** *If there exists $\alpha \geqslant 0$ such that System (2.8) is α-STLC at $(0,0)$, then it satisfies the LARC at $(0,0)$.*

The converse is not true. For example, system

$$\begin{cases} \dot{y}_1 &= y_2^2, \\ \dot{y}_2 &= u, \end{cases} \tag{2.13}$$

satisfies the LARC at $((0,0),0)$ but is not controllable, because necessarily $y_2 \geqslant 0$.

This rather trivial example suggests that the LARC is not a very sharp necessary condition: it encompasses too many uncontrollable cases. Unfortunately, there does not exist better ones in the general case, to the best of my knowledge. We state in the following a few finer results that hold in the scalar case ($m = 1$). Let us first present the sufficient conditions in the general case.

Sufficient conditions. We start with a few notations, taken in [Cor07, Section 3.4]. Let $\mathfrak{S}_m$ be the set of permutations of $\{1,\dots,m\}$. For $\pi \in \mathfrak{S}_m$, let $\tilde{\pi}$ be the function that maps $(f_0, f_1, \dots, f_m)$ on $(f_0, f_{\pi(1)}, \dots, f_{\pi(m)})$ in a given bracket. This way, for g in $\mathrm{Br}(f_0,\dots,f_m)$, we can define

$$\sigma(g) = \sum_{\pi \in \mathfrak{S}_m} \tilde{\pi}(g).$$

For example, if $m = 2$ and $g = [f_1, [f_2, [f_1, f_0], f_0]]$, then

$$\sigma(g) = [f_1, [f_2, [f_1, f_0], f_0]] + [f_2, [f_1, [f_2, f_0], f_0]].$$

Finally, given g a bracket in $\mathrm{Br}(f_0,\dots,f_m)$ and $i \in \{0,\dots,m\}$, we denote by :

— $\delta_i(g)$ the number of times f_i appears in g. In the above example $\delta_0(g) = 2$, $\delta_1(g) = 2$, and $\delta_2(g) = 1$,

— for $\theta \in [0,1]$, $\rho_\theta(g) = \theta\delta_0(g) + \sum_{i=1}^m \delta_i(g)$,

— for $\eta > 0$, H_η the subspace of $\mathbb{R}^n$ generated by the brackets g of $\mathrm{Br}(f_0,\dots,f_m)$ such that $\rho_\theta(g) < \eta$, taken at 0.

Let us now introduce the well-known Sussmann condition [Sus87].

Definition 2.16 (Sussmann condition)**.** Let $\theta \in [0,1]$. System (2.8) is said to satisfy $S(\theta)$ at $(0,0)$ if

— it satisfies the LARC at $(0,0)$;

— for all g in $\mathrm{Br}(f_1,\dots,f_m)$ such that $\delta_0(g)$ is odd and $\delta_i(g)$ is even for all $i \in \{1,\dots,m\}$,

$$\sigma(g)(0) \in H_{\rho_\theta(g)}.$$

Then, one has the following result :

Theorem 2.17 ([Sus87, Theorem 7.3]). *If there exists $\theta \in [0,1]$ such that System (2.8) satisfies $S(\theta)$ at $(0,0)$, then System (2.8) is STLC at $(0,0)$.*

Theorem 2.17 states that the STLC property for System (2.8) depends on the behaviour of brackets with an odd number of times f_0 and an even number of times the other fields. These brackets have often been called *bad* ones, because it is their directions at 0 that seem to obstruct controllability if the Sussmann condition does not hold. On the contrary, for a given bracket h and $\theta \in [0,1]$, the brackets in $H_{\rho_\theta(g)}$ are called *good* brackets: the system is controllable if these brackets encompass enough directions at 0 and are therefore able to "neutralise" the bad brackets.

However, as Kawski noticed in [Kaw86, Example 2.5.1], goodness or badness of high-order brackets is not intrinsic and depends on the basis chosen for the Lie bracket subspaces generated by the fields f_i. For convenience, and because this phenomenon does not occur for the low-order brackets that we consider here, we will occasionnally say that some brackets are good or bad. It should nonetheless be kept in mind that this is an imprecise terminology.

STLC conditions for scalar-input systems. From now on, we study the case $m = 1$, called *scalar-input* or *single-input*:

$$\dot{y} = f_0(y) + f_1(y)u_1. \tag{2.14}$$

For $k \in \mathbb{N}$, let S_k be the set of iterated Lie brackets of $f_0, \dots, f_m$ containing at most k times f_0. For $y \in \mathbb{R}^n$, let $S_k(0)$ be the subspace of $\mathbb{R}^n$ generated by the elements of S_k taken at 0.

Remark 2.18. We have of course $S_k \subset S_{k+1}$ for all k.

Theorem 2.19 ([Sus83]). *Assume that, at an equilibrium $(0,0)$:*

- *System (2.14) satisfies the LARC at $(0,0)$;*
- *for all positive integer k,*

$$S_{2k}(0) \subset S_{2k-1}(0). \tag{2.15}$$

Then, System (2.14) is STLC at $(0,0)$.

Theorem 2.19 slightly improves and simplifies the Sussmann condition (Def. 2.16) in the scalar-input case. It states that System (2.14) is STLC provided that the "bad" brackets g with an even number of f_1 do not create new directions at 0 compared to the directions created by the "good" brackets with at most $(\delta_1(g) - 1)$ times f_1.

Let us now investigate what happens when condition (2.15) does not hold. The lowest-order violation of this condition occurs when $[f_1, [f_0, f_1]](0) \notin S_1(0)$. The following theorem deals with this case. Let

$$B_1 = [f_1, [f_0, f_1]]. \tag{2.16}$$

B_1 is called the "first bad bracket".

Theorem 2.20 ([Sus83, Proposition 6.3]). *Assume $B_1(0)$ does not belong to $S_1(0)$. Then, for all $\alpha \geqslant 0$, System (2.14) is not α-STLC at $(0,0)$.*

This theorem establishes that the bracket B_1 obstructs STLC when its direction at 0 is outside of $S_1(0)$. Similarly, we would like to state that the presence inside $S_1(0)$ of the other

elements of $S_2(0)$ is necessary for STLC. Unfortunately, it is not the case: things get more complicated as soon as we look at the "second bad bracket"

$$B_2 = [[f_0, f_1], [f_0, [f_0, f_1]]]. \tag{2.17}$$

Indeed, if $B_1(0) \in S_1(0)$ and $B_2(0) \notin S_1(0)$, then (2.14) *may or may not* be STLC. For example, the following system (taken from [Sus83, p.711]):

$$\begin{cases} \dot{y}_1 &= u, \\ \dot{y}_2 &= y_1, \\ \dot{y}_3 &= y_1^3 + y_2^2, \end{cases} \tag{2.18}$$

is STLC at 0 even if $B_2(0) \notin S_1(0)$.

Adding new directions to S_1 allows to state a new necessary condition:

Theorem 2.21 ([Kaw87])**.** *Let* $S' = \mathrm{Span}\{\mathrm{ad}_{f_0}^k(\mathrm{ad}_{f_1}^3 f_0), k \in \mathbb{N}\}$*. If* $B_2(0) \notin S_1(0) + S'(0)$*, then* (2.14) *is not STLC at* $(0,0)$*.*

This theorem does not exclude the system from being α-STLC for $\alpha > 0$. In [Kra98, Théorème 1.2], M. Krastanov establishes necessary conditions for α-STLC in the case $B_2(0) \notin S_1(0) + S'(0)$, where α depends in particular of the value at 0 of brackets of order 5. These conditions are very technical, so we will not reproduce them here. They tend to confirm that it is unrealistic to hope to be able to obtain necessary conditions as nice and simple as Theorem 2.20 for all other cases where condition (2.15) does not hold.

In [Ste86], G. Stefani states a necessary condition that encompasses Theorem 2.20 and is, to the best of my knowledge, the most complete condition to this day:

Theorem 2.22 ([Ste86])**.** *If there exists* k *in* $\mathbb{N}$ *such that*

$$\mathrm{ad}_{f_1}^{2k} f_0(0) \notin S_{2k-1}(0),$$

then, for all $\alpha \geqslant 0$*, System* (2.14) *is not* α*-STLC at* $(0,0)$*.*

Finally, let us mention a new result obtained by K. Beauchard and F. Marbach in [BM18], that uses a different notion of local controllability requiring the control to be small for a different norm.

Given an interval I of R, we say that a function f belongs to the Sobolev space $\mathrm{W}^{k,\infty}(I)$ if, for all p in $\{0, \dots, k\}$, $f^{(p)} \in \mathrm{L}^\infty(I)$. The norm of f on this space is given by

$$\|f\|_{\mathrm{W}^{k,\infty}} = \max_{p \in \{0,\dots k\}} \|f^{(p)}\|_{\mathrm{L}^\infty(I)}.$$

Definition 2.23. Let $k \in \mathbb{N}$. System (2.14) is $\mathrm{W}^{k,\infty}$-STLC ar $(y_{\mathrm{eq}}, u_{\mathrm{eq}})$ if, for all $\varepsilon > 0$, there exists $\eta > 0$ such that, for all y_0 and y_1 in $B_\eta(y_{\mathrm{eq}})$, there exists $u \in \mathrm{L}^\infty([0,\varepsilon], \mathbb{R})^m$ such that the solution of (2.14) with $y(0) = y_0$ satisfies $y(\varepsilon) = y_1$ and

$$\|u - u_{\mathrm{eq}}\|_{\mathrm{W}^{k,\infty}[0,\varepsilon]} \leqslant \varepsilon. \tag{2.19}$$

Remark 2.24. For $k = 0$, this notion is identical to STLC. Moreover, the different notions of STLC from Definitions 2.5, 2.6 and 2.23 can be ranked on an implication chain: let k and

k' in $\mathbb{N}$ such that $k \geqslant k'$ and α and α' in $\mathbb{R}$ such that $\alpha \geqslant \alpha'$. Then, we have

$$\mathrm{W}^{k,\infty}\text{-STLC} \Rightarrow \mathrm{W}^{k',\infty}\text{-STLC} \Rightarrow \mathrm{STLC} \Rightarrow \alpha'\text{-STLC} \Rightarrow \alpha\text{-STLC}. \tag{2.20}$$

Let $d = \dim S_1(0)$ and $k \in \{1, \dots, d\}$. By analogy with (2.16) and (2.17), define

$$B_k = [\mathrm{ad}_{f_0}^{k-1} f_1, \mathrm{ad}_{f_0}^{k} f_1]. \tag{2.21}$$

Theorem 2.25 ([BM18, Theorem 3])**.** *Let $k \in \{2, \dots, d\}$. If $B_k(0) \notin S_1(0)$, then (2.14) is not $\mathrm{W}^{2k-3,\infty}$-STLC at $(0,0)$.*

Remark 2.26. This result, in its version stated in [BM18], is also true for $k = 1$, with the convention that the function $u : [0, \epsilon] \to \mathbb{R}$ is in $\mathrm{W}^{-1,\infty}([0,\epsilon])$ if $t \mapsto \int_0^t u(s)\mathrm{d}s$ belongs to $\mathrm{L}^\infty([0,\epsilon])$.

Let us give an illustration of this Theorem by considering again Sussmann's example (2.18), that we know to be STLC at 0. Theorem 2.25 for $k = 2$ states that it is however not $\mathrm{W}^{1,\infty}$-STLC, which means that the derivative of the required controls cannot be too small. One has to use, for example, strongly oscillating controls.

In a sense, this result suggests that the greater k is, the less strong is the obstruction to controllability constituted by B_k when it is outside of $S_1(0)$.

2.2.2 Thesis contributions : necessary condition of local controllability for a particular class of systems with two controls

The work conducted during my PhD, that is the subject of this section, states an extension of Theorem 2.20 in the case of control-affine systems having not one, but two controls. This work had led to an article submitted to *ESAIM:COCV*, reproduced in Chapter 3.

Consider a control-affine system like (2.8) with $m = 2$:

$$\dot{y} = f_0(y) + f_1(y)u_1 + f_2(y)u_2. \tag{2.22}$$

Assume that

$$f_0(0) = 0, f_2(0) = 0, \tag{2.23}$$

i.e., for all $u_2^{\mathrm{eq}} \in \mathbb{R}$, $(0, (0, u_2^{\mathrm{eq}}))$ is an equilibrium point: the second control u_2 cannot act on the system when at equilibrium position $y = 0$. I have studied the role played by this additional control in this system's controllability properties, in comparison with the scalar case.

The idea of studying systems of this form came from the study of magnetically controlled micro-swimmers – see section 2.4 and Part II. The system governing the dynamics of these swimmers is indeed of the form (2.22). I showed several results of controllability for these systems – see Theorems 2.55 and 2.60 and Chapters 5 and 6. The spirit of this section is to generalise the results obtained about the swimmers, by dealing with the controllability problem associated to System (2.22).

By analogy with the previous section, define:

— R_1 the space generated by the Lie brackets of f_0, f_1, f_2 containing at most f_1 ;

— $R_1(0)$ the subspace of $\mathbb{R}^n$ generated by the elements of R_1 evaluated at 0.

Recall also that the "bad" bracket B_1 is defined by $B_1 = [f_1, [f_0, f_1]]$.

My main result is the following necessary condition:

Theorem 2.27 ([GLMP19] and Chapter 3, Theorem 3.16)**.** *Assume $B_1(0) \notin R_1(0)$.*

1. *If $B_1(0) \in R_1(0) + \mathrm{Span}([f_1, [f_2, f_1]](0))$, let $\beta \in \mathbb{R}$ such that*

$$B_1(0) + \beta[f_1, [f_2, f_1]](0) \in R_1(0).$$

   Then, for all $u_2^{eq} \in \mathbb{R}$ such that $u_2^{eq} \neq \beta$, System (2.22) is not STLC at $(0, (0, u_2^{eq}))$.

2. *If $B_1(0) \notin R_1(0) + \mathrm{Span}([f_1, [f_2, f_1]](0))$, then, for all $u_2^{eq} \in \mathbb{R}$ and all $\alpha \geqslant 0$, System (2.22) is not α-STLC at $(0, (0, u_2^{eq}))$.*

According to Theorem 2.20, the "bad" bracket B_1 obstructs controllability if its value at 0 lies outside of $R_1(0)$. Theorem 2.27 stated right above completes this result by indicating that, for System (2.22) with two controls, the bracket $[f_1, [f_2, f_1]]$ can *neutralise* the bracket B_1, *i.e.* contribute to restore STLC even if $B_1(0) \notin R_1(0)$. This is possible only in case 1., *i.e.* when the value of these brackets at 0 share a common direction outside of $R_1(0)$, embodied by the constant β. The value of β is then the *only* value of u_2 around which System (2.22) may be STLC.

A striking illustration of this phenomenon can be found in the numerical simulations of the motion of a magnetic micro-swimmer presented on Figures 2.4 and 2.5 in section 2.4.3. As explained later on, the trajectories plotted on these figures are those of a system like System (2.22). They are chosen in order to roughly cover the accessible space around $(0, (0, u_2^{\mathrm{eq}}))$ for a given value of u_2^{eq}. As prescribed by Theorem 2.27, only the "critical" value β allows the accessible space to contain a neighbourhood of the origin. Else, the accessible space remains locally either to the right or to the left of the origin. This may be interpreted as the effect of the drift generated by the bad bracket $[f_1, [f_0, f_1]]$.

Śketch of proof of Theorem 2.27. The proof of this result is inspired of that of Theorem 2.20 conducted in [Sus83]. It is based on the study of a sort of asymptotic expansion of (2.22) around the equilibrium, called the *Chen-Fliess series* – see Definition 2.28 below.

Let us start with a few notations. Let $k \in \mathbb{N}$ and $I = (i_1, \ldots, i_k)$ a multi-index in $\{0, 1, 2\}^k$. We denote by $f_{i_1} f_{i_2} \ldots f_{i_k}$ the iterated composition of the fields $f_{i_1}, \ldots, f_{i_k}$ seen as differential operators.

Given $u = (u_1, u_2)$ a control in $\mathrm{L}^\infty([0, T], \mathbb{R})^2$, we define the iterated integral $\int_0^T u_I$ by

$$\int_0^T u_{i_k}(\tau_k) \int_0^{\tau_k} u_{i_{k-1}}(\tau_{k-1}) \int_0^{\tau_{k-1}} \ldots u_{i_2}(\tau_2) \int_0^{\tau_2} u_{i_1}(\tau_1) \mathrm{d}\tau_1 \mathrm{d}\tau_2 \ldots \mathrm{d}\tau_k,$$

with $u_0 = 1$ by convention.

Lastly, let y_u be the solution of (2.22) with $y(0) = 0$ and control u.

Définition 2.28. Let $\Phi : \mathbb{R}^n \to \mathbb{R}$ a real analytic function defined on a neighbourhood of 0, and $u = (u_1, u_2)$ a control in $\mathrm{L}^\infty([0, T], \mathbb{R})^2$. The Chen-Fliess series [Fli78, Fli75, Che57] associated to (2.22), Φ, u and T is defined by

$$\Sigma(u, f, \Phi, T) = \sum_I \left(\int_0^T u_I \right) (f_I \Phi)(0), \tag{2.24}$$

where the sum is made over all the multi-indices $I = (i_1, \dots, i_k)$ in $\{0,1,2\}^k$ with $k \in \mathbb{N}$.

Proposition 2.29 ([Sus83, Proposition 4.3, p. 698])**.** *For all $A > 0$, there exists $T_0(A) > 0$ such that the series (2.24) converges for all $T \leqslant T_0$ and u such that $\|u\|_{\mathrm{L}^\infty([0,T],\mathbb{R})^2} \leqslant A$, uniformly in u and T, to $\Phi(y_u(T))$, i.e.*

$$\Phi(y_u(T)) = \Sigma(u, f, \Phi, T). \tag{2.25}$$

The proof of Theorem 2.27 is structured as follows:

1. define local coordinates for the state y, and Φ a smart choice of real analytic function that maps y to one of these coordinates.
2. show that there exists $T_0 > 0$ such that, for all $T \in [0, T_0]$ and all control $u = (u_1, u_2)$ satisfying assumptions matching the right definition of STLC (STLC or α-STLC depending on the cases), one has
$$\Phi(y_u(T)) \geqslant 0. \tag{2.26}$$
3. deduce that the set $\{x \in \mathbb{R}^n | \Phi(x) < 0\}$ is not locally reachable for System (2.22), and therefore that this system is not locally controllable for the appropriate STLC definition.

Let p_1 be the term of the Chen-Fliess series $\Sigma(u, f, \Phi, T)$ associated to $I_2 = (1,1,0)$. It is precisely the term associated to the bad bracket B_1. Then, for a well-chosen function Φ and under the right assumptions on u and T stated at step 2 above, we show that

$$p_1 > 0 \quad \text{et} \quad |\Sigma(u, f, \Phi, T) - p_1| \leqslant p_1; \tag{2.27}$$

which allows to deduce (2.26) using (2.25).

The detailed calculations leading to (2.27) are developed in section 3.5 of Chapter 3.

2.2.3 Perspectives

Extensions of Theorem 2.27

Theorem 2.27 deals with the case for which $B_1(0)$ does not belong to $R_1(0)$. By analogy with the scalar case, one can naturally wonder which controllability properties System (2.22) has when $B_1(0)$ belongs to $R_1(0)$ and some higher-order brackets do not. In the scalar case, we have seen that Theorem 2.21 provides a result when the value at 0 of the bracket B_2 of order 5 lies outside of $R_1(0)$. I am working on stating a similar result for the case with two controls.

Theorem 2.27, that is about brackets of order 3, shows that only the "good" bracket $[f_1, [f_2, f_1]]$ can "neutralise" the "bad" bracket $[f_1, [f_0, f_1]]$, provided they share a common direction outside of $R_1(0)$.

At order 5, I established that there are two bad brackets that need to be neutralised: the bracket B_2 as well as the bracket $C_2 = [[f_2, f_1], [f_0, [f_2, f_1]]]$. The problem then splits into two cases, depending on whether the good brackets that can neutralise B_2 and C_2 are of lower order, or also of order 5.

Neutralisation by $[f_1, [f_2, f_1]]$

By analogy with Theorem 2.25 and our results, we conjecture that the bracket $[f_1, [f_2, f_1]]$ (and possibly others of higher order) could neutralise the bad brackets like B_2, C_2 or even B_k with $k > 2$, provided it shares with them a direction outside $R_1(0)$. This would allow System (2.22) to be $\mathrm{W}^{2k-3,\infty}$-STLC, which it cannot be in the scalar case according to Theorem 2.25. Example 3.27 in Chapter 3 supports this conjecture: it gives an example of a system which is $\mathrm{W}^{1,\infty}$-STLC and which satisfies:

— $B_1(0) \in R_1(0)$;

— $B_2(0) \notin R_1(0)$;

— $[f_1, [f_2, f_1]](0) = B_2(0)$.

Neutralisation by same-order brackets

If no lower-order bracket is able to neutralise B_2 and C_2, six brackets of order 5 can play a neutralising role, analogous to that of $[f_1, [f_2, f_1]]$ in Theorem 2.27. These brackets are given by

$$[[f_2, f_1], [f_0, [f_0, f_1]]], [[f_0, f_1], [f_0, [f_2, f_1]]], [[f_0, f_1], [f_2, [f_0, f_1]]],$$
$$[[f_2, f_1], [f_2, [f_0, f_1]]], [[f_0, f_1], [f_2, [f_2, f_1]]], [[f_2, f_1], [f_2, [f_2, f_1]]].$$

One still needs to determine precisely which assumptions on the values of these brackets at 0 allow to conclude that System (2.22) is locally controllable or not, and for which notion of controllability (STLC, α-STLC, *etc.*). My research on this subject is currently ongoing.

2.3 Controllability of parabolic equations with nonnegative state constraint

2.3.1 State of the art

The usual results of controllability ensure that a target can be reached from a starting point, without really knowing about the behaviour of the state between these two states. Yet, many systems describe physical phenomena with nonnegative variables (temperature, concentration...). Hence, it is natural to require to be able to control them while ensuring that the state remains nonnegative – or, more generally, in a given region of the state space. This problem has known growing interest in the last few years with promising advances: for example [LTZ18] for ODEs and [LTZ17, PZ17] for PDEs.

State constraints lead to interesting phenomena. Controllability with nonnegative state is not always possible, even for a system that is controllable without constraint [PZ17]. In the cases where it is possible, a positive minimal time may exist [LTZ17].

I will consider in this section parabolic PDEs featuring a second-order elliptic operator in space and the first time-derivative of the state. The evolution of this type of equations is characterised by phenomena of diffusion, regularisation and dissipation in the linear case, and possible finite-time blowup in the nonlinear case. For the heat equation, controllability [LR95, FI96] and controllability with nonnegative state [LTZ17] are solved.

My thesis' contribution is constituted by similar results for coupled linear parabolic systems. I established that, under good assumptions:

— if the diffusion coupling matrix is the identity matrix, then one can control to trajectories with nonnegative state (Theorem 2.38),

— if the diffusion coupling matrix is diagonalizable, then one can control to globally bounded trajectories while ensuring that state remains approximately nonnegative (Theorem 2.41).

The current section 2.3.1 briefly describes the state of the art on this domain. My results are displayed in section 2.3.2 and section 2.3.3 is dedicated to future perspectives. In particular, we give details on a possible extension to semilinear parabolic equations with internal control.

In all of section 1.3, d is a positive integer, Ω is a connected open bounded nonempty set of $\mathbb{R}^d$ with smooth boundary and ω a nonempty open subset of Ω. Δ denotes the Laplacian operator on Ω.

Control of heat equation

Let $T > 0$. Consider the heat equation with internal control and Neumann boundary conditions

$$\begin{cases} \partial_t y - \Delta y &= \mathbf{1}_\omega u & \text{on } (0,T)\times\Omega, \\ \frac{\partial y}{\partial n} &= 0 & \text{on } (0,T)\times\partial\Omega, \\ y(0,\cdot) &= y_0 & \text{on } \Omega. \end{cases} \tag{2.28}$$

Given $y_0 \in \mathrm{L}^\infty(\Omega)$, we call *free trajectory starting at* y_0 the solution of (2.28) with initial condition y_0 and control $u = 0$.

Definition 2.30 (Controllability to trajectories)**.** Let $T > 0$. System (2.28) is *controllable to trajectories* in time T if, for all $y_0, \bar{y}_0 \in \mathrm{L}^\infty(\Omega)$, there exists a control v in $\mathrm{L}^\infty((0,T)\times\omega)$ such that the solution y of (2.28) with initial condition y_0 and control v satisfies

$$y(T,\cdot) = \bar{y}(T,\cdot). \tag{2.29}$$

where $\bar{y}$ is the free trajectory starting at $\bar{y}_0$.

The following result was shown for $d = 1$ in [FR71] and for any d in [LR95, FI96].

Theorem 2.31. *System (2.28) is controllable to trajectories for all time $T > 0$.*

More recently, in [LTZ17], J. Lohéac, E. Trélat and E. Zuazua have shown that the equation is also controllable to positive steady states while keeping the state nonnegative. However, controllability in any time is not preserved: there exists a positive minimal time depending on the initial condition and target.

Theorem 2.32 ([LTZ17, Theorem 4.1])**.** *Let $y_0 \in \mathrm{L}^\infty(\Omega)$ non identically zero such that $y_0 \geqslant 0$, and y_1 a steady state of (2.28). Assume there exists $\zeta > 0$ such that $y_1 \geqslant \zeta$ sur Ω. Then, there exists $T > 0$ and a control $u \in \mathrm{L}^2((0,T)\times\omega)$ such that the solution y of (2.28) with initial condition y_0 and control u satisfies $y(T) = y_1$ and moreover*

$$\forall (t,x) \in (0,T)\times\Omega, y(t,x) \geqslant 0.$$

Remark 2.33. A similar result with boundary control is stated in [LTZ17] as well.

The proofs of my results (Theorems 2.38 and 2.41 below) are inspired by the proof of this theorem. For that reason, let us explain its main arguments. The proof is mainly based on the following lemma:

Lemma 2.34 ([LTZ17, Lemma 4.1])**.** *Let $y_0 \in \mathrm{L}^\infty(\Omega)$, $y_1 \in \mathbb{R}$ and $\tau > 0$. There exists $C(\tau) > 0$ and a control $u \in \mathrm{L}^2((0,\tau)\times\omega)$ such that the solution y of (2.28) with initial condition y_0 and control u satisfies $y(\tau) = y_1$ and moreover*

$$\forall t \in (0,T), \|y(t) - \tilde{y}(t)\|_{\mathrm{L}^\infty(\Omega)} \leqslant C(\tau)\|y_0 - y_1\|_{\mathrm{L}^2(\Omega)},$$

where $\tilde{y}$ the free solution of (2.28) starting at y_0.

Let $\tau > 0$, $\varepsilon > 0$ and y_0 and y_1 defined as in Theorem 2.32. We build the controlled trajectory in several steps:

1. starting at y_0, we let the system evolve without control. Then, the state converges in norm L^2 to the constant equilibrium $\bar{y}_0 = \frac{1}{|\Omega|}\int_\Omega y_0$ (we have $\bar{y}_0 > 0$ because y_0 is not identically zero). We wait long enough to reach a state y^0 very close (*i.e.* ε-close in L^2 norm) to $\bar{y}_0$.
2. control from y^0 to $\bar{y}_0$ in time τ. These two states are close to each other, so Lemma 2.34 ensures that the controlled trajectory stays close in norm L^∞ to the free trajectory starting at y^0, and therefore nonnegative for ε (defined at the previous step) small enough.
3. take N in $\mathbb{N}$ such that $N \geqslant \frac{|y_1 - \bar{y}_0|}{\varepsilon}$ and define a path of N steady states by

$$\forall k \in \{1,\dots,N\}, y^k = (1 - \frac{k}{N})\bar{y}_0 + \frac{k}{N}y_1. \tag{2.30}$$

   Then, define N controls steering from $\bar{y}_0$ to y^1 then, for $k \in \{1,\dots,N\}$, from y^k to y^{k+1} in time τ, and use at each step Lemma 2.34 to ensure that the controlled trajectory between y^k and y^{k+1} stays close in norm L^∞ to the free trajectory starting at y^k, and therefore nonnegative for ε small enough.

Finally, concatenate the controls defined at steps 1, 2 and 3: the obtained control steers the system from y_0 to y_1 while keeping the state nonnegative.

Remark 2.35. The method used by the authors of [LTZ17] at step 3 of this proof, that consists in going towards the target trajectory by a path made of successive equilibria close to each other, is called the "staircase" method. Combining the closeness of these steps with a lemma of the form of Lemma 2.34, one can make sure that the controlled trajectory remains close to the steps, which allows to conclude that the state remains nonnegative.

I use the staircase method in the following to show similar results in the case of a coupled parabolic system. For Theorem 2.38, the "staircase" is made of trajectories that are not equilibria (see Figure 2.1), but the spirit of the proof remains unchanged.

Control of linear parabolic systems

Let us now study the controllability properties of several coupled parabolic equations. Let R be a second-order self-adjoint elliptic operator given by

$$R = \sum_{i,j=1}^{d} \partial_i (r_{ij}(x)\partial_j) + c(x), \tag{2.31}$$

with $c \in \mathrm{L}^\infty(\Omega)$, and $r_{ij} \in \mathrm{W}^{1,\infty}(\Omega)$ for $i, j \in \{1, \dots, d\}$ satisfying

$$r_{ij}(x) = r_{ji}(x) \tag{2.32}$$

and the ellipticity condition

$$\exists \alpha > 0, \forall \xi \in \mathbb{R}^d, \sum_{i,j=1}^{d} r_{ij}(x)\xi_i\xi_j \geqslant a_0|\xi|^2 \tag{2.33}$$

almost everywhere on Ω.

Let n, m be positive integers. Consider the linear system with Neumann boundary condition

$$\begin{cases} \partial_t Y - DRY &= AY + Bu\mathbf{1}_\omega \quad \text{on } (0,T)\times\Omega; \\ \frac{\partial Y}{\partial n} &= 0 \quad \text{on } (0,T)\times\partial\Omega; \\ Y(0,\cdot) &= Y_0(\cdot) \quad \text{on } \Omega. \end{cases} \tag{2.34}$$

with $A \in \mathcal{M}_n(\mathbb{R})$, $B \in \mathcal{M}_{n,m}(\mathbb{R})$, and $D \in \mathcal{M}_n(\mathbb{R})$ diagonalizable.

Being a self-adjoint operator, $-R$ has got a real sequence $(\lambda_p)_{p\in\mathbb{N}}$ of eigenvalues satisfying

$$0 = \lambda_0 < \lambda_1 \leqslant \lambda_2 \leqslant \dots, \quad \lim_{p\to+\infty} \lambda_p + \infty,$$

associated to eigenfunctions $(\phi_p)_{p\in\mathbb{N}}$ constituting an orthonormal basis of $\mathrm{L}^2(\Omega)$.

Given two matrices A in $\mathcal{M}_n(\mathbb{R})$ and B in $\mathcal{M}_{n,m}(\mathbb{R})$, we denote by

$$[A|B] = \left(B \mid AB \mid \dots \mid A^{n-1}B\right). \tag{2.35}$$

the Kalman matrix associated to A and B.

Controllability of System (2.34) depends on a Kalman-type condition (see Theorem 2.3.

Theorem 2.36 ([AKBDGB09b])**.** *System (2.34) is controllable to trajectories for all time if and only if, for all p in $\mathbb{N}$,*

$$\operatorname{rank}\left[(-\lambda_p D + A)|B\right] = n. \tag{2.36}$$

Remark 2.37. In the case $D = I_n$, condition (2.36) simply becomes

$$\operatorname{rank}\left[A|B\right] = n. \tag{2.37}$$

2.3.2 Thesis contributions

During my PhD, I studied controllability properties of System (2.34) between two positive states with nonnegative state constraint. As seen above, Theorem 2.32 gives a result of this type for the heat equation. My contribution consists in two similar results for System (2.34): Theorems 2.38 and 2.41 below.

General case: D diagonalizable

System (2.34) is not necessarily dissipative (in particular, the coupling between components of Y can lead to oscillationg behaviours), therefore we cannot wait for Y to converge to a constant steady state as in the proof of Theorem 2.32.

Under reasonable assumptions, controllability with (almost) nonnegative state can however be obtained. In the following, for $r \geqslant 0$, $\mathrm{H}^r(\Omega)$ denotes the Sobolev space $W^{r,2}(\Omega)$.

Theorem 2.38 (Chapter 4, Theorem 4.10)**.** *Assume the following conditions hold :*

1. *A is quasipositive, i.e.*

$$\forall i, j \in \{1, \dots, n\}, i \neq j \Rightarrow a_{i,j} \geqslant 0, \tag{2.38}$$

2. *A is such that*

$$\forall \xi \in \mathbb{R}^n, \langle A\xi, \xi \rangle \leqslant 0, \tag{2.39}$$

3. *the eigenvalues of $-R$ are such that we have (2.36).*

Let $\tilde{Y}$ and Y^{f} in $\mathrm{L}^\infty(\mathbb{R}_+ \times \Omega)^n$ be trajectories of (2.34), starting respectively at Y_0 and Y_0^{f} in $\mathrm{L}^\infty(\Omega)^n$ and such that $Y_0 \geqslant 0$ and $Y_0^{\mathrm{f}} \geqslant 0$. Let

$$\zeta = \min\left(\inf_{(\mathbb{R}_+ \times \Omega)^n} Z(t,x), \inf_{(\mathbb{R}_+ \times \Omega)^n} Y(t,x) \right) \geqslant 0.$$

Then, for all $\varepsilon > 0$, there exists $T > 0$ and $u \in (\mathrm{L}^2((0,T), \mathrm{H}^r(\omega)) \cap \mathrm{H}^s((0,T), \mathrm{L}^2(\omega)))^m$ with r, s large enough (in a sense that is precisely defined in Chapter 4) such that the solution Y of (2.34) with initial condition Y_0 and control u satisfies

$$Y(T, \cdot) = Y^{\mathrm{f}}(T, \cdot), \tag{2.40}$$

and, for all t in $[0,T]$,

$$Y(t, \cdot) \geqslant \zeta - \varepsilon. \tag{2.41}$$

Remark 2.39. In particular, if $\zeta > 0$, one can control towards Y^{f} while preserving nonnegativity of the state.

Remark 2.40. The quasipositivity condition (2.38) ensures that the free trajectories of System (2.34) remain nonnegative [Pie10, Lemma 1.1]. Condition (2.39) ensures that the free trajectories are globally bounded.

The proof of Theorem 2.38 is developed in Chapter 4. It is based on the staircase method described above for Theorem 2.32. Starting from the free trajectory $\tilde{Y}_0$ with initial

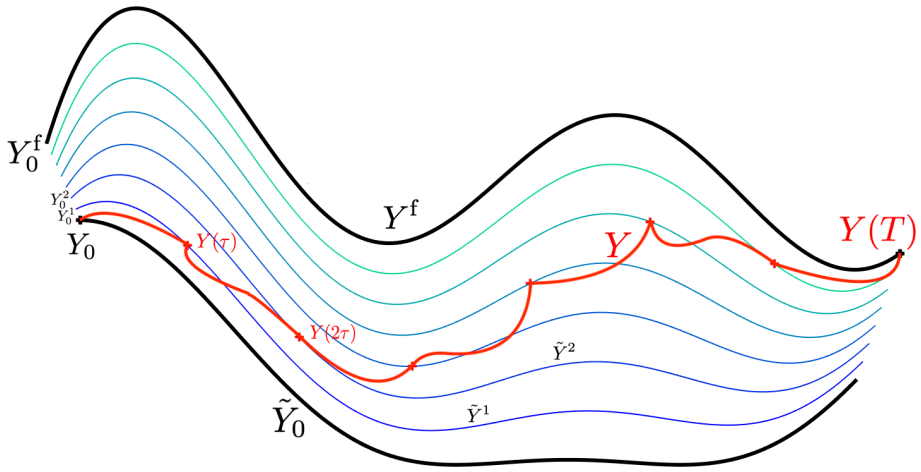

Figure 2.1 – Construction of the controlled trajectory using staircase method for proof of Theorem 2.38.

condition Y_0, we steer the solution towards Y^{f}, going through a path made of free nonnegative trajectories "close" to each other (see Figure 2.1). We ensure that the controlled trajectory remains close to these free trajectories, and therefore approximately nonnegative, thanks to a lemma similar to Lemma 2.34 : see Chapter 4, Lemma 4.13.

Case $D = I_n$

In this particular case, the conclusion of Theorem 2.38 is slightly improved.

Theorem 2.41 (Chapter 4, Theorem 2.41)**.** *Assume the following conditions holds :*

1. $D = I_n$*;*
2. A *is quasipositive (see* (2.38)*),*
3. A *and* B *satisfy the Kalman condition* (2.37)*.*

Let Y_0*,* Y_0^{f} *in* $\mathrm{L}^\infty(\Omega)^n$ *and* Y^{f} *the trajectory starting at* Y_0^{f}*. Assume that*

$$Y_0 \geqslant 0, Y_0^{\mathrm{f}} \geqslant 0 \tag{2.42}$$

and that none of the components of Y_0 *and* Y_0^{f} *is a.e. zero on* Ω*. Then, there exists* $T > 0$ *and* $u \in (\mathrm{L}^2((0,T), \mathrm{H}^r(\omega)) \cap \mathrm{H}^s((0,T), \mathrm{L}^2(\omega)))^m$ *with* r, s *large enough (in a sense that is precisely defined in Chapter 4) such that the solution* Y *of* (2.34) *with initial condition* Y_0 *and control* u *satisfies*

$$Y(T, \cdot) = Y^{\mathrm{f}}(T, \cdot), \tag{2.43}$$

and, for all t *in* $[0, T]$*,*

$$Y(t, \cdot) \geqslant 0. \tag{2.44}$$

The proof of this theorem is given in detail in Chapter 4. We present the main arguments here. The first step is to perform a change of variables that makes System (2.34) uncoupled.

Indeed, for $t \geqslant 0$, let

$$Z = e^{-tA}Y. \tag{2.45}$$

Note that, if Y is a solution of System (2.34), then Z is a solution of system

$$\begin{cases} \partial_t Z - RZ &= e^{-tA}Bu\mathbf{1}_\omega & \text{on } (0,T)\times\Omega; \\ \frac{\partial Z}{\partial n} &= 0 & \text{on } (0,T)\times\partial\Omega; \\ Z(0,\cdot) &= Y(0,\cdot) & \text{on } \Omega. \end{cases} \tag{2.46}$$

The idea is to show that there exists $T>0$ and $u \in (\mathrm{L}^2((0,T),\mathrm{H}^r(\omega)) \cap \mathrm{H}^s((0,T),\mathrm{L}^2(\omega)))^m$ such that the solution Z of (2.46) with initial condition Y_0 and control u satisfies

$$Z(T,\cdot) = Z^{\mathrm{f}}(T,\cdot), \tag{2.47}$$

and, for all t in $[0,T]$,

$$Z(t,\cdot) \geqslant 0. \tag{2.48}$$

According to (2.45) and (2.46), such a control u is such that the solution Y of (2.34) with initial condition Y_0 satisfies (2.43) and (2.44).

Without control, System (2.46) is simply made of n uncoupled parabolic equations. Using a spectral expansion, it can be shown that the trajectories $\tilde{Z}_0$ and Z^{f}, starting respectively at Y_0 at Y_0^{f}, converge in L^2 norm (and any other norm) to

$$\bar{Z}_0 = \frac{1}{|\Omega|}\int_\Omega Y_0 \quad \text{and} \quad \bar{Z}_0^{\mathrm{f}} = \frac{1}{|\Omega|}\int_\Omega Y_0^{\mathrm{f}}.$$

We know from assumption (2.42) that Y_0 and Y_0^{f} are nonnegative and none of their components is everywhere zero. Therefore, all the components of $\bar{Z}_0$ and $\bar{Z}_0^{\mathrm{f}}$ are positive. Therefore there exists $\zeta>0$ such that $\bar{Z}_0 \geqslant \zeta$ and $\bar{Z}_0^{\mathrm{f}} \geqslant \zeta$.

Let $\tau>0$ and $\delta>0$. We build the control u in several steps (that resembles those used for the proof of Theorem 2.32) :

1. Define a time T_0 such that, for all $t \geqslant T_0$,

   $$\|\tilde{Z}_0(t) - \bar{Z}_0\|_{\mathrm{L}^2(\Omega)^n} \leqslant \delta \quad \text{and} \quad \|Z^{\mathrm{f}}(t) - \bar{Z}^{\mathrm{f}}\|_{\mathrm{L}^2(\Omega)^n} \leqslant \delta,$$

   and take null control $u=0$ on $[0,T_0]$.

2. Control from $\tilde{Z}_0(T_0)$ to $\bar{Z}_0$ in time τ.

3. Control from $\bar{Z}_0$ to $\bar{Z}_0^{\mathrm{f}}$ using the staircase method, *i.e.* going through N constant steady states "close" to each other, with every step lasting time τ.

4. Control from $\bar{Z}_0^{\mathrm{f}}$ to the trajectory Z^{f} in time τ.

At each step, one ensures that the controlled trajectory Z remains nonnegative thanks to a lemma similar to Lemma 2.34 (see Chapter 4, Lemma 4.15). Finally, define $T = T_0 + (N+2)\tau$ and $u \in (\mathrm{L}^2((0,T),\mathrm{H}^r(\omega)) \cap \mathrm{H}^s((0,T),\mathrm{L}^2(\omega)))^m$ by concatenating the controls defined at steps 1, 2, 3 and 4.

This control u is such that Z satisfies (2.47) and (2.48). Hence Y satisfies (2.43) and (2.44).

2.3.3 Perspectives

Nonnegative state control

A possible improvement of Theorem 2.38 would be to replace ε by 0 in equation (2.41). Intuitively, it seems doable, especially if the target trajectory Z remains positive for all time. My research on this subject is ongoing.

Controllability of semilinear parabolic equations with nonnegative state constraint

I also studied the case of a semilinear parabolic equation, *i.e.* the heat equation (2.28) with an additional nonlinear term $f : \mathbb{R} \to \mathbb{R}$ depending on the state:

$$\begin{cases} \partial_t y - \Delta y + f(y) &= \mathbf{1}_\omega u & \text{on } (0,T)\times\Omega, \\ y &= 0 & \text{on } (0,T)\times\partial\Omega, \\ y(0,\cdot) &= y_0 & \text{on } \Omega. \end{cases} \tag{2.49}$$

This type of systems behaves in a less friendly way than the linear heat equation. Indeed, if f grows to fast, the solution may experience finite-time blowup. In this case, an interesting question is whether it is possible to control the equation such that the solution is globally defined in time [LB20]. In more favourable cases in which the free trajectories are globally defined in time, the controllability of trajectories is still more difficult to obtain. Indeed, in the linear case, one can always reduce the cost of the control (*i.e.* its norm) by controlling in larger time. In the nonlinear case, this is not true anymore.

Let us define two other notions of controllability :

Definition 2.42 (Null-controllability)**.** Let $T > 0$. System (2.28) is *null-controllable* in time T if, for all $y_0 \in \mathrm{L}^2(\Omega)$, there exists a control u in $\mathrm{L}^\infty((0,T)\times\omega)$ such that the solution y of (2.28) with initial condition y_0 and control u satisfies

$$y(T,\cdot) = 0. \tag{2.50}$$

Definition 2.43 (Approximate controllability)**.** Let $T > 0$. System (2.28) is *approximately controllable* in time T if, for all $\varepsilon > 0$, and $y_0, y_1 \in \mathrm{L}^2(\Omega)$, there exists a control u in $\mathrm{L}^\infty((0,T)\times\omega)$ such that the solution y of (2.28) with initial condition y_0 and control u satisfies

$$\|y(T,\cdot) - y_1\|_{\mathrm{L}^2(\Omega)} \leqslant \varepsilon. \tag{2.51}$$

Remark 2.44. Controllability to trajectories (Definition 2.30 above) implies null-controllability. The converse is false in general, unless the equation is linear. Indeed, define $y^* = y - \bar{y}$ to immediately deduce that both notions are equivalent.

Moreover, in the linear case, assume that the following backwards uniqueness property holds:

$$\left.\begin{cases} \partial_t y - \Delta y &= \mathbf{1}_\omega u & \text{on } (0,T)\times\Omega, \\ \frac{\partial y}{\partial n} &= 0 & \text{on } (0,T)\times\partial\Omega, \\ y(T,\cdot) &= 0 & \text{on } \Omega. \end{cases}\right\} \Rightarrow y \equiv 0,$$

Then, the set of extremities of trajectories at time T is dense in $\mathrm{L}^2(\Omega)$, so null-controllability implies approximate controllability.

E. Fernández-Cara and E. Zuazua showed in [FCZ00] conditions on f to obtain null-controllability of System (2.49) :

Theorem 2.45 ([FCZ00, Theorems 1.2, 1.4])**.** *Let $q = 1 + \frac{4}{d}$. Assume the nonlinearity f satisfies the following conditions :*

1. *f is locally Lipschitz-continuous ;*
2. *$\exists C > 0, \forall s \in \mathbb{R}, |f'(s)| \leqslant C(1 + |s|^q)$ p.p. ;*
3. *$\frac{f(s)}{|s| \ln^{\frac{3}{2}}(1+|s|)} \to 0$ when $|s| \to +\infty$.*

Assume moreover that there exists (at least) one globally defined bounded solution to (2.49). Then (2.49) is null-controllable and approximately controllable.

Remark 2.46. Condition 3 is crucial for controllability. Actually, if there exists $p > 2$ such that

$$|f(s)| \sim |s| \ln^p(1 + |s|) \quad \text{when} \quad |s| \to +\infty, \tag{2.52}$$

then System (2.49) may not be null-controllable in any time ([FCZ00, Theorem 1.1]).

In the intermediary case $p \in]\frac{3}{2}, 2]$ recently dealt with by K. Le Balc'h [LB20], one has local null-controllability (*i.e.* null-controllability for initial condition close to zero in some sense) in large time, and blowup controllability (*i.e.* one can find a control so that the solution is globally defined in time).

As for the heat equation, some results have recently be found on controllability of these equations with nonnegative state constraint. For an equation *with boundary control*, some results have been found by D. Pighin and E. Zuazua in [PZ17]: consider the system

$$\begin{cases} \partial_t y - \Delta y + f(y) &= 0 & \text{on } (0,T) \times \Omega, \\ y &= \mathbf{1}_\Gamma u & \text{on } (0,T) \times \partial\Omega, \\ y(0,\cdot) &= y_0 & \text{on } \Omega, \end{cases} \tag{2.53}$$

where Γ is a non empty subset of $\partial\Omega$, relatively open with respect to $\partial\Omega$.

Theorem 2.47 ([PZ17, Theorems 1.2 et 1.3])**.** *1. (Steady-state controllability). Let y_0 and y_1 in $\mathrm{L}^\infty(\Omega)$ be two positive steady states of (2.53). Assume y_0 and y_1 are connected, i.e. there exists a continuous map $\gamma = [0,1] \to \mathrm{L}^\infty(\Omega)$ such that $\gamma(0) = y_0$ and $\gamma(1) = 1$. Moreover, assume that for all $s \in [0,1]$, $\gamma(s) > 0$.*
Then, there exists a time $T > 0$ and a control $u \in \mathrm{L}^\infty((0,T) \times \Gamma)$ such that the solution y of (2.53) with initial condition y_0 satisfies $y(T) = y_1$ and, for all t in $(0,T)$, $y(t) \geqslant 0$.

2. *(Controllability in the dissipative case). In the dissipative case ($sf(s) \geqslant 0$ for all $s \in \mathbb{R}$), System (2.53) is controllable to trajectories in large time with nonnegative state.*

The proof of the first point of Theorem 2.47 uses the staircase method, which explains the necessity of assuming that they are connected through γ (unlike in the linear case, a simple linear combination of y_0 and y_1 is not necessarily an equilibrium of System (2.53)).

This theorem establishes results in rather specific cases of System (2.53): connected steady states and dissipative case. On the other hand, it is also shown in [PZ17, Proposition 1] an example in which the system is not controllable with nonnegative state if none of these two conditions hold.

These results are valid only for boundary control. The behaviour of System (2.49) might be different with internal control. One of my objectives is to study what happens in the internal control case, in order to state a result similar to Theorem 2.47 or a counterexample to constrained controllability for System (2.49).

However, even in a favourable case where the nonlinearity f is globally Lipschitz or a linear potential ($f(y) = ay, a \in \mathbb{R}$), the staircase method does not work in general, because the trajectories might move away from each other exponentially in time. Therefore, small fixed-size steps do not ensure that the controlled trajectory will eventually reach the target.

At the current state of my research, I conjecture that System (2.49) with globally Lipschitz nonlinearity is not controllable with nonnegative state constraint in general, and I am working on building a counterexample.

2.4 Micro-swimming

2.4.1 Context

Propulsion at low Reynolds number

Swimming is the action of moving inside a fluid by changing form. At our scale, swimming strategies generally appeal to the *inertia* of the fluid. A classic example is that of the scallop, which opens it shell slowly and closes it quickly, thereby using the inertia to produce a net movement in the opposite direction of its opening. The situation is very different for a microscopic organism or robot. The Reynolds number, which measures the ratio between the inertial effects and the viscous effects, is proportional to the characteristic length of the object under consideration, and has a value of approximately 10^3 to 10^4 for a human swimming in water. For a micro-organism, like a sperm cell, which measures a few tens to a few hundreds of micrometres, this number is much smaller than 1 (10^{-4} to 10^{-5}); in that case, we are in a regime called *Stokes flow* where the inertial effects are negligible in relation to the viscous effects. In a presentation [Pur77] which is considered to have founded the field of micro-swimming, Purcell calls this phenomenon the *scallop theorem*: at low Reynolds number, reversible movements leads to immobility. This peculiar Stokes regime justifies the fact that micro-swimming constitutes a field in its own right.

Micro-swimmer robots

One of the main goals of the study of micro-swimming is to conceive robots that are capable of moving efficiently at this small scale. Such robots would offer numerous applications in the biomedical field: delivery robots [CHS+17] capable of delivering medication to a precise location in the human body by moving within blood vessels or through tissues; sensor robots [BKJH+11] that collect information at locations that are inaccessible to ordinary sensors; cleaning robots [WLdÁ+15] which capture undesirable substances (such as those which are toxic to the organism) and eliminate them or transport them elsewhere; surgical robots [LRB+09] that could perform little intrusive surgical acts.

In all cases, such micro-swimmers have to be able to move efficiently, rapidly and precisely. Different strategies of propulsion can be considered: propulsion thanks to a chemical reaction [SMBU+09], a magnetic field [PZN13, GSM+10, GF09], a biological micro-swimmer [MMSC+15], an acoustic pressure field [GGOS+13], a temperature gradient, *etc.*. Figure 2.2 presents a few examples.

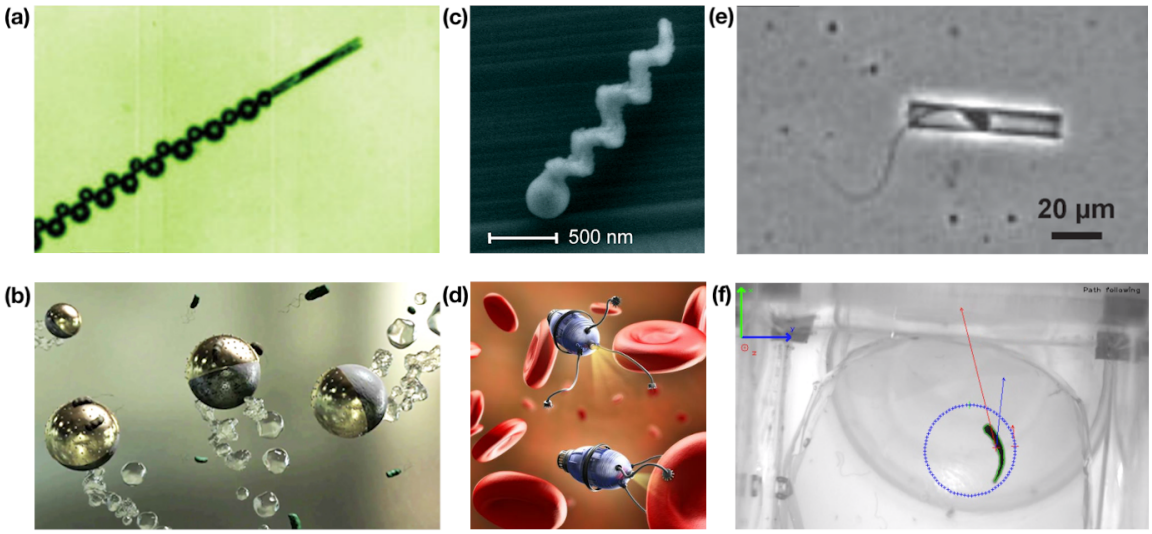

Figure 2.2 – Some examples and illustrations of swimming micro-robots. (a) Chemical robot powered by the production of gas bubbles [SMBU+09]. (b) Artist's view of chemical robots called "Janus spheres" [GLA05]. (c) Magnetic robot in the shape of a corkscrew [PZN13]. (d) Artist's interpretation of surgical micro-robots. (e) Biological robot powered by a spermatozoid which is captured in a magnetic tube, enabling the choice of the desired direction [MMSC+15]. (f) Magnetic robot of the type that is studied in the thesis, here forced to swim along a circle [AFPRG19].

See [Wan13, LdÁG+17, PF18] for a more complete review of the state of the art in terms of swimming micro-robots and their applications.

Controllability

At low Reynolds number, the dynamic of a generic swimmer is expressed as a system of ordinary differential equations, linearly dependent on the derivatives of the position parameters. This system can be seen as a control system, and studied from the controllability point of view.

The first works in this field [SW89] suppose that the control is given by the swimmer's deformation. Purcell's swimmer, for example, consists of three segments held together by elastic links. The links move with respect to each other in order to produce a displacement. The magnetic version of this robot will be studied in the following. Other studies about controllability of swimmers by deformation are carried out in [MTT07, Loh12, LM14, LST13, ADGZ13, GMZ13, LST13]. In this case, dynamics are governed by a driftless control-affine system. Then, strong results of controllability due to sub-Riemannian geometry, such as the Rashevskii-Chow theorem, become available. In this context, numerous results of optimal control have also been obtained: see for example [TH07, ADL08, ADH+13, CGM14].

When the deformation of the swimmer is indirectly acted upon *via* a magnetic field, like in the following, controllability can be more difficult to obtain. This can be understood intuitively: in this case, there are only two or three controls (the components of the magnetic field in 2D or 3D) that act on all of the position and shape parameters of the swimmer. The associated control system presents a drift. As explained in section 2.2, controllability results for systems with a drift are less powerful in general and no necessary and sufficient condition of local controllability is known.

I have studied the controllability of a planar elastic micro-robot model, controlled with an exterior magnetic field [GO14, ADGZ15]. The controllability of the two-link magnetic swimmer has first been studied in [GP17]. The authors show that the standard techniques (study of the linearised system, Sussmann condition) fail to establish the local controllability of the robot around its equilibrium position. They obtain a "weak" local controllability result (α-STLC, see Definition 2.6) by adapting Jean-Michel Coron's [Cor07, Chapter 6] return method, which was first conceived to establish local controllability of PDEs.

During my PhD, I have introduced a new approach, inspired by Sussmann's work [Sus83], which consists, in a nutshell, in the construction of a smart expansion of the controlled solution in the neighbourhood of the equilibrium position. As a result, I have been able to show the non-controllability of the two link magnetic swimmer at the zero equilibrium [GLMP18]. I have then generalised this approach in order to deduce the more general necessary condition for local controllability presented in section 2.2 (Theorem 2.27), and to resolve in a more complete manner the question of local controllability of two- and three-link swimmers around their equilibria. Theorems 2.55 et 2.60 show that small-time local controllability of such swimmers is only possible if the magnetic field applied to the robot remains close to a specific constant value, which depends on the magnetisation parameters of the robot.

Section 2.4.2 briefly describes the model, and section 2.4.3 presents the obtained results of controllability for the swimmers, and illustrates these results by numerical simulations. Lastly, section 2.4.4 is dedicated to future perspectives.

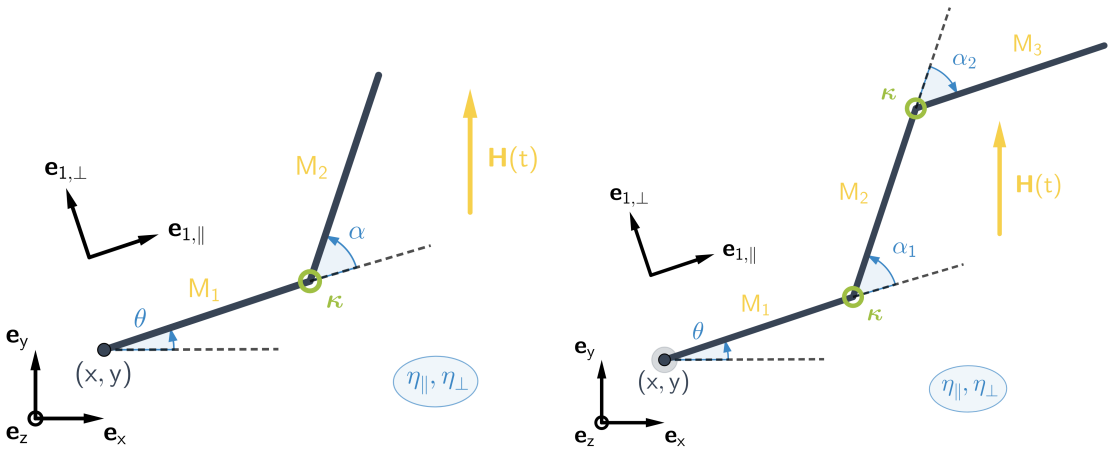

Figure 2.3 – Parametrisation of the two- and three-link swimmers.

The results of this section have been published in [GLMP18] and [Mor19], and are reproduced in Chapters 5 et 6.

2.4.2 Magnetic micro-swimmer model

In this section, we study a magnetic micro-swimmer robot made of two or three rigid links, connected by torsional springs. The swimmers' movement is assumed to be planar. Figure 2.3 displays a diagram of the robots.

When this does not imply any ambiguity, some notations are identical for the two- and three-link swimmers in the following.

The links are noted S_1 and S_2 for the two-link swimmer and S_1, S_2, S_3 for the three-link swimmer. Each segment has length ℓ and hydrodynamic coefficients $\eta_{\|}$ and $\eta_{\perp}$, with $\eta_{\perp} > \eta_{\|} > 0$. Moreover, each segment S_i is seen as a magnetic dipole in its own direction, with a magnetic moment M_i. Consecutive segments are connected by elastic joints, modelled as torsional springs of stiffness κ.

The swimmers move in the reference plane $(O, \mathbf{e}_x, \mathbf{e}_y)$. Let $\mathbf{e}_z = \mathbf{e}_x \times \mathbf{e}_y$. The first link S_1 has its endpoint at coordinates $\mathbf{x} = (x, y)$ and is oriented at an angle θ with respect to $\mathbf{e}_x$. For the two-link swimmer, we denote by α the angle between S_1 and S_2. For the three-link swimmer, we respectively denote by α_1 and α_2 the angle between S_1 and S_2 and the angle between S_2 and S_3. Lastly, we denote by $(\mathbf{e}_{i,\|}, \mathbf{e}_{i,\perp})$ the orthonormal basis associated to segment S_i.

Hence, the two-link swimmer is fully described by the four variables $\mathbf{z}_2 = (x, y, \theta, \alpha)^T$ and the three-link swimmer by the five variables $\mathbf{z}_3 = (x, y, \theta, \alpha_1, \alpha_2)^T$. As a complement, we occasionally write $\mathbf{x}_i$ for the position of the extremity of segment S_i for $i = 1, 2, 3$.

The swimmer is submitted to a uniform in space, time-varying magnetic field, denoted by $\mathbf{H}(t)$. We decompose it in the moving basis associated to S_1 : $\mathbf{H}(t) = (H_{\|}(t), H_{\perp}(t))$.

The magnetic field $\mathbf{H}(t)$ induces a torque in each of the segments. Moreover, as it moves, the swimmer experiences hydrodynamic drag, as well as elastic restoring torques at the joints between the segments.

1. **Elasticity**: the torsional springs which connect the swimmer segments exert a torque

$\mathbf{T}^{\text{el}}$ proportional to the stiffness κ and the shape angles α_1 and α_2. Hence the torque $\mathbf{T}_2^{\text{el}}$ exerted on S_2 is given by $\mathbf{T}_2^{\text{el}} = \kappa\alpha_1\mathbf{e}_z$ and the torque $\mathbf{T}_3^{\text{el}}$ exerted on S_3 is given by $\mathbf{T}_3^{\text{el}} = \kappa\alpha_2\mathbf{e}_z$.
The springs tend to get the swimmer back to a straight shape, in which S_1, S_2 and S_3 are aligned.

2. **Magnetism**: The magnetic field exerts a torque $\mathbf{T}_i^m$ on S_i which is proportional to its magnetisation coefficient M_i: $\mathbf{T}_i^m = M_i\mathbf{e}_{i,\parallel} \times \mathbf{H}$.
3. **Hydrodynamics**: We use the Resistive Force Theory [GH55] to model this interaction. In this approximation, the drag force per unit of length is proportional to the velocity and to the hydrodynamics coefficients $\eta_\parallel$ and $\eta_\perp$. The hydrodynamic force exerted on segment S_i is called $\mathbf{F}_i^h$ and the hydrodynamic torque with respect to a given point $\mathbf{x}_0$ is called $\mathbf{T}_{i,\mathbf{x}_0}^h$. The detailed expressions of $\mathbf{F}_i^h$ and $\mathbf{T}_{i,\mathbf{x}_0}^h$ are displayed in Chapter 6, section 6.2.

Since we are at low Reynolds number, inertia can be neglected. Therefore, balance of forces and torques holds at all time [LP09]. For the two-link swimmer, we obtain four equations by writing :

— balance of forces on the swimmer projected on axis (Ox) and (Oy),
— balance of torques on the swimmer at point $\mathbf{x}$,
— balance of torques on segment S_2 at point $\mathbf{x}_2$,

which yields the following system:

$$\left\{\begin{array}{lll} \mathbf{F}_1^h + \mathbf{F}_2^h & & = 0, \\ \mathbf{T}_{1,\mathbf{x}}^h + \mathbf{T}_{2,\mathbf{x}}^h & + \mathbf{T}_1^m + \mathbf{T}_2^m & = 0, \\ \underbrace{\mathbf{T}_{2,\mathbf{x}_2}^h}_{\text{hydrodynamics}} & + \underbrace{\mathbf{T}_2^m}_{\text{magnetism}} + \underbrace{\mathbf{T}^{\text{el}}}_{\text{elasticity}} & = 0. \end{array}\right. \tag{2.54}$$

For the three-link swimmer, we obtain five equations by writing :

— balance of forces on the swimmer projected on axis (Ox) and (Oy),
— balance of torques on the swimmer at point $\mathbf{x}$,
— balance of torques on the set $\{S_2 + S_3\}$ at point $\mathbf{x}_2$,
— balance of torques on segment S_3 at point $\mathbf{x}_3$,

which yields the following system:

$$\left\{\begin{array}{lll} \mathbf{F}_1^h + \mathbf{F}_2^h + \mathbf{F}_3^h & & = 0, \\ \mathbf{T}_{1,\mathbf{x}}^h + \mathbf{T}_{2,\mathbf{x}}^h + \mathbf{T}_{3,\mathbf{x}}^h & + \mathbf{T}_1^m + \mathbf{T}_2^m + \mathbf{T}_3^m & = 0, \\ \mathbf{T}_{2,\mathbf{x}_2}^h + \mathbf{T}_{3,\mathbf{x}_2}^h & + \mathbf{T}_2^m + \mathbf{T}_3^m + \mathbf{T}_2^{\text{el}} & = 0, \\ \underbrace{\mathbf{T}_{3,\mathbf{x}_3}^h}_{\text{hydrodynamics}} & + \underbrace{\mathbf{T}_3^m}_{\text{magnetism}} + \underbrace{\mathbf{T}_3^{\text{el}}}_{\text{elasticity}} & = 0. \end{array}\right. \tag{2.55}$$

Let $R_{\theta,2} = \left(\begin{array}{cc|c} \cos\theta & \sin\theta & 0 \\ -\sin\theta & \cos\theta & 0 \\ \hline 0 & 0 & I_2 \end{array}\right)$ et $R_{\theta,3} = \left(\begin{array}{cc|c} \cos\theta & \sin\theta & 0 \\ -\sin\theta & \cos\theta & 0 \\ \hline 0 & 0 & I_3 \end{array}\right)$.

Expressing every contribution inside systems (2.54) and (2.55) with respect to the position variables, their time derivative and the system parameters, we get the following differential systems:

— for the two-link swimmer:

$$A_2(\alpha)R_{-\theta,2}\dot{\mathbf{z}}_2 = \begin{pmatrix} 0 \\ 0 \\ 0 \\ -\kappa\alpha \end{pmatrix} + H_{\parallel} \begin{pmatrix} 0 \\ 0 \\ M_2 \sin\alpha \\ M_2 \sin\alpha \end{pmatrix} - H_{\perp} \begin{pmatrix} 0 \\ 0 \\ M_1 + M_2 \cos\alpha \\ M_2 \cos\alpha \end{pmatrix}, \tag{2.56}$$

— for the three-link swimmer:

$$\begin{aligned} A_3(\alpha_1,\alpha_2)R_{-\theta,3}\dot{\mathbf{z}}_3 \quad = & \begin{pmatrix} 0 \\ 0 \\ 0 \\ -\kappa\alpha_1 \\ -\kappa\alpha_2 \end{pmatrix} + H_{\parallel} \begin{pmatrix} 0 \\ 0 \\ M_2 \sin\alpha_1 + M_3 \sin(\alpha_1+\alpha_2) \\ M_2 \sin\alpha_1 + M_3 \sin(\alpha_1+\alpha_2) \\ M_3 \sin(\alpha_1+\alpha_2) \end{pmatrix} \\ & - H_{\perp} \begin{pmatrix} 0 \\ 0 \\ M_1 + M_2 \cos\alpha_1 + M_3 \cos(\alpha_1+\alpha_2) \\ M_2 \cos\alpha_1 + M_3 \cos(\alpha_1+\alpha_2) \\ M_3 \cos(\alpha_1+\alpha_2) \end{pmatrix}. \end{aligned} \tag{2.57}$$

The detailed expressions of A_2 and A_3 are given in the Appendix, section A.1.

Straightforward calculations, detailed in section A.2 in the Appendix, show that A_2 and A_3 are always invertible. Therefore, we can express the swimmers' dynamics as control-affine systems, in which the magnetic field is seen as the control and noted

$$\dot{\mathbf{z}}_2 = \mathbf{G}_0 + H_{\parallel}(t)\mathbf{G}_1 + H_{\perp}(t)\mathbf{G}_2 \tag{2.58}$$

for the two-link swimmer, and

$$\dot{\mathbf{z}}_3 = \mathbf{F}_0 + H_{\parallel}(t)\mathbf{F}_1 + H_{\perp}(t)\mathbf{F}_2 \tag{2.59}$$

for the three-link swimmer.

The expression of the right hand sides of (2.56) and (2.57) immediately yields the following proposition :

Proposition 2.48. *Let $x, y, \theta, \beta \in \mathbb{R}$.*

1. *For the two-link swimmer, states of the form $((x, y, \theta, 0), (\beta, 0))$ are equilibria of System (2.58).*
2. *For the three-link swimmer, states of the form $((x, y, \theta, 0, 0), (\beta, 0))$ are equilibria of System (2.59).*

Remark 2.49. Actually, x and y do not appear in the dynamics and θ only appears through a rotation matrix. Therefore, systems (2.58) and (2.59) are invariant by translation and rotation. Therefore, in the following, we will study without loss of generality systems (2.58) and (2.59) around the equilibria $((0,0,0,0),(\beta,0))$ and $((0,0,0,0,0),(\beta,0))$, both $(0,(\beta,0))$ for legibility.

Remark 2.50. The fields $\mathbf{G}_0$, $\mathbf{G}_1$, $\mathbf{F}_0$, $\mathbf{F}_1$ vanish at the aforementioned equilibria. Therefore, Systems (2.58) and (2.59) are of the form (2.22) studied in section 2.2 of this chapter. Theorem 2.27 constitute a generalisation of the work conducted on the micro-swimmers.

The following theorem, taken from [GP17], states a partial controllability result for the two-link swimmer .

Theorem 2.51 ([GP17, Theorem 5]). *For all $\varepsilon > 0$, the two-link swimmer is $(2|\gamma_2| + \epsilon)$-STLC at $(0,(0,0))$ with*

$$\gamma_2 = \kappa \left(\frac{1}{M_1} + \frac{1}{M_2} \right).$$

Remark 2.52. The result from [GP17] is more general, for it does not assume that the lengths and hydrodynamic coefficients of S_1 and S_2 are equal.

During my PhD, I contributed to improve this result and state its equivalent for the three-link swimmer.

2.4.3 Thesis contributions

This section summarises results that were published in [GLMP18] with Laetitia Giraldi, Pierre Lissy and Jean-Baptiste Pomet and in [Mor19].

These results describe the controllability properties of the two- and three-link swimmers at the neighbourhood of their equilibrium. For each swimmer, a few particular cases are ruled out in Propositions 2.53 and 2.57 before stating the main results in Theorems 2.55 and 2.60.

The following properties use the notion of STLC, introduced in Definition 1.5.

Proposition 2.53. *The two-link swimmer is :*

- *STLC at $(0,(0,0))$ if $M_1 + M_2 = 0$;*
- *not STLC at $(0,(\beta,0))$ for all $\beta \in \mathbb{R}$ if $M_1 = 0$, $M_2 = 0$ or $M_1 - M_2 = 0$.*

The proof of this proposition is developed in Chapter 6 (Proposition 6.17).

Assumption 2.54. For the two-link swimmer, assume the magnetisations M_1 and M_2 satisfy $M_1 \neq 0$, $M_2 \neq 0$, $M_1 - M_2 \neq 0$ and $M_1 + M_2 \neq 0$.

My main result for the two-link swimmer is the following:

Theorem 2.55 ([Mor19] and Chapter 6, Theorem 6.21). *Under Assumption 2.54, the two-link swimmer is STLC at $(0,(\gamma_2,0))$ with*

$$\gamma_2 = \kappa \left(\frac{1}{M_1} + \frac{1}{M_2} \right).$$

Moreover, it is not STLC at $(0,(\beta,0))$ if $\beta \neq \gamma_2$.

Sketch of proof. The proof of Theorem 2.55 is carried out in two steps:

Proof of non-STLC. Let $\beta \neq \gamma_2$. We use the necessary condition from 2.27. Indeed, System (2.58) satisfies :

- $\mathbf{G}_0(0) = \mathbf{G}_1(0) = 0$
- $[\mathbf{G}_2,[\mathbf{G}_0,\mathbf{G}_2]](0) \notin R_1(0)$;
- $[\mathbf{G}_2,[\mathbf{G}_0,\mathbf{G}_2]](0) = \gamma_2[\mathbf{G}_2,[\mathbf{G}_1,\mathbf{G}_2]](0)$.

(recall that $R_1(0)$ is the subspace of $\mathbb{R}^4$ spanned by the iterated Lie brackets of $\mathbf{G}_0, \mathbf{G}_1, \mathbf{G}_2$ containing at most $\mathbf{G}_2$ and evaluated at 0.)

Applying Theorem 2.27, we conclude that the swimmer is not STLC at $(0,(\beta,0))$.

Proof of STLC at $(0,(\gamma_2,0))$. Define $\widetilde{H}_{\|} = H_{\|} + \gamma_2$ to obtain the new system

$$\dot{z} = \widetilde{\mathbf{G}}_0 + \widetilde{H}_{\|}\widetilde{\mathbf{G}}_1 + H_{\perp}\widetilde{\mathbf{G}}_2. \tag{2.60}$$

with $\widetilde{\mathbf{G}}_0 = \mathbf{G}_0 - \gamma_2\mathbf{G}_1$, $\widetilde{\mathbf{G}}_1 = \mathbf{G}_1$ and $\widetilde{\mathbf{G}}_2 = \mathbf{G}_2$. We then check that

— (2.60) satisfies the LARC at $(0,(0,0))$ (see Definition 2.11),

— (2.60) satisfies the Sussmann condition with $\theta = 1$ (see Definition 2.16).

According to Theorem 2.17, this implies that System (2.60) is STLC at $(0,(0,0))$, and therefore System (2.58) is STLC at $(0,(\gamma_2,0))$. □

The detailed proof is done in Chapter 6.

Remark 2.56. Theorem 2.55, published in [Mor19], extends a first result on the two-link swimmer, published in [GLMP18], in which it is shown that the two-link swimmer is not STLC at $(0,(0,0))$. This result is contained in 2.55. However, the proof developed in [GLMP18], more constructive, brings an interesting complement to the arguments used in [Mor19]. See remark 3.19 in Chapter 3, and Chapter 4 which reproduces [GLMP18].

We now turn to the case of the three-link swimmer.

Proposition 2.57. *Assume one of this conditions holds:*

— $M_1 - M_3 = 0$*;*

— $(M_1 + M_3 = 0 \ \ et \ \ M_2 = 0)$*;*

— $9M_2(M_1 + M_3) - 5M_1M_3 - 7M_2^2 = 0$*;*

Then, the three-link swimmer is not STLC at $(0,(\beta,0))$ *with* $\beta \in \mathbb{R}$.

The proof of this proposition is developed in Chapter 6 (Assumption 6.8)

Assumption 2.58. For the three-link swimmer, assume the magnetisations M_1, M_2 et M_3 are such that

$$\begin{aligned} M_1 - M_3 &\neq 0; \\ (M_1 + M_3 \neq 0 \ \text{ ou } \ M_2 &\neq 0); \\ 9M_2(M_1 + M_3) - 5M_1M_3 - 7M_2^2 &\neq 0; \\ P(M_1, M_2, M_3) &\neq 0, \end{aligned} \tag{2.61}$$

with

$$P(x,y,z) = 49y^3 - 91y^2(x+z) + 36y(x+z)^2 - (45y + 65(x+z))xz.$$

Remark 2.59. The last of these four conditions, which we do not deal with in Proposition 2.57, corresponds to an expressions appearing in the calculations for the proof of Theorem 2.60. The question of whether the swimmer is STLC or not when $P(M_1, M_2, M_3) = 0$ is still open. Numerical simulations show that, in that case and with $H_{\|}$ close to γ_3, we have approximately $\alpha_1 = \alpha_2$ for all time (see Figure 2.5). This suggests that the swimmer's movement is limited in this situation, and that the system is not controllable.

My main result for the three-link swimmer is the following:

Theorem 2.60 ([Mor19] and Chapter 6, Theorem 6.10)**.** *Under Assumption 2.58, the three-link swimmer is STLC at* $(0,(\gamma_3,0))$ *with*

$$\gamma_3 = \kappa \frac{17(M_1+M_3)-16M_2}{9M_2(M_1+M_3)-5M_1M_3-7M_2^2}.$$

Moreover, it is not STLC at $(0,(\beta,0))$ *if* $\beta \neq \gamma_3$.

The proof of this Theorem, very similar to that of Theorem 2.55, is developed in Chapter 6.

Remark 2.61. Theorems 2.55 and 2.60 show in particular that the swimmers are not, in general, controllable at $(0,(0,0))$, *i.e.* with "small" magnetic fields. This lack of controllability is due to the fact that the fields $\mathbf{G}_1$ and $\mathbf{F}_1$ vanish at 0: the parallel component of the magnetic field cannot act on the swimmer when all the segments are aligned.

These results are of interest from the theoretical point of view, and also provide important information for applications to micro-swimming. The explicit expression of the controls required to obtain STLC, as well as the numerical simulations, contribute to better understand the way these swimmers move.

Numerical simulations

In order to numerically visualise the results of Theorems 2.55 and 2.60, we compute trajectories starting from the equilibrium position 0, with controls remaining "close" to a given equilibrium control. Let $\beta \in \mathbb{R}$ and $\varepsilon > 0$. Define the controls

$$\begin{aligned} H_{\parallel}(t) &= \beta + \varepsilon(h_1 + h_2\cos(10t) + h_3\cos(100t)), \\ H_{\perp}(t) &= \varepsilon(h_4 + h_5\cos(10t) + h_3\cos(100t)), \end{aligned} \tag{2.62}$$

with h_1 to h_6 taken randomly in $[-1,1]$. By simulating a few of these trajectories on a short interval of time and plotting them, one can expect them to roughly cover the reachable space, allowing to observe potential unaccessible regions.

Figures 2.4 for the two-link swimmer, and 2.5 for the three-link swimmer, display the simulations results, where we can indeed observe that only the values $\beta = \gamma_2$ and $\beta = \gamma_3$ allow the trajectories to cover a neighbourhood of the origin in the (x,y) plane.

For the three-link swimmer, we also observe on Figure 1.5 (middle bottom plot) the phenomenon described in Remark 2.59, that occurs for angles α_1 and α_2 when $P(M_1,M_2,M_3)$ defined in Equation (2.61) vanishes. The simulations suggest that in that case, $\alpha_1 = \alpha_2$ for all time around control $(\gamma_3,0)$, which is not the case when $P(M_1,M_2,M_3) \neq 0$. Thus, the swimmer seems "less" controllable in this particular case. The question of its controllability is however still open.

2.4.4 Perspectives

Extension to N links

By analogy, the model for two and three links can be generalised into a N-link formulation with $N \geqslant 4$. The N-link magnetic swimmers are studied in [ADGZ15], where the authors show that they can move in certain directions when submitted to an oscillating magnetic

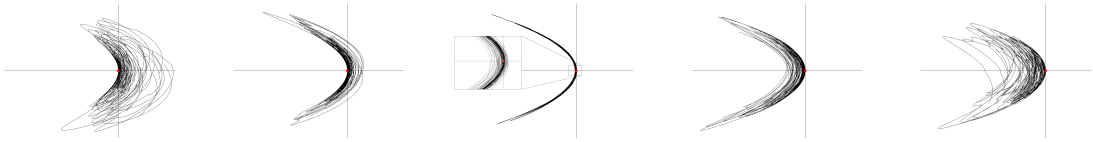

(a) $\beta = 0.5\gamma_2$ (b) $\beta = 0.9\gamma_2$ (c) $\beta = \gamma_2$ (d) $\beta = 1.1\gamma_2$ (e) $\beta = 1.25\gamma_2$

Figure 2.4 – Illustration of the controllability properties of the two-link swimmer. On each plot, the evolution of (x, y) for 30 trajectories has been drawn with realisations of controls (2.62) taken around $(\beta, 0)$. When β is different from the critical value γ_2, the trajectories remain either all to the left or all to the right of the origin. Only the control $(\gamma_2, 0)$ enables the trajectories to cover a neighbourhood of the origin (middle plot). Numerical values: $\eta = 4$, $\xi = 2$, $\ell = 1$, $M_1 = 1$, $M_2 = 3$, $k = 1$, $\varepsilon = 10^{-2}$, $T = 1$.

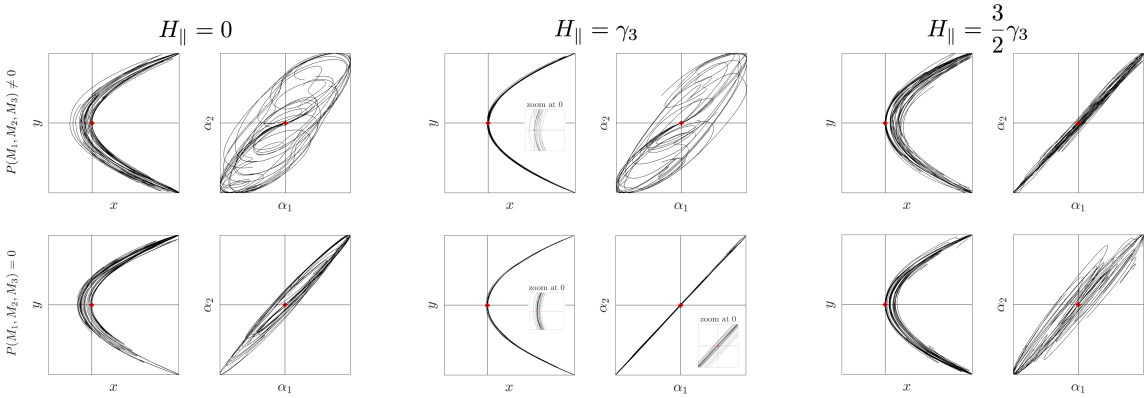

Figure 2.5 – Illustration of the controllability properties of the three-link swimmer. On each couple of plots, the evolution of (x, y) and (α_1, α_2) for 15 trajectories has been drawn with realisations of controls (2.62) taken around $(\beta, 0)$. When β is different from the critical value γ_3, the trajectories remain either all to the left or all to the right of the origin. Only the control $(\gamma_3, 0)$ enables the trajectories to cover a neighbourhood of the origin. The second row of plots illustrates the change in the swimmer's behaviour in the (α_1, α_2) plane when $\beta = \gamma_3$ and $P(M_1, M_2, M_3) = 0$. Numerical values: $\eta = 4$, $\xi = 2$, $\ell = 1$, $M_1 = 8$ (first row), $M_1 = 7.069$ (second row), $M_2 = 10$, $M_3 = 4$, $k = 1$, $\varepsilon = 10^{-2}$, $T = 1$.

field. Experiments conducted in [AFPRG19] (see Figure 2.3-(f)) validate a 3D version of this model and solve an optimal control problem to maximise the swimmer's displacement over a period.

Similarly to the two- and three-link swimmers, the dynamics are governed by the system

$$\dot{\mathbf{z}}_N = \mathbf{F}_0 + H_{\parallel}(t)\mathbf{F}_1 + H_{\perp}(t)\mathbf{F}_2. \tag{2.63}$$

and we study controllability around $(0,(\beta,0))$ with $\beta \in \mathbb{R}$.

However, for $N \leqslant 4$, the expressions of the vector fields are too complex to allow to compute explicitly the Lie brackets of interest and critical values such as γ_2 and γ_3, even with the help of a formal calculation software. I nevertheless proved the following result:

Proposition 2.62. *For the N-link swimmer, $[\mathbf{F}_2,[\mathbf{F}_0,\mathbf{F}_2]](0)$ and $[\mathbf{F}_2,[\mathbf{F}_1,\mathbf{F}_2]](0)$ are colinear.*

The proof of this proposition is developed in section A.3 of the Appendix.

We deduce from 2.62 that :

— if there exists a value γ_N such that $[\mathbf{F}_2,[\mathbf{F}_0,\mathbf{F}_2]](0) = \gamma_N[\mathbf{F}_2,[\mathbf{F}_1,\mathbf{F}_2]](0)$, then this value is the only one for which the system *could* be STLC, *i.e.* System (2.63) is not STLC at $(0,(\beta,0))$ for $\beta \neq \gamma_N$.

— γ_N exists in general, that is only excluding generic conditions on the magnetisations similar to Assumptions 2.54 and 2.58.

Furthermore, in section 2.5 and Chapters 7 and 8, we also use a N-link model in order to study nonmagnetised elastic filaments at low Reynolds number.

Bent swimmer at equilibrium

Following Remark 2.61, one could wonder if it would be better to consider a "bent" swimmer that would not be aligned at its equilibrium, so that the control $H_{\parallel}$ can have an effect on it. In [GLMP16], I studied the equations of such a bent swimmer, for which the elastic torque $\mathbf{T}_3^{\text{el}} = \kappa\alpha_2$ is replaced by $\mathbf{T}_3^{\text{el}} = \kappa(\alpha_2 - \alpha_0)$, with $\alpha_0 \neq 0$. The state $((0,0,0,0,\alpha_0),(0,0))$, noted $(\mathbf{z}_0,(0,0))$, is now an equilibrium. Let us briefly describe the results developed in [GLMP16]. First, we define *partial STLC for variables x and y*:

Definition 2.63. The control system associated to the bent swimmer is *partially STLC at $(\mathbf{z}_0,(0,0))$ for variables x and y* if, for all $\varepsilon > 0$, there exists neighbourhoods $\mathcal{V}$ of $\mathbf{z}_0$ and $\mathcal{W}$ of $(0,0)$ such that, for all $\mathbf{z}_\text{i}$ in $\mathcal{V}$ and (x_1,y_1) in $\mathcal{W}$, there exists a control $(H_{\parallel},H_{\perp})$ defined on $[0,\epsilon]$ such that the trajectory of the swimmer starting at $\mathbf{z}_\text{i}$ satisfies :

— $x(\varepsilon) = x_1$ and $y(\varepsilon) = y_1$;

— forall t in $[0,\varepsilon]$, $|H_{\parallel}| \leqslant \varepsilon$ and $|H_{\perp}| \leqslant \varepsilon$.

Remark 2.64. For a broader overview of partial controllability, see for example [Dup15, Chapitres I et IV].

By linearising System (2.63) around its equilibrium $(\mathbf{z}_0,(0,0))$ and calculating the Kalman matrix, I showed the following result:

Proposition 2.65. *The bent three-link swimmer is partially STLC at $(\mathbf{z}_0,(0,0))$ for variables x and y.*

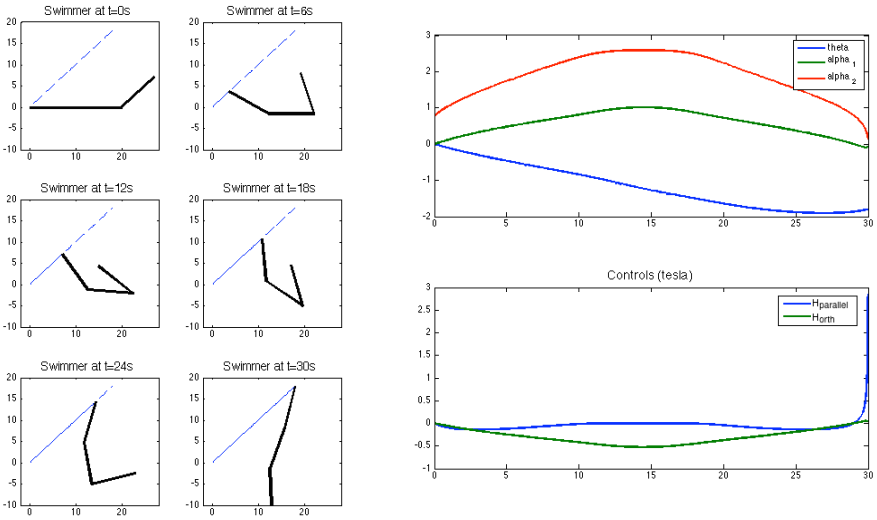

Figure 2.6 – Illustrations of the bent swimmer following a prescribed straight line. On the last plot, representing the swimmer at $t = 30s$, observe that its shape gets close to the straight shape $\alpha_1 = \alpha_2 = 0$ (this can also be seen on the top right plot, which represents the evolution of α_1 (green line) and α_2 (red line) with respect to time). The graph on the bottom right corner shows the evolution of the controls with respect to time. The parallel component $H_{\|}$ (blue line) required to carry on blows up at the end of the simulation.

Actually, since there are two controls and that we want to control only the two variables x and y, that can be done by simply inverting a system to make the swimmer follow a prescribed trajectory $(x(t), y(t))$... until the three segments become aligned, that is $\alpha_1(t) = \alpha_2(t) = 0$ for some time t. When it happens, this (naive) method fails (see Figure 2.6). The question of whether it is possible to control the bent swimmer while avoiding the straight shape to appear at some point is still open.

Extension to a 3D model

The entirety of this section is about planar swimmers. In the three-dimensional case, controllability with shape control has been studied in [LM14, GMZ13]. It would be interesting to know to which extent the controllability properties of the swimmer are preserved or modified in 3D for the magnetic control case.

2.5 Modeling of microfilaments and applications

This section is a synthesis of work done in collaboration with H. Gadêlha and L. Giraldi which is developped in Part III.

2.5.1 Context

A considerable diversity of micro-swimmers using all sorts of strategies to move in their surrounding fluid can be found in nature. Like sperm or certain bacteria, they often use

one or more flagella to do so [GL95, TS04, GGSKB10, SK18]; others, including some cells and micro-algae, move their cilia in a synchronised fashion [GGS+11]. In each case, the interaction between flexible filaments and the fluid creates movement. This constitutes the framework and motivation behind the following section.

Elastic microfilaments are not merely used as a means for moving around in micro-organisms. For example, the cytoskeleton is a set of microtubules and actin microfilaments that gives a cell its structure and mechanical properties. Understanding how the filaments that make up the cytoskeleton react to the constraints applied to them is a fundamental problem in cellular biology [How01, CSRB08].

In order to describe and simulate the dynamics of inextensible microfilaments, many models have been put forward, including discrete [HSF10, SZ11, ADGZ13, GMZ13, Bro14, SK18], and continuous [HB79, WROG98, TS04, Ant05, LP09, GGSKB10] formulations. Determining unknown contact forces along the filament [Ant05] usually requires the computation of Lagrange multipliers [BW77, LP09, SZ11] in order to keep a constant length. This can lead to numerical instability which requires adding corrective terms [TS04, GGSKB10, MJGS15].

The first objective in this part of my thesis was to describe an efficient model that would be numerically robust and adaptable. This would allow us to numerically study a great variety of phenomena revolving around microfilaments. I validated the model by comparing it with the results of a continuous model that had been experimentally validated [TS04, GGSKB10, MJGS15]. I then conceived a ready to use Matlab code that is easily adaptable to various situations and made it available it online. It can be accessed here:

`https://github.com/Clementmoreau/Filament`

The model has notably been reused and rendered in 3D in [WIG19], adapted to take into account interactions with a wall in [WIGG19], and to take into account non local hydrodynamic interactions in [HMMJG+19].

I then focused on the dynamics of buckling in microfilaments [BS01, TS04, BT09, Gad18], one of the possible applications of the model. I did a precise numerical analysis of this phenomenon. We can notably observe the emergence of three different final forms depending on the characteristic parameter of buckling, as well as other phenomena developped in Chapter 8.

2.5.2 Thesis contributions

Modeling of microfilaments at low Reynolds number

This section summarises the results published in [MGG18], reproduced in Chapter 7.

The model I worked on is based on the discretisation of an inextensible elastic filament on length L in N elements denoted by $S_1, \dots, S_N$, as shown in Figure 2.7. The derivation of the equations of the model shows many similarities with the magnetic swimmer of the preceding section, both in terms of notation and in the expression of forces and moments.

Each element is of length $\Delta s = L/N$, with hydrodynamic coefficients $\eta_{\parallel}$ and $\eta_{\perp}$, and two consecutive segments are linked together by an elastic joint modelled by a torsional spring of stiffness κ. The filament is assumed to move in the reference plane $(O, \mathbf{e}_x, \mathbf{e}_y)$, and described by the vector

$$\mathbf{x}_N = (x, y, \theta, \alpha_2, \dots, \alpha_N)^T \in \mathbb{R}^{N+2}.$$

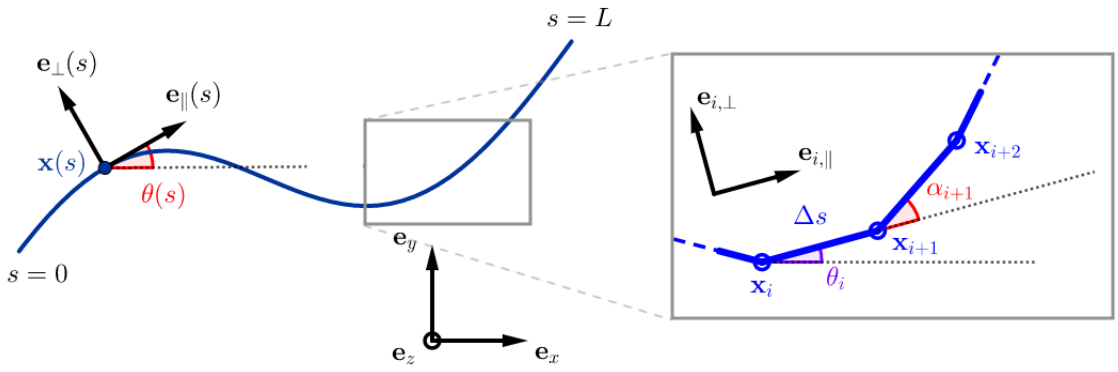

Figure 2.7 – From the continuous filament to a N-links model

In $\mathbf{x}_N$, $\mathbf{x} = (x, y)$ are the coordinates of the extremity of S_1, θ is the angle between $\mathbf{e}_x$ and S_1, and the angles between two consecutive segments, denoted by $\alpha_2, \dots, \alpha_N$, indicate the shape of the filament (see Figure 2.7).

For a segment S_i, hydrodynamic force, denoted by $\mathbf{F}_i^{\mathrm{h}}$, and the hydrodynamic couple of a point $\mathbf{x}_0$, denoted by $\mathbf{T}_i^{\mathrm{h},\mathbf{x}_0}$, are modelled using the Resistive Force Theory (see [GH55] and section 2.4.2). The elastic interaction $\mathbf{T}_i^{\mathrm{el}}$ between segments S_i and S_{i-1} is proportional to stiffness κ and angle α_i.

Assuming, like in section 2.4, that the Reynolds number is small enough for inertial effects to be negligible (Stokes regime), we have balance of forces and moments at each instant. We get $N + 2$ equations writing:

— two equations for the force balance on the filament, projected on axes (Ox) et (Oy);

— one equation for the torque balance on the filament in relation to point $\mathbf{x}$;

— $N-1$ equations for the torque balance on the set $\{S_k + \cdots + S_N\}$ for all k in $\{2, \dots, N\}$, with respect to $\mathbf{x}_k$,

which yields

$$\begin{cases} \sum_{i=1}^{N} \mathbf{F}_i^h &= 0, \\ \sum_{i=1}^{N} \mathbf{T}_i^{h,\mathbf{x}_1} &= 0, \\ \sum_{i=2}^{N} \mathbf{T}_i^{h,\mathbf{x}_2} &= -\mathbf{T}_2^{\mathrm{el}}, \\ \vdots & \vdots \quad \vdots \\ \mathbf{T}_N^{h,\mathbf{x}_N} &= -\mathbf{T}_N^{\mathrm{el}}, \end{cases} \tag{2.64}$$

rewritten in matricial form as

$$AQ\dot{\mathbf{x}}_N = B. \tag{2.65}$$

The detailed expressions for A, Q and B are presented in section 7.7.1 of Chapter 7.

The numerical resolution of (2.65) can be done using a standard ODE solver (*e.g.* Matlab's `ode45`). To ensure the numerical validity of the model, I confronted it to the results given by a PDE model based on the continuous formulation [TS04, GGSKB10, MJGS15] linked to an *ad hoc* numerical scheme that has been experimentally validated. The test consists in considering two initial shapes for the filament (a semicircle and a parabola arc) and

Flexible filament			
Test	Model discrete N=70	Tolerance	Model PDE
Semicircle 	2	1% 0.1% 0.01%	1.3 249 3750
Parabola 	1.5	1% 0.1% 0.01%	90 1820 $>$ 1h
Rigid filament			
Test	Model discrete N=70	Tolerance	Model PDE
Semicircle 	3	1% 0.1% 0.01%	1.3 850 $>$ 1h
Parabola 	1.7	1% 0.1% 0.01%	90 $>$ 1h $>$ 1h

Table 2.1 – Computation time (in seconds) for two initial conditions and two different stiffnesses.

let them evolve until they reach straight equilibrium. Even with a low number of segments, the discrete model reproduces the behaviour of the PDE model very accurately (see Figure 7.3 in Chapter 7).

The PDE model used for the validation features a corrective term to make sure the total length of the filament remains constant. The system of equations (2.65) does not need such a term since the inextensibility of the filament is directly embedded in the model's geometry. This makes the discrete model significantly more robust, in particular in "stiff" cases, where the filament's curvature is locally high (as is the case of the parabola arc). For the same precision on the total length of the filament, the discrete model therefore requires a considerably lower computation time than the PDE model with which it is compared (see Table 2.1).

The numeric framework of our model allows a quick and easy adaptation to numerous cases. Here are a few examples, some of which are detailed in section 7.5 of Chapter 7:

— the addition of an internal couple along the filament, modeling resistance to sliding, which can trigger a phenomenon for which a curvature applied to one end of the filament leads to the appearance of an opposite curvature at the opposite end. This phenomenon, observed in bio-flagella like sperm [CG17, IGG+18], is called *counterbend* [LML05, GGG13]. See section 7.5.3;

— the addition of contact forces at the endpoints of the filament to model buckling, [Ant05, BS01, TS04, BT09, Gad18] *i.e.* the behaviour of a filament undergoing compression forces. See the next section and Chapter 8;

— the addition of terms modeling exterior effects like a magnetic field (see section 7.5.2), and inertial effect, current in the fluid. . . ;

— the addition of terms modeling the nonlocal hydrodynamic interactions that are not taken into account by Resistive Force Theory [HMMJG+19] ;

— adapting the model to 3D [WIG19] ;

— *etc.*

The numerical and analytical study of problems in this list using the framework offered by the N-segments model, constitutes a range of future prospects for my research, in collaboration with H. Gadêlha.

Numerical study of buckling phenomena

This study summarises an article in preparation, reproduced in Chapter 8.

Buckling is the particular behaviour that a material exhibits when subjected to compression or shearing forces. Microfilaments are largely exposed to this phenomenon under the action of a moving fluid [GG06] or internal forces [BT09].

I am more specifically interested in an initially straight elastic filament the ends of which are pushed towards one another. In this situation, which was first studied by Euler during the 18^{th} century [Eul44], we know analytical solutions for static equilibrium.

These classical solutions do not take into account the dynamic aspect: the competition between the characteristic time of relaxation necessary to the establishment of static equilibrium and the speed at which the ends are moving. This competition leads to more complex dynamic behaviours, which strongly vary with respect to the parameters.

In my thesis, I conducted a numerical study of this dynamic buckling problem. The originality of my work lies in particular in the fact that the movement of the ends of the filament is carried beyond the instant when they cross each other. The simulations I ran therefore allow us to distinguish different regimes leading to the appearance of different shapes for the filament, depending on the parameters of the system. My results are succinctly presented here and further developped in Chapter 8.

Equations of the model. We use the filament model developped in the previous section. At initial time, the filament is straight and "almost" horizontal, meaning that we introduce a Gaussian noise of very weak amplitude in the curvature (angles α_i) to numerically model the infinitesimal asymmetry which triggers the buckling phenomenon. We then push the ends of the filament towards each other according to the following kinematic constraints:

$$\begin{aligned} &\dot{y}_1(t) = 0, && \dot{y}_{N+1}(t) = 0, \\ &\dot{x}_1(t) = (1-a)V_p, && \dot{x}_N(t) = -(1+a)V_p, \end{aligned} \tag{2.66}$$

where V_p is the pushing speed and $a \in [0,1]$ an asymmetry parameter. When $a = 0$, both ends move towards one another at the same speed; conversely, when $a = 1$, only one of the ends moves while the other does not. These two parameters do not exist in the static case. They describe the manner in which the ends get closer over time and therefore represent the dynamic aspect of the system.

The system of equations determining the filament's dynamics (given by System (2.64) augmented with equations (2.66)) is nondimensionalised to obtain a characteristic parameter

of buckling called the buckling number, denoted by Bu:

$$\mathrm{Bu} = \frac{\eta_{\|} \mathrm{L}^3 V_p}{E_b}.$$

In this expression, $\eta_{parallel}$ corresponds to the hydrodynamic drag coefficient, L corresponds to the length of the filament and E_b to its stiffness (see Chapter 7). The buckling number expresses the relation between the characteristic relaxation time of the filament and the speed at which the ends are moving. When Bu is very low, the behaviour is the same as the static case.

Appearance of three different shapes. Figure 2.8 shows the different behaviours presented by the filament depending on Bu. We can observe three distinct regimes.

— for $\mathrm{Bu} = 10^{-1}$ to $\mathrm{Bu} = 1$, the filament flips soon after the ends meet.

— for $\mathrm{Bu} = 10^{1}$ to $\mathrm{Bu} = 10^{2}$, we can see a loop appearing, which is present until the end of the simulation.

— for $\mathrm{Bu} = 10^{3}$ and beyond, the filament takes in some cases a shape reminding that of a knot.

For some values of Bu, two different shapes can coexist. Figure 2.8-(b) shows the prevalence of each form depending on Bu. We can notably see that the "loops" and "knots" seem to appear equiprobably for larger Bu values.

Figure 2.8-(c) shows the influence of the asymmetry parameter a on the appearance of different shapes. When a increases, the loops and knots start appearing from higher values of Bu. The appearance of the loop and the knot are therefore favored when values of a are closer to 0, that is rather symmetrical situations.

Evolution of Fourier modes' amplitudes. I completed this analysis of shapes appearing in large time by a study of the behaviour of the filament in small time. During the first instants, we observe that the filament presents several "waves" (see for example the filament in the bottom-left corner of Figure 2.8-(a)), which quickly disappear. These waves correspond to higher order Fourier modes of the curvature of the filament. Figure 2.9 shows the evolution of the amplitude of these Fourier modes over time for different values of Bu. In each case, each mode appears, reaches a maximum of amplitude, then decays. These maxima take place in succession, in decreasing order of the modes. Denoting $T^k_{\max}$ the time when mode k reaches its maximum, we numerically established that the decrease follows a law of the form:

$$T^k_{\max} = T_0 \exp(-\alpha k^{1/4}), \tag{2.67}$$

with $T_0 > 0$ and $\alpha > 0$ roughly independent from Bu (see the graph on the right hand side of Figure 2.9).

Perspectives. These numerical observations shed light on interesting phenomena compared with other numerical and experimental studies [CDK17], but also from the point of view of the mathematical behaviour of the system. In particular, I have noticed that for certain values of Bu, the final shape of the filament seemed very impredictible, even at an advanced stage of the simulation. Besides, the amplitudes of the first three Fourier modes of

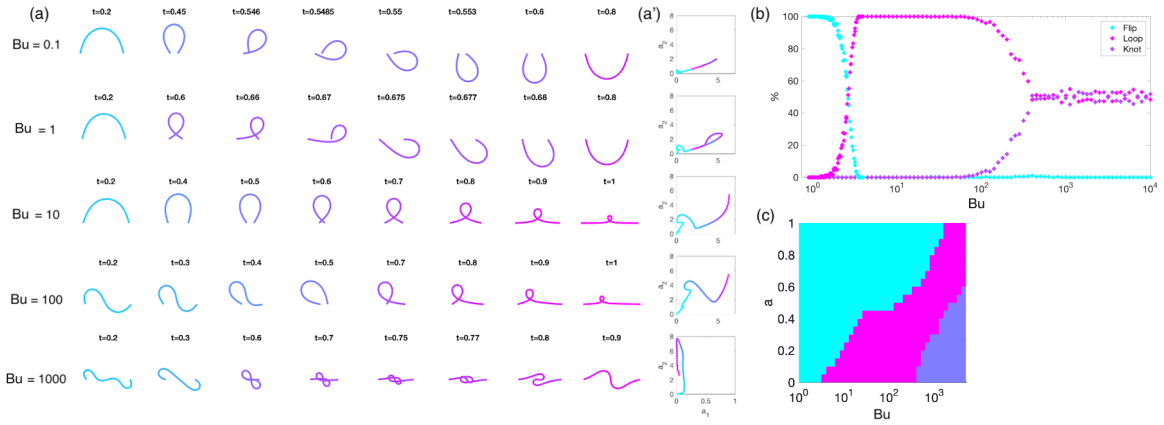

Figure 2.8 – Visualising of the appearance of different shapes during buckling (a). Evolution of the filament's shape over time for different values of Bu. We can see the three shapes (flip, loop and knot) corresponding to the three buckling regimes. (a'). Evolution of the amplitude of the first two Fourier modes of the curvature of the filament for each of the simulations displayed in (a). The point of these graphs is further developped in Chapter 8. (b). Prevalence of each shape as a function of Bu, expressed in proportion of appearance over 500 simulations. (c). Prevalence of each shape as a function of Bu and a.

.

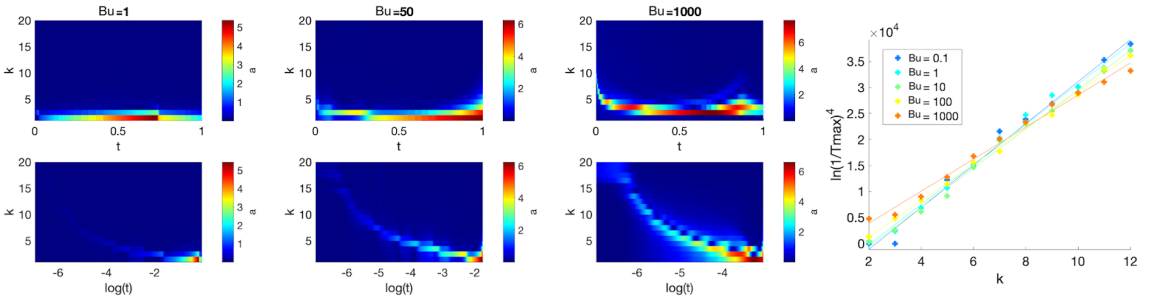

Figure 2.9 – Results obtained on the decrease of Fourier modes of the curvature of the filament. For three different values of Bu, we represented the amplitude of the first 20 Fourier modes (y-axis) over time (x-axis). The time scale is linear on the top row, allowing us to see that only the first two or three modes appear most of the time. The time scale on the bottom row is logarithmic, we can therefore observe the appearance and subsequent decrease of high modes' amplitude in short time, following a law modeled by (2.67), represented in the graph on the right hand side.

the curvature, which seem to play a major role in the behaviour of the filament during buckling, follow complex paths containing bifurcations (see Figure 8.5, Chapter 8). The analytical study of this system to better understand these behaviours is a promising prospect.

Part I

Some controllability results in finite and infinite dimension

Chapter 3

Necessary conditions for local controllability of a particular class of systems with two scalar controls

This chapter reproduces [GLMP19], written in collaboration with Laetitia Giraldi, Pierre Lissy and Jean-Baptiste Pomet, under revision for resubmission in the journal ESAIM:COCV. *NB*: In accordance with the usages in the mathematics field, the authors for this publication are in alphabetical order, regardless of the fact that I provided the dominant contribution.

3.1 Introduction

Let n, m be positive integers. Let $\mathcal{X}$ be the set of real analytic vector fields on $\mathbb{R}^n$. Consider a general affine control system with m controls:

$$\dot{z(t)} = f_0(z(t)) + \sum_{k=1}^{m} u_k(t)\, f_k(z(t))\,, \tag{3.1}$$

where z is the state in $\mathbb{R}^n$, $t \in [0, T]$ for some $T > 0$, the u_k are measurable functions on $[0, T]$ called the controls, and the f_k are vector fields in $\mathcal{X}$. Such a system is called *controllable* if, for any two points z_0 and z_1 in the state space, there exists controls u_k ($k \in 1, \ldots, m$) producing a trajectory z that starts from z_0 at time 0 and ends at z_1 at time T (see classical textbooks like [LM67, Son13, Cor07]). It is *locally* controllable around a point z_{eq} in the state space and controls $u_{k,\text{eq}}$ —assumed to be an equilibrium throughout all this paper, we do not discuss local controllability around a trajectory— if for every positive time T and every positive control bound M, there exists an open neighborhood of $(X_{\text{eq}}, u_{\text{eq}})$ such that for every pair of states X and Y in this neighborhood, there exists a control bounded by M that joins X to Y in time T. There are different notions of local controllability, some stronger than others, depending on the topology used on the control, and possibly requiring that the difference with the reference control be bounded rather than arbitrarily small, see Section 3.2.

Some sufficient conditions (see [Her76, Her82, Sus87]) and some necessary conditions (see [Sus87, Ste86, Kaw87, Kra98]) are given in the literature for local controllability of control affine systems of the form (3.1) around an equilibrium, with a rather big gap between them

that makes the subject intriguing. These conditions all allow us to decide controllability or non-controllability based on the value of a finite number of Lie brackets of the underlying vector fields at the equilibrium point, i.e. on the truncation at a certain order of the series defining the real analytic vector fields; an even more intriguing question is pointed out in [Agr99]: it is not clear whether or not, in general (for systems lying in the above mentioned gap), a finite number of such terms of series, or Lie brackets, is enough to decide local controllability or non controllability. See for example [Cor07] and [Son13] for more results on the important questions around local controllability that emerged in nonlinear control theory and for the advances in the last decades.

This paper is specifically concerned with control systems with two scalar inputs, of the form

$$\dot{z} = f_0(z) + u_1\, f_1(z) + u_2\, f_2(z)\,, \tag{3.2}$$

where the state z is in $\mathbb{R}^n$, f_0, f_1, f_2 are three real analytic vector fields on $\mathbb{R}^n$ such that f_0 and f_2 vanish at the origin while f_1 does not:

$$f_0(0) = 0,\ \ f_2(0) = 0,\ \ f_1(0) \neq 0\,. \tag{3.3}$$

Such systems have two controls but the effect of one of them vanishes at the point of interest. In a sense, the contribution of this paper is to study to what extent the second control helps controllability or to what extent, on the contrary, obstructions to controllability of the single input system $\dot{z} = f_0(z)+u_1\, f_1(z)$ carry over when the second control u_2 is turned on.

Studying this very situation stemmed out of previous work from the authors on the controllability of magnetic micro-swimmers [GP17, GLMP18, Mor19]. See these references for a description of these devices and their interest (for instance in micro-robotics and biomedical applications). The corresponding control systems are particular cases of (3.2)-(3.3), for which the authors have proved various controllability and non-controllability results, with the various notions of local controllability introduced in 3.2.1.

We believe that a more general treatment of systems of type (3.2)-(3.3), beyond the case of magnetic micro-swimmers, is of interest to the controllability problem in control theory. It is the purpose of the present paper.

The paper is structured as follows. Section 3.2 is devoted to precise definitions of various notions of local controllability and to recalling known controllability conditions for single-input systems. Our main result is presented in Section 3.3. Section 3.4 illustrates the results with several examples. Section 3.5 is dedicated to the proof of the main result. To finish, conclusions as well as some perspectives on further research are provided in Section 3.6.

3.2 Problem statement

3.2.1 Definitions of local controllability

In the following, we endow $\mathbb{R}^m$ with any norm that we denote by $|.|$. We will keep the notations $\|.\|$ for functional norms when the control is assigned to be a function of time $t \mapsto u(t)$.

We say that $(z^{\mathrm{eq}}, u^{\mathrm{eq}}) \in \mathbb{R}^n \times \mathbb{R}^m$ is an equilibrium point of the system if $f_0(z^{\mathrm{eq}}) + \sum_{k=1}^m u_k^{\mathrm{eq}} f_k(z^{\mathrm{eq}}) = 0$.

Let us start with two different notions of local controllability around an equilibrium. For $\eta \in \mathbb{R}$ such that $\eta > 0$ and $z \in \mathbb{R}^n$, we denote by $B(0, \eta)$ the open ball for the Euclidian norm in $\mathbb{R}^n$, centered at z and with radius η.

Definition 3.1 (STLC)**.** The control system (3.1) is *STLC at* (z^{eq}, u^{eq}) if, for every $\varepsilon > 0$, there exists $\eta > 0$ such that, for every z_0, z_1 in $B(z^{\mathrm{eq}}, \eta)$, there exists a control $u(\cdot)$ in $\mathrm{L}^\infty([0, \varepsilon], \mathbb{R}^m)$ such that the solution of the control system $z(\cdot) : [0, \varepsilon] \to \mathbb{R}^n$ of (3.1) satisfies $z(0) = z_0$, $z(\varepsilon) = z_1$, and

$$\|u - u^{\mathrm{eq}}\|_{\mathrm{L}^\infty([0,\varepsilon],\mathbb{R}^m)} \leqslant \varepsilon\,.$$

Definition 3.2 (α-STLC)**.** Let $\alpha \geqslant 0$. The control system (3.1) is *α-STLC at* (z^{eq}, u^{eq}) if, for every $\varepsilon > 0$, there exists $\eta > 0$ such that, for every z_0, z_1 in $B(z^{\mathrm{eq}}, \eta)$, there exists a control $u(\cdot)$ in $\mathrm{L}^\infty([0, \varepsilon], \mathbb{R}^m)$ such that the solution of the control system $z(\cdot) : [0, \varepsilon] \to \mathbb{R}^n$ of (3.1) satisfies $z(0) = z_0$, $z(\varepsilon) = z_1$, and

$$\|u - u^{\mathrm{eq}}\|_{\mathrm{L}^\infty([0,\varepsilon],\mathbb{R}^m)} \leqslant \alpha.$$

Remark 3.3. We can easily see that 0-STLC is then identical to STLC. If $\alpha > 0$, the second notion is weaker than the first one, as the norm of the control can remain "far" from the equilibrium control as the ball radius η gets arbitrary small.

Remark 3.4. For a given control system that is α-STLC, the smallest possible value of α depends on the norm $|\cdot|$ chosen for the control. However, it does not depend on the norm we put on the state space, justifying the choice of a particular norm on $\mathbb{R}^n$.

Remark 3.5. Note that our definition for STLC requires the time to be arbitrarily small and the control to be arbitrarily close to the equilibrium control, matching the notion used for instance by Kawski in [Kaw86, Kaw87] and later by Coron in [Cor07, Def. 3.2, p. 125]. Historically, the term "STLC" was however first used in the works of Hermes [Her82] and Sussmann [Sus83] among others, to describe what we chose to call 1-STLC [1]. With this other formalism, the notion described in Definition 3.1 has been referred to as *small-time local controllability with small controls*.

More recently, a new notion has been introduced by Beauchard and Marbach in [BM18, Definition 4]. The idea is to ensure the smallness, not only of the control, but also of its derivatives, by requiring its norm to be bounded in Sobolev spaces. For I an interval and k a nonnegative integer, we recall that a function $f : I \to \mathbb{R}$ belongs to $\mathrm{W}^{k,\infty}(I)$ if, for all $p \in \{0, \dots, k\}$, $f^{(p)} \in \mathrm{L}^\infty(I)$. In this case, the norm of f on this space reads

$$\|f\|_{\mathrm{W}^{k,\infty}} = \max_{p\in\{0,\dots k\}} \|f^{(p)}\|_{\mathrm{L}^\infty(I)}.$$

Definition 3.6 ($\mathrm{W}^{k,\infty}$-STLC)**.** Let $k \in \mathbb{N}$. The control system (3.1) is *$\mathrm{W}^{k,\infty}$-STLC at* (z^{eq}, u^{eq}) if, for every $\varepsilon > 0$, there exists $\eta > 0$ such that, for every z_0, z_1 in $B(z^{\mathrm{eq}}, \eta)$, there exists a control $u(\cdot)$ in $\mathrm{W}^{k,\infty}([0, \varepsilon], \mathbb{R}^m)$ such that the solution of the control system $z(\cdot) : [0, \varepsilon] \to \mathbb{R}^n$ of (3.1) satisfies $z(0) = z_0$, $z(\varepsilon) = z_1$, and

$$\|u - u^{\mathrm{eq}}\|_{\mathrm{W}^{k,\infty}([0,\varepsilon],\mathbb{R}^m)} \leqslant \varepsilon\,.$$

1. The exact definition given in [Sus83] supposes an *a priori* bound on the control, uses the notion of reachable space, and is hence written in a more condensed manner than in Definition 3.2; we rephrased it here to match the structure of Definition 3.1.

Remark 3.7. Like 0-STLC in Remark 3.3, $\mathrm{W}^{0,\infty}$-STLC is identical to STLC. When $k > 0$, $\mathrm{W}^{k,\infty}$-STLC is stronger than STLC, because it requires the control to be sufficiently smooth.

Remark 3.8. The different STLC notions can be ordered in an implication chain. With $0 < \alpha_1 < \alpha_2$ and $k_1 < k_2$ in $\mathbb{N}$, and for a given norm on the control space, one has

$$\mathrm{W}^{k_2,\infty}\text{-STLC} \Rightarrow \mathrm{W}^{k_1,\infty}\text{-STLC} \Rightarrow \text{STLC} \Rightarrow \alpha_1\text{-STLC} \Rightarrow \alpha_2\text{-STLC}$$

3.2.2 Known results for single-input systems

Consider an affine control system like (3.1) with $m = 1$:

$$\dot{z} = f_0(z) + u_1(t) f_1(z) \tag{3.4}$$

with z in $\mathbb{R}^n$, f_0, f_1 in $\mathcal{X}$ and u_1 a control function in $\mathrm{L}^1([0,T])$. For some T_0 in $]0,T]$, (3.4) admits a unique maximal solution (see e.g. [BM18, Proposition 2]). Up to a translation, we can assume that $(0,0)$ is an equilibrium of (3.4) (which means in particular that $f_0(0) = 0$).

Since $m = 1$, we can assume here without loss of generality that $|\cdot|$ is the usual absolute value.

If f and g are two vector fields in $\mathcal{X}$, $[f,g]$ denotes the Lie bracket of f and g and $\mathrm{ad}_f^k g$ is defined by induction with $\mathrm{ad}_f^0 g = g$ and $\mathrm{ad}_f^k g = [f, \mathrm{ad}_f^{k-1} g]$.

Following [Sus87] formalism, given $\mathcal{F}$ a family of elements of $\mathcal{X}$, we denote by $\mathrm{Br}(\mathcal{F})$ the set of formal iterated Lie brackets of $\mathcal{F}$, and $\mathrm{Lie}(\mathcal{F})$ the Lie algebra generated by the vector fields in $\mathcal{F}$, For $k \in \mathbb{N}$, S_k the subspace of $\mathcal{X}$ spanned by all the elements of $\mathrm{Br}(f_0, f_1)$ containing f_1 at most k times, and $S_k(0)$ the subspace of $\mathbb{R}^n$ spanned by the value at 0 of the elements of S_k.

Definition 3.9. System (3.4) satisfies the Lie Algebra Rank Condition (LARC) at 0 if

$$\{g(0), g \in \mathrm{Lie}(f_0, f_1)\} = \mathbb{R}^n. \tag{3.5}$$

It is well-known [Her63, Nag66] that the LARC is necessary for any form of STLC, but not sufficient. Stronger assumptions on the structure of Lie bracket spaces have to be made to obtain a sufficient condition:

Proposition 3.10 ([Sus83, Theorem 2.1, p.688])**.** *If system (3.4) satisfies the LARC at 0 and, for all k in $\mathbb{N}$,*

$$S_{2k+2}(0) \subset S_{2k+1}(0), \tag{3.6}$$

then it is STLC.

Condition (3.6) is violated if for some $k \in \mathbb{N}$, some brackets in S_{2k+2}, once evaluated at 0, do not belong to $S_{2k+1}(0)$. Such brackets were historically called *bad* ones, since they appear in Proposition 3.10 as potential *obstructions* to local controllability. The bad brackets can be seen as directions towards which the system drifts, thus potentially (but not necessarily) preventing local controllability. Dealing with this issue can be done by finding other brackets sharing directions at 0 with the bad brackets, in order to "compensate" the drift. We say that those new brackets help to *neutralize* the bad ones.

However, as Kawski showed in [Kaw86, Example 2.5.1], the goodness or badness of high-order brackets is not intrinsic and depends on the basis chosen for the formal Lie brackets

homogeneous subspaces. This kind of phenomenon occurs when $k > 1$ in (3.6). Since our work is concerned only with the case where (3.6) is violated for $k = 1$, we will still call some brackets of interest "bad" ones; it must nonetheless be kept in mind that the "good" and "bad" terminology does not account for the full reality of the general behavior of system (3.4).

The lowest-order possible obstruction to (3.6) occurs if the bad bracket in S_2

$$B_1 = [f_1, [f_0, f_1]] \tag{3.7}$$

is such that $B_1(0)$ does not belong to $S_1(0)$. We call B_1 the *first bad bracket*. The following result has been shown by Sussmann in [Sus83, Proposition 6.3, p.707]:

Proposition 3.11. *Assume $f_0(0) = 0$ and $B_1(0) \notin S_1(0)$. Then, (3.4) is not 1-STLC.*

It is worth mentioning that this result has been extended to higher-order bracket spaces by Stefani in [Ste84]:

Proposition 3.12. *Assume that there exists k in $\mathbb{N}$ such that*

$$\mathrm{ad}_{f_1}^{2k} f_0(0) \notin S_{2k-1}(0).$$

Then, for all $\alpha \geqslant 0$, (3.4) is not α-STLC.

Assume that the hypothesis of Proposition 3.11 is not satisfied and that $B_1(0)$ does belong to $S_1(0)$. The next lowest-order bracket in S_2 that can obstruct controllability is what we call the *second bad bracket* and denote by B_2:

$$B_2 = [[f_0, f_1], [f_0, [f_0, f_1]]]. \tag{3.8}$$

For scalar-input systems, Sussmann noticed in [Sus83, p.710] that one may or may not get STLC under the hypothesis $B_2(0) \notin S_1(0)$ (see System (3.14) at the beginning of section 3.4.2). In [Kaw87], Kawski obtained a new necessary condition by refining the space S_1:

Proposition 3.13. *Let $S' = \mathrm{Span}(\{\mathrm{ad}_{f_0}^k(\mathrm{ad}_{f_1}^3 f_0), k \in \mathbb{N}\})$.*
If $B_2(0) \notin S_1(0) + S'(0)$, then, for any $\alpha \geqslant 0$, (3.4) is not STLC.

More recently, in [BM18, Theorem 3], Beauchard and Marbach showed another result by using another notion of local controllability.

Proposition 3.14. *If $B_2(0) \notin S_1(0)$, then (3.4) is not $\mathrm{W}^{1,\infty}$-STLC.*

Proposition 3.13 states that B_2 can be neutralized if it shares its direction at 0 with a particular class of brackets in S_3, while Proposition 3.14 states that B_2 can only be neutralized if the derivative of the control is "not too small".

Concerning systems with control in $\mathbb{R}^m, m \geqslant 2$, a general sufficient condition for local controllability, in the vein of Proposition 3.10 but more complex, can be found in [Sus87], but no necessary condition is known, to the best of our knowledge. The main result of this paper, stated in the next section, is a step in this direction in the sense that they give an extension of the necessary condition contained in Proposition 3.11 to the case where the system has two scalar controls, and the vector field associated to the second control vanishes at the equilibrium.

In addition to this result, we also provide in section 3.4 a few examples that illustrate the behaviour of System (3.2) in the case where $B_1(0) \in R_1(0)$ and $B_2(0) \notin R_1(0)$, that can be seen as exploratory work that could lead to an extension to two-control systems of the necessary condition contained in 3.14.

3.3 Main result

We now consider the affine control system (3.2) (which is also system (3.1) with $m = 2$):

$$\dot{z} = f_0(z) + u_1(t)f_1(z) + u_2(t)f_2(z),$$

with $z \in \mathbb{R}^n$, f_0, f_1, f_2 in $\mathcal{X}$ and u_1, u_2 control functions in $\mathrm{L}^1([0,T])$.

We assume that (3.3) is satisfied, i.e. $f_0(0) = 0, f_2(0) = 0, f_1(0) \neq 0$, and we study local controllability for $(z,(u_1,u_2))$ close to the equilibria $(0,(0,u_2^{\mathrm{eq}}))$, with u_2^{eq} arbitrary.

Remark 3.15. A more general situation than (3.3) would be to consider an equilibrium $(z^{\mathrm{eq}},(u_1^{\mathrm{eq}},u_2^{\mathrm{eq}}))$ (i.e. $f_0(z^{\mathrm{eq}})+u_1^{\mathrm{eq}}\,f_1(z^{\mathrm{eq}})+u_2^{\mathrm{eq}}\,f_2(z^{\mathrm{eq}}) = 0$) such that the rank of $\{f_1(z^{\mathrm{eq}}), f_2(z^{\mathrm{eq}})\}$ is 1. In that case, one may recover (3.3) by defining new variables and controls (Z,U_1,U_2) with the linear transformation $z = Z + z^{\mathrm{eq}}, u_1 = \lambda_2 U_1 + \lambda_1 U_2, u_2 = -\lambda_1 U_1 + \lambda_2 U_2$ where (λ_1,λ_2) nonzero such that $\lambda_1\, f_1(z^{\mathrm{eq}}) + \lambda_2\, f_2(z^{\mathrm{eq}}) = 0$. This transformation brings us back to the study of a system of type (3.2)-(3.3).

Let R_1 be the subspace of $\mathcal{X}$ containing the brackets of $\mathrm{Br}(f_0,f_1,f_2)$ containing f_1 at most one time, and $R_1(0)$ the subspace of $\mathbb{R}^n$ spanned by the value at 0 of the elements of R_1.

3.3.1 Obstruction coming from the first bad bracket

Let us now state our main results. Recall that $B_1 = [f_1,[f_0,f_1]]$ and $B_2 = [[f_0,f_1],[f_0,[f_0,f_1]]]$.

Theorem 3.16. *Consider system (3.2) under Assumption (3.3). Assume $B_1(0) \notin R_1(0)$.*

1. *If $B_1(0) \in R_1(0) + \mathrm{Span}([f_1,[f_2,f_1]](0))$, let $\beta \in \mathbb{R}$ be such that*

$$B_1(0) + \beta[f_1,[f_2,f_1]](0) \in R_1(0).$$

   Then, for any $u_2^{eq} \in \mathbb{R}$ such that $u_2^{eq} \neq \beta$, system (3.2) is not STLC at $(0,(0,u_2^{eq}))$.

2. *If $B_1(0) \notin R_1(0) + \mathrm{Span}([f_1,[f_2,f_1]](0))$, then, for any $u_2^{eq} \in \mathbb{R}$ and any $\alpha \geqslant 0$, system (3.2) is not α-STLC at $(0,(0,u_2^{eq}))$.*

Remark 3.17. In case 2., the second control does not improve controllability with respect to the single-input system obtained by taking $u_2 = 0$.

Remark 3.18. In case 1., the fact that the brackets $[f_1,[f_2,f_1]](0)$ and $B_1(0)$ share a common direction is crucial. It allows the bracket $[f_1,[f_2,f_1]]$ to possibly neutralize the bad bracket B_1 through the particular control $u_2^{\mathrm{eq}} = \beta$. This critical value of the control is the only value around which system (3.2) may be STLC.

Remark 3.19. In [GLMP18], a result similar to case 1. is shown for a particular system of type (3.2)-(3.3) describing the movement of a magnetized micro-swimmer. This particular

result led to the generalizations presented in this paper. Furthermore, the proof of Theorem 3.16 is based on the existence of a suitable local change of coordinates, that is performed explicitly in [GLMP18] for the micro-swimmer system.

Remark 3.20. Up to a translation, one can always study controllability around the null equilibrium $(0,(0,0))$. Let us define the affine feedback transformation on the control u_2: $\tilde{u}_2 = u_2 - \beta$. With this transformed control, system (3.2) becomes

$$\dot{z} = \tilde{f}_0(z) + u_1 \tilde{f}_1(z) + \tilde{u}_2 \tilde{f}_2(z) \tag{3.9}$$

with $\tilde{f}_0 = f_0 + \beta f_2$, $\tilde{f}_1 = f_1$ and $\tilde{f}_2 = f_2$.

Note that $[\tilde{f}_1,[\tilde{f}_0,\tilde{f}_1]](0) = [f_1,[f_0,f_1]](0) + \beta[f_1,[f_2,f_1]](0) \in R_1(0)$. Assume that system (3.9) is STLC at $(0,(0,0))$. Let ε be a positive real number. Let η be the associated parameter from Definition 3.1, and z_0, z_1 in $B(0,\eta)$. There exists controls u_1 and $\tilde{u}_2$ in $\mathrm{L}^\infty([0,\varepsilon])$ such that the solution of (3.9) with $z(0) = z_0$ and these controls satisfy $z(\varepsilon) = z_1$, and

$$\|u_1\|_{\mathrm{L}^\infty([0,\varepsilon],\mathbb{R})} \leqslant \varepsilon\,, \|\tilde{u}_2\|_{\mathrm{L}^\infty([0,\varepsilon],\mathbb{R})} \leqslant \varepsilon.$$

Hence, the solution of system (3.2) with $z(0) = z_0$ and controls $u_2 = \beta + \tilde{u}_2$ and u_1 satisfies $z(\varepsilon) = z_1$. Moreover, $\|u_2 - \beta\|_{\mathrm{L}^\infty([0,\varepsilon],\mathbb{R})} \leqslant \varepsilon$ and $\|u_1\|_{\mathrm{L}^\infty([0,\varepsilon],\mathbb{R})} \leqslant \varepsilon$.

Therefore, if system (3.9) is STLC at $(0,(0,0))$, then system (3.2) is STLC at $(0,(0,\beta))$.

3.4 Illustrating examples and applications

3.4.1 Examples for the first bracket obstruction

Case where the second control cannot help to neutralize B_1

In case 2. of Theorem 3.16, the second control u_2 cannot neutralize the obstruction to local controllability induced by B_1. The following example illustrates that case.

Example 3.21. Consider the system

$$\left\{\begin{array}{ll} \dot{x} &= y^2 + yu_1, \\ \dot{y} &= 2y - u_1 + xu_2. \end{array}\right. \tag{3.10}$$

It is of the form (3.2) with

$$f_0 = \begin{pmatrix} y^2 \\ 2y \end{pmatrix}, \quad f_1 = \begin{pmatrix} y \\ -1 \end{pmatrix}, \quad f_2 = \begin{pmatrix} 0 \\ x \end{pmatrix}.$$

Straightforward computations show that

$$R_1(0) = \mathrm{Span}(\mathbf{e}_2), \quad [f_1,[f_0,f_1]](0) = -6\mathbf{e}_1, \quad [f_1,[f_2,f_1]](0) = \mathbf{e}_2,$$

so we are in the case 2. of Theorem 3.16. Therefore, for any $\alpha \geqslant 0$ and any $u_2^{\mathrm{eq}} \in \mathbb{R}$, system (3.10) is not α-STLC at $(0,(0,u_2^{\mathrm{eq}}))$.

Case where STLC is obtained thanks to the second control

In case 1., Theorem 3.16 states that the system is not STLC around the equilibria $(0,(0,u_2^{\text{eq}}))$, unless u_{eq} is equal to a particular value β, that allows the bracket $[f_1,[f_2,f_1]]$ to neutralize the bad bracket B_1. Around the equilibrium $(0,(0,\beta))$, the system can then be STLC, like in the next example. The method used in the following example to show STLC was introduced in [Mor19] to show local controllability of magnetically driven micro-swimming robots. We reproduce it here on a simpler system.

Example 3.22. Consider the system

$$\begin{cases} \dot{x} &= y^2 + yu_1 - \dfrac{2}{\alpha}y^2u_2, \\ \dot{y} &= 2y - u_1 - \dfrac{1}{\alpha}yu_2, \end{cases} \tag{3.11}$$

for some $\alpha \neq 0$. Here we have

$$f_0 = \begin{pmatrix} y^2 \\ 2y \end{pmatrix}, \quad f_1 = \begin{pmatrix} y \\ -1 \end{pmatrix}, \quad f_2 = -\frac{1}{\alpha}\begin{pmatrix} 2y^2 \\ y \end{pmatrix}.$$

Straightforward computations show that

$$R_1(0) = \text{Span}(\mathbf{e}_2), \quad [f_1,[f_0,f_1]](0) = -6\mathbf{e}_1, \quad [f_1,[f_2,f_1]](0) = \frac{6}{\alpha}\mathbf{e}_1,$$

so we are in the case 1. of Theorem 3.16. Therefore, the system (3.11) is not STLC at $(0,(0,u_2^{\text{eq}})$ for any $u_2^{\text{eq}} \neq \alpha$.

As in Remark 3.20, we define the feedback control $\tilde{u}_2$ such that $u_2 = \alpha + \tilde{u}_2$, that neutralizes the bracket B_1. With this control, the transformed system 3.11 reads

$$\begin{cases} \dot{x} &= -y^2 + yu_1 - \dfrac{2}{\alpha}y^2\tilde{u}_2, \\ \dot{y} &= y - u_1 - \dfrac{1}{\alpha}y\tilde{u}_2, \end{cases} \quad \text{so that } \tilde{f}_0 = \begin{pmatrix} -y^2 \\ y \end{pmatrix}. \tag{3.12}$$

Let us show that this system is STLC at $(0,(0,0))$. To this end, we use the sufficient Sussmann condition for controllability [Sus87, Theorem 7.3] with $\theta = 1$ and the notation for G_η introduced in [GP17, Definition III.10]. Since $[f_1,[f_2,f_1]](0) = \frac{6}{\alpha}\mathbf{e}_1$, the Lie brackets of order 3 generate the whole space, i.e. G_η is the whole tangent space if $\eta > 3$. The only Lie brackets of order at most 3 with an even number of 1 and 2 are $[f_1,[\tilde{f}_0,f_1]]$ and $[f_2,[\tilde{f}_0,f_2]]$, which are both zero and therefore belong trivially to G_3.

Hence, the Sussmann condition from [Sus87] is satisfied and system (3.12) is STLC at $(0,(0,0))$. We conclude that the system (3.11) is STLC at $(0,(0,\alpha))$ (see Remark 3.20 for details).

Application to micro-swimmer robots

The present paper was motivated by the work on controllability of micro-swimmer robot models made in [GP17, GLMP18, Mor19]. The two swimmers studied in these papers are made of two (respectively three) magnetized rigid segments, linked together with torsional

springs, immersed in a low-Reynolds number fluid, and driven by a uniform in space, time-varying magnetic field $\mathbf{H}$. The swimmers' movement is assumed to be planar. The magnetic field $\mathbf{H}$ belongs to the swimmers' plane and can therefore be decomposed, in the moving basis associated to the first segment, in two components called $(H_\perp, H_\parallel)$.

Seeing the magnetic field as a control function, the dynamics of both swimmers write as control systems that are exactly of type (3.2)-(3.3):

$$\dot{\mathbf{z}} = f_0(\mathbf{z}) + H_\perp f_1(\mathbf{z}) + H_\parallel f_2(\mathbf{z}), \tag{3.13}$$

with the state $\mathbf{z}$ in $\mathbb{R}^4$ for the two-link swimmer (resp. $\mathbb{R}^5$ for the three-link swimmer). The detailed expressions of f_0, f_1 and f_2 with respect to the system parameters are given in [GP17, Equations (12) to (16)] (resp. [Mor19, Appendix]).

Moreover, assumptions (3.3) are satisfied. Hence, for all $H_\parallel$ in $\mathbb{R}$, $(0,(0,H_\parallel))$ is an equilibrium point (the first zero is short for $(0,0,0,0)$ in $\mathbb{R}^4$ (resp. $(0,0,0,0,0)$ in $\mathbb{R}^5$)). One also has $R_1(0) = \mathrm{Span}(\mathbf{e}_2, \mathbf{e}_3, \mathbf{e}_4)$ (resp. $R_1(0) = \mathrm{Span}(\mathbf{e}_2, \mathbf{e}_3, \mathbf{e}_4, \mathbf{e}_5)$) and the brackets of interest for Theorem 3.16 read:

$$[f_1,[f_0,f_1]](0) = (a_2,0,0,0) \quad (\text{resp. } [f_1,[f_0,f_1]](0) = (a_3,0,0,0,0))$$

and

$$[f_1,[f_2,f_1]](0) = (b_2,0,0,0) \quad (\text{resp. } [f_1,[f_2,f_1]](0) = (b_3,0,0,0,0))$$

with a_2, a_3, b_2, b_3 constants that are nonzero under generic assumptions on the system parameters – see [GP17, Assumption III.2] (resp. [Mor19, Assumption 1]).

We can therefore apply Theorem 3.16, case 1. and conclude that the two-link swimmer (resp. three-link swimmer) is not STLC at $(0,(0,H_\parallel))$ for any $H_\parallel$ such that $H_\parallel \neq \frac{a_2}{b_2}$ (resp. $H_\parallel \neq \frac{a_3}{b_3}$).

In [Mor19], it is shown that the two-link swimmer (resp. the three-link swimmer) is indeed STLC at $(0,(0,\frac{a_2}{b_2}))$ (resp. $(0,(0,\frac{a_3}{b_3}))$), using the technique displayed in Example 3.22. However, the question of STLC at *other* equilibria of type $(0,(0,H_\parallel))$ was left open in [Mor19, Remark 5]. Theorem 3.16 allows to answer that question: $(0,(0,\frac{a_2}{b_2}))$ (resp. $(0,(0,\frac{a_3}{b_3}))$) is the *only* equilibrium of this type for which the swimmer is STLC.

Remark 3.23. Former studies on the two-link swimmer had led to the following results: in [GP17], it is shown that the control system (3.13) associated to the 2-link swimmer is $\left(2\frac{a_2}{b_2}\right)$-STLC at $(0,(0,0))$; in [GLMP18], it is shown that it is moreover not STLC at $(0,(0,0))$. The proof of this last result features an explicit construction of the function Φ that is used in the proof of Theorem 3.16 below.

3.4.2 Examples for the second bracket obstruction

The following examples provide a prospective insight on the role that u_2 can play when $B_1(0) \in R_1(0)$ and $B_2(0) \notin R_1(0)$. In particular, Example 3.27 displays a case where, similarly to Example 3.22, the second control helps restoring $\mathrm{W}^{1,\infty}$-STLC through the bracket $[f_1,[f_2,f_1]]$.

We start by recalling the classical scalar-input example given by Sussmann in [Sus83,

Equation (6.12), p. 711]:

$$\begin{cases} \dot{x} &= u_1, \\ \dot{y} &= x, \\ \dot{z} &= x^3 + y^2. \end{cases} \tag{3.14}$$

For this system, $B_2(0)$ is outside of $S_1(0)$. Yet is shown in [Sus83] that it is 1-STLC (and STLC as well, as shown for instance in [BM18, Example 12]). Furthermore, Proposition 3.14 shows that it is *not* $\mathrm{W}^{1,\infty}$-STLC: it can only be controlled around $(0,0)$ with small controls if those control's derivatives are "not too small".

In the following examples, we add a second control to this system and look at the effect of this second control on controllability, i.e. if the second control can or cannot help neutralize the bad bracket B_2 to restore controllability with u_1 small in $\mathrm{W}^{1,\infty}$.

From now on, we consider the control system

$$\begin{cases} \dot{x} &= u_1, \\ \dot{y} &= x + \phi(x,y,z)u_2, \\ \dot{z} &= x^3 + y^2 + \psi(x,y,z)u_2, \end{cases} \tag{3.15}$$

with ϕ and ψ real analytic functions from $\mathbb{R}^3$ to $\mathbb{R}$ that vanish at $(0,0,0)$.

Straightforward computations show that $B_1(0) = 0$ (so it trivially belongs to $R_1(0)$), and $B_2(0) = -2\mathbf{e}_3$.

We noticed that several different brackets can neutralize B_2 depending on ϕ and ψ, (whereas in Theorem 3.16, only the bracket $[f_1,[f_2,f_1]]$ can neutralize the bracket B_1). This is illustrated in the following examples, where we choose two different sets of functions ϕ and ψ in order to make the bad bracket B_2 neutralized by the bracket $[[f_0,f_1],[f_2,[f_0,f_1]]]$, then by the bracket $[f_1,[f_2,f_1]]$.

We introduce a new notion of STLC.

Definition 3.24. Let $k \in \mathbb{N}$ and α in $\mathbb{R}$ such that $\alpha \geqslant 0$. The control system (3.2) is $(\mathrm{W}^{k,\infty},\alpha)$-STLC at $(z^{\mathrm{eq}},(u_1^{\mathrm{eq}},u_2^{\mathrm{eq}}))$ if, for every $\varepsilon > 0$, there exists $\eta > 0$ such that, for every z_0, z_1 in $B(z^{\mathrm{eq}},\eta)$, there exists a control $(u_1(\cdot),u_2(\cdot))$ in $\mathrm{W}^{k,\infty}([0,\varepsilon],\mathbb{R}) \times \mathrm{L}^\infty([0,\varepsilon],\mathbb{R})$ such that the solution of the control system $z(\cdot) : [0,\varepsilon] \to \mathbb{R}^n$ of (3.2) satisfies $z(0) = z_0$, $z(\varepsilon) = z_1$, and

$$\|u_1 - u_1^{\mathrm{eq}}\|_{\mathrm{W}^{k,\infty}([0,\varepsilon],\mathbb{R})} \leqslant \varepsilon, \quad \|u_2 - u_2^{\mathrm{eq}}\|_{\mathrm{L}^\infty([0,\varepsilon],\mathbb{R})} \leqslant \alpha + \varepsilon.$$

Remark 3.25. The norms used for each control are different in this STLC notion. It fits the nature of system (3.2), where the second control plays a particular role due to the fact that f_2 vanishes at 0. This could be seen as a form of "hybrid" small-time local controllability.

Example 3.26. Take $\phi(x,y,z) = 0$ and $\psi(x,y,z) = y^2$. Then

$$f_2 = \begin{pmatrix} 0 \\ 0 \\ y^2 \end{pmatrix},$$

and one can compute that $R_1(0) = \mathrm{Span}(\mathbf{e}_1,\mathbf{e}_2)$, $[f_1,[f_2,f_1]](0) = 0$ and $[[f_0,f_1],[f_2,[f_0,f_1]]](0) =$

$-2\mathbf{e}_3$. Let $\epsilon > 0$ and set $u_2 = -1$ on $[0, \epsilon]$. System (3.15) then becomes

$$\begin{cases} \dot{x} &= u_1, \\ \dot{y} &= x, \\ \dot{z} &= x^3, \end{cases} \tag{3.16}$$

which is locally controllable with smooth controls. Therefore (3.15) is $(\mathrm{W}^{1,\infty}, 1)$-STLC: the bad bracket B_2 has seemingly been neutralized by the bracket $[[f_0, f_1], [f_2, [f_0, f_1]]]$.

Example 3.27. Consider the control system (3.15) with $\phi(x, y, z) = 0$ and $\psi(x, y, z) = x^2$. One can check that: $R_1(0) = \mathrm{Span}(\mathbf{e}_1, \mathbf{e}_2)$, $B_1(0) = 0$ (so it trivially belongs to $R_1(0)$), and $B_2(0) = 2\mathbf{e}_3$. Moreover, $[f_1, [f_2, f_1]](0) = 2\mathbf{e}_3$, so $B_2(0) \in R_1(0) + \mathrm{Span}([f_1, [f_2, f_1]](0))$.

Let us show that in this case, system (3.15) is $\mathrm{W}^{1,\infty}$-STLC.

The first step, inspired by the return method of Coron [Cor07, Chapter 6], is to construct a loop trajectory, that goes from and back to 0. We define u_1 and u_2 on $[0, 2\pi\varepsilon]$ by

$$\begin{aligned} u_1(t) &= \tfrac{1}{4}\varepsilon^2 \sin\left(\tfrac{t}{\varepsilon}\right) - \tfrac{1}{2}\varepsilon^2 \sin\left(\tfrac{2t}{\varepsilon}\right); \\ u_2(t) &= \tfrac{5}{16}\varepsilon^2 \cos\left(\tfrac{t}{\varepsilon}\right) - \tfrac{3}{4}\varepsilon^2 \cos\left(\tfrac{2t}{\varepsilon}\right). \end{aligned} \tag{3.17}$$

One can check that, with these controls, the solution of (3.15) starting at $(0, 0, 0)$ satisfies $x(2\pi\varepsilon) = y(2\pi\varepsilon) = z(2\pi\varepsilon) = 0$. Now let us show that a small perturbation of this loop trajectory allows to access a neighbourhood of 0. We define the perturbed control

$$u_{1,\mathrm{per}}(t) = \tfrac{1}{4}\varepsilon^2 \sin\left(\tfrac{t}{\varepsilon}\right) - \tfrac{1}{2}\varepsilon^2 \sin\left(\tfrac{2t}{\varepsilon}\right) + a + bt + ct^3 \tag{3.18}$$

for $(a, b, c) \in \mathbb{R}^3$ such that $|a|, |b|$ and $|c|$ are smaller than ε. Note that for all $|a|, |b|$ and $|c|$ small enough, $\|u_{1,\mathrm{per}}\|_{\mathrm{W}^{1,\infty}} \leqslant \varepsilon$ and $\|u_2\|_{\mathrm{W}^{1,\infty}} \leqslant \varepsilon$. Let $F : \mathbb{R}^3 \to \mathbb{R}^3$ be the function that maps (a, b, c) to
$(x_{\mathrm{per}}(2\pi\varepsilon), y_{\mathrm{per}}(2\pi\varepsilon), z_{\mathrm{per}}(2\pi\varepsilon))$, solution of (3.15) starting at $(0, 0, 0)$ with controls $u_{1,\mathrm{per}}$ and u_2. Integrating system (3.15), $(x_{\mathrm{per}}(2\pi\varepsilon), y_{\mathrm{per}}(2\pi\varepsilon), z_{\mathrm{per}}(2\pi\varepsilon))$ reads

$$\begin{aligned} x(2\pi\varepsilon) &= \textstyle\int_0^{2\pi\varepsilon} u_{1,\mathrm{per}}(t)\mathrm{d}t, \\ y(2\pi\varepsilon) &= \textstyle\int_0^{2\pi\varepsilon}\int_0^t u_{1,\mathrm{per}}(\tau)\mathrm{d}\tau\mathrm{d}t, \\ z(2\pi\varepsilon) &= \textstyle\int_0^{2\pi\varepsilon} \left(\left(\int_0^t u_{1,\mathrm{per}}(\tau)\mathrm{d}\tau\right)^3 + (1 + u_2(t)) \left(\int_0^t \int_0^\tau u_{1,\mathrm{per}}(\sigma)\mathrm{d}\sigma\mathrm{d}\tau\right)^2 \right) \mathrm{d}t, \end{aligned} \tag{3.19}$$

which allows, substituting (3.17) and (3.18) in (3.19), to explicitly calculate the value of $F(a, b, c)$. With the help of a computer algebra software, we can then calculate the determinant of the Jacobian matrix of F at $(0, 0, 0)$, which is equal to

$$-\pi^5\varepsilon^{14}\left(\frac{12}{5}\pi^2\varepsilon - \frac{45}{4}\varepsilon - \frac{184}{27}\pi^2 + \frac{8102}{81}\right),$$

which is nonzero for $\varepsilon > 0$. Therefore, F is onto and we apply the inverse mapping theorem: for every (x, y, z) in a neighborhood of $(0, 0, 0)$, there exists $(a, b, c) \in \mathbb{R}^3$ such that the associated control $(u_{1,\mathrm{per}}, u_2)$ drives the system from $(0, 0, 0)$ to (x, y, z). Hence (3.15) is $\mathrm{W}^{1,\infty}$-STLC at 0.

This example suggests that the bracket $[f_1, [f_2, f_1]]$ plays a strong role in the controllability of the system, as it allows to recover the $\mathrm{W}^{1,\infty}$-STLC that is unattainable in that case

with only one scalar control.

Starting from these examples, we expect to soon be able to state a necessary condition similar to the one in Theorem 3.16 in the case $B_2(0) \not\subset R_1(0)$.

3.5 Proof of the Theorem

We start with a few notations. Given controls u_1, u_2 in $\mathrm{L}^\infty([0,T])$, we denote by $z_u(T)$ the solution of (3.2) with the controls u_1, u_2 at time T, with $z(0) = 0$.

For a vector field f in $\mathcal{X}$ with components $a_1, \dots, a_n$ (n real analytic functions) in coordinates $x = (x_1, \dots, x_n)$, we identify

$$f(x) = \begin{pmatrix} a_1(x) \\ \vdots \\ a_n(x) \end{pmatrix} \quad \text{and} \quad f = \sum_{k=1}^{n} a_k \frac{\partial}{\partial x_k}.$$

Considering f as a differential operator, for a smooth function ϕ, $f\phi$ is given by $f\phi = \sum_{k=1}^{n} a_k \frac{\partial \phi}{\partial x_k}$. For $f, g \in \mathcal{X}$, we define the composed operator (of order 2) fg as $(fg)\phi = f(g\phi)$. In coordinates, and if $g = \sum_{k=1}^{n} b_j \frac{\partial}{\partial x_j}$, one has

$$fg = \sum_{k=1}^{n}\sum_{j=1}^{n} a_k b_j \frac{\partial^2}{\partial x_k \partial x_j} + \sum_{j=1}^{n} \left(\sum_{k=1}^{n} a_k \frac{\partial b_j}{\partial x_k} \right) \frac{\partial}{\partial x_j}.$$

Remark 3.28. When f and g are considered as differential operators, their Lie bracket is simply their commutator: $[f, g] = fg - gf$, and it turns out to be a differential operator of order 1 (i.e. a vector field) because the higher order terms cancel in virtue of Schwarz's theorem.

For a multi-index $I = (i_1, \dots, i_k) \in \{0, 1, 2\}^k$, we denote by f_I the iterated composition of operators $f_{i_1} f_{i_2} \dots f_{i_k}$ associated to (3.2).

Let $u = (u_1, u_2)$ in $\mathrm{L}^\infty([0,T])$. For a multi-index $I = (i_1, \dots, i_k) \in \{0, 1, 2\}^k$, the iterated integral $\int_0^T u_I$ is defined as

$$\int_0^T \int_0^{\tau_k} \int_0^{\tau_{k-1}} \dots \int_0^{\tau_2} u_{i_k}(\tau_k) u_{i_{k-1}}(\tau_{k-1}) \dots u_{i_2}(\tau_2) u_{i_1}(\tau_1) \mathrm{d}\tau_1 \mathrm{d}\tau_2 \dots \mathrm{d}\tau_k, \tag{3.20}$$

with the convention $u_0 = 1$.

Let $\Phi : \mathbb{R}^n \to \mathbb{R}$ a real analytic function defined in a neighbourhood of 0 in $\mathbb{R}^n$. The Chen-Fliess series associated to Φ is defined as

$$\Sigma(u, f, \Phi, T) = \sum_I \left(\int_0^T u_I \right) (f_I \Phi)(0). \tag{3.21}$$

The summation is made over all the multi-indices $I = (i_1, \dots, i_k)$ in $\{0, 1, 2\}^k$ with $k \in \mathbb{N}$. The Chen-Fliess series appears in a range of works in control theory and geometry (see [Fli78, Fli75, Che57]). It is shown in [Sus83, Proposition 4.3, p. 698] that for all $A > 0$, there exists $T_0(A) > 0$ such that the series converges for any $T \leqslant T_0$ and u such that

$\|u\|_{\mathrm{L}^\infty[0,T]} \leqslant A$, uniformly with respect to u and T, to $\Phi(z_u(T))$, i.e. we can write

$$\Phi(z_u(T)) = \Sigma(u, f, \Phi, T). \tag{3.22}$$

It is worth mentioning that the convergence is valid because of the analyticity of the vector fields f_i.

A wisely chosen function Φ conveniently allows, through the series Σ, to focus on the brackets of interest, and highlights their role in the following proofs.

3.5.1 Proof of Theorem 3.16

The following proof relies on similar arguments than those used to show Proposition 3.11 in [Sus83, pp.707-710]. We treat both Case 1. and Case 2. together.

Given u_2^{eq} in $\mathbb{R}$ satisfying moreover $u_2^{\mathrm{eq}} \neq \beta$ in case 1., we can always perform the linear transformation $(u_1, u_2) \mapsto (u_1, u_2 - u_2^{\mathrm{eq}})$ from Remark 3.20 to return to the equilibrium $(0,(0,0))$. One can easily check that the transformed system falls within the same case for the equilibrium $(0,(0,0))$ as the original system for the equilibrium $(0,(0,u_2^{\mathrm{eq}}))$. Therefore, we assume from now on that $u_2^{\mathrm{eq}} = 0$ and we study controllability around $(0,(0,0))$.

The next step is to define suitable local coordinates, and a suitable real analytic function $\Phi : \mathbb{R}^n \to \mathbb{R}$ mapping the state z to one of these local coordinates.

We shall prove that we have, for this suitable choice of Φ,

$$\Phi(z_u(T)) \geqslant 0 \tag{3.23}$$

for any small positive T and any control $u(\cdot) = (u_1(\cdot), u_2(\cdot))$ satisfying the norm requirements from the STLC definitions (3.1 in case 1. or 3.2 in case 2.), with $z_u(\cdot)$ defined on the first line of section 3.5. Provided Φ is a coordinate function, inequality (3.23) obviously contradicts local controllability (STLC in case 1. or α-STLC for any α in case 2.): it means that the halfspace $\{x \in \mathbb{R}^n | \Phi(x) < 0\}$ is locally unreachable.

Let $d_1 = \dim R_1(0)$ and $d_2 = \dim(R_1(0) + \mathrm{Span}([f_1,[f_2,f_1]](0)))$ (d_2 might be equal to d_1 or d_1+1). Let $(g_1, \ldots, g_n)$ be vector fields in $\mathrm{Lie}(f_0, f_1, f_2)$ such that:

- $g_1 = f_1$,
- $(g_1(0), \ldots, g_n(0))$ is a basis of $\mathbb{R}^n$,
- in Case 1., $(g_1(0), \ldots, g_{d_1}(0))$ is a basis of $R_1(0)$ and $g_{d_1+1} = [f_1,[f_0,f_1]]$,
- in Case 2., $(g_1(0), \ldots, g_{d_2}(0))$ is a basis of $R_1(0) + \mathrm{Span}([f_1,[f_2,f_1]](0))$ and $g_{d_2+1} = [f_1,[f_0,f_1]]$.

For $s \in \mathbb{R}$ and g a vector field, let e^{sg} denote the flow of g at time s. The real analytic map $(s_1, \ldots, s_n) \mapsto e^{s_1 g_1} \circ e^{s_2 g_2} \circ \cdots \circ e^{s_n g_n}(0)$ sends 0 to 0. Moreover, its Jacobian at 0 is invertible (for its columns are the components of $g_1(0), \ldots, g_n(0)$). In virtue of the inverse mapping theorem, it has a real analytic inverse $\zeta \mapsto (s_1(\zeta), \ldots, s_n(\zeta))$, defined a certain neighborhood $\mathcal{V}$ of $z = 0$ in $\mathbb{R}^n$. One then has, for all ζ in $\mathcal{V}$,

$$\zeta = e^{s_1(\zeta) g_1} \circ e^{s_2(\zeta) g_2} \circ \cdots \circ e^{s_n(\zeta) g_n}(0),$$

i.e., $(s_1, \ldots, s_n)$ are local coordinates for ζ. Then:

- in case 1., we define $\Phi(\zeta) = s_{d_1+1}(\zeta)$,

— in case 2., we define $\Phi(\zeta) = s_{d_2+1}(\zeta)$.

The function Φ is real analytic on $\mathcal{V}$ and has, by construction, the following properties:

$$\Phi(0) = 0, \tag{3.24}$$
$$\text{(Case 2.)} \quad \forall g \in R_1, (g\Phi)(0) = 0, \tag{3.25}$$
$$\text{(Case 1.)} \quad \forall g \in R_1 + \mathrm{Span}([f_1, [f_2, f_1]]), (g\Phi)(0) = 0, \tag{3.26}$$
$$f_1\Phi = 0 \text{ on } \mathcal{V}, \tag{3.27}$$
$$([f_1, [f_1, f_0]]\Phi)(0) = 1. \tag{3.28}$$

We then consider the Chen-Fliess series $\Sigma(u, f, \Phi, T)$ associated to Φ (see (3.21)) and split its terms into six different types:

$$\Sigma(u, f, \Phi, T) = P_1 + P_2 + P_3 + P_4 + P_5 + P_6,$$

where each P_i contains the terms with multi-indices I defined as follows:

— $P_1 : I = (2, \dots)$, or $I = (0, \dots)$,

— $P_2 : I = (\dots, 1)$,

— $P_3 : I = (1, J)$ with J containing only 0's and 2's,

— $P_4 : I = (1, 1, 0)$,

— $P_5 : I = (1, 1, 2)$,

— P_6 : all the remaining terms.

The first three parts are easily dealt with:

Lemma 3.29. *One has* $P_1 = P_2 = P_3 = 0$.

Proof. We have $P_1 = P_2 = 0$ because, from (3.27) and assumption (3.3), $f_I\Phi(0) = 0$ for I of these types.

We also have $P_3 = 0$; indeed, let $I = (1, i_2, \dots, i_k)$ with $i_j = 0$ or 2 for all $j \in \{2, \dots k\}$. Then we can write that:

$$f_1 f_{i_2} \dots f_{i_k} = [f_1, f_{i_2}] f_{i_3} \dots f_{i_k} + f_{i_2} f_1 \dots f_{i_k},$$

and $(f_{i_2} f_1 \dots f_{i_k}\phi)(0) = 0$ because of assumption (3.3) and the fact that $i_2 = 0$ or 2. Similarly, we have

$$[f_1, f_{i_2}] f_{i_3} \dots f_{i_k} = [[f_1, f_{i_2}], f_{i_3}] f_{i_4} \dots f_{i_k} + f_{i_3}[f_1, f_{i_2}] \dots f_{i_k},$$

and $((f_{i_3}[f_1, f_{i_2}] \dots f_{i_k})\phi)(0) = 0$ because of assumption (3.3) and the fact that $i_3 = 0$ or 2. Repeating this operation $k - 3$ more times, we eventually get that

$$(f_1 f_{i_2} \dots f_{i_k}\phi)(0) = ([\dots [f_1, f_{i_2}], \dots, f_{i_k}]\phi)(0).$$

But $[\dots [f_1, f_{i_2}], \dots, f_{i_k}]$ is in R_1, so $(f_1 f_{i_2} \dots f_{i_k}\phi)(0) = 0$ because of (3.25). □

The terms P_4 and P_5, associated to the brackets $[[f_1, f_0], f_1]$ and $[[f_1, f_2], f_1]$, are the key

parts of the proof. Let us compute their value. For P_4, we write

$$\begin{aligned} f_1 f_1 f_0 &= f_1 f_0 f_1 + f_1[f_1, f_0] \\ &= f_1 f_0 f_1 - [f_1, f_0] f_1 - [[f_1, f_0], f_1]. \end{aligned}$$

The first two terms on the right-hand side vanish when evaluated at 0 against Φ because of (3.27), so $(f_{(1,1,0)}\Phi)(0) = -([[f_1, f_0], f_1]\Phi)(0) = 1$ by (3.28). Moreover, the control integral part is given by

$$\begin{aligned} \int_0^T u_{(1,1,0)} &= \int_0^T \int_0^s u_1(\sigma) \int_0^\sigma u_1(\tau) \mathrm{d}\tau \mathrm{d}\sigma \mathrm{d}s \\ &= \int_0^T \int_0^s v_1'(\sigma) v_1(\sigma) \mathrm{d}\sigma \mathrm{d}s \\ &= \frac{1}{2} \int_0^T v_1^2(s) \mathrm{d}s \end{aligned}$$

with

$$v_1(t) = \int_0^t u_1(s) \mathrm{d}s, \tag{3.29}$$

so overall $P_4 = \frac{1}{2}\|v_1\|_{\mathrm{L}^2}^2$.

For P_5, using assumption (3.3) and (3.27) again, we obtain

$$(f_1 f_1 f_2 \Phi)(0) = ([f_1, [f_1, f_2]]\Phi)(0).$$

This is where the two different cases of the theorem appear. Indeed:

— Case 2.: we have $(f_1 f_1 f_2 \Phi)(0) = 0$ thanks to (3.26), so $P_5 = 0$.

— Case 1.: $[f_1, [f_0, f_1]](0) \in R_1(0) + \mathrm{Span}([f_1, [f_2, f_1]](0))$.

Here, we write that $[f_1, [f_2, f_1]] = -\beta[f_1, [f_0, f_1]] + g$, with $g \in R_1$ and $\beta \in \mathbb{R}^*$. Thanks to (3.25) and (3.28), we conclude that

$$(f_1 f_1 f_2 \Phi)(0) = -\beta.$$

The control integral associated to P_5 reads

$$\begin{aligned} \int_0^T u_{(1,1,2)} &= \int_0^T u_2(s) \int_0^s u_1(\sigma) \int_0^\sigma u_1(\tau) \mathrm{d}\tau \mathrm{d}\sigma \mathrm{d}s \\ &\leqslant \frac{1}{2} \|u_2\|_{\mathrm{L}^\infty} \|v_1\|_{\mathrm{L}^2}^2 \end{aligned}$$

and therefore P_5 is bounded:

$$|P_5| \leqslant \frac{1}{2}|\beta| \, \|u_2\|_{\mathrm{L}^\infty} \|v_1\|_{\mathrm{L}^2}^2. \tag{3.30}$$

Finally, we show that the terms of P_6 add up to a small remainder, through the following technical lemma:

Lemma 3.30. *There exists $T_0 > 0$ and a constant $D(T_0) > 0$ such that, for all T in $[0, T_0]$,*

$$|P_6| \leqslant T D(T_0) \|v_1\|_{\mathrm{L}^2}^2. \tag{3.31}$$

Proof. Let I be a multi-index such that the associated term in the series is in P_6. Then $I = (1, J, 1, K)$ with $K = (k_1, \dots, k_q)$ and $J = (j_1, \dots, j_r)$ such that $q \geqslant 1$, $q + r \geqslant 2$ and J contains only 0's and 2's. Let us denote by J_2 the number of 2's in J, and K_1 and K_2 respectively the number of 1's and 2's in K. The control integral associated to I reads

$$\int_0^T u_I = \int_0^T \int_0^{s_q} \int_0^{s_{q-1}} \dots \int_0^{s_2} u_{k_q}(s_q) u_{k_{q-1}}(s_{q-1}) \dots u_{k_1}(s_2) W_r(s_1) \mathrm{d}s_1 \dots \mathrm{d}s_q, \tag{3.32}$$

with

$$W_r(s) = \int_0^s u_1(\tau_{r+1}) \int_0^{\tau_{r+1}} u_{j_r}(\tau_r) \dots \int_0^{\tau_1} u_{j_1}(\tau_1) \int_0^{\tau_0} u_1(\tau_0) \mathrm{d}\tau_0 \dots \mathrm{d}\tau_{r+1}.$$

Applying triangular inequality, bounding u_2 by $\|u_2\|_{\mathrm{L}^\infty}$ and using $u_0 = 1$ yields

$$\left| \int_0^T u_I \right| \leqslant \|u_2\|_{\mathrm{L}^\infty}^{K_2} \|u_1\|_{\mathrm{L}^\infty}^{K_1} \int_0^T \int_0^{s_q} \int_0^{s_{q-1}} \dots \int_0^{s_2} |W_r(s_1)| \mathrm{d}s_1 \dots \mathrm{d}s_q, \tag{3.33}$$

which rewrites as

$$\left| \int_0^T u_I \right| \leqslant \|u_2\|_{\mathrm{L}^\infty}^{K_2} \|u_1\|_{\mathrm{L}^\infty}^{K_1} \frac{1}{(q-1)!} \int_0^T (T-s)^{q-1} |W_r(s)| \mathrm{d}s. \tag{3.34}$$

The study of $W_r(s)$ splits in three cases.

— **Case r=0.** In this case, we have

$$W_0(s) = \frac{1}{2} v_1^2(s), \tag{3.35}$$

where v_1 is defined in (3.29).

— **Case r=1.** In this case, we integrate by parts to get

$$W_1(s) = v_1(s) \int_0^s u_{j_1}(\tau) v_1(\tau) \mathrm{d}\tau - \int_0^s u_{j_1}(\tau) v_1^2(\tau) \mathrm{d}\tau, \tag{3.36}$$

and we apply triangular inequality to bound the u_{j_1} term:

$$\|W_1(s)\| \leqslant \|u_2\|_{\mathrm{L}^\infty}^{J_2} \left(|v_1(s)| \int_0^\tau |v_1(\tau)| \mathrm{d}\tau - \int_0^s v_1^2(\tau) \mathrm{d}\tau \right). \tag{3.37}$$

(recall that, here, $J_2 = 1$ if $j_1 = 2$ and $J_2 = 0$ if $j_1 = 0$.)

— **Case r>1.** In this case, we integrate by parts to get

$$\begin{aligned} W_r(s) = \; & v_1(s) \int_0^s u_{j_r}(\tau_r) \int_0^{\tau_r} u_{j_{r-1}}(\tau_{r-1}) \dots \int_0^{\tau_2} u_{j_1}(\tau_1) v(\tau_1) \mathrm{d}\tau_1 \dots \mathrm{d}\tau_r \\ & - \int_0^s v_1(\tau_r) u_{j_r}(\tau_r) \int_0^{\tau_r} u_{j_{r-1}}(\tau_{r-1} \dots \int_0^{\tau_2} u_{j_1}(\tau_1) v(\tau_1) \mathrm{d}\tau_1 \dots \mathrm{d}\tau_r, \end{aligned} \tag{3.38}$$

and we use triangular inequality to bound the u_{j_p} terms:

$$\begin{aligned} |W_r(s)| \leqslant \; & \|u_2\|_{\mathrm{L}^\infty}^{J_2} \Big(|v_1(s)| \int_0^s \int_0^{\tau_r} \dots \int_0^{\tau_1} |v_1(\tau_1)| \mathrm{d}\tau_1 \dots \mathrm{d}\tau_r \\ & - \int_0^s |v_1(s)| \int_0^{\tau_r} \dots \int_0^{\tau_1} |v_1(\tau_1)| \mathrm{d}\tau_1 \dots \mathrm{d}\tau_r \Big), \end{aligned} \tag{3.39}$$

which rewrites as

$$|W_r(s)| \leqslant \|u_2\|_{\mathrm{L}^\infty}^{J_2}\Big(\frac{|v_1(s)|}{(r-1)!}\int_0^s (s-\sigma)^{r-1}|v_1(\sigma)|\mathrm{d}\sigma - \frac{1}{(r-2)!}\int_0^s |v_1(\tau)|\int_0^\tau (\tau-\sigma)^{r-2}|v_1(\sigma)|\mathrm{d}\sigma\mathrm{d}\tau\Big). \tag{3.40}$$

The Cauchy-Schwarz inequality yields

$$\int_0^s (s-\sigma)^{r-1}|v_1(\sigma)|\mathrm{d}\sigma \leqslant \frac{s^{r-1/2}}{\sqrt{2r-1}}\|v_1\|_{\mathrm{L}^2} \quad . \tag{3.41}$$

We then apply (3.41) to (3.40), once to the first term and twice to the second term, which leads to the following upper bound:

$$|W_r(s)| \leqslant \|u_2\|_{\mathrm{L}^\infty}^{J_2}\left(|v_1(s)|\frac{\|v_1\|_{\mathrm{L}^2}}{(r-1)!}\frac{s^{r-1/2}}{\sqrt{2r-1}} + \frac{\|v_1\|_{\mathrm{L}^2}^2}{(r-2)!}\frac{s^{r-1}}{\sqrt{(2r-3)(2r-2)}}\right). \tag{3.42}$$

Substituting (3.35), (3.37), and (3.42) in (3.34), and bounding $(T-s)$ by T, we have:

$$\left|\int_0^T u_I\right| \leqslant \|u_2\|_{\mathrm{L}^\infty}^{K_2+J_2}\|u_1\|_{\mathrm{L}^\infty}^{K_1}\frac{AT^{q+r-1}}{(q-1)!(r-2)!}\|v_1\|_{\mathrm{L}^2}^2, \tag{3.43}$$

where $(r-2)!$ is replaced by 1 if $r \in \{0,1\}$. Here and hereafter, A is a constant that may vary from line to line.

The fields f_i and the function Φ are real analytic. Under these assumptions, it is stated in [Sus83, Lemma 4.2, p.697] that we have, for some constant C independent of I,

$$|(f_I\Phi)(0)| \leqslant C^{q+r+2}(q+r+2)!. \tag{3.44}$$

Combining (3.43) and (3.44), we find an upper bound for the whole term of index I from the series:

$$\left|\left(\int_0^T u_I\right)(f_I\Phi)(0)\right| \leqslant B(q,r)\|Tu_2\|_{\mathrm{L}^\infty}^{K_2+J_2}\|u_1\|_{\mathrm{L}^\infty}^{K_1},$$

with

$$B(q,r) = AC^{q+r+2}T^{q+r-2}\frac{(q+r)!(q+r+2)^5}{q!r!}\|v_1\|_{\mathrm{L}^2}^2,$$

where we bounded $\frac{(q+r+2)}{(q-1)!(r-2)!}$ by $\frac{(q+r)!(q+r+2)^5}{q!r!}$ to encompass the cases $r=0$ and $r=1$.

For any given q and r, there are 2^r3^q corresponding indices I. More precisely:

— for any given q, K_2, K_1, there are $\binom{q}{K_1}$ choices to place the 2's and then $\binom{q-K_1}{K_2}$ choices to place the 1's.

— for any given r, J_2, there are $\binom{r}{J_2}$ choices to place the 1's.

Therefore, summing all the terms in P_6, we obtain an upper bound:

$$|P_6| \leqslant T\sum_{\substack{r\geqslant 0, q\geqslant 1\\ r+q\geqslant 2}} B(q,r)\sum_{J_2=0}^{r}\binom{r}{J_2}\|u_2\|_{\mathrm{L}^\infty}^{J_2}\sum_{K_1=0}^{q}\binom{q}{K_1}\|u_1\|_{\mathrm{L}^\infty}^{K_1}\sum_{K_2=0}^{q-K_1}\binom{q-K_1}{K_2}\|u_2\|_{\mathrm{L}^\infty}^{K_2}. \tag{3.45}$$

This rewrites as

$$|P_6| \leqslant T \sum_{\substack{r\geqslant 0, q\geqslant 1\\ r+q\geqslant 2}} B(q,r)(1+\|u_2\|_{\mathrm{L}^\infty})^r(1+\|u_2\|_{\mathrm{L}^\infty}+\|u_1\|_{\mathrm{L}^\infty})^q. \tag{3.46}$$

Using $(1+\|u_2\|_{\mathrm{L}^\infty}) \leqslant (1+\|u_2\|_{\mathrm{L}^\infty}+\|u_1\|_{\mathrm{L}^\infty})$ and renumbering the terms of the sum for $p \geqslant 2$ and $0 \leqslant r \leqslant p$ (such that $p = r+q$ in equations (3.45) and (3.46)), one obtains

$$|P_6| \leqslant T \sum_{p\geqslant 2} \sum_{r=0}^{p} B(p-r,r)(1+\|u_2\|_{\mathrm{L}^\infty}+\|u_1\|_{\mathrm{L}^\infty})^p. \tag{3.47}$$

There exists T_0 such that the series in (3.47) converges for all T in $[0,T_0]$.

Including its limit for $T = T_0$ and the other constants in a new constant $D(T_0)$, we finally obtain (3.31) for any $T \in [0,T_0]$. □

We now end the proof of the theorem in both cases.

In case 2., we obtain that

$$\Sigma(u,f,\Phi,T) = \frac{1}{2}\|v_1\|_2^2 + P_6. \tag{3.48}$$

Let T_0 and $D(T_0)$ be as defined in Lemma 3.30. Let ε_0 be a real positive number such that $\varepsilon_0 D(T_0) \leqslant \frac{1}{2}$. Let $\varepsilon = \min(T_0, \varepsilon_0)$. Using (3.31) in (3.48), we obtain that $\Sigma(u,f,\Phi,T) \geqslant 0$ for all $T \leqslant \varepsilon$, i.e. we have proven (3.23). Hence, system (3.2) is not α-STLC at $(0,(0,0))$ for any $\alpha \geqslant 0$.

In case 1., we have

$$\Sigma(u,f,\Phi,T) = \frac{1}{2}\|v_1\|_2^2 + P_5 + P_6, \tag{3.49}$$

knowing, thanks to (3.30) and Lemma 3.30 that

$$|P_5 + P_6| \leqslant \frac{1}{2}|\beta|\|u_2\|_{\mathrm{L}^\infty}\|v_1\|_{\mathrm{L}^2}^2 + TD(T_0)\|v_1\|_{\mathrm{L}^2}^2. \tag{3.50}$$

Let ε_0 be a real positive number such that $\varepsilon(\frac{1}{2}|\beta| + D(T_0)) \leqslant \frac{1}{2}$. Let $\varepsilon = \min(T_0, \varepsilon_0)$. Assume $T \leqslant \varepsilon$ and $\|u_2\|_{\mathrm{L}^\infty} \leqslant \varepsilon$. Using (3.50) in (3.49), we obtain that $\Sigma(u,f,\Phi,T) \geqslant 0$ for all $T \leqslant \varepsilon$ and $\|u_2\|_{\mathrm{L}^\infty} \leqslant \varepsilon$, i.e. we have proven (3.23). Hence, system (3.2) is not STLC at $(0,(0,0))$.

This ends the proof of Theorem 3.16.

3.6 Conclusion

In this paper, we explored the controllability properties of systems with two controls (3.2), satisfying the assumption (3.3). Theorem 3.16 provides a necessary condition for local controllability around equilibria. This result extends the classical necessary conditions stated for scalar-control systems in [Sus83]. Moreover, it is, to the best of our knowledge, the first result of this nature for non-scalar-input systems.

This work does not only present a theoretical interest for control theory. Using Theorem 3.16, we were able to solve the open question of the local controllability of magnetically

controlled micro-swimming robots (see paragraph). One can use our results to easily and systematically address local controllability issues in similar applied situations.

Our necessary condition is only based on the "bad" bracket B_1 and (see equation (3.7)), but there are higher-order brackets that may prevent $S_2(0)$ to be contained in $S_1(0)$ (in the single-input case see for instance [BM18]). Giving necessary conditions based on these brackets, for instance adapting the results from [BM18] to the situation (3.2)-(3.3), is a possible continuation of the present work. The complexity of the higher-order terms structure in the Chen-Fliess series however makes the analysis very intricate.

Chapter 4

Controllability of semi-linear parabolic equations with positive state constraint

This chapter presents unpublished results obtained in collaboration with Pierre Lissy.

4.1 Introduction

Let d be an integer such that $d \geqslant 1$. Let Ω be a bounded open connected set of $\mathbb{R}^d$, and ω an open subset of Ω. Let R be a second-order self-adjoint elliptic operator given by

$$R = \sum_{i,j=1}^{d} \partial_i(r_{ij}(x)\partial_j) + c(x), \tag{4.1}$$

with $c \in \mathrm{L}^\infty(\Omega)$, and $r_{ij} \in W^{1,\infty}(\Omega)$ for $i, j \in \{1, \dots, d\}$ satisfying

$$r_{ij}(x) = r_{ji}(x) \tag{4.2}$$

and the ellipticity condition

$$\exists \alpha > 0, \forall \xi \in \mathbb{R}^d, \sum_{i,j=1}^{d} r_{ij}(x)\xi_i\xi_j \geqslant a_0|\xi|^2 \tag{4.3}$$

almost everywhere on Ω.

Let n, m in $\mathbb{N}^*$ and $T > 0$. We consider the parabolic linear system of n scalar equations

$$\begin{cases} \partial_t Y - DRY &= AY + Bu\mathbf{1}_\omega \quad \text{on } (0,T)\times\Omega; \\ \frac{\partial Y}{\partial n} &= 0 \quad \text{on } (0,T)\times\partial\Omega; \\ Y(0,\cdot) &= Y_0(\cdot) \quad \text{on } \Omega. \end{cases} \tag{PL}$$

In (PL), D is a diagonalizable matrix in $\mathcal{M}_n(\mathbb{R})$, A is a square matrix in $\mathcal{M}_n(\mathbb{R})$ and B is a matrix in $\mathcal{M}_{n,m}(\mathbb{R})$.

Controllability of (PL) to trajectories under a Kalman-type condition is known since [AKBDGB09b] (see Proposition 4.6). The question we address in this paper is the following

: is it possible to ensure that the states remains nonnegative while controlling (PL) between two nonnegative trajectories? This question is relevant because systems like (PL) frequently model phenomena in which the state is nonnegative (*e.g.* concentrations of chemicals). In these cases, a controlled trajectory that does not remain nonnegative would have no interest for applications.

State-constrained controllability is a challenging subject that has gained popularity in the last few years. Results have been obtained in [LTZ17] for the heat equation, in [LTZ18] for linear ODE systems, and in [PZ17] for semilinear parabolic equations. They can be summarized this way: when the system is controllable in the classical sense, controllability with nonnegative state is usually possible *in large time*. Moreover, the results about parabolic equations are valid under restrictive hypothesis on initial condition and target (e.g. they are constant steady states).

In the following, we state similar results for coupled parabolic systems of the form (PL). In the general case, we show that under reasonable assumptions on the coupling matrix A, (PL) is controllable in large time, with state remaining "approximately" nonnegative (*i.e.* greater than $-\epsilon$ for any $\epsilon > 0$). When $D = I_n$, this result is slightly improved: the hypothesis on A can be relaxed and controllability in large time with nonnegative state is achieved.

4.2 Properties of system (PL)

In the following, for Y a vector in $\mathbb{R}^n$ and $\alpha \in \mathbb{R}$, we write $Y \geqslant \alpha$ and $Y > 0$ if all the n components of Y are respectively greater or equal to α and greater than α. Moreover, $|Y|$ is the usual Euclidean norm of Y on $\mathbb{R}^n$ and $\max Y$ designates the greatest component of Y. Finally, for $r \geqslant 0$, $\mathrm{H}^r(\Omega)$ denotes the Sobolev space $W^{r,2}(\Omega)$.

It is well-known that, for every $Y_0 \in \mathrm{L}^2(\Omega)^n$ and $u \in \mathrm{L}^2((0,T)\times\omega)^m$, the Cauchy problem given by system (PL) possesses a unique solution $Y \in \mathrm{L}^2((0,T), H^1(\Omega)^n) \cap C^0([0,T], \mathrm{L}^2(\Omega)^n)$.

Moreover, the solutions satisfy the following standard well-posedness estimation for PDE systems, that will be useful to the proof of our result:

Proposition 4.1 (Well-posedness)**.** *Let $T > 0$, $Y_0 \in \mathrm{L}^\infty(\Omega)^n$. There exists $r, s \geqslant 0$ such that, for all $u \in (\mathrm{L}^2((0,T), \mathrm{H}^r(\omega)) \cap \mathrm{H}^s((0,T), \mathrm{L}^2(\omega)))^m$, there exists $C(T) > 0$ (also depending on r and s) such that the solution of (PL) with initial condition Y_0 and control u satisfies*

$$\forall t \in [0,T], \|Y(t,\cdot) - \tilde{Y}(t,\cdot)\|_{\mathrm{L}^\infty(\Omega)^n} \leqslant C(T)\|u\|_{\mathrm{L}^2((0,T),\mathrm{H}^r(\omega))^m} + \|u\|_{\mathrm{H}^s((0,T),\mathrm{L}^2(\omega))^m}, \quad (4.4)$$

where $\tilde{Y}$ is the solution of (PL) with initial condition Y_0 and without control.

From now on, we take r and s such that (4.4) holds.

Assume that the coupling matrix A is quasipositive, i.e.

$$\forall i, j \in \{1, \dots, n\}, i \neq j \Rightarrow a_{i,j} \geqslant 0. \quad (4.5)$$

and that it also satisfies

$$\forall \xi \in \mathbb{R}^n, \langle A\xi, \xi \rangle \leqslant 0. \quad (4.6)$$

Proposition 4.2 (Positivity [Pie10, Lemma 1.1])**.** *Let $Y_0 \in \mathrm{L}^\infty(\Omega)^n$ such that $Y_0 \geqslant 0$. The solution Y of (PL) with initial condition Y_0 satisfies $Y(t,\cdot) \geqslant 0$ for all time t if and only if (4.5) is satisfied.*

Remark 4.3. Our goal is to control the system with a positivity constraint on the state Y. Therefore, it seems reasonable to assume that uncontrolled solutions naturally stay nonnegative, hence assumption (4.5).

Proposition 4.4 (Boundedness)**.** *Let $Y_0 \in \mathrm{L}^\infty(\Omega)^n$. If (4.6) is satisfied, then the solution Y of (PL) with initial condition Y_0 and no control satisfies $\|Y(t,\cdot)\|_{\mathrm{L}^2(\Omega)^n} \leqslant \int_\Omega |Y_0|^2$ for all time t.*

Proof. Let Y be a solution of (PL) with $u = 0$. Let $t > 0$. Take scalar product of (PL) with Y and integrate over Ω:

$$\int_\Omega \langle \partial_t Y, Y\rangle - \int_\Omega \langle DRY, Y\rangle = \int_\Omega \langle AY, Y\rangle, \tag{4.7}$$

which rewrites as

$$\frac{1}{2}\frac{d}{dt}\int_\Omega |Y|^2 = \int_\Omega \langle DRY, Y\rangle + \int_\Omega \langle AY, Y\rangle \leqslant 0 \tag{4.8}$$

because of assumption (4.6). Hence, for all $t > 0$,

$$\int_\Omega |Y(t)|^2 \leqslant \int_\Omega |Y_0|^2. \tag{4.9}$$

□

Finally, let us recall the controllability results for system (PL).

Definition 4.5 (Controllability to trajectories)**.** Let $T > 0$. System (PL) is *controllable to trajectories* in time T if, for all $Y_0 \in \mathrm{L}^\infty(\Omega)^n$, and for all Y^{f} solution of (PL) with initial condition $Y_0^{\mathrm{f}} \in \mathrm{L}^\infty(\Omega)^n$, there exists a control u in $\mathrm{L}^\infty([0,T]\times\omega)^m$ such that the solution Y of (PL) with initial condition Y_0 and control u satisfies

$$Y(T,\cdot) = Y^{\mathrm{f}}(T,\cdot). \tag{4.10}$$

The operator $-R$ with Neumann boundary admits a sequence of eigenvalues $(\lambda_p)_{p\in\mathbb{N}}$ such that

$$0 = \lambda_0 < \lambda_1 \leqslant \lambda_2 \leqslant \dots, \quad \lim_{p\to+\infty} \lambda_p + \infty,$$

with an associated sequence of eigenfunctions $(\phi_p)_{p\in\mathbb{N}}$ that forms an orthonormal basis of $\mathrm{L}^2(\Omega)$.

Given two matrices A in $\mathcal{M}_n(\mathbb{R})$ and B in $\mathcal{M}_{n,m}(\mathbb{R})$, we use the following notation for the *Kalman matrix* associated to A and B:

$$[A|B] = \left[A^{n-1}B \mid A^{n-2}B \mid \dots \mid B\right]. \tag{4.11}$$

Controllability to trajectories is ensured for the system (4.5) under a Kalman-type condition, established in [AKBDGB09b]:

Proposition 4.6 (Controllability [AKBDGB09b, Theorem 1.1])**.** *System (PL) is controllable to trajectories at any time T if and only if, for all $p \in \mathbb{N}$,*

$$\operatorname{rank}\left[(-\lambda_p D + A)|B\right] = n. \tag{4.12}$$

Remark 4.7. In the case $D = I_n$, condition (4.6) simply becomes

$$\operatorname{rank}[A|B] = n. \tag{4.13}$$

The authors of [AKBDGB09b] also state a useful estimation on the control cost:

Proposition 4.8 (Control cost [AKBDGB09b, Theorem 5.2])**.** *Assume (4.12) holds. Let $Y_0 \in \mathrm{L}^\infty(\Omega)^n$ and Y^1 a trajectory of system (PL) associated to the initial condition $Y_0^1 \in \mathrm{L}^\infty(\Omega)^n$. Let $u \in (\mathrm{L}^2((0,T),\mathrm{H}^r(\omega)) \cap \mathrm{H}^s((0,T),\mathrm{L}^2(\omega)))^m$ a control such that $Y(T,\cdot) = Y^1(T,\cdot)$. Then, there exists $K(T)$ such that*

$$\|u\|_{\mathrm{L}^2((0,T),\mathrm{H}^r(\omega))^m} + \|u\|_{\mathrm{H}^s((0,T),\mathrm{L}^2(\omega))^m} \leqslant K(T)\|Y_0 - Y_0^1\|_{\mathrm{L}^2(\Omega)^n}. \tag{4.14}$$

Remark 4.9. Theorem 5.2 in [AKBDGB09b] states this control cost inequality with $u \in \mathrm{L}^2((0,T),\omega)^m$, using an observability inequality. As noted in [LTZ17, p. 1616], it still holds with u taken more regular, hence (4.14).

4.3 Main results

We now state our main results :

Theorem 4.10 (General case)**.** *Assume (4.5), (4.6) and (4.12). Let $\tilde{Y}$ and Y^{f} in $\mathrm{L}^2(\mathbb{R}_+\times\Omega)^n$ be trajectories of (PL), starting respectively at Y_0 and Y_0^{f} in $\mathrm{L}^\infty(\Omega)^n$ and such that $Y_0 \geqslant 0$ and $Y_0^{\mathrm{f}} \geqslant 0$. Let*

$$\zeta = \min\left(\inf_{(\mathbb{R}_+\times\Omega)^n} Y(t,x), \inf_{(\mathbb{R}_+\times\Omega)^n} Y^{\mathrm{f}}(t,x)\right) \geqslant 0.$$

Then, for all $\varepsilon > 0$, there exists $T > 0$ and $u \in (\mathrm{L}^2((0,T),\mathrm{H}^r(\omega)) \cap \mathrm{H}^s((0,T),\mathrm{L}^2(\omega)))^m$ such that the solution Y of (PL) with initial condition Y_0 and control u satisfies

$$Y(T,\cdot) = Y^{\mathrm{f}}(T,\cdot), \tag{4.15}$$

and, for all t in $[0,T]$,

$$Y(t,\cdot) \geqslant \zeta - \varepsilon. \tag{4.16}$$

Remark 4.11. In particular, if $\zeta > 0$, (PL) is controllable with nonnegative state.

In the particular case $D = I_n$, one can remove condition (4.6) and actually ensure that the state remains nonnegative:

Theorem 4.12 (Case $D = I_n$)**.** *Assume that $D = I_n$ and that A and B satisfy (4.5) and (4.13).*

Let Y_0, Y_0^{f} in $\mathrm{L}^\infty(\Omega)^n$ and Y^{f} the trajectory starting at Y_0^{f}. Assume that

$$Y_0 \geqslant 0, Y_0^{\mathrm{f}} \geqslant 0 \tag{4.17}$$

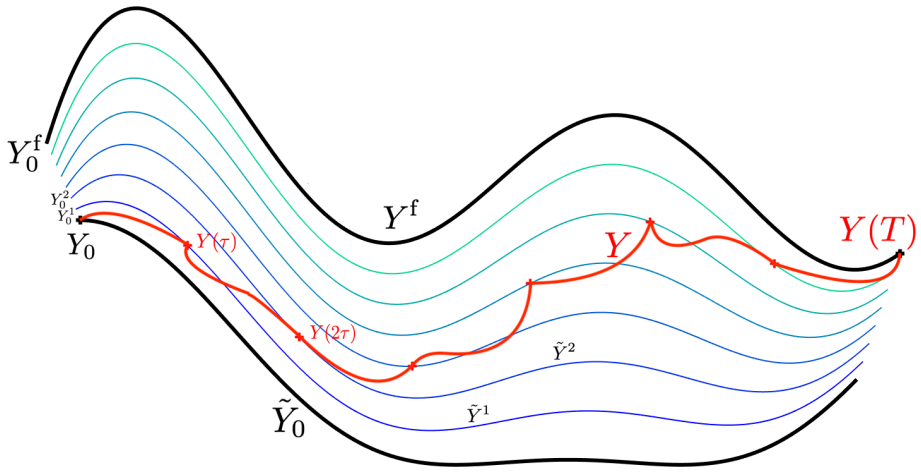

Figure 4.1 – Schematic representation of the staircase method used for the proof of Theorem 4.10.

and that none of the components of Y_0 *and* Y_0^{f} *is a.e. zero on* Ω.

Then, there exists $T > 0$ *and* $u \in (\mathrm{L}^2((0,T),\mathrm{H}^r(\omega)) \cap \mathrm{H}^s((0,T),\mathrm{L}^2(\omega)))^m$ *such that the solution* Y *of* (PL) *with initial condition* Y_0 *and control* u *satisfies*

$$Y(T,\cdot) = Y^{\mathrm{f}}(T,\cdot), \tag{4.18}$$

and, for all t *in* $[0,T]$,

$$Y(t,\cdot) \geqslant 0. \tag{4.19}$$

Proof of Theorem 4.10. Let $\tau > 0$, $\varepsilon > 0$, $Y^0 \in \mathrm{L}^\infty(\Omega)^n$ such that $Y_0 \geqslant 0$, and Y^{f} in $\mathrm{L}^\infty(\mathbb{R}_+ \times \Omega)^n$ a trajectory of (PL) associated to the initial condition $Y_0^{\mathrm{f}} \geqslant 0$. Let ζ defined as in Theorem 4.10.

The proof is based on what may be called a "staircase" or "quasistatic" strategy. Starting from the free trajectory $\tilde{Y}$ originated at Y_0, we make small steps towards Y^{f} following a path of trajectories such that the controlled trajectory stays always close to a nonnegative free trajectory, and therefore almost nonnegative (see Figure 4.1). The same strategy is used for a similar result of state constrained controllability on the linear heat equation in [LTZ17] and between two steady states of a semilinear parabolic equation in [PZ17].

Let us start with a useful lemma.

Lemma 4.13. *Let* $Y_0 \in \mathrm{L}^\infty(\Omega)^n$, $\tilde{Y}$ *the solution of* (PL) *with initial condition* Y_0 *and no control, and* Y_1 *a trajectory of* (PL) *with an initial condition* Y_1^0. *Then, for all* $T > 0$, *there exists a control* u *and* $C(T)$ *such that the solution* Y *of* (PL) *with initial condition* Y_0 *and control* u *satisfies* $Y(T,\cdot) = Y_1(T,\cdot)$ *and*

$$\forall t \in [0,T], \|Y(t) - \tilde{Y}(t)\|_{\mathrm{L}^\infty(\Omega)^n} \leqslant C(T)\|Y_0 - Y_1^0\|_{\mathrm{L}^2(\Omega)^n}. \tag{4.20}$$

Proof. Combine Propositions 4.1 and 4.8 for r, s such that (4.4) holds. □

Let $\delta > 0$. Let $N \in \mathbb{N}^*$ such that $\frac{1}{N}\|Y_0 - Y_0^{\mathrm{f}}\|_{\mathrm{L}^2(\Omega)^n} \leqslant \delta$. For $k \in \{0, \dots, N\}$, we define

$$Y_0^k = (1 - \frac{k}{N})Y_0 + \frac{k}{N}Y_0^{\mathrm{f}}, \tag{4.21}$$

(this way one has $Y_0^0 = Y_0$ and $Y_0^N = Y_0^{\mathrm{f}}$.) Let $\tilde{Y}^k$ be the free solution of system (PL) with initial condition $\tilde{Y}_0^k$ and no control. The following lemma shows that these "step" solutions stay close to each other.

Lemma 4.14. *There exists $M > 0$ such that, for any $\delta > 0$ and for all $k \in \{0, \dots, N-1\}$, one has*

$$\|\tilde{Y}^{k+1} - \tilde{Y}^K\|_{\mathrm{L}^2(\mathbb{R}_+ \times \Omega)} \leqslant \delta M. \tag{4.22}$$

Proof. According to Propositions 4.2 and 4.4, $\tilde{Y}$ and Z are globally bounded in L^2 and nonnegative. Let $M > 0$ be such that $\|\tilde{Y}\|_{\mathrm{L}^2(\mathbb{R}_+ \times \Omega)} \leqslant M$ and $\|Y^{\mathrm{f}}\|_{\mathrm{L}^2(\mathbb{R}_+ \times \Omega)} \leqslant M$. Then, one has

$$\|\tilde{Y} - Y^{\mathrm{f}}\|_{\mathrm{L}^2(\mathbb{R}_+ \times \Omega)} \leqslant M,$$

and (4.22) follows by linearity and the definition of the Y^k. □

Note that, by linearity of system (PL), one has, for all $k \in \{0, \dots, N\}$,

$$\inf_{(\mathbb{R}_+ \times \Omega)^n} \tilde{Y}^k(t, x) \geqslant \zeta.$$

We now build the controlled trajectory.

Let us start by steering the system from Y_0 to the trajectory $\tilde{Y}^1$. According to Proposition 4.6, there exists a control $u_1 \in (\mathrm{L}^2((0,T), \mathrm{H}^r(\omega)) \cap \mathrm{H}^s((0,T), \mathrm{L}^2(\omega)))^m$ (with r, s large enough) such that the solution of (PL) with initial condition Y_0 and control u_1 satisfies

$$Y(\tau, \cdot) = \tilde{Y}^1(\tau, \cdot). \tag{4.23}$$

Moreover, according to Lemma 4.13, one has, for all $t \in [0, \tau]$,

$$\|Y(t) - \tilde{Y}(t)\|_{\mathrm{L}^\infty(\Omega)^n} \leqslant C(\tau)\|Y_0 - Y_0^1\|_{\mathrm{L}^2(\Omega)^n}. \tag{4.24}$$

Using (4.22) and the definition of ζ, we get

$$\forall t \in [0, \tau], Y(t) \geqslant \zeta - C(\tau)M\delta. \tag{4.25}$$

Next, let $k \in \{1, \dots, N-1\}$. We repeat the step above to steer the trajectory Y from $\tilde{Y}^k(\cdot, k\tau)$ to $\tilde{Y}^{k+1}(\cdot, (k+1)\tau)$ in time τ with a control $u_{k+1} \in (\mathrm{L}^2((0,T), \mathrm{H}^r(\omega)) \cap \mathrm{H}^s((0,T), \mathrm{L}^2(\omega)))^m$ such that, for all $t \in [k\tau, (k+1)\tau]$,

$$\|Y(t) - \tilde{Y}^k(t)\|_{\mathrm{L}^\infty(\Omega)^n} \leqslant C(\tau)\|\tilde{Y}^k(\cdot, k\tau) - \tilde{Y}^{k+1}(\cdot, k\tau)\|_{\mathrm{L}^2(\Omega)^n}. \tag{4.26}$$

Using (4.22) again, we have

$$\forall t \in [k\tau, (k+1)\tau], Y(t) \geqslant \zeta - C(\tau)M\delta. \tag{4.27}$$

Overall, let us set

$$\delta = \frac{\epsilon}{MC(\tau)}, \tag{4.28}$$

$T = N\tau$, and u the control defined on $[0,T]$ by $u(t) = u_k(t)$ if $t \in (k\tau,(k+1)\tau)$. The solution Y of (PL) starting at Y_0 and with control u satisfies (4.15) and (4.16), which concludes the proof. □

Proof of Theorem 4.12. For $t \geqslant 0$ and $Y \in \mathbb{R}^n$, define

$$Z = e^{-tA}Y. \tag{4.29}$$

Note that, if Y is a solution of (PL), then Z is solution of the following system:

$$\begin{cases} \partial_t Z - RZ &= e^{-tA}Bu\mathbf{1}_\omega & \text{on } (0,T)\times\Omega; \\ \frac{\partial Z}{\partial n} &= 0 & \text{on } (0,T)\times\partial\Omega; \\ Z(0,\cdot) &= Y(0,\cdot) & \text{on } \Omega. \end{cases} \tag{4.30}$$

Let Z^{f} be the solution of (4.30) with initial condition Y_0^{f} and no control. We are going to show the existence of $T > 0$ and a control u such that the solution Z of (4.30) with initial condition Y_0 and control u satisfies

$$Z(T,\cdot) = Z^{\mathrm{f}}(T,\cdot) \tag{4.31}$$

and, for all $(t,x) \in [0,T]\times\Omega$,

$$Z(t,x) \geqslant 0. \tag{4.32}$$

From the definition of Z, it is clear that such a control u is such that the solution Y of (PL) with initial condition Y_0 and control u satisfies

$$Y(T,\cdot) = Y^{\mathrm{f}}(T,\cdot). \tag{4.33}$$

Moreover, for all $(t,x) \in [0,T]\times\Omega$,

$$Y(t,x) = e^{tA}Z(t,x) \geqslant 0, \tag{4.34}$$

because of (4.32) and the fact that the exponential of a quasipositive matrix has only nonnegative entries (if A is quasipositive, write $A = P + \alpha I_n$ with $\alpha \in \mathbb{R}$ such that P has only nonnegative entries, then it is clear that e^P is nonnegative and so is $e^A = e^{\alpha I_n}e^P = e^\alpha e^P$ [BP94]).

When $u = 0$, (4.30) becomes a system of n independent parabolic equations. Then, using a spectral expansion, we immediately have that the solutions $\tilde{Z}_0$ and Z^{f} starting respectively at Y_0 and Y_0^{f} converge in norms L^∞ and L^2 (and any other norm) to

$$\bar{Z}_0 = \frac{1}{|\Omega|}\int_\Omega Y_0 \quad \text{and} \quad \bar{Z}_0^{\mathrm{f}} = \frac{1}{|\Omega|}\int_\Omega Y_0^{\mathrm{f}}.$$

Assumption (4.17) in Theorem 4.12 ensure that all the components of $\bar{Z}_0$ and $\bar{Z}$ are positive. Therefore, there exists $\zeta > 0$ such that $\bar{Z}_0 \geqslant \zeta$ and $\bar{Z}_0^{\mathrm{f}} \geqslant \zeta$.

It is shown in [AKBDGB09a, Theorem 1.1] that System (4.30) is controllable to trajectories under assumption (4.13) and we have an estimation similar to (4.20):

Lemma 4.15. *Let $Y_0 \in \mathrm{L}^\infty(\Omega)^n$, $\tilde{Y}$ the solution of (4.30) with initial condition Y_0 and no control, and Y_1 a trajectory of (PL) with an initial condition Y_1^0. Then, for all $T > 0$, there exists a control u and $C(T)$ such that the solution Y of (4.30) with initial condition Y_0 and control u satisfies $Y(T,\cdot) = Y_1(T,\cdot)$ and*

$$\forall t \in [0,T], \|Y(t) - \tilde{Y}(t)\|_{\mathrm{L}^\infty(\Omega)^n} \leqslant C(T)\|Y_0 - Y_1^0\|_{\mathrm{L}^2(\Omega)^n}. \tag{4.35}$$

Proof. Combine Proposition 4.1 and [AKBDGB09a, Theorem 5.2], that states the same estimation as in Proposition 4.8 for time-dependent systems like (4.30). □

We are now in a position to build the trajectory Z going from Y_0 to Z^{f}. This will take several steps:

Let $\delta > 0$ and $\tau > 0$.

1. Define a time T_0 such that, for all $t \geqslant T_0$,

$$\|\tilde{Z}_0(t) - \bar{Z}_0\|_{\mathrm{L}^2(\Omega)^n} \leqslant \delta \quad \text{and} \quad \|Z^{\mathrm{f}}(t) - \bar{Z}^{\mathrm{f}}\|_{\mathrm{L}^2(\Omega)^n} \leqslant \delta, \tag{4.36}$$

and take the null control on $[0,T_0]$. The positivity of the initial conditions ensures that

$$\forall (t,x) \in [0,T_0] \times \Omega, Z(t,x) = \tilde{Z}_0(t,x) \geqslant 0. \tag{4.37}$$

2. Control from $\tilde{Z}_0(T_0)$ to $\bar{Z}_0$ in time τ. Lemma 4.15 ensures that the control can be taken such that, for all $t \in [T_0, T_0+\tau]$,

$$\|Z(t) - Z_0(t)\|_{\mathrm{L}^\infty((0,T)\times\Omega)^n} \leqslant C(\tau)\|\tilde{Z}_0(T_0) - \bar{Z}_0\|_{\mathrm{L}^2((0,T)\times\Omega)^n}, \tag{4.38}$$

and therefore, using (4.36), for all $(t,x) \in [T_0, T_0+\tau] \times \Omega$,

$$Z(t,x) \geqslant \zeta - C(\tau)\delta. \tag{4.39}$$

3. Let $M = \max(1, \max \bar{Z}_0, \max \bar{Z}_0^{\mathrm{f}})$ and $N \in \mathbb{N}^*$ such that $\frac{M}{N} \leqslant \delta$. By reproducing the staircase method developed in the proof of Theorem 4.10 in equations (4.21) to (4.28), build a control u that steers Z from $\bar{Z}_0$ to $\bar{Z}^{\mathrm{f}}$, following a path of N steps with every step lasting time τ. Using Lemma 4.15 again yields, for all $(t,x) \in [T_0+\tau, T_0+(N+1)\tau] \times \Omega$,

$$Z(t,x) \geqslant \zeta - C(\tau)M\delta. \tag{4.40}$$

4. Control from $\bar{Z}_0^{\mathrm{f}}$ to Z^{f} in time τ. Lemma 4.15 ensures one more time that the control can be taken such that for all $t \in [T_0 + (N+1)\tau, T_0 + (N+2)\tau]$,

$$\|Z(t) - \bar{Z}_0^{\mathrm{f}}\|_{\mathrm{L}^\infty(\Omega)^n} \leqslant C(\tau)\|Z^{\mathrm{f}}(T_0 + (N+1)\tau) - \bar{Z}_0^{\mathrm{f}}\|_{\mathrm{L}^2(\Omega)^n}, \tag{4.41}$$

which gives, using (4.36): for all $(t,x) \in [T_0 + (N+1)\tau, T_0 + (N+2)\tau] \times \Omega$,

$$Z(t,x) \geqslant \zeta - C(\tau)\delta. \tag{4.42}$$

Overall, taking $T = T_0 + (N+2)\tau$ and

$$\delta = \frac{\zeta}{C(\tau)M},$$

we have found a control u on $[0,T]$ such that Z satisfies (4.31) and (4.32). □

4.4 Discussion and open problems

We have studied the problem of nonnegative controllability for coupled systems of linear parabolic equations. Our results show that one can control such a system in large time to bounded trajectories using the staircase method with approximately nonnegative state. In the case $D = I_n$, the boundedness hypothesis can be removed and controllability in large time with nonnegative state holds. Our research is still at an early stage, so we have not yet investigated whether the assumptions we made on the matrix A are sharp. We list some open questions below.

Controllability with nonnegative state in the general case. It would be interesting to know if it is possible to replace ζ with 0 in Theorem 4.10. Without restrictive assumptions on the behaviour of system (PL), it seems however difficult to control with positivity constraint towards a trajectory whose some components converge rapidly to zero.

Controllability without assumption (4.6). Assumption (4.6) ensures that the solution of (PL) remain globally bounded. In the general case, controllability with positivity constraint is still an open problem.

Nonlinear case. A few results of controllability with state constraint have been given in [PZ17] for semilinear equations with boundary control. We have started to investigate the case with internal control. We believe that in that case, controllability with state constraint does not hold, even with strong growth assumptions on the linearity. Research to find a counterexample is ongoing.

Part II

Applications to micro-swimming

Chapter 5

Note on local controllability of the two-link magneto-elastic micro-swimmer

This chapter reproduces [GLMP18], written in collaboration with Laetitia Giraldi, Pierre Lissy and Jean-Baptiste Pomet, and published in 2018 in the journal *IEEE Transactions on Automatic Control*. It features an addendum to [GP17], in which a study of controllability of the two-link magnetic swimmer introduced in section 2.4 is conducted. *NB*: In accordance with the usages in the mathematics field, the authors for this publication are in alphabetical order, regardless of the fact that I provided the dominant contribution.

5.1 Model of the magneto-elastic micro-swimmer

Keeping the same notations as in [GP17] (see fig. 1 there), the planar micro-swimmer's dynamics are given by

$$\dot{\mathbf{z}} = \mathbf{F}_0(\mathbf{z}) + H_{\parallel}\,\mathbf{F}_1(\mathbf{z}) + H_{\perp}\,\mathbf{F}_2(\mathbf{z})\,. \tag{5.1}$$

The state is $\mathbf{z} = (x, y, \theta, \alpha)$ with α an angle describing the swimmer's shape and x, y, θ two coordinates and an angle describing its position. The control is $(H_{\perp}, H_{\parallel})$, the coordinate vector of the external magnetic field in a moving frame.

The norm on the control space $\mathbb{R}^2$ is the sup-norm:

$$\|(H_{\perp}, H_{\parallel})\| = \max\{\,|H_{\perp}|\,,\,|H_{\parallel}|\,\}\,.$$

Denoting $f_{i,j}$ twelve functions [1] explicitly derived from [GP17, Prop. II.1 and (12)-(16)], the $\mathbf{F}_i$'s may be expressed as follows:

$$\mathbf{F}_i(\mathbf{z}) = \begin{pmatrix} \cos\theta & \sin\theta & 0 & 0 \\ -\sin\theta & \cos\theta & 0 & 0 \\ 0 & 0 & 1 & 0 \\ 0 & 0 & 0 & 1 \end{pmatrix} \begin{pmatrix} f_{i,1}(\alpha) \\ f_{i,2}(\alpha) \\ f_{i,3}(\alpha) \\ f_{i,4}(\alpha) \end{pmatrix}. \tag{5.2}$$

1. The notation $f_{i,j}$ is not present in [GP17].

In [GP17], the dynamics, hence the functions $f_{i,j}$, depend on: the length ℓ_i of each segment ($i = 1, 2$), its magnetization M_i, its longitudinal and transversal hydrodynamic drag constants ξ_i, η_i, and an elastic constant κ. It is assumed that $\kappa > 0$ and that, for each i, $\ell_i > 0$, $\xi_i > 0$, $\eta_i > 0$ and $M_i \neq 0$. In this addendum, we further assume that the two links have the same length and hydrodynamic constants, i.e. we define:

$$\ell = \ell_1 = \ell_2,\ \xi = \xi_1 = \xi_2,\ \eta = \eta_1 = \eta_2. \tag{5.3}$$

This assumption makes the redaction easier to follow but it does not alter the nature of the proofs.

The equilibria of interest are $((x^e, y^e, \theta^e, 0), (0, 0))$ in the state-control space, with (x^e, y^e, θ^e) arbitrary in $\mathbb{R}^2 \times [0, 2\pi]$. Using invariance by translation and rotation [GP17], one may, without loss of generality, suppose $(x_e, y_e, \theta_e) = (0, 0, 0)$ and consider only the equilibrium $\mathbf{O} = ((0, 0, 0, 0), (0, 0))$.

5.2 Some local controllability concepts

Consider a smooth continuous-time control system

$$\dot{z} = f(z, u) \tag{5.4}$$

with state z in $\mathbb{R}^n$ and control u in $\mathbb{R}^m$. We endow $\mathbb{R}^m$ with a norm $\|\cdot\|$ and always assume that the control is measurable as a function of time.

Let (z_e, u_e) be an equilibrium of (5.4), i.e. $f(z_e, u_e) = 0$. The following definition introduces an ad hoc notion of controllability for the sake of clarity.

Definition 5.1 (STLC(q))**.** Let q be a non-negative number. The control system (5.4) is *STLC(q) at* (z_e, u_e) if and only if, for every $\varepsilon > 0$, there exists $\eta > 0$ such that, for every z_0, z_1 in the ball centered at z_e with radius η, there exists a control $u(\cdot)$ such that the solution of the control system $z(\cdot) : [0, \varepsilon] \to \mathbb{R}^n$ of (5.4) satisfies $z(0) = z_0$, $z(\varepsilon) = z_1$, and, for almost all t in $[0, \varepsilon]$,

$$\|u(t) - u_e\| \leqslant q + \varepsilon\,.$$

Let us also recall the classical definition of STLC.

Definition 5.2 (STLC)**.** The system (5.4) is *STLC (small-time locally controllable) at* (z_e, u_e) if and only if it is STLC(0) at (z_e, u_e).

The following necessary condition for STLC will be used.

Lemma 5.3 (Loop trajectories)**.** *If (5.4) is STLC at (z_e, u_e), then, for any $\varepsilon > 0$, there exists a control $u^\varepsilon(\cdot)$ such that the solution $t \mapsto z^\varepsilon(t)$ of (5.4), defined for t in $[0, \varepsilon]$, satisfies*

- *$z^\varepsilon(0) = z^\varepsilon(\varepsilon) = z_e$,*
- *$z^\varepsilon(t) \neq z_e$ for at least one t in $[0, \varepsilon]$,*

and, for almost all t in $[0, \varepsilon]$,

$$\|u^\varepsilon(t) - u_e\| \leqslant \varepsilon.$$

Proof. Let $\varepsilon > 0$. There exists $\eta > 0$ such that, for every $z_\star$ in the ball centered at z_e with radius η, there is a control $u^\varepsilon(\cdot)$ such that the solution $z^\varepsilon(\cdot) : [0, \varepsilon/2] \to \mathbb{R}^n$ of (5.4)

satisfies $z^\varepsilon(0) = z_e$, $z^\varepsilon(\varepsilon/2) = z_\star$, and, for almost all t, $\|u^\varepsilon(t) - u_e\| \leqslant \varepsilon/2$. Pick one such $z_\star$ different from z_e. System (5.4) being autonomous, there also exists a control $u^\varepsilon(\cdot)$ such that the solution $z^\varepsilon(\cdot) : [\varepsilon/2, \varepsilon] \to \mathbb{R}^n$ of (5.4) satisfies $z(\varepsilon/2) = z_\star$, $z(\varepsilon) = z_e$, and, for almost all t in $[\varepsilon/2, \varepsilon]$, $\|u(t) - u_e\| \leqslant \varepsilon/2$. Then, the control $u^\varepsilon(\cdot) : [0, \varepsilon] \to \mathbb{R}^m$ and solution $z^\varepsilon(\cdot) : [0, \varepsilon] \to \mathbb{R}^n$ verify all the desired properties. □

5.3 Complements to the original note

The following proposition reformulates the results from [GP17]. Without assumption (5.3), $\xi \neq \eta$ would be replaced by $(\xi_1, \xi_2) \neq (\eta_1, \eta_2)$ and $M_1 \neq M_2$ by [GP17, eqn. (20)].

Proposition 5.4 ([GP17], Thm. III.4 and Prop. III.1)**.** *Assume (5.3). The control system (5.1) is STLC$(2\kappa\,|M_1 + M_2|/\,|M_1 M_2|)$ at $\boldsymbol{O}$ if $\xi \neq \eta$ and $M_1 \neq M_2$. Otherwise, it is not STLC(q) for any $q \geq 0$.*

Unless $M_1 + M_2 = 0$, STLC$(2\kappa\,|M_1 + M_2|/\,|M_1 M_2|)$ does not imply STLC. The purpose of the present addendum is to prove the following result:

Theorem 5.5. *Consider the control system given by (5.1). Suppose that the length of the links and the hydrodynamics constants satisfy (5.3). If $\xi \neq \eta$, $M_1 \neq M_2$ and $M_1 + M_2 \neq 0$, then the system is not STLC at $\boldsymbol{O}$.*

Proof. From [GP17, Prop. II.1 and (12)-(16)], one readily verifies that the functions $f_{i,j}$ introduced in (5.2) have the following expansions around $\alpha = 0$:

$$
\begin{aligned}
&f_{2,j}(\alpha) = \mathcal{O}(\alpha), && j \in \{1,2,3,4\},\\
&f_{0,1}(\alpha) = a_1\alpha^2 + \mathcal{O}(\alpha^3), && f_{1,1}(\alpha) = b_1\alpha + \mathcal{O}(\alpha^2),\\
&f_{0,2}(\alpha) = \mathcal{O}(\alpha^2), && f_{1,2}(\alpha) = b_2 + \mathcal{O}(\alpha),\\
&f_{0,3}(\alpha) = \frac{a}{2}\alpha + \mathcal{O}(\alpha^2), && f_{1,3}(\alpha) = b_3 + \mathcal{O}(\alpha),\\
&f_{0,4}(\alpha) = -a\,\alpha + \mathcal{O}(\alpha^2), && f_{1,4}(\alpha) = b_4 + \mathcal{O}(\alpha),
\end{aligned}
\tag{5.5}
$$

with

$$
\begin{aligned}
&a_1 = \frac{3\kappa}{\ell^2\eta},\ b_1 = \frac{3}{2}\frac{M_2 - M_1}{\ell^2\eta} - \frac{3}{8}\frac{M_1 + M_2}{\ell^2\xi},\ b_2 = \frac{3}{4}\frac{M_1 + M_2}{\ell^2\eta},\\
&a_2 = \frac{24\,\kappa}{\ell^3\eta},\ b_3 = \frac{3(5M_2 - 3M_1)}{2\,\ell^3\eta},\ b_4 = \frac{12(M_1 - M_2)}{\ell^3\eta}.
\end{aligned}
\tag{5.6}
$$

The assumptions before (5.3) and these of the theorem imply $b_4 \neq 0$, $a_2 \neq 0$, $M_1 + M_2 \neq 0$ and $M_1 - M_2 \neq 0$, hence

$$
z_4 = \frac{1}{b_4}\,\alpha,\ z_3 = \frac{8\,(M_1 - M_2)}{a_2\,(M_1 + M_2)}\Big(b_4\,\theta - b_3\,\alpha\Big) \tag{5.7}
$$

defines a change of coordinates[2] $(x, y, \theta, \alpha) \mapsto (x, y, z_3, z_4)$. Since $8(M_1 - M_2)/(M_1 + M_2) = 1/(1/2 + b_3/b_4)$, one deduces from (5.1), (5.2), (5.5), and (5.7) the following expressions of $\dot{z}_3$

2. For the reader's information: the linear approximation of (5.1) is in (non-controllable) Brunovsky form in coordinates $(x,\ y - b_2 z_3\ , z_3, z_4)$.

and $\dot{z}_4$, where $r_{i,j}$ $(i = 0, 1, 2,\ j = 3, 4)$ are smooth functions of one variable:

$$\begin{aligned} \dot{z}_3 &= z_4 \left(1 + z_4\, r_{0,3}(z_4) + H_\perp\, r_{1,3}(z_4) + H_\parallel\, r_{2,3}(z_4) \right), \\ \dot{z}_4 &= H_\perp - z_4 \Big(a_2 + z_4\, r_{0,4}(z_4) + H_\perp\, r_{1,4}(z_4) + H_\parallel\, r_{2,4}(z_4) \Big). \end{aligned} \tag{5.8}$$

Substituting $\alpha = b_4\, z_4$ and $\theta = b_3\, z_3 + \dfrac{a_2\,(M_1 + M_2)}{8 b_4\,(M_1 - M_2)}\, z_4$ in (5.2), expanding $\sin(\theta)$ and $\cos(\theta)$ around 0 and using (5.5) one gets, with c_1, c_2, c_3 three constants that may easily be computed from $a_1, a_2, b_1, b_2, b_3, b_4$, the expression:

$$\dot{x} = c_3\, z_4^2 + (c_1 z_3 + c_2 z_4) H_\perp + z_4^2 R_1 + z_3 z_4\, R_2 + z_3^2 R_3 \tag{5.9}$$

$$\begin{aligned} \text{with } R_1 &= z_4\, \rho_1(z_3, z_4) + \rho_2(z_3, z_4)\, H_\perp + \rho_3(z_3, z_4)\, H_\parallel, \\ R_2 &= \rho_4(z_3, z_4) + \rho_5(z_3, z_4)\, H_\perp + \rho_6(z_3, z_4)\, H_\parallel, \\ R_3 &= \rho_7(z_3, z_4) + \rho_8(z_3, z_4)\, H_\perp + \rho_9(z_3, z_4)\, H_\parallel, \end{aligned} \tag{5.10}$$

and ρ_i, $i = 1 \dots 9$, nine smooth functions of two variables. Then, defining $\zeta = x - c_1 z_3 z_4 - \frac{1}{2} c_2 z_4^2$, one has

$$\begin{aligned} &\dot{\zeta} = z_4^2 (c_0 + \widetilde{R}_1) + z_3 z_4\, \widetilde{R}_2 + z_3^2\ \widetilde{R}_3 \\ &\text{with } c_0 = c_3 + a_2 c_2 - c_1 \end{aligned} \tag{5.11}$$

with $\widetilde{R}_1, \widetilde{R}_2, \widetilde{R}_3$ three functions of z_3, z_4, $H_\perp, H_\parallel$ that can be expended similarly to R_1, R_2 and R_3 in (5.10). Computing c_0 from the expressions of c_1, c_2, c_3, one finds that it is nonzero from the assumptions of Theorem 5.5:

$$c_0 = \frac{108\kappa}{\ell^8 \eta^3 \xi} (M_2^2 - M_1^2)(\eta - \xi) \neq 0. \tag{5.12}$$

From Lemma 5.3, for each $\varepsilon > 0$, there exists a "loop"

$$t \mapsto (x^\varepsilon(t), y^\varepsilon(t), \theta^\varepsilon(t), \alpha^\varepsilon(t), H_\perp^\varepsilon(t), H_\parallel^\varepsilon(t)\,)$$

defined on $[0, \varepsilon]$, solution of (5.1), and such that

$$|H_\perp^\varepsilon(t)| \leqslant \varepsilon \text{ and } |H_\parallel^\varepsilon(t)| \leqslant \varepsilon \text{ for all } t \text{ in } [0, \varepsilon], \tag{5.13}$$

$$\begin{aligned} (x^\varepsilon(0), y^\varepsilon(0), z_3^\varepsilon(0), z_4^\varepsilon(0)) &= (0,0,0,0), \\ (x^\varepsilon(\varepsilon), y^\varepsilon(\varepsilon), z_3^\varepsilon(\varepsilon), z_4^\varepsilon(\varepsilon)) &= (0,0,0,0), \end{aligned} \tag{5.14}$$

$$(x^\varepsilon(t), y^\varepsilon(t), z_3^\varepsilon(t), z_4^\varepsilon(t)) \neq (0,0,0,0) \text{ for one } t \text{ in } [0, \varepsilon], \tag{5.15}$$

where $z_3^\varepsilon(t), z_4^\varepsilon(t)$ are defined from $(\theta^\varepsilon(t), \alpha^\varepsilon(t))$ as in (5.7). Along these solutions, the functions $r_{i,j}$ and ρ_i are bounded uniformly with respect to t in $[0, \varepsilon]$ and ε in $(0, \varepsilon_0]$ for some small enough $\varepsilon_0 > 0$. In particular, using (5.7) and (5.11), we deduce that for each $\varepsilon \in (0, \varepsilon_0]$,

there are three functions $u^\varepsilon(.)$, $v^\varepsilon(.)$, $w^\varepsilon(.)$ such that

$$\dot{z}_3^\varepsilon(t) = z_4^\varepsilon(t)\, u^\varepsilon(t)\,, \tag{5.16}$$

$$\dot{\zeta}^\varepsilon(t) = z_4^\varepsilon(t)^2(c_0 + \varepsilon\, w^\varepsilon(t)) + z_3^\varepsilon(t) z_4^\varepsilon(t)\; v^\varepsilon(t) + z_3^\varepsilon(t)^2 s^\varepsilon(t)\,, \tag{5.17}$$

$$|u^\varepsilon(t)| \leqslant K,\ |v^\varepsilon(t)| \leqslant K,\ |w^\varepsilon(t)| \leqslant K,\ |s^\varepsilon(t)| \leqslant K\,. \tag{5.18}$$

Here and hereafter, $K > 0$ denotes a constant independent of ε and t that may vary from line to line.

From (5.16) and (5.18), one gets, for any ε in $(0, \varepsilon_0]$,

$$|z_3^\varepsilon(t)| \leqslant K\int_0^t |z_4^\varepsilon(\tau)|\,\mathrm{d}\tau, \quad \int_0^\varepsilon |z_3^\varepsilon(t)|\mathrm{d}t \leqslant K\varepsilon\int_0^\varepsilon |z_4^\varepsilon(\tau)|\mathrm{d}\tau\,.$$

It follows that

$$\begin{aligned}\int_0^\varepsilon |z_3^\varepsilon(t) z_4^\varepsilon(t)|\,\mathrm{d}t &\leqslant K\iint_{0\leqslant\tau\leqslant t\leqslant\varepsilon} |z_4^\varepsilon(t) z_4^\varepsilon(\tau)|\,\mathrm{d}t\,\mathrm{d}\tau \\ &\leqslant K\iint_{(t,\tau)\in[0,\varepsilon]^2} |z_4^\varepsilon(t) z_4^\varepsilon(\tau)|\mathrm{d}t\,\mathrm{d}\tau = K\big(\int_0^\varepsilon |z_4^\varepsilon(t)|\mathrm{d}t\,\big)^2,\end{aligned}$$

$$\begin{aligned}\int_0^\varepsilon z_3^\varepsilon(t)^2\mathrm{d}t &\leqslant K\iint_{0\leqslant\tau\leqslant t\leqslant\varepsilon} |z_3^\varepsilon(t) z_4^\varepsilon(\tau)|\,\mathrm{d}t\mathrm{d}\tau \\ &\leqslant K\iint_{(t,\tau)\in[0,\varepsilon]^2} |z_3^\varepsilon(t) z_4^\varepsilon(\tau)|\mathrm{d}t\mathrm{d}\tau \\ &= K\big(\int_0^\varepsilon |z_3^\varepsilon(t)|\mathrm{d}t\big)\big(\int_0^\varepsilon |z_4^\varepsilon(t)|\mathrm{d}t\big) \leqslant K^2\varepsilon\big(\int_0^\varepsilon |z_4^\varepsilon(t)|\mathrm{d}t\big)^2.\end{aligned}$$

Applying the Cauchy-Schwartz inequality, we get

$$\int_0^\varepsilon |z_3^\varepsilon(t) z_4^\varepsilon(t)|\mathrm{d}t \leqslant K\varepsilon\int_0^\varepsilon z_4^\varepsilon(t)^2\mathrm{d}t \tag{5.19}$$

and

$$\int_0^\varepsilon z_3^\varepsilon(t)^2\mathrm{d}t \leqslant K^2\varepsilon^2\int_0^\varepsilon z_4^\varepsilon(t)^2\mathrm{d}t. \tag{5.20}$$

Equations (5.14) imply $\int_0^\varepsilon \dot{\zeta}^\varepsilon(t)\mathrm{d}t = 0$. Substituting $\dot{\zeta}^\varepsilon(t)$ from (5.17) and using the inequalities (5.18), (5.19) and (5.20) yields, for any ε in $(0, \varepsilon_0]$,

$$|c_0|\int_0^\varepsilon z_4^\varepsilon(t)^2\mathrm{d}t \leqslant \left(2K\varepsilon + K^2\varepsilon^2\right)\int_0^\varepsilon z_4^\varepsilon(t)^2\mathrm{d}t\,. \tag{5.21}$$

Since $c_0 \neq 0$, this implies that $z_4^\varepsilon(t)$ is identically zero on $[0, \varepsilon]$ for $\varepsilon > 0$ small enough. From (5.8), this implies that the control $H_\perp^\varepsilon(t)$ is identically zero. Since all the maps $f_{i,j}$ with $i \neq 1$ are zero at zero (see (5.2) and (5.5)), all state variables are constant if z_4^ε and $H_\perp^\varepsilon$ are identically zero, meaning that $(x^\varepsilon(t), y^\varepsilon(t), \theta^\varepsilon(t))$ are identically zero on $[0, \varepsilon]$ for $\varepsilon > 0$ small enough. Therefore, any small enough loop with small enough control is trivial, which

contradicts (5.15) and hence contradicts STLC. □

5.4 Conclusion

We proved that the local controllability results in [GP17] are sharp in the sense that STLC occurs only for the values of the parameters for which it was already proved in that note.

On the one hand, from the theoretical point of view of controllability, although it deals with a very specific class of systems, Theorem 5.5 is a necessary condition for STLC. Conditions for STLC have been much studied in the last decades, see for instance [Cor07] or [Kaw90] and references therein. Many sophisticated and powerful sufficient conditions have been stated, but necessary conditions are always specific, see for instance [Kaw87, Kra98]. Theorem 5.5 is not, to the best of our knowledge, a consequence of known necessary conditions.

On the other hand, the implications for locomotion at low Reynolds number via an external magnetic field are not clear. Comments on that matter are left to further research.

Chapter 6

Local controllability of two- and three-link magneto-elastic swimmers

This chapter reproduces [Mor19], published in 2019 in the journal *IEEE Control Systems Letters*.

6.1 Introduction

Micro-swimming robots offer potential high-impact applications in the biomedical field, such as targeted drug delivery or non-invasive surgery. For that reason, the interest in building such robots has been growing in the past years. The shapes and propulsion techniques of these new robots could be inspired by biology, since micro-organisms such as sperm cells or bacterias developed efficient ways to move through a surrounding fluid (see [PZN13]). One promising technique consists of using an external magnetic field to drive a magnetized swimmer (see [GKP+12, DBR+05, GF09]).

In this paper, we focus on this type of propulsion, applied on a simple model of micro-swimmer consisting of three magnetized segments linked by elastic joints. Such models, with different numbers of segments, have been studied for instance in [GO14] and [ADGZ13], in which the authors show that sinusoidal magnetic fields allow the swimmer to move forward in a prescribed direction. The 3-link articulated swimmer was introduced by Purcell in a founding talk about micro-swimming [Pur77].

At the microscopic scale, the Reynolds number is typically very small (around 10^{-6}), which means that the intensity of inertial forces is negligible compared to those of viscous ones. Therefore, we can assume that the fluid is governed by the Stokes equations. We model the hydrodynamic interaction between the swimmer and the fluid by the local drag approximation of Resistive Force Theory introduced in [GH55].

We state a local controllability result for the 3-link swimmer. Under generic conditions on the links magnetizations, we show that it is controllable around its equilibrium position (a straight line), but with controls that cannot be made arbitrarily small. This is due to the fact that the parallel component of the magnetic field cannot act on the swimmer when all its links are aligned. The proof gives an explicit bound on the controls to achieve small-time local controllability (STLC).

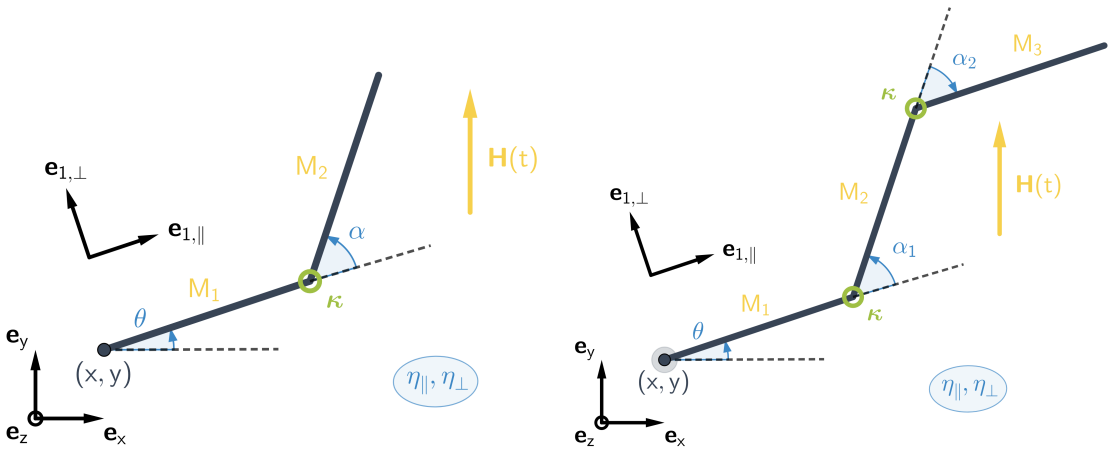

Figure 6.1 – 3-link microswimmer model

In [GP17], the authors show a similar local controllability result for the 2-link model around its straight position. The method that we present here to obtain our controllability result allows to improve this result with a stronger form of local controllability. In addition to its interest for applications and experiments, our result raises potential new STLC conditions for a particular class of control systems.

The paper is organized as follows. In Section 6.2, we describe the micro-swimmer model and derive the dynamics equations. In Section 6.3, we recall definitions and results regarding small-time local controllability (STLC), state our main result, and extend it to the 2-link swimmer model. Section 6.4 is dedicated to a discussion about the results as well as some numerical simulations.

6.2 Micro-swimmer model

6.2.1 Formulation of the problem

We mostly follow the notations and model used in [ADGZ15], [GP17] and [GLMP16]. We focus on a micro-swimmer consisting of 3 rigid magnetized segments – see Figure 6.1 – connected by two torsional springs with stiffness κ, subject to a uniform in space, time-varying magnetic field $\mathbf{H}$. The 3 segments, called S_1,S_2 and S_3, have same length ℓ, same hydrodynamic drag coefficients ξ and η, and respective magnetic moments M_1, M_2 and M_3. The swimmer can move in the 2d-plane defined by the vectors $\mathbf{e}_x$ and $\mathbf{e}_y$. Let $\mathbf{e}_z = \mathbf{e}_x \times \mathbf{e}_y$. Let $\mathbf{x} = (x, y)$ be the coordinates of the end of S_1, θ the angle between (Ox) and S_1, and α_1 and α_2 the angles between S_1 and S_2 and between S_2 and S_3. The swimmer is then completely described by the five state variables $(x, y, \theta, \alpha_1, \alpha_2)$: the pair (x, y) represents the position of the swimmer, θ its orientation and the pair (α_1, α_2) its shape. Let us also define the moving frames associated to S_i for $i = 1, 2, 3$ as $(\mathbf{e}_{i,\parallel}, \mathbf{e}_{i,\perp})$.

The magnetic field $\mathbf{H}(t)$ induces a torque in each of the segments. As it moves, the swimmer experiences hydrodynamic drag, as well as elastic restoring torques at the joints between the segments.

Elasticity

The torsional springs which connect the swimmer segments exert a torque $\mathbf{T}^{\text{el}}$ proportional to the shape angles α_1 and α_2. Hence the torque $\mathbf{T}_2^{\text{el}}$ exerted on S_2 is given by $\mathbf{T}_2^{\text{el}} = \kappa\alpha_1\mathbf{e}_z$ and the torque $\mathbf{T}_3^{\text{el}}$ exerted on S_3 is given by $\mathbf{T}_3^{\text{el}} = \kappa\alpha_2\mathbf{e}_z$.

The springs tend to get the swimmer back to a straight shape, in which S_1, S_2 and S_3 are aligned.

Hydrodynamics

The fluid surrounding the swimmer exerts a hydrodynamic drag on it. We use the Resistive Force Theory [GH55] to model this interaction, i.e. the drag force per unit of length is proportional to the velocity and to the hydrodynamics coefficients ξ and η. For $s \in [0, \ell]$, let $\mathbf{x}_s$ be the point of arclength s on one of the segments S_i. Its velocity $\mathbf{u}_i(\mathbf{x}_s)$ is given in the moving frame $(\mathbf{e}_{i,\parallel}, \mathbf{e}_{i,\perp})$ by $\mathbf{u}_i(\mathbf{x}_s) = u_{i,\parallel}\mathbf{e}_{i,\parallel} + u_{i,\perp}\mathbf{e}_{i,\perp}$. The drag force exerted on this point is then given by

$$\mathbf{f}_i(\mathbf{x}_s) = -\xi u_{i,\parallel}\mathbf{e}_{i,\parallel} - \eta u_{i,\perp}\mathbf{e}_{i,\perp}.$$

Integrating over S_i to obtain the total force $\mathbf{F}_i^h$ exerted on S_i:

$$\mathbf{F}_i^h = \int_{S_i} \mathbf{f}_i(\mathbf{x}_s) d\mathbf{x}_s.$$

Moreover, given a point $\mathbf{x}_0$, the drag torque for S_i with respect to $\mathbf{x}_0$ takes the form

$$\mathbf{T}_{i,\mathbf{x}_0}^h = \int_{S_i} (\mathbf{x}_s - \mathbf{x}_0) \times \mathbf{f}_i(\mathbf{x}_s) d\mathbf{x}_s.$$

Hydrodynamic drag effects are resistant: without a magnetic field, the swimmer tends to immobilize at its equilibrium straight shape.

Magnetism

The magnetic field exerts a torque $\mathbf{T}_i^m$ on S_i which is proportional to its magnetization coefficient M_i: $\mathbf{T}_i^m = M_i\mathbf{e}_{i,\parallel} \times \mathbf{H}$.

Dynamics equations

The swimmer is considered sufficiently small to be at low Reynolds number regime, and, as a result, inertia may be neglected [Pur77]. Newton's second law says that the total force applied to $\{S_1 + S_2 + S_3\}$ is zero, and so is the total torque with respect to $\mathbf{x}$. Same holds for the subsystems $\{S_2 + S_3\}$ and $\{S_3\}$, with torques computed with respect to the end of, respectively, S_2 and S_3. This leads to the following system of equations:

$$\begin{cases} \mathbf{F}_1^h + \mathbf{F}_2^h + \mathbf{F}_3^h & & & = & 0, \\ \mathbf{T}_{1,\mathbf{x}}^h + \mathbf{T}_{2,\mathbf{x}}^h + \mathbf{T}_{3,\mathbf{x}}^h & + \mathbf{T}_1^m + \mathbf{T}_2^m + \mathbf{T}_3^m & & = & 0, \\ \mathbf{T}_{2,\mathbf{x}_2}^h + \mathbf{T}_{3,\mathbf{x}_2}^h & + \mathbf{T}_2^m + \mathbf{T}_3^m & + \mathbf{T}_2^{\text{el}} & = & 0, \\ \underbrace{\mathbf{T}_{3,\mathbf{x}_3}^h}_{\text{hydrodynamic terms}} & + \underbrace{\mathbf{T}_3^m}_{\text{magnetic terms}} & + \underbrace{\mathbf{T}_3^{\text{el}}}_{\text{elastic terms}} & = & 0. \end{cases} \tag{6.1}$$

This system gives five scalar equations by projecting the first line on (Ox) and (Oy) and the last three on (Oz). We project the uniform time-varying magnetic field $\mathbf{H}(t)$ in the moving frame associated to S_1: $\mathbf{H}(t) = H_{\parallel}\mathbf{e}_{1,\parallel} + H_{\perp}\mathbf{e}_{1,\perp}$, seeing them as control functions. After computing the different contributions with respect to the parameters, the system can be written as an implicit differential system

$$M(\alpha_1, \alpha_2) R_{-\theta} \dot{Z} = Y, \tag{6.2}$$

with $Z = \begin{pmatrix} x & y & \theta & \alpha_1 & \alpha_2 \end{pmatrix}^T$,

$$R_\theta = \left(\begin{array}{cc|c} \cos\theta & \sin\theta & 0 \\ -\sin\theta & \cos\theta & 0 \\ \hline 0 & 0 & I_3 \end{array}\right),$$

$$Y = \begin{pmatrix} 0 \\ 0 \\ H_{\parallel}(M_2 \sin\alpha_1 + M_3 \sin(\alpha_1+\alpha_2)) \\ \quad -H_{\perp}(M_1 + M_2\cos\alpha_1 + M_3\cos(\alpha_1+\alpha_2)) \\ -\kappa\alpha_1 + H_{\parallel}(M_2\sin\alpha_1 + M_3\sin(\alpha_1+\alpha_2)) \\ \quad -H_{\perp}(M_2\cos\alpha_1 + M_3\cos(\alpha_1+\alpha_2)) \\ -\kappa\alpha_2 + H_{\parallel}M_3\sin(\alpha_1+\alpha_2) - H_{\perp}M_3\cos(\alpha_1+\alpha_2) \end{pmatrix},$$

and M is a matrix that depends only on α_1 and α_2. Its expression is given in the Appendix, section A.1.

Remark 6.1. If the orthogonal magnetic field is equal to zero, (i.e. $H_\perp = 0$ for all times), for any $H_\parallel$, states of the form $(x, y, \theta, 0, 0)$ with $(x, y, \theta) \in \mathbf{R}^3$ are equilibrium positions. In particular, the parallel component of the magnetic field has no action on the swimmer when its shape is a straight line. This makes the system more difficult to control around the equilibrium. This issue is being dealt with in [GLMP16], where a modified swimmer model that is bent at equilibrium is introduced.

Remark 6.2. The problem is invariant by translation and rotation, as can be seen from the absence of x and y in the dynamics, and the special way in which the dynamics depends on θ. Therefore, we focus on the equilibrium position $(0, 0, 0, 0, 0)$, without loss of generality.

Straightforward computations show that the determinant of M remains negative for all values of α_1 and α_2, so M is invertible and we can rewrite the system (S) as a nonlinear control system given by

$$\dot{Z} = \mathbf{F}_0 + H_{\parallel}\mathbf{F}_1 + H_{\perp}\mathbf{F}_2, \tag{S}$$

where $\mathbf{F}_0$,$\mathbf{F}_1$ and $\mathbf{F}_2$ are combinations of the third, fourth and fifth columns of $(MR_{-\theta})^{-1}$, denoted respectively by $\mathbf{X}_3$,$\mathbf{X}_4$ and $\mathbf{X}_5$:

$$\begin{aligned} \mathbf{F}_0 = \; & -\kappa(\alpha_1\mathbf{X}_4 + \alpha_2\mathbf{X}_5); \\ \mathbf{F}_1 = \; & (M_2\sin\alpha_1 + M_3\sin(\alpha_1+\alpha_2))(\mathbf{X}_3 + \mathbf{X}_4) \\ & + M_3\sin(\alpha_1+\alpha_2)\mathbf{X}_5; \\ \mathbf{F}_2 = \; & -M_1\mathbf{X}_3 \\ & -(M_2\cos\alpha_1 + M_3\cos(\alpha_1+\alpha_2))(\mathbf{X}_3 + \mathbf{X}_4) \\ & - M_3\cos(\alpha_1+\alpha_2)\mathbf{X}_5. \end{aligned}$$

6.3 Local controllability around equilibrium states

6.3.1 Small-time local controllability (STLC)

We start with some useful definitions and properties. Let

$$\dot{z} = f_0(z) + u_1(t)f_1(z) + u_2(t)f_2(z). \tag{6.3}$$

be a general nonlinear control-affine system, with z in $\mathbf{R}^n$, f_0, f_1, f_2 real analytic vector fields in $\mathbf{R}^n$ and u_1, u_2 control functions in $L^\infty([0,T])$ for some $T > 0$. For $\eta > 0$, and $z \in \mathbf{R}^n$, let $B(z,\eta)$ be the open ball centered at z with radius η. The following definition appears in [Cor07, Definition 3.2].

Definition 6.3 (STLC)**.** Let z_e in $\mathbf{R}^n$, and $u_e = (u_{1e}, u_{2e})$ constant controls such that (z_e, u_e) is an equilibrium of the system (6.3). The control system (6.3) is *STLC at* (z_e, u_e) if, for every $\varepsilon > 0$, there exists $\zeta > 0$ such that, for every z_0, z_1 in $B(z_e, \zeta)$, there exists controls $u_1(\cdot)$ and $u_2(\cdot)$ in $L^\infty([0,\varepsilon])$ such that the solution of the control system $z(\cdot) : [0,\varepsilon] \to \mathbf{R}^n$ of (6.3) satisfies $z(0) = z_0$, $z(\varepsilon) = z_1$, and

$$\|u_1 - u_{1e}\|_{L^\infty} \leqslant \varepsilon\,, \|u_2 - u_{2e}\|_{L^\infty} \leqslant \varepsilon.$$

In the following, we assume that $f_0(0) = 0$, such that $(0,(0,0))$ (state and controls equal to zero) is an equilibrium of the system 6.3.

The following definitions and theorem provide a sufficient condition for STLC, that we will use later to prove our controllability result on the 3-link swimmer.

Definition 6.4 (LARC)**.** System (6.3) satisfies the Lie Algebra Rank Condition (LARC) at 0 if the values at 0 of all iterated Lie brackets of the vector fields f_0, f_1, f_2 span a vector space of dimension n.

Let us introduce some notions of weight and orders of iterated Lie brackets (see [Sus87, pp.184-185] for details). For h an iterated Lie bracket involving the vector fields f_0, f_1, f_2, let g the iterated Lie bracket obtained by exchanging f_1 and f_2 in h (e.g., if $h = [f_1,[f_1,[f_0,f_2]]]$, then $g = [f_2,[f_2,[f_0,f_1]]]$). Let $\sigma(h) = h + g$, and let $\delta_i(h) \in \mathbf{N}$ $(i = 0,1,2)$ be the number of times f_i appears in h, and $\rho(h) = \delta_0(h) + \delta_1(h) + \delta_2(h)$ (i.e. ρ is the order of h). Let $G_{\rho(h)}$ be the subspace of $\mathbf{R}^n$ spanned by the value at 0 of all the iterated brackets g such that $\rho(g) < \rho(h)$ (i.e. all the brackets of order inferior to the order of h).

Definition 6.5 (Sussmann's condition S)**.** System (6.3) satisfies the condition S at 0 if it satisfies the LARC and any iterated Lie bracket h of the vector fields f_0, f_1, f_2 such that $\delta_0(h)$ is odd and $\delta_1(h)$ and $\delta_2(h)$ are even (those are called the "bad" brackets) satisfies $\sigma(h)(0) \in G_{\rho(h)}$.

Remark 6.6. Condition S is called $S(1)$ in [Sus87, Theorem 7.3], where a more general condition $S(\theta)$ is defined for $\theta \in [0,1]$.

Theorem 6.7 ([Sus87], Theorem 7.3)**.** *If the Sussmann condition S holds, system (6.3) is STLC.*

6.3.2 Controllability result for the 3-link swimmer

In this section, we state a local controllability result for system (S), around the equilibrium position $(0,0,0,0,0)$ (that we will denote by 0 for the sake of readability) with nonzero controls.

From now on, we assume that the physical constants ℓ, η, ξ, κ are positive, and that $\eta > \xi$. This is usually true in the swimmer's physical setting (for thin filaments, one typically has $\eta = 2\xi$, see [GH55]), and avoid dealing with numerous subcases.

Let $m = M_1 + M_3$ and $\mu = M_1 - M_3$. Before stating the result, we need to make a few technical assumptions about the magnetizations.

Assumption 6.8. The magnetizations M_1, M_2 and M_3 are such that

$$\begin{aligned} \mu &\neq 0; \\ (m \neq 0 \ \text{ or } \ M_2 &\neq 0); \\ -7M_2^2 + 9M_2 m - 5M_1 M_3 &\neq 0; \\ P(M_1, M_2, M_3) &\neq 0, \end{aligned} \tag{6.4}$$

with

$$\begin{aligned} P(x,y,z) = 49y^3 - 91y^2(x+z) \\ +36y(x+z)^2 - (45y + 65(x+z))xz. \end{aligned}$$

Remark 6.9. It is shown in [ADGZ17, Section3.1], using a symmetry argument, that if $\mu = 0$, the swimmer starting from the straight shape verifies $\alpha_1(t) = -\alpha_2(t)$ for all times. A similar argument shows that if $m = 0$ and $M_2 = 0$, one has $\alpha_1(t) = \alpha_2(t)$ for all times. Therefore, the system is not controllable in both of these cases.

If $-7M_2^2 + 9M_2 m - 5M_1 M_3 = 0$, then the constant γ expressed in Theorem 6.10 below is not defined. In that case, the swimmer is not STLC at $(0, (\beta, 0))$ for any $\beta \in \mathbf{R}$; see Remark 6.15 for further discussion about the uniqueness of γ.

The first three conditions in equation (6.4) are hence necessary for controllability. It is unclear whether the last one is also necessary. The polynomial expression P seems to be of importance in the swimmer's dynamics, as it appears in all the determinants computed in the proof of Lemma 6.11 below. The values of (M_1, M_2, M_3) for which P vanishes may therefore correspond with cases where the swimmer's movement ability is limited. It seems nonetheless difficult to confirm this hypothesis analytically or numerically.

We now state our main result.

Theorem 6.10. *System (S) is STLC at $(0, (\gamma, 0))$ with*

$$\gamma = \kappa \frac{17m - 16M_2}{-7M_2^2 + 9M_2 m - 5M_1 M_3}.$$

Proof. Let $T > 0$. Let $H_\parallel$ and $H_\perp$ be control functions defined on $[0, T]$. We define $\widetilde{H}_\parallel$ as the affine feedback transformation $\widetilde{H}_\parallel = H_\parallel + \gamma$. With this new control, system (S) can be written as a different control system

$$\dot{Z} = \widetilde{\mathbf{F}}_0 + \widetilde{H}_\parallel \widetilde{\mathbf{F}}_1 + H_\perp \widetilde{\mathbf{F}}_2, \tag{$\tilde{S}$}$$

with $\widetilde{\mathbf{F}}_0 = \mathbf{F}_0 - \gamma\mathbf{F}_1$, $\widetilde{\mathbf{F}}_1 = \mathbf{F}_1$ and $\widetilde{\mathbf{F}}_2 = \mathbf{F}_2$.

For $i_1, \dots, i_m$ indices in $\{0,1,2\}$, we denote by $F_{i_1 i_2 \dots i_m}$ the value at 0 of the iterated Lie bracket $[\mathbf{F}_{i_1}, [\mathbf{F}_{i_2}, \dots \mathbf{F}_{i_m}] \dots]$ of vector fields $\mathbf{F}_0$, $\mathbf{F}_1$, $\mathbf{F}_2$, and by $\widetilde{F}_{i_1 i_2 \dots i_m}$ the value at 0 of the iterated Lie bracket $[\widetilde{\mathbf{F}}_{i_1}, [\widetilde{\mathbf{F}}_{i_2}, \dots \widetilde{\mathbf{F}}_{i_m}] \dots]$ of vector fields $\widetilde{\mathbf{F}}_0$, $\widetilde{\mathbf{F}}_1$, $\widetilde{\mathbf{F}}_2$. For example, $F_{102} = [\mathbf{F}_1, [\mathbf{F}_0, \mathbf{F}_2]](0)$ and $\widetilde{F}_{102} = [\widetilde{\mathbf{F}}_1, [\widetilde{\mathbf{F}}_0, \widetilde{\mathbf{F}}_2]](0)$.

We start with two lemmas on the Lie brackets of the systems (S) and ($\tilde{S}$).

Lemma 6.11. *One has*

$$\widetilde{F}_{101} = 0, \quad \widetilde{F}_{202} = 0, \tag{6.5}$$

and

$$\mathrm{Span}\{\widetilde{F}_2, \widetilde{F}_{02}, \widetilde{F}_{12}, \widetilde{F}_{212}, \widetilde{F}_{2202}, \widetilde{F}_{2212}\} = \mathbf{R}^5. \tag{6.6}$$

Proof. Using a computer algebra software (for example Mathematica), we compute Lie brackets and show (6.5). We also show that only the first component of $\widetilde{F}_{212}$ is nonzero, and its value is equal to

$$48\frac{(\xi-\eta)\mu}{5\ell^8\xi^3\eta}(-7M_2^2 + 9M_2 m - 5M_1 M_3),$$

that is nonzero thanks to Assumption 1. Moreover, the determinants of $(\widetilde{F}_2, \widetilde{F}_{02}, \widetilde{F}_{12}, \widetilde{F}_{212}, \widetilde{F}_{2202})$ and $(\widetilde{F}_2, \widetilde{F}_{02}, \widetilde{F}_{12}, \widetilde{F}_{212}, \widetilde{F}_{2212})$ cannot be both zero if Assumption 1 holds. Hence (6.6) is verified. □

Lemma 6.12. *One has*

$$F_{101} = 0, \quad F_{202} = \gamma F_{212}, \tag{6.7}$$

and

$$\mathrm{Span}\{F_2, F_{02}, F_{12}, F_{212}, F_{2202}, F_{2212}\} = \mathbf{R}^5. \tag{6.8}$$

Proof. Since $\mathbf{F}_0 = \widetilde{\mathbf{F}}_0 + \gamma\mathbf{F}_1$, $\mathbf{F}_1 = \widetilde{\mathbf{F}}_1$ and $\mathbf{F}_2 = \widetilde{\mathbf{F}}_2$, one immediately has (6.7) and (6.8). □

Lemmas 6.11 and 6.12 allow to prove the following results:

Proposition 6.13. *System (S) does not satisfy the Sussmann condition S.*

Theorem 6.14. *System ($\tilde{S}$) is STLC at $(0,(0,0))$.*

Proof. We prove simultaneously Proposition 6.13 and Theorem 6.14. System (S) (resp. system ($\tilde{S}$)) satisfies the LARC thanks to (6.8) (resp. (6.6)). Moreover, all the "bad" brackets h such that $\rho(h) > 4$ trivially belong to $G_{\rho(h)} = \mathbf{R}^5$. The only bad brackets of lower order that remain are the ones with two times $\mathbf{F}_1$ or $\mathbf{F}_2$ and one time $\mathbf{F}_0$ (resp. $\widetilde{\mathbf{F}}_0$). The Sussmann condition S requires $F_{101} + F_{202}$ (resp. $\widetilde{F}_{101} + \widetilde{F}_{202}$) to belong to the subspace spanned by the brackets of order smaller than 2, which is $\mathrm{Span}\{F_2, F_{02}, F_{12}\}$ (resp. $\mathrm{Span}\{\widetilde{F}_2, \widetilde{F}_{02}, \widetilde{F}_{12}\}$).

Equations (6.7) and (6.8) show that $F_{101} + F_{202} = \gamma F_{212} \notin \mathrm{Span}\{F_2, F_{02}, F_{12}\}$, which proves Proposition 6.13. On the other hand, (6.5) shows that $\widetilde{F}_{101} + \widetilde{F}_{202} = 0 \in \mathrm{Span}\{\widetilde{F}_2, \widetilde{F}_{02}, \widetilde{F}_{12}\}$, which proves that the condition S is true for ($\tilde{S}$). Then, thanks to Theorem 6.7, ($\tilde{S}$) is STLC at $(0,(0,0))$. □

We now conclude the proof of Theorem 6.10, as a corollary to Theorem 6.14. Let $\varepsilon > 0$. Let ζ be the associated parameter from Definition 6.3, and Z_0, Z_1 in $B(0,\zeta)$. There exists controls $\widetilde{H}_\parallel$ and $H_\perp$ defined on $[0,\varepsilon]$ such that the solution of $(\widetilde{S})$ with $Z(0) = Z_0$ and these controls verifies $Z(\varepsilon) = Z_1$, and

$$\|\widetilde{H}_\parallel\|_{L^\infty} \leqslant \varepsilon\,, \|H_\perp\|_{L^\infty} \leqslant \varepsilon.$$

Hence, the solution of system (S) with $Z(0) = Z_0$ and controls $H_\parallel = \widetilde{H}_\parallel - \gamma$ and $H_\perp$ verifies $Z(\varepsilon) = Z_1$. Moreover, $\|H_\parallel - \gamma\|_{L^\infty} \leqslant \varepsilon$ and $\|H_\perp\|_{L^\infty} \leqslant \varepsilon$. □

Remark 6.15. In a forthcoming paper [GLMP19], we show that γ is unique: system (S) is not STLC around any control different from $(\gamma, 0)$. In particular, one cannot hope to control the system at $(0,(0,0))$ (i.e. with small controls) or at $(0,(\delta,0))$ with $\delta < \gamma$. Our result is optimal in that sense.

The uniqueness of γ is due to the fact that it is the only value that allows to "neutralize" the bracket F_{202} with the bracket F_{212} at 0. Around another control $(0,(\delta,0))$ with $\delta \neq \gamma$, one has to check that F_{202} obstructs local controllability and that all the other brackets cannot "neutralize" it. This requires a careful study of the higher-order brackets. The calculations in their full length would exceed the scope of the present study. The reader is invited to refer to [GLMP19] for more details.

6.3.3 A similar result for the 2-link swimmer

In [GP17], the authors conduct a study on the 2-link magnetic swimmer and state a local controllability result. However, the result they state is weaker than STLC. In this section, we improve this result, using the same arguments than for the 3-link swimmer.

The notations used in the following are the same as in their paper, and as above: each of the two segments has length ℓ, hydrodynamic coefficients η and ξ; the segments are magnetized with magnetizations M_1 and M_2 and connected by a torsional spring with stiffness κ. The swimmer is submitted to a magnetic field $(H_\parallel, H_\perp)$. The state variables are x, y, θ, defined as for the 3-link swimmer, and α, the angle between the two links. We assume that ℓ, η, ξ and κ are positive and that $\eta > \xi$.

The derivation of the dynamics equation leads to a system analog to system (S)

$$\dot{Y} = \mathbf{G}_0 + H_\parallel(t)\mathbf{G}_1 + H_\perp(t)\mathbf{G}_2, \tag{Σ}$$

with $Y = (x, y, \theta, \alpha)$.

Without loss of generality (thanks to an argument similar to Remark 6.2), we focus on controllability around the position 0 (i.e. $(0,0,0,0)$) with nonzero controls. Using the "return method" from [Cor07, Chapter 6], the following result is shown in [GP17, Theorem III.4]:

Theorem 6.16. *Assume $M_1 M_2 \neq 0$ and $M_1 \neq M_2$. Let $\varepsilon > 0$. For any Y_0, Y_1 in $B(0,\zeta)$, there exist $H_\parallel$ and $H_\perp$ in $L^\infty[0,\epsilon]$ such that the solution of (Σ) with $Y(0) = Y_0$ and these controls verifies $Y(\varepsilon) = Y_1$, and*

$$\|H_\parallel\|_{L^\infty} \leqslant 2\kappa \left|\frac{1}{M_1} + \frac{1}{M_2}\right| + \varepsilon, \quad \|H_\perp\|_{L^\infty} \leqslant \varepsilon.$$

Before stating our result, let us point out a few particular cases, as for the 3-link swimmer.

Proposition 6.17. *If $M_1 = 0$ or $M_2 = 0$, the swimmer is not STLC.*

Proof. We start with a useful lemma.

Lemma 6.18. *If $\mathbf{G}_1 = 0$, and $G_{202} \notin \mathrm{Span}\{G_2, G_{02}, \dots, G_{0\dots02}, \dots\}$, then System ($\Sigma$) is not STLC.*

Proof. This is a direct application of the necessary condition stated in [Sus83, Prop. 6.3, p.707], for scalar-input control systems. □

The symmetry of the system makes both cases $M_1 = 0$ and $M_2 = 0$ equivalent. Moreover, in the case $M_1 = 0$, a straightforward computation shows $\mathbf{G}_1 = 0$ and $G_{202} \notin \mathrm{Span}\{G_2, G_{02}, \dots, G_{0\dots02}, \dots\}$, so we can apply Lemma 6.18. □

From now on, we make the following assumptions on the magnetizations:

Assumption 6.19. The magnetizations M_1, and M_2 are such that $M_1 \neq 0$, $M_2 \neq 0$, $M_1 - M_2 \neq 0$ and $M_1 + M_2 \neq 0$.

Remark 6.20. It is shown in [GP17, Section III] that the system is not controllable if $M_1 - M_2 = 0$, and STLC at $(0, (0, 0))$ if $M_1 + M_2 = 0$. Moreover, it is shown in [GLMP18] that, unless $M_1 + M_2 = 0$, the 2-link swimmer is not STLC at $(0, (0, 0))$.

We now state our result for the 2-link swimmer.

Theorem 6.21. *System (Σ) is STLC at $(0, (\gamma', 0))$ with*

$$\gamma' = \kappa \left(\frac{1}{M_1} + \frac{1}{M_2} \right).$$

Remark 6.22. This improves the result from Theorem 6.16, for it shows that the system is STLC at $(\gamma', 0)$, whereas Theorem 6.16 does not require the control $H_\parallel$ to stay arbitrarily close to the upper bound $2\kappa \left| \frac{1}{M_1} + \frac{1}{M_2} \right|$. This upper bound on $H_\parallel$ is also improved in our result.

Proof. Let $T > 0$. Let $H_\parallel$ and $H_\perp$ be control functions defined on $[0, T]$. Let

We define $\widetilde{H}_\parallel = H_\parallel + \gamma'$ as above, to get the feedback system

$$\dot{Y} = \widetilde{\mathbf{G}}_0 + \widetilde{H}_\parallel \widetilde{\mathbf{G}}_1 + H_\perp \widetilde{\mathbf{G}}_2, \tag{$\tilde{\Sigma}$}$$

with $\widetilde{\mathbf{G}}_0 = \mathbf{G}_0 - \gamma' \mathbf{G}_1$, $\widetilde{\mathbf{G}}_1 = \mathbf{G}_1$ and $\widetilde{\mathbf{G}}_2 = \mathbf{G}_2$.

We will use the same notations as above for the Lie brackets associated to systems (Σ) and ($\tilde{\Sigma}$), evaluated at 0. For example, $G_{102} = [\mathbf{G}_1, [\mathbf{G}_0, \mathbf{G}_2]](0)$ and $\widetilde{G}_{102} = [\widetilde{\mathbf{G}}_1, [\widetilde{\mathbf{G}}_0, \widetilde{\mathbf{G}}_2]](0)$.

Lemma 6.23. *One has $\mathrm{Span}\{G_2, G_{12}, G_{212}, G_{2202}\} = \mathbf{R}^4$ and*

$$G_{101} = 0, \quad G_{202} = \gamma' G_{212}. \tag{6.9}$$

Proof. Using a computer algebra software, we compute Lie brackets and show (6.9). We also show that the first component of each of the three vectors G_2, G_{12}, G_{2202} is zero. The determinant D of the matrix formed with the three last components of these vectors expresses

$$D = \frac{209952\kappa M_1 M_2(\eta-\xi)\left(M_1^2-M_2^2\right)^2}{\eta^7 l^{20}\xi}.$$

D is nonzero thanks to Assumption 6.19. Moreover, only the first component of G_{212} is nonzero, and its value is equal to

$$\frac{216 M_1 M_2(\eta-\xi)(M_1-M_2)}{\eta^3 l^8 \xi}$$

that is nonzero thanks to Assumption 6.19. Hence (6.8) is verified. □

Lemma 6.24. *One has* $\mathrm{Span}\{\widetilde{G}_2, \widetilde{G}_{12}, \widetilde{G}_{212}, \widetilde{G}_{2202}\} = \mathbf{R}^4$ *and*

$$\widetilde{G}_{101} = 0, \quad \widetilde{G}_{202} = \gamma' \widetilde{G}_{212} \tag{6.10}$$

Proof. Since $\widetilde{\mathbf{G}}_0 = \mathbf{G}_0 - \gamma \mathbf{G}_1$, $\widetilde{\mathbf{G}}_1 = \mathbf{G}_1$ and $\widetilde{\mathbf{G}}_2 = \mathbf{G}_2$, one immediately has (6.10). □

Proposition 6.25. *System* (Σ) *does not satisfy the Sussmann condition S.*

Remark 6.26. This proposition is stated and shown in [GP17, Prop. III.11].

Theorem 6.27. *System* ($\tilde{\Sigma}$) *is STLC at* $(0,(0,0))$.

Proof. See the proofs of Proposition 6.13 and Theorem 6.14 in the previous section. □

We conclude the proof of Theorem 6.21 as in the previous section. □

6.4 Discussion

6.4.1 Comments on the main results

The feedback systems ($\tilde{S}$) and ($\tilde{\Sigma}$) are defined this way because they "neutralize" the bad bracket $[\mathbf{F}_2, [\widetilde{\mathbf{F}}_0, \mathbf{F}_2]]$ (or $[\mathbf{G}_2, [\widetilde{\mathbf{G}}_0, \mathbf{G}_2]]$). In the original systems (S) and (Σ), the value of this bracket at 0 is nonzero, which seems to be an obstruction to STLC. In fact, since no other control than $(\gamma, 0)$ (resp. $(\gamma', 0)$ for the 2-link swimmer) neutralizes the bad bracket, our result is optimal (see Remark 6.15): as we show in a forthcoming paper [GLMP19], the system is not STLC around any other control. In particular, one cannot locally control the swimmer with a parallel control inferior, in absolute value, to γ (resp. γ').

Theorem 6.10 is, to our knowledge, the first local controllability result for this magnetically actuated 3-link swimmer. It shows, rather counterintuitively, that the parallel component of the magnetic field needs to remain large in order to control the swimmer, even when the target state is very close to its equilibrium position. In the particular case $16m - 17M_2 = 0$, the constant γ is equal to 0, and the standard STLC at $(0,(0,0))$ is retrieved. We improved the existing result on the 2-link swimmer in Theorem 6.21.

Physically, these results reflect the fact that the parallel component of the magnetic field has no effect on the swimmer when it is at its equilibrium shape, i.e. when all the segments are aligned. This may be seen as a loss of controllability at the equilibrium. The parallel control $H_{\parallel}$ plays however a crucial role in the controllability properties of the swimmers.

This result provides a useful insight for experiments, by showing that the 2- and 3-link swimmers may not be driven easily in any direction from an equilibrium point, and giving an explicit lower bound on the control needed to achieve local controllability. Further work on the subject of micro-swimmers, currently under our investigation, is to consider swimmers with more links, that describe more realistically flexible filaments. This work also addresses the question of the existence of necessary conditions for local controllability for systems with non-scalar controls, for which little is known.

6.4.2 Numerical simulations

In order to numerically observe the local behavior of the system, we steer it from an equilibrium state with different controls that stay "close" to the equilibrium control. Let β be a real number and $\epsilon > 0$ be a small parameter; we set

$$\begin{aligned} H_{\parallel}(t) &= \beta + \varepsilon(h_1 + h_2\cos(10t) + h_3\cos(100t)) \\ H_{\perp}(t) &= \varepsilon(h_4 + h_5\cos(10t) + h_3\cos(100t)) \end{aligned} \tag{6.11}$$

with h_1 to h_6 constants taken randomly in $[-1, 1]$. We take N realizations of these random controls and solve the 2-link swimmer system starting from $(0, 0, 0, 0)$ over the time interval $[0, T]$. With such a range of randomized oscillating controls close to $(\beta, 0)$, we expect the obtained trajectories to roughly cover the reachable space in small time T, which allows to observe the unattainable regions if there are any. The results of the simulations, performed with MATLAB, for the 2-link swimmer with these controls are displayed on Figure 6.2. When β is different from the critical value γ', the trajectories remain, locally, either always left or always right of $(0, 0)$ in the 2d-plane, which tends to validate the non-STLC of the swimmer. On the contrary, for $\beta = \gamma'$, where the swimmer can be locally controlled according to our result, the trajectories seem to cover a neighborhood of 0.

The dynamics of the 3-link swimmer are more complex and appear to be numerically unstable. The oscillating controls generate numerical artifacts over the trajectories; hence the numerical simulations in this case are less conclusive than for the two-link swimmer.

6.4.3 Remark on the definition of STLC

The STLC definition given in Definition 6.3 is quite standard, used for instance in [Cor07]. Another definition that only requires boundedness of the control (and not for the controls to be arbitrarily close to a certain reference control) can be found in the works of Hermes [Her82] and Sussmann [Sus83] [1] among others. This second definition, while not equivalent to the first one, is sometimes called STLC as well. In order to avoid the confusion, we will call it γ-STLC:

1. The exact definition given in [Sus83] supposes an *a priori* bound on the control, uses the notion of reachable space, and is hence written in a more condensed manner. We rephrase it here to match the structure of Definition 6.3.

Definition 6.28 (γ-STLC)**.** Let $\gamma \geqslant 0$. Let z_e in $\mathbf{R}^n$, and $u_e = (u_{1e}, u_{2e})$ constant controls such that (z_e, u_e) is an equilibrium of the system (6.3). The control system (S) is *γ-STLC at* (z_e, u_e) if, for every $\varepsilon > 0$, there exists $\zeta > 0$ such that, for every z_0, z_1 in $B(z_e, \zeta)$, there exists controls $u_1(\cdot)$ and $u_2(\cdot)$ in $L^\infty([0, \varepsilon])$ such that the solution of the control system $z(\cdot) : [0, \varepsilon] \to \mathbf{R}^n$ of (6.3) satisfies $z(0) = z_0$, $z(\varepsilon) = z_1$, and

$$\|u_1 - u_{1e}\|_{L^\infty} \leqslant \gamma + \varepsilon\,, \|u_2 - u_{2e}\|_{L^\infty} \leqslant \gamma + \varepsilon.$$

One can see that "0-STLC" at (z_e, u_e) is identical to STLC at (z_e, u_e). If $\gamma > 0$, Definition 6.28 is weaker than Definition 6.3, for the norm of the control can remain "large" as the ball radius ζ gets arbitrarily small. Theorem 6.16 is equivalent to the $(2\gamma')$-STLC at $(0, (0, 0))$ for system (Σ). In a forthcoming paper [GLMP19], we prove that a particular class of systems with two controls, with properties similar to those of the 2- and 3-link swimmers, may be γ-STLC for $\gamma > 0$, but not STLC, at an equilibrium.

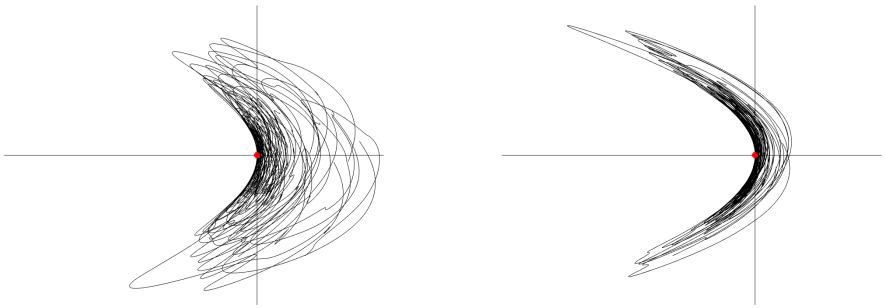

(a) $\beta = 0.5\gamma'$ (b) $\beta = 0.9\gamma'$

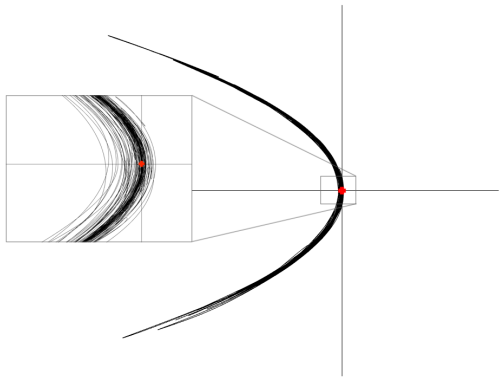

(c) $\beta = \gamma'$

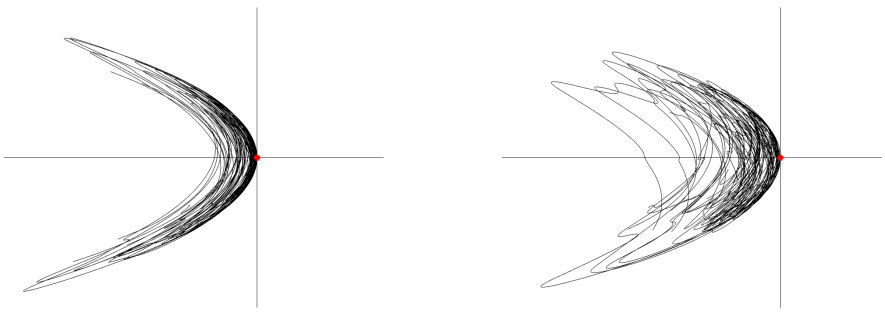

(d) $\beta = 1.1\gamma'$ (e) $\beta = 1.25\gamma'$

Figure 6.2 – Illustration of the role played by the constant γ'. On each graph are plotted $N = 30$ trajectories in the 2d-plane of the extremity of the 2-link swimmer, starting at state (0,0,0,0) and with the randomized controls (6.11) taken "around" $(\beta, 0)$, for 5 different values of β. The origin $(0, 0)$ is indicated by the red dot on each graph. One can observe that a certain region seems to be unattainable for every case, except for the case $\beta = \gamma'$ (graph (c)) where controllability at $(0, 0)$ is theoretically retrieved (a zoom-in around the origin is added on the graph to show that the trajectories cover a neighborhood of $(0, 0)$. The numerical values used are $\eta = 4$, $\xi = 2$, $l = 1$, $M_1 = 1$, $M_2 = 3$, $k = 1$, $\varepsilon = 10^{-2}$, and $T = 1$.

Part III

Modelling and numerical aspects of elastic microfilaments in a low Reynolds number fluid

Chapter 7

The asymptotic coarse-graining formulation of slender-rods, bio-filaments and flagella

This chapter reproduces [MGG18], written in collaboration with Laetitia Giraldi and Hermes Gadêlha, and published in 2018 in the *Journal of the Royal Society Interface*.

7.1 Introduction

The fluid-structure interactions of semi-flexible filaments are found everywhere in nature [Ant05, Alb02, How01], from the mechanics of DNA strands and the movement of polymer chains to complex interaction involving cytoskeletal microtubules and actin cross-linking architectures and filament-bundles and flagella [GGSKB10, CJP99, BDE+95, GL95, FWP08, YLH06, OLC13, TS04, KG12, SCD+12, BMK+06, PTD+16, HSF10, CSRB08, CBFB06]. The elastohydrodynamics of filaments permeate different branches in mathematical sciences, physics and engineering, and their cross-fertilising intersects with biology and chemistry. The wealth of theoretical and experimental studies on the movement of semi-flexible filaments, termed here as filaments, is extensive, thus reflecting the fundamental importance of the physical interactions marrying fluid and elastic phenomena. Hitherto the elastohydrodynamics of active and passive filaments have shed new light into bending, buckling, active matter and self-organisation, as well as bulk material properties of interacting active and passive fibres across disciplines [HB79, GGSKB10, CJP99, BDE+95, GL95, FWP08, YLH06, OLC13, TS04, KG12, SCD+12, CG17, SK18].

The movement of semi-flexible filaments bridges complex fluid and elastic interactions within a hierarchy of different approximations [LP09]. Here, we focus on systems governed by low Reynolds number inertialess hydrodynamics [Pur77]. Both the hydrodynamic and elastic interactions of filaments are greatly simplified by exploiting the filament slenderness [LP09, Ant05], reducing the dynamics to effectively a one-dimensional system [HB78]. A variety of model families have been developed exploiting such slenderness property, and thus it would be a challenging task to review the wealth of theoretical and empirical developments to date here. Instead we direct the reader to excellent reviews on the subject [LP09, Pow10, SZ11, BW77].

In a nutshell, two theoretical descriptions are popularly used: the discrete and continuous

formulation. In discrete models, such as the beads model, gears model, n-links model, or similarly worm-like chain models (see [ADGZ13, ADGZ15, GMZ13, GMZ15, SK18, DCP15, PTD+16, HSF10, CLPL05, SZ11, MJGS15, Bro14, JB79]), the filament is broken into a discrete number of units, such as straight segments, spheres or ellipsoids. The elastic interaction coupling neighboring nodes/joints is described via constitutive energy functionals or via discrete elastic connectors encoding the filament's resistance to bending. The shape of each discrete unit defines the hydrodynamical interaction, i.e. hydrodynamics of spheres for the beads and gear model, and slender-body hydrodynamics for straight rod-like elements. Continuous models, on the other hand, recur to partial differential equation (PDE) systems to describe the combined action from fluid-structure interactions [HB79, TS04]. The dynamics arises through the total balance of contact forces and moments along the filament [Ant05]. This formalism results invariably in a nonlinear PDE system coupling a hyperdiffusive fourth-order PDE with a second-order boundary value problem (BVP) required to ensure inextensibility via Lagrange multipliers [HB79, TS04, GGSKB10], in addition to six boundary conditions and initial configuration for closeness. The geometrical coupling guarantees that the order of the PDE remains unchanged under transformation of variables, from the position of filament centerline $X(s,t)$ at an arclength s and time t relative to a fixed frame of reference, to tangent angle $\theta(s,t)$ or curvature $\kappa(s,t)$ of the filament [GL95, WG98]. While the equivalence between discrete and continuous models is generally not available, both theoretical frameworks suffer from numerical instability and stiffness arising from the nonlinear geometrical coupling between the filament's curvature and its inextensibility constraint [Kla96, TS04]. Nonlinearities originated from curvature are well known to drive numerical instability in moving boundary systems, as found in pattern formation of interfacial flows driven by surface tension [HLS94], as well as in elastic and fluid stresses in shells and fluid membranes [HKS98, RAMB15]. The latter often requires numerical regularisation, such as the small-scale decomposition [HLS94, HKS98].

Contact forces of inextensible filaments are not determined constitutively [Ant05], and require Lagrange multipliers to ensure strict length constraints. The resulting systems in both discrete and continuous models are thus prone to numerical instabilities [LP09, Pow10, SZ11, BW77, HB78, MJGS15, Bro14, JB79, Kla96, CJP99, SK18, DCP15, PTD+16, HSF10]. This is despite the fact that discrete models automatically satisfy the length constraint by construction [LP09, HB78, Bro14, PTD+16, CJP99, SK18, DCP15, CLPL05, Low03, CLPL05], or equivalently the tangent angle formulation $\theta(s,t)$ for continuous models [CJP99, HB78, WROG98, You09], which intrinsically preserves lengths by definition. In continuum models, penalization strategies are required to regularize length errors that vary dynamically [TS04, GGSKB10, MJGS15]. The number of boundary conditions is large, and the non-linear coupling makes complex boundary systems challenging [MJGS15], as we discuss below. The latter imposes severe spatiotemporal discretisation constraints, increases the computational time and numerical errors, especially for deformations involving large curvatures.

The aim of this paper is to resolve the bottleneck arising from the interaction between the hyperdiffusive elastohydrodynamics and the inextensibility constraint. For this, we consider a hybrid continuum-discrete approach. The coarse-graining formulation is a direct consequence of the asymptotic integration of the moment balance system along coarse-grained rod-like elements. No explicit length constraint is required, and the resulting linear system is structurally stable and does not require explicit computation of the unknown force distribution aforementioned. Numerical implementation is straightforward and allows for faster computation, over than a hundred times faster, with increasingly better performance for tol-

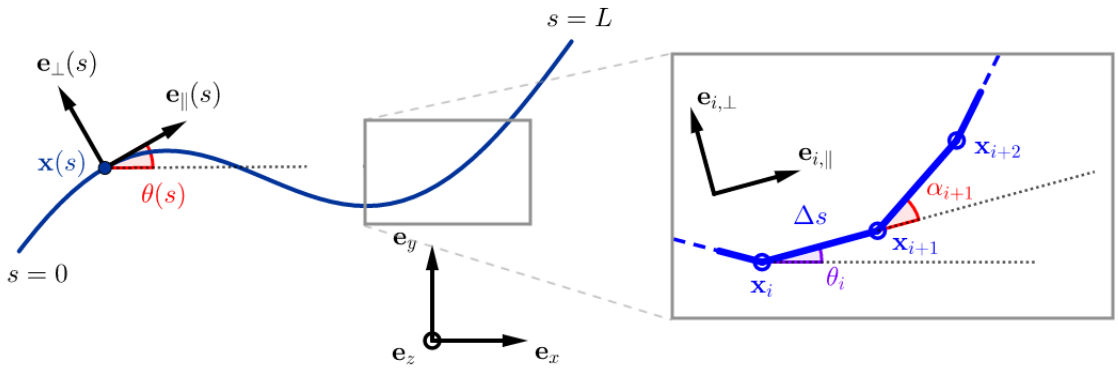

Figure 7.1 – Parametrisation of the continuous and discrete filaments

erance to error below 1%. This greatly decreases the implementation complexity, the number of boundary conditions required, computational time and numerical stiffness. The coarse-graining framework can be readily applied to systems that would be prohibitive using the classical system, as we discuss in section 7.4. Furthermore, we show that the coarse-graining implementation is simple, and generalisations for complex interaction of multiple rods, Brownian polymer dynamics, active filaments and non-local hydrodynamics are straightforward.

This paper is structured as follows: first, we describe the momentum balance for an inextensible filament embedded in an inertialess fluid, and re-derive the classical elastohydrodynamic system in Section 7.2. For this, we employ the standard elastic theory for slender-rods and lowest order hydrodynamic approximation for slender-bodies, i.e. Resistive Forces Theory [GH55]. In Section 7.3, we introduce the asymptotic coarse-graining formulation. In Section 7.4, we contrast the classical elastohydrodynamics and the coarse-graining formulations and their respective numerical performances. Finally, we abandon the classical elastohydrodynamic formulation and explore several systems with the coarse-graining approach in Section 7.5. We investigate the buckling instability of a bio-filament [BDE+95, TS04], magnetically-driven micro-swimmers [ADGZ15, GP17, GO14, Gad13], the counterbend phenomenon for effectively one-dimensional filament-bundles [GGG13, Gad18, CG17] and the driven motion of a two-filament bundle assembly. Except from the magnetic swimmer, the other bio-filament systems are entirely novel in the literature. We also provide the Matlab code via github free repository that can be used as a basis for further generalisations. The link to this repository is available at the end of the paper.

7.2 Classical elastohydrodynamic filament theory

Consider an inextensible elastic rod of length L, parametrised by its arclength. The position of a point of arclength s on the filament is denoted by $\mathbf{x}(s)$. The filament can experience two types of forces [Ant05]: contact forces $\mathbf{n}(s)$ within the filament, and external forces, that have a force density $\mathbf{f}(s)$ (by unit of length) ? later this will incorporate the hydrodynamic interaction. The second Newton's law ensures the momentum balance:

$$\mathbf{n}_s + \mathbf{f} = 0, \tag{7.1}$$

$$\mathbf{m}_s + \mathbf{x}_s \times \mathbf{n} = 0, \tag{7.2}$$

where the subscripts denote derivatives with respect to arclength s, $\mathbf{m}(s)$ is the contact moment, and external moments are neglected. The dynamical system (7.1)-(7.2) is further specified by the geometry of the deformation and the constitutive relations characterising the filament. Here we focus on inextensible, unshearable hyperelastic filaments undergoing planar deformations. Thus the contact forces are not defined constitutively whilst the bending moment is linearly related to the local curvature [Ant05].

The position of the filament centerline is denoted by $\mathbf{x}(s,t)$. The Frenet basis moving with the filament is given by $(\mathbf{e}_\parallel, \mathbf{e}_\perp)$, tangent and normal vector respectively. The angle between the x-axis of frame of reference and $\mathbf{e}_\parallel$ is θ, where the normal vector to the plane in which deformation occurs is $\mathbf{e}_z$, see Figure 7.1. The filament is characterised by a bending stiffness E_b, and thus elastic moments are simply $\mathbf{m}(s) = E_b\theta_s\mathbf{e}_z$. The latter can be used in conjuction with (7.2), using $\theta_{ss}\mathbf{e}_\perp = \mathbf{x}_{sss}$, to get

$$\mathbf{n}(s) = -E_b\mathbf{x}_{sss}\mathbf{e}_\perp + \tau\mathbf{e}_\parallel, \tag{7.3}$$

where $\tau(s)$ is the unknown Lagrange multiplier. The hydrodynamical friction experienced by a slender-body in low Reynolds number regime can be simplified asymptotically by employing the Resistive Force Theory [GH55], in which hydrodynamic friction is related with to velocity via an anisotropic operator

$$\mathbf{f}(s) = -\xi(\mathbf{e}_\perp \cdot \mathbf{x}_t)\mathbf{e}_\perp - \eta(\mathbf{e}_\parallel \cdot \mathbf{x}_t)\mathbf{e}_\parallel\,, \tag{7.4}$$

where η and ξ are the parallel and perpendicular drag coefficients, respectively. Using (7.1) and nondimensionalizing the system with respect to the length scale L, time scale ω^{-1}, force density E_b/L^3, and noticing that $\mathbf{e}_\parallel = \mathbf{x}_s$, the dimensionless elatohydrodynamic equation for a passive filament deforming in a viscous environment reads:

$$\mathrm{Sp}^4\mathbf{x}_t = -\mathbf{x}_{ssss} - (\gamma-1)(\mathbf{x}_s \cdot \mathbf{x}_{ssss})\mathbf{x}_s + (\tau\mathbf{x}_{ss} + \gamma\tau_s\mathbf{x}_s), \tag{7.5}$$

with the dimensionless parameters $\mathrm{Sp} = L(\omega\xi/E_b)^{1/4}$ and $\gamma = \xi/\eta$. The unknown line tension is obtained by invoking the inextensibility constraint

$$\frac{\partial}{\partial t}(\mathbf{x}_s \cdot \mathbf{x}_s) = 0, \tag{7.6}$$

which together with (7.1) provides a nonlinear second-order boundary value problem for the line tension, or Lagrange multiplier,

$$\gamma\tau_{ss} - (\mathbf{x}_{ss} \cdot \mathbf{x}_{ss})\tau = -3\gamma(\mathbf{x}_{sss} \cdot \mathbf{x}_{sss}) - (3\gamma+1)(\mathbf{x}_{ss} \cdot \mathbf{x}_{ssss}). \tag{7.7}$$

In practice, however, this inextensibility condition is prone to numerical errors [TS04] causing the filament length to vary over time. A penalisation term is thus added on the right-hand side of (7.7) to remove spurious incongruousnesses of the tangent vector [TS04, GGSKB10, MJGS15].

The non-linear, geometrically exact elastohydrodynamical system Eqs. (7.5) and (7.7) requires a set of initial and boundary conditions for closeness. At the filament boundaries, either the force/torque are specified or the endpoints kinematics is imposed. Here we consider

the distal end free from external forces and moments

$$\forall t, \quad -\mathbf{x}_{sss}(L,t) + \tau \mathbf{x}_s(L,t) = 0, \quad \mathbf{x}_{ss}(L,t) = 0.$$

At the proximal end, several scenarios may be considered: (i) Free torque and force condition, thus the above equations are satisfied at $s = 0$. (ii) Pivoting, pinned or hinged condition: the extremity has a fixed position but it is free rotate around it, $\mathbf{x}_t(0,t) = 0, \mathbf{x}_{ss}(0,t) = 0$. (iii) Clamped condition: the extremity has a fixed position and orientation, $\mathbf{x}_t(0,t) = 0, \mathbf{x}_{st}(0,t) = 0$. Finally, initial conditions are required for closeness. Boundary conditions for the Lagrange multiplier τ boundary value problem (7.7) are derived from the above boundary constraints accordingly, and are generally unknown. Thus the PDE system Eqs. (7.5) and (7.7) is solved simultaneously.

7.3 Asymptotic coarse-grained elastohydrodynamics

In this section we describe the asymptotic coarse-graining formulation by integrating the moment balance system (7.1)-(7.2). The aim of this formulation is to bypass the complexity arising from the unknown contact forces (7.3), not defined constitutively, thus requiring the Lagrange multiplier τ to ensure inextensibility (7.7). Integrating the balance of contact forces over the whole filament (7.1), we get

$$\mathbf{n}(L) - \mathbf{n}(0) + \int_0^L \mathbf{f}(s)\,\mathrm{d}s = 0,$$

where external contact forces are given by $\mathbf{n}(L) = \mathbf{n}(0) = 0$. The filament is conveniently divided in N rod-like segments with $\Delta s = L/N$. In the asymptotic limit of a small nonzero Δs, the filament can be coarse-grained via a semi-Riemann sum

$$\sum_{i=1}^{N} \int_{(i-1)\Delta s}^{i\Delta s} \mathbf{f}(s)\,\mathrm{d}s = \sum_{i=1}^{N} \mathbf{F}_i = 0, \tag{7.8}$$

so that $\mathbf{F}_i$ represents the total contact force experienced by the i-th element. For a filament free from external torques, $\mathbf{m}(L) = \mathbf{m}(0) = 0$, the total moment balance (7.2) simply reads

$$\sum_{i=1}^{N} \int_{(i-1)\Delta s}^{i\Delta s} \mathbf{x}_s(s) \times \mathbf{n}(s)\,\mathrm{d}s = 0.$$

After partial integration, and exploiting the force balance (7.1), we find

$$\sum_{i=1}^{N} \int_{(i-1)\Delta s}^{i\Delta s} (\mathbf{x}(s) - \mathbf{x}_0) \times \mathbf{f}(s)\mathrm{d}s = \sum_{i=1}^{N} \mathbf{M}_{i,\mathbf{x}_0} = 0, \tag{7.9}$$

which is independent of $\mathbf{n}(s)$. Similarly, $\mathbf{M}_{i,\mathbf{x}_0}$ is the i-th moment about $\mathbf{x}_0 = \mathbf{x}(0)$. As required, the total moment balance above is independent of the bending moment. Integration by parts of (7.2) for the j-th element instead introduces the effect of the elastic bending

moments via

$$\sum_{i=j}^{N} \mathbf{M}_{i,\mathbf{x}_j} = \mathbf{m}_j, \tag{7.10}$$

where $\mathbf{m}_j = \mathbf{m}((j-1)L/N)$ and $j = 2, \ldots, N$. Here, it is convenient to write the moment $\mathbf{M}_{i,\mathbf{x}_j}$ relative to $\mathbf{x}_j$, whilst $\mathbf{m}_j$ is the bending moment contribution from the j-th element and, as previously, it is linearly related to the curvature $\mathbf{m}(s) = E_b\theta_s\mathbf{e}_z$. Distinct finite difference approximations maybe employed for θ_s [GGSKB10, DCP15, TS04]. For simplicity, we use the backward difference formulae,

$$\mathbf{m}_i = \kappa\,\alpha_i\mathbf{e}_z = \kappa\,(\theta_i - \theta_{i-1})\mathbf{e}_z, \tag{7.11}$$

where $\kappa = E_b/\Delta s$. The contact force $\mathbf{f}(s)$ in (7.8)-(7.10) is given by the hydrodynamic coupling (7.4).

We introduce now the geometry of deformation for centerline $\mathbf{x}(s,t)$ for the the coarse-grained elastohydrodynamic system. It is convenient to describe filament centerline in terms of the tangent angle θ, see Fig. 7.1, where $\mathbf{x}(s,t) = \mathbf{x}_0 + \int_0^L(\cos\theta, \sin\theta)\mathrm{d}s$, so that in the coarse-graining limit, we have

$$\mathbf{x}_i = \mathbf{x}_0 + \sum_{k=1}^{i-1}(\cos\theta_k, \sin\theta_k)\Delta s \tag{7.12}$$

for $i = 1, \ldots, N$, thus $\mathbf{x}_i = \mathbf{x}((i-1)L/N) = (x_i, y_i)$, where θ_k is the angle between $\mathbf{e}_x$ and $\mathbf{e}_{k,\parallel}$ of the k-th element, $\mathbf{e}_{k,\parallel} = (\cos\theta_k, \sin\theta_k), \mathbf{e}_{k,\perp} = (-\sin\theta_k, \cos\theta_k)$, thus ensuring inextensibility intrinsically. Due to the curvature dependence in (7.10), it is simpler to define the tangent angle in terms of the backward difference angle, $\alpha_i = \theta_i - \theta_{i-1}$, i.e. the angle between $\mathbf{e}_{i-1,\parallel}$ and $\mathbf{e}_{i,\parallel}$,

$$\theta_i = \sum_{k=1}^{i} \alpha_k, \tag{7.13}$$

by setting $\alpha_1 = \theta_1$. This reduces the filament centerline $\mathbf{x}(s,t)$ to only $N+2$ parameters $(x_0, y_0, \alpha_1, \ldots, \alpha_N)$ (see [ADGZ13]). The total force balance (7.8) and torque balance (7.9), together with $N-1$ equations for the internal moment balance (7.10), further closes the elastohydrodynamic system with $N+2$ scalar equations.

The resistive force theory approximation (7.4) allows for further analytical progress, as described in the seminal work by Gray and Hancock [GH55], by expressing the anisotropic operator in terms of tangent angle. Thus $\mathbf{F}_i$ and $\mathbf{M}_{i,\mathbf{x}_j}$ can be integrated analytically over the coarse-grained elements and expressed in terms of $(\dot{\mathbf{x}}_i, \dot{\theta}_i)$, where the overdots represent time derivatives. For simplicity, we assume linear interpolation of the shape function along the length s' of each coarse-grained element. Thus from (7.12) the velocity of the centreline can be expressed as

$$\dot{\mathbf{x}}_i(s) = \dot{\mathbf{x}}_i + (s - (i-1)\Delta s)\,\dot{\theta}_i\mathbf{e}_{i,\perp}.$$

At the fixed frame of reference, the contact forces over the i-th coarse-element reads [ADGZ15, GP17]

$$\mathbf{F}_i = \eta\Delta s\;\Lambda(\theta_i)^T \begin{pmatrix} \dot{\mathbf{x}}_i \\ \Delta s\,\dot{\theta}_i \end{pmatrix}, \tag{7.14}$$

where

$$\Lambda(\theta) = \begin{pmatrix} -\cos^2\theta - \gamma\sin^2\theta & (\gamma-1)\cos\theta\sin\theta \\ (\gamma-1)\cos\theta\sin\theta & -\gamma\cos^2\theta - \sin^2\theta \\ \frac{1}{2}\sin\theta & -\frac{1}{2}\cos\theta \end{pmatrix}.$$

Similarly, the contact moment at the i-th element relative to $\mathbf{x}_j$ takes the form

$$\mathbf{M}_{i,\mathbf{x}_j} = \eta\Delta s \begin{pmatrix} \Delta s \\ x_i - x_j \\ y_i - y_j \end{pmatrix}^T G(\theta_i) \begin{pmatrix} \dot{x}_i \\ \dot{y}_i \\ \Delta s\,\dot{\theta}_i \end{pmatrix} \mathbf{e}_z \tag{7.15}$$

with

$$G(\theta) = \begin{pmatrix} -\frac{1}{2}\cos\theta & \frac{1}{2}\sin\theta & -\frac{1}{3} \\ (1-\gamma)\cos\theta\sin\theta & -\cos^2\theta - \gamma\sin^2\theta & -\frac{1}{2}\cos\theta \\ \gamma\cos^2\theta + \sin^2\theta & (\gamma-1)\cos\theta\sin\theta & -\frac{1}{2}\sin\theta \end{pmatrix}, \tag{7.16}$$

where the above set of $3N$ variables $\mathbf{X}_{3N} = (x_1, \ldots, x_N, y_1, \ldots, y_N, \theta_1, \ldots, \theta_N)$ can be reduced to $N+2$ variables $\mathbf{X} = (x_1, y_1, \theta_1, \ldots, \alpha_N)$ via $\mathbf{X}_{3N} = \mathbf{Q}\mathbf{X}$, as described in detail in the Appendix. The coarse-grained elastohydrodynamics (7.8)-(7.15) reduces to a nondimensional system of ordinary differential equations

$$\mathrm{Sp}^4\mathbf{A}\mathbf{Q}\dot{\mathbf{X}} = \mathbf{B}, \tag{7.17}$$

where Sp is the "sperm number" as defined in (7.5), following the same recalling used for the classical system in the previous section. The general form of the matrices $\mathbf{A}$ and $\mathbf{B}$ are also defined in the Appendix.

7.4 Comparison between the classical and coarse-grained formulations

The classical elastohydrodynamic system is solved using the numerical scheme used in [GGSKB10, TS04, MJGS15], briefly described here for comparison purpose. The system (7.5)-(7.7) couples nonlinearly a fourth-order partial differential equations with a second-order boundary value problem for the unknown line tension, yielding severe constraints for the time-stepping size if all terms are treated explicitly [GGSKB10, TS04]. This is resolved by employing a second-order implicit-explicit method (IMEX) [ARW95], where only the higher-order terms are treated implicitly, and before any previous time level is available, the second-order IMEX is replaced by the first-order IMEX [ibid]. The arclength discretization is uniform with N intervals, while second-order divided differences are used to approximate spatial derivatives, in which skew operators are applied at the boundaries [GGSKB10, TS04]. The timestep thus can be chosen to be the same order of magnitude as the grid spacing, yielding a first-order constraint for timestepping. Each iteration is made in two steps: first the boundary value problem for the Lagrange multiplier τ, Eq. (7.7), is solved for a given filament configuration $\mathbf{x}$ at time t_n, from which Eq. (7.5) can be timestepped to obtain new filament configuration $\mathbf{x}$ at t_{n+1}. Theoretical and empirical validation of this scheme is provided in Refs. [GGSKB10, TS04, MJGS15].

The coarse-grained elastohydrodynamic system (7.17) does not require evaluation of Lagrange multipliers. The inextensibility is satisfied by model construction, while the asymp-

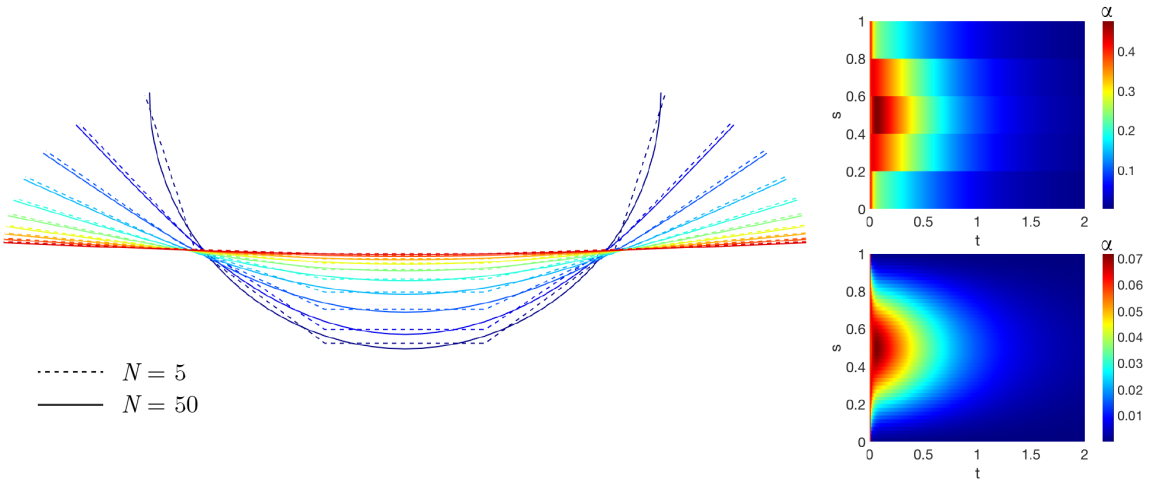

Figure 7.2 – Relaxation dynamics of a filament from a half-circle configuration with 5 elements (dotted line) and 50 elements (continuous line) and $Sp = 4$. The filaments are drawn on the left plot at $t = 0$ (dark blue) and at regular time increment of 0.2. The colormaps on the right show the spatiotemporal transient dynamics of the angle $\alpha_i = \theta_i - \theta_{i-1}$ between consecutive elements, i.e. the discrete curvature. The colormap above (below) corresponds to the coarse-grained filament with $N = 5$ ($N = 50$) elements. Note that the values of α are smaller for the finer case, as refinement induces a smoother spatiotemporal map, hence smaller angle difference between segments.

totic corse-graining allows for a straightforward semi-analytic relation between the filament kinematics and the elastohydrodynamic forces and torques. The ODE system (7.17) is straightforward to implement using any solver or numerical scheme of choice. To illustrate this, we solved (7.17) using the built-in `ode15s` MATLAB solver, which uses a variable-order, variable-step method based on the numerical differentiation formulas of orders 1 to 5 [SR97]. All computations for both the classical and coarse-grained formulation were conducted on an Intel Core i5-6500 processor 3.20 GHz, using MATLAB software.

In what follows, we study the transient dynamics of a filament decaying from an initial configuration [CG17, WROG98, WG98], set to be a half-circle and a parabola. The filament thus unbends to its straight equilibrium configuration. Fig. 7.2 contrasts the coarse-grained filament configuration and difference angle α for $N = 5$ and $N = 50$. A remarkable agreement between the dynamics of a very coarse filament (with only 5 segments) and $N = 50$ is observed. Indeed, the bulk-part elastohydrodynamics is well captured by the the coarser system. This is despite the shape inaccuracies associated with high curvatures. The shape discrepancies are continuously reduced as the the filament approaches the equilibrium state. A higher number of segments smoothes the elastohydrodynamic hyperdiffusion profile, thus acting as an effective spatial spline interpolation for each filament configuration in time (compare the angle plots in Fig. 7.2). De facto, the coarse-grained system is able to capture the filament elastohydrodynamics with excellent accuracy even for very coarse filaments when compared with the classical system. This is agreement with Fig. 7.3 which depicts the

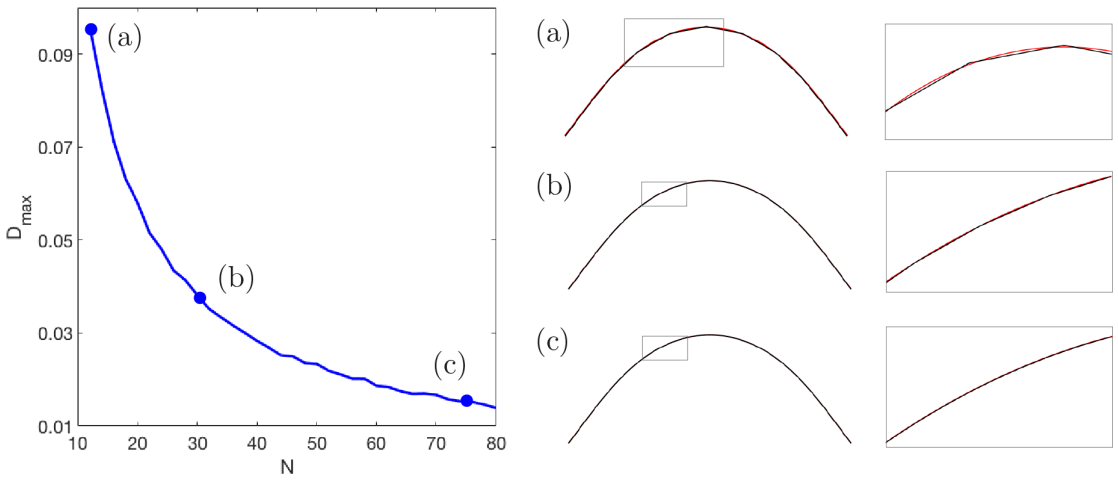

Figure 7.3 – Comparison between the classical and of the coarse-grained systems for increasing N. A fine discretisation for the classical solution is fixed for all cases. (a-c) show the aspect compare the classical (red) and the corse-grained (black) for $N = 10, 30, 75$, as indicated on the $D_{\max}$ plot. The right-hand column exposes the detailed shape of small parts of the filaments, indicated by the small gray rectangles. The good accuracy of the corse-grained solution is observed even for very small number of segments N.

discrepancy between the classical, $\mathbf{x}_{\mathrm{c}}$, and the coarse-grained, $\mathbf{x}_{\mathrm{cg}}$, solutions via

$$D_{\max} = \max_{s,t} |\mathbf{x}_{\mathrm{c}} - \mathbf{x}_{\mathrm{cg}}|,$$

so that $D_{\max} = 0$ if the agreement is exact [GGSKB10]. For $D_{\max} \approx 0.1$ or less, the agreement is observed to be very good, as illustrated by the shapes in (a)-(c) for an increasing N (Fig. 7.3). For $D_{\max} < 0.05$ the difference between the classical and coarse-grained solutions is almost undistinguishable, see for example the detailed insets in Fig. 7.3(b,c) on the right column. $D_{\max}$ decays approximately with $1/N$ in Fig 7.3, as expected from linear interpolation of curves. The dynamics is thus weakly influenced by the coarse-graining refinement level of the system. This feature may be exploited to reduce the dimensionality of the linear system while keeping a reasonable accuracy of the dynamics. By construction the asymptotic integrals along coarse-grained segments will tend to zero for infinitesimal Δs, as detailed in Eqs. (7.8) and (7.9). This introduces a higher bound for N. For $N > 80$, or equivalently for $\Delta s/L < 1\%$, the system becomes numerically stiff and requires an excessive time-stepping refinement.

We further compare the computational time of both formulations in Table 7.1. We focus on the numerically stiff regime of the classical system, occurring at low sperm number Sp, for effectively stiff filaments, and high curvatures. $N = 70$ was used for all simulations of the coarse-grained model. The classical system however requires distinct spatiotemporal discretisations according to total length error associated to each parameter regime [TS04], chosen to give the smallest computing time. Table 7.1 shows that the coarse-grained model has a maximum time duration of 3 seconds for Sp $= 2$. The computational time for the

Sp = 4			
Test	Coarse-grained system N=70	Tolerance length error	Classical system
Half-circle 	2	1% 0.1% 0.01%	1.3 249 3750
Parabola 	1.5	1% 0.1% 0.01%	90 1820 > 1h
Sp = 2			
Test	Coarse-grained system N=70	Tolerance length error	Classical system
Half-circle 	3	1% 0.1% 0.01%	97 850 > 1h
Parabola 	1.7	1% 0.1% 0.01%	> 1h > 1h > 1h

Table 7.1 – Computing times in seconds for the two relaxation tests and two different sperm numbers. Tolerance of the length error only applies to the classical system.

coarse-grained system increases as the Sp is reduced, although the accretion is marginal. On the other hand, the classical system suffers dramatically from numerical stiffness. For the lowest length-error tolerance imposed, 1%, the computational time increases by a factor of 74 for the half-circle case when Sp is reduced. The time required for the the parabola is on the order of hours. The latter is exacerbated when length-error tolerance is reduced to 0.01%. In this case, even for Sp = 4, the computational times surpasses one hour to solve the parabola initial shape. De facto, this regime is known to be numerically challenging, as one approaches the limit of validity of the resistive-force theory. Elastic forces and torques are very large compared to the viscous dissipation, characterised by a snap-through, fast unbending of the filament towards the relaxation state, thus requiring very fine time-stepping to resolve this fast transient phase. Table 7.1 demonstrates how the coarse-grained approach outperforms the classical elastohydrodynamic system.

7.5 Bio-applications

In this section we apply the coarse-grained formulation for a variety of elastohydrodynamic systems and boundary conditions found in biology, emphasising the simplicity and robustness of this approach. We focus on the filament buckling problem (Subsection 7.5.1), well known for its numerical stiffness, instability and challenges associated with boundary forces. We also study the magnetic actuation of swimming filament (Subsection 7.5.2) and the dynamics of cross-linked filament-bundles and flagella (Subsection 7.5.3), including explicit elastic coupling among coarse-grained filaments. Other interactions, via boundary forces/torques or their distribution along the filament, such as in gravitational and elec-

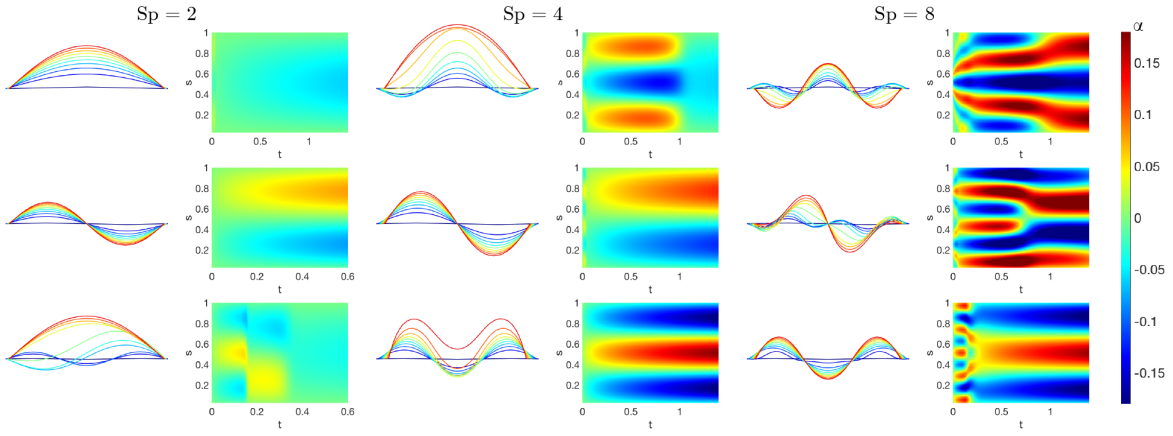

Figure 7.4 – Visualisation of the buckling phenomenon for three different sperm numbers (Sp= 2 on the left, Sp= 4 on the middle and Sp= 8 on the right). Here $N = 36$ and $k = 1.5$. The filament is displayed at regular intervals of time, coloured from blue (beginning) to red (end). Three different initial conditions lead to different outcomes. The colormap graphs show time on the x-axis and link number (discrete arclength) on the y-axis. The colours show the curvature (angles) over time, from blue for a highly negative curvature to red for a highly positive one. The filament quickly takes a waveform with fewer waves as time goes on. The higher the sperm number is, the longer it takes for the waves to vanish (note that the total time on the graphs is longer as the sperm number increases).

tromagnetic effects, as well as background flows, may be accounted effortlessly within this formulation.

7.5.1 Filament buckling instability

The coarse-grained system Eq. (7.17) is particularly suitable for non-trivial boundary constraints, such as in a fixed or moving boundary cases. In such situations, either the position (angle) or the force (torque) is imposed at the extremities. Here we consider an initially straight filament with the proximal end, $s = 0$, pinned, so that the position is fixed but free from external torques. The distal boundary, $s = 1$, moves with an imposed velocity towards the proximal end, although free from external torques. Post-transient dynamics, at the steady-state, leads to the celebrated Euler-elastica boundary value problem which admits exact solutions in terms of elliptic functions [Ant05, Gad18]. In this limit, contact forces balance exactly the the imposed load, and the shape is defined by the torque balance [Ant05, Gad18]. The transient dynamics of a filament buckling in a viscous fluid however depends to the distribution of both contact forces and torques that evolves in time. This requires the evaluation of unknown boundary forces at the proximal end, $s = 0$, while the distal end, $s = 1$, follows prescribed kinematics. We consider that the two endpoints are driven towards each other at a constant speed. This is a nontrivial task within the classical elastohydrodynamic formulation, as the usual separation between Eqs. (7.5) and (7.7) for the customary free force/torque condition is not possible. Instead, the unknown tension line at the boundary, required for the inextensibility constraint, is non-linearly coupled with the hyperdiffusive elastohydrodynamics (7.5). This difficulty is augmented by the fact that the

buckling instability is instigated by excessive compressive force distribution to a critical level in which the filament cannot uphold and buckles. This occurs via a pitchfork bifurcation with equal chances to buckle in either direction, as $\theta \to -\theta$ is also a solution [Gad18]. The initial straight configuration thus requires an infinitesimal bias to trigger the unstable modes dynamically.

The buckling phenomena is however straightforward within the coarse-grained framework. For this, we introduce unknown contact forces, respectively, for the proximal and distal ends $\mathbf{P}_0$ and $\mathbf{P}_N$, and associated moments in the coarse-grained system Eq. (7.17), which reduces to

$$\begin{aligned} \sum_{i=1}^{N} \mathbf{F}_i + \mathbf{P}_0 + \mathbf{P}_N &= 0 \\ \sum_{i=j}^{N} \mathbf{M}_{i,\mathbf{x}_j} + \mathbf{L}_{N,\mathbf{x}_j} &= \mathbf{m}_j \delta_j, \end{aligned} \tag{7.18}$$

for $j = 1, \ldots, N$ and δ_j is defined $\delta_1 = 0$ and $\delta_{j\neq 1} = 1$, where $\mathbf{L}_{N,\mathbf{x}_i}$ is the moment induced by $\mathbf{P}_N$ with respect to the point $\mathbf{x}_i$, $\mathbf{L}_{N,\mathbf{x}_i} = (\mathbf{x}_{N+1} - \mathbf{x}_i) \times \mathbf{P}_N$. The unknown forces are supplemented by the kinematic constraints $\dot{\mathbf{x}}_0 = (k/2, 0)$ and $\dot{\mathbf{x}}_N = (-k/2, 0)$, where k is positive parameter. The detailed form of the linear system may be found in the Appendix, section 7.7.3.

Fig. 7.4 depicts the shape evolution for the first three initially unstable modes at the onset of the instability and beyond, for $\mathrm{Sp} = 2, 4, 8$ from Eqs. (7.18). They capture the fast transient solutions for an effectively stiff filament, $\mathrm{Sp} = 2$ (also the numerically stiff case), which rapidly collapses into the static, steady-state Euler-elastica solutions for the first two modes, top and middle plots in Fig. 7.4 for $\mathrm{Sp} = 2$. Complex mode competition is easily accessible. This is demonstrated by the third mode dynamics (bottom row). The coarse-grained system thus unveils the cascade of unstable modes towards the stable shape, see third-mode for $\mathrm{Sp} = 8$. For $\mathrm{Sp} = 2$, these transitions occur via fast distal-proximal travelling waves, with distinct wave duration and speed, as demonstrated by the spatiotemporal-α profiles. As Sp increases, more unstable modes are instigated, giving rise to a wide diversity of nonlinear phenomena and interactions among the participating modes, in particular mode-coupling competition, see for exemple $\mathrm{Sp} = 4, 8$ in Fig. 7.4. Investigation of mode stability at advanced, nonlinear stages is also possible using this formulation, for instance, by studying the energy landscape and bifurcation diagrams. Despite the current gap in the literature, detailed nonlinear investigation of the buckling phenomenon in a viscous environment is outside the scope of the present paper and will be explored elsewhere.

7.5.2 Magnetic swimmer

Following recent resurgence of interest on magnetically driven elastic fibres for the purpose of locomotion at micro or macro-scale [ADGZ15, DBR+05, Gad13], we solve the coarse-graining of a magnetic filament under the influence of an external magnetic field. In this section, we consider a magnetic filament with a homogeneous magnetic moment μ along its arclength, directed towards the tangential direction, under the action of an uniform, time-varying sinusoidal oscillatory magnetic field $\mathbf{H}(t)$. The new terms arising from external torques are thus straightforward, as it only requires the addition of a distribution of the

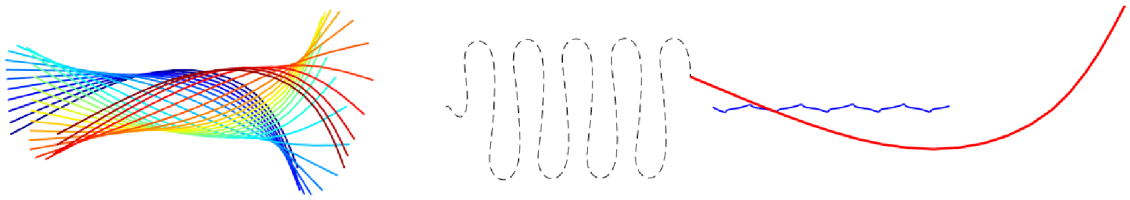

Figure 7.5 – Example of magnetic drive with a sinusoidal orthogonal magnetic field. One quarter of the length of the filament (i.e. the first five elements) is not magnetized, and the other part is constantly magnetized. Here $\mathrm{Sp} = 4$, $N = 20$, $M = 1$, $\mathbf{H}(t) = \cos(t)\mathbf{e}_y/15$. On the left, the filament is displayed at regular intervals of time over a time period, coloured from blue (beginning) to red (end). On the right, the red line shows the position of the filament at the end of the simulation. The thin dotted and thick blue lines respectively show the trajectory of the non-magnetized end and the centroid of the filament.

magnetic moments in Eq. (7.17), $\mathbf{m}_i^m = \mu_i \mathbf{e}_{i,\parallel} \times \mathbf{H}$, and reads

$$\begin{aligned} \sum_{i=1}^{N} \mathbf{F}_i &= 0 \\ \sum_{i=j}^{N} (\mathbf{M}_{i,\mathbf{x}_j} + \mathbf{m}_i^m) &= \mathbf{m}_j \delta_j, \text{ for } j = 1 \ldots N. \end{aligned} \tag{7.19}$$

Fig. 7.5 shows an example of a partially magnetised swimmer moving according to the applied sinusoidal magnetic field, with $N = 20$ and $\mathrm{Sp} = 4$, starting from a straight configuration for approximately 5 cycles. The coarse-grained system is numerically cheap, as it has a reduced number of mesh points. Thus it allows for optimisation studies involving the continuous evaluation of objective function across a large parameter space. Previous studies demonstrated that the classical system leads to very expensive numerical simulations [Gad13, MJGS15], making any parameter search very challenging. This open new possibilities for investigations within control theory, as well as optimal control [GP17, GLMP18] by using this approach.

7.5.3 Cross-linked filament bundles and flagella

In this section we focus on biological systems involving time-dependent load distributions. This could arise, for example, via mechano-sensory coupling in biological structures and biochemical landscapes. Flagella and cilia found in eukaryotes are perfect exemplars of the latter [GGS+11]. They are composed by a geometrical arrangement of semi-flexible filaments interconnected by elastic linking proteins, called axoneme [WS74]. Its generic form is composed by $9 + 2$ microtubule doublets surrounding a central pair [GGG13, LML05, PBLL09], observed in both motile and non-motile form. Flagella is a challenging mathematical system. It couples nanometric scales from the molecular motor biochemical activation with microscopic properties of the elastic structure, as observed for the purpose of spermatozoa transport [GGS+11, IGG+18]. A geometrical abstraction of this system based on the sliding filament mechanism was first proposed by Brokaw [Bro72]. In the static case, for steady-state deformations, flagella is prone to the so-called *counterbend phenomenon* [LML05, GGG13].

This occurs when distant parts of a passive flagellum (in absence of motor activity) bend in opposition to an imposed curvature elsewhere along the flagellum, for example, using the tip of a micropipete [LML05, PBLL09, XWO+16]. Theoretical models encoding the mean cross-linked filament-bundle mechanics where able to recover the counterbend phenomenon [GGG13, Gad18], from which material parameters could be measured directly from the resulting counter-curvature. The dynamics of passive flagellar bundles have been investigated using linear theory [GGG13], and prediction of counter-travelling waves instigated by the non-local cross-linking moments reported. To date, a geometrically exact investigation is still lacking in the literature.

We consider the geometrically exact cross-linked filament bundle system for a passive bundle, that is a flagellum without molecular motor actuation, using the coarse-grained formulation. The sliding filament model [Bro72, CG17] is particularly cumbersome within the classical elastohydrodynamic framework [GGSKB10]. The boundary conditions are non-local due to the accumulative dependence of sliding moments along the bundle, and generally unknown during the dynamics. This becomes even more challenging when the bundle is driven via the molecular motor activity [OGC17, CG17], which may explain the reason why numerical investigation of geometrically exact bundle systems is still lacking, for both active and passive cases [OGC17]. The coarse-grained formulation breaks the contribution of the sliding filament moments for each segment simply as

$$\mathbf{m}_j^s = \kappa^s \sum_{i=j}^{N} \Delta s(\theta_i - \theta_1), \tag{7.20}$$

this last sum being a discretisation of the sliding displacement integrated along the part of the filament going from $j\Delta s$ to L, and κ^s an effective resistance to sliding between the sliding filaments [CG17]. The balance of forces and moments then reads

$$\begin{aligned} \sum_{i=1}^{N} \mathbf{F}_i &= 0 \\ \sum_{i=j}^{N} \mathbf{M}_{i,\mathbf{x}_j} &= \mathbf{m}_j \delta_j + \mathbf{m}_j^s \,, \text{for } j = 1 \ldots \text{N}, \end{aligned} \tag{7.21}$$

and describes an effective sliding filament bundle free from forces/torques at endpoints. We consider instead that the bundle is fixed and angularly actuated at the proximal end. Thus the first three equations in Eq. (7.21) are replaced with the kinematic conditions $\dot{\mathbf{x}}_1 = 0$ and $\dot{\theta} = a\cos t$ for an angular amplitude a. Numerical solutions of the the coarse-graining system for a filament bundle angularly actuated at $s = 0$ with amplitude $a = 0.4362\,\text{rad}$ and $\kappa^s \Delta s/\kappa = 0.06$ is shown in Fig. 7.6. They confirm analytical prediction of counter-wave phenomenon from linear theory reported in ([CG17], Fig. 2), where waves are instigated non-locally, and travel in opposition to the imposed angular oscillation. The wavespeed and amplitudes involved depend on the cross-linking elastohydrodynamic parameters and the sperm number, compare Sp = 7 and Sp = 15 in Fig. 7.6. It is worth noting that coarse-graining system in Eq. (7.21) allows for straightforward generalisation to include different motor-control hypothesis - central for the current flagella and cilia self-organisation current debate [CG17, SGS+16, OGC17].

Finally, we consider the dynamics of two individual filaments embedded in a viscous fluid

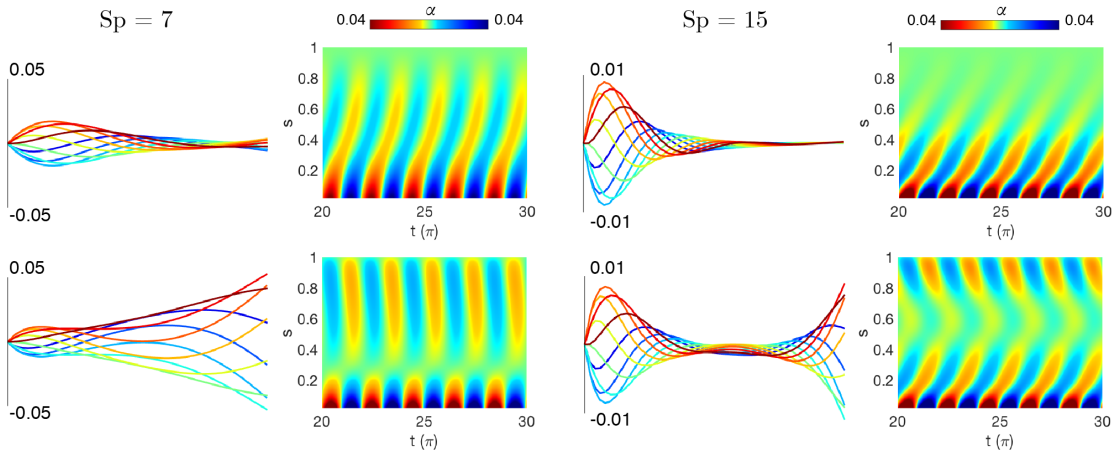

Figure 7.6 – Simulation of the counterbend phenomenon for two different sperm numbers (parameters are chosen in order to match those used in [CG17]: $\kappa^s \Delta s/\kappa = 0.06$, $a = 0.4362\,\text{rad}$; and $N = 50$). The top row shows the behaviour of an actuated filament when no sliding resistance is added. The right column shows the same oscillation applied to the bundle model. For each case, the filament is displayed at regular intervals of time over a time period, coloured from blue (beginning) to red (end). The color plots show the curvature (angles α) with respect to the time in x and the arclength in y. The travelling curvature wave generated by the actuation is visible at the bottom of all of the color plots. For the counterbend case, a second travelling wave appears at the free end of the filament in the bundle case (bottom row).

and coupled elastically via Hookean elastic springs, see Fig. 7.7. The system thus involves the geometrically non-linear elastohydrodynamics of two interacting elastic fibres. Once again, the classical elastohydrodynamic formulation is ill-posed. The discrete distribution of elastic springs introduces unknown point forces via Eqs. (7.5) and (7.7) for each filament. We consider that the two-filament assembly is angularly actuated at one end, see Fig. 7.7. We assume that the connecting elastic springs have an effective spring constant K connecting opposite nodes between the two filaments, placed at each coarse-grained segment junction for simplicity, see Fig. 7.7. The equilibrium bundle diameter is d_0 at rest. The elastic force $\mathbf{F}_i^{\text{int}}$ exerted by the i-th spring on the filament S (top filament) reads

$$\mathbf{F}_i^{\text{int}} = K \left(1 - \frac{d_0}{\|\mathbf{x}_i - \mathbf{x}_i'\|}\right) (\mathbf{x}_i - \mathbf{x}_i'),$$

where primes refer to the second filament. The coarse-grained formulation for S and S' is thus augmented by the elastic reactions from each connecting spring, and their associated moments along each filament. Hence the coupled system for the filaments S and S' reads,

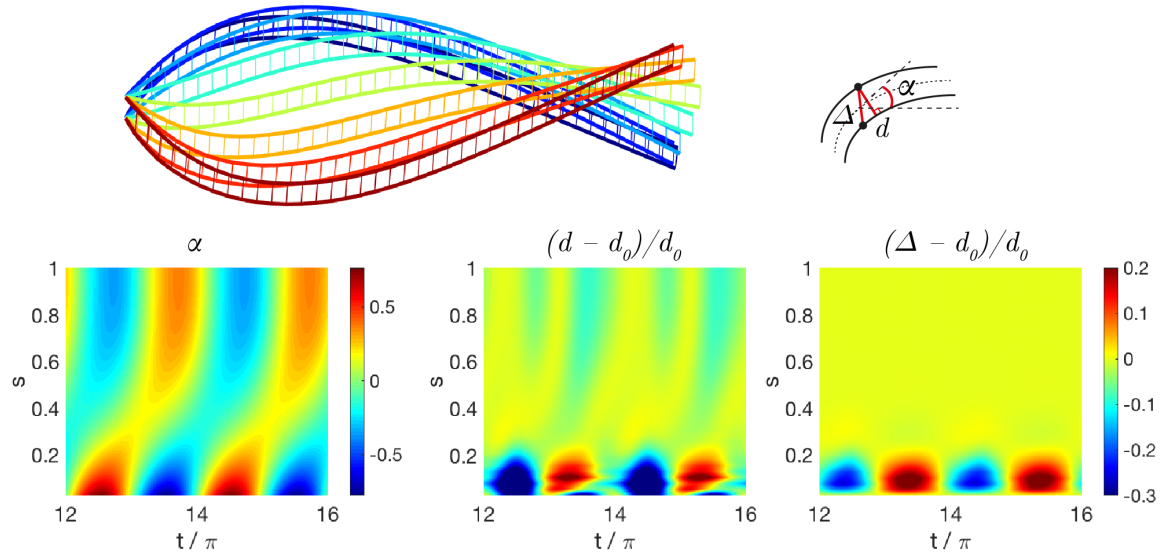

Figure 7.7 – Coupling between two filaments obtained with the coarse-grained approach. Here Sp = 4, $a = 0.88\,\text{rad}$, $K/\kappa = 1/25$. On the top, the actuated filament is represented at regular intervals of time over half a time period, coloured from blue (beginning) to red (end). The three colormaps display three parameters with respect to time and arclength: the angle α of the centerline (left), the distance d between the two filaments (middle) and the distance Δ between two facing nodes, normalised by their resting length d_0. Note that the beginning time for the graphs has been chosen big enough to skip transient phase and display only steady state. A travelling wave of curvature generated by the actuation of the top filament is visible in graph at the bottom left. The graph at the bottom in the middle shows the distance between the two filaments. Moreover, the graph at the bottom right captures the sliding distance between the two filaments.

respectively,

$$\begin{aligned}
\sum_{i=1}^{N}(\mathbf{F}_i + \mathbf{F}_i^{\text{int}}) &= 0 \\
\sum_{i=j}^{N}(\mathbf{M}_{i,\mathbf{x}_j} + \mathbf{F}_i^{\text{int}} \times (\mathbf{x}_j - \mathbf{x}_i)) &= \mathbf{m}_j\delta_j, \\
\sum_{i=1}^{N}(\mathbf{F}'_i - \mathbf{F}_i^{\text{int}}) &= 0 \\
\sum_{i=j}^{N}(\mathbf{M}'_{i,\mathbf{x}_j} - \mathbf{F}_i^{\text{int}} \times (\mathbf{x}'_j - \mathbf{x}'_i)) &= \mathbf{m}'_j\delta_j.
\end{aligned} \tag{7.22}$$

The proximal end of both constituent filaments is fixed, but the angle at $s = 0$ of the filament S (top filament) is actuated via $\theta_1(t) = a \sin t$. The filament S' (bottom filament) is free from external actuation, thus its movement solely arises via the elastic coupling between them. A detailed description of the resulting two-filament system is provided in the appendix, section 7.7.5.

Fig. 7.7 shows numerical simulations for time evolution of the two-filament assembly, demonstrating the effectiveness of the connecting springs while transmitting bending moment from the top filament to the bottom one. A synchronous traveling wave of curvature is observed, see for exemple the tangent angle α of the centreline of the filament-pair in Fig. 7.7. The axial diameter d however evolves asymmetrically (middle plot in Fig. 7.7). The angular actuation of the top filament modify the diametral distance between the filaments near the base, in an oscillatory motion, from where axial waves are propagated down the structure. Axial extensional waves (light yellow regions) propagate more easily than compressional waves in the axial direction (light green regions). The resulting sliding displacement Δ between the filament-pair is also depicted in the right graph in Fig. 7.7. Similarly to the radial distance, the relative sliding motion is concentrated towards the basal end, however, it is not propagated along the filament-pair. This is despite the fact that both filament are inextensible, and tangential motion is easily propagated. Conversion of curvature into relative sliding motion between the filaments is not observed nor the counterbend phenomenon observed in Fig. 7.6, see the light yellow region for $\Delta \approx 0$ in Fig. 7.7. This suggests that simple elastic connectors between filaments are not effective while transmitting sliding moments. Instead, axial distortions are prevailed and propagated along the filament-pair assembly. The connecting springs contribute to forces along its direction, but mostly on the radial direction, perpendicular to centreline. The elastic springs are hinged at each connecting node, thus the constituent filaments are free from bending moments arising from the interfilament sliding (in contrast with Fig. 7.6). This supports the so-called geometric clutch mechanism proposed by Lindemann [Lin94], where axial displacements are central for flagellar mechanics. These results further show that the sliding filament mechanism present in flagellar systems [Bro72, GGG13, LML05] is far more complex than this simplistic two-filament cross-linked assembly [CJP99, SGS+16, OGBMC14, CG17, Bro72].

7.6 Conclusions

This paper studies inertialess fluid-structure interaction of inextensible filaments commonly found in biological systems. The nonlinear coupling between the geometry of deforma-

tion and the physical effects invariably results on intricate governing equations that negotiate elastohydrodynamical interactions with non-holonomic constraints, as a direct consequence of the filament inextensibility. As a result, the classical elastohydrodynamical formulation is prone to numerical instabilities, requires penalization methods and high-order spatiotemporal propagators. Here, we exploit the momentum balance in the asymptotic limit of small rod-like elements, from which the system can be integrated semi-analytically. This bypasses the bottleneck associated with the inextensibilty constraint, and does not require the use of Lagrange multipliers to solve the system. We further show the equivalence between the two formalisms, as well as a direct comparison between the their numerical performances. The coarse graining formalism was shown to outperform the classical approach, in particular for numerically stiff regimes where the classical system performs poorly. The coarse-graining structure also allowed faster computations, over than a hundred times faster than previous implementations. The coarse-graining approach is simple and intuitive to implement, and generalisations for complex interaction of multiple rods, active filaments, flagella, Brownian polymer dynamics and non-local hydrodynamics are straightforward.

We employed the coarse-grained formulation to study distinct biologically inspired systems: the buckling instability of bio-filaments, the magnetic actuation of a microswimmer and the dynamics of cross-linked filament bundles and flagella. With the exception of the magnetic swimmer case, the results obtained here for the other systems are new in the literature. For the buckling problem, travelling waves are generated and propagated with different speeds, depending on the elastohydrodynamic properties of the filament and its interaction with other competing modes, Fig. 7.4; thus relevant to biological systems in which buckling is a naturally occurring phenomenon [BDE+95]. The coarse-graining approach successfully captured the counterbend phenomenon in cross-linked filament-bundles [CG17, GGG13], Fig. 7.6, including geometrical nonlinearities. Finally, motivated by mathematical abstractions of flagellar systems [CJP99, SGS+16], we solved the dynamics of interactions between two individual filaments interconnected with elastic springs. Numerical simulations indicated that the sliding between the filaments is not instigated by changes in curvature, as assumed by the sliding-filament mechanism [Bro72]. Instead, axial distortions are propagated along the two-filament assembly, in agreement with the geometric clutch hypothesis [Lin94]. These modes of deformation are central for the molecular-motor control debate in flagellar systems [SGS+16, CG17].

The results presented here offer new possibilities for theoretical investigations, for instance, on the elastohydrodynamic self-organisation of fibres, many interacting filaments, cytoskeleton modelling, manoeuvrability of micro-magnetic robots [GP17, GLMP18], as well as optimal strategy of deformation for micro-locomotion [WGD+18]. Only basic knowledge of systems of linear equations is required and implementation achieved with any solver of choice. We hope that the simplicity of the formalism, the numerical robustness and easy-to-implement generalisations will appeal to the biology, soft-matter and interdisciplinary community at large.

7.7 Appendix

7.7.1 Parametrization in the coarse-graining model

In the asymptotic description, the filament can be described with two different sets of parameters (see Fig. 7.1) :

— the $N+2$ parameters $\mathbf{X} = (x_1, y_1, \theta_1, \alpha_2, \dots, \alpha_N)$.

— the $3N$ parameters $\mathbf{X}_{3N} = (x_1, \dots, x_N, y_1, \dots, y_N, \theta_1, \dots, \theta_N)$,

The second set uses $3N$ parameters where $N+2$ are sufficient. However, it makes the computations easier to read. Going from $\dot{\mathbf{X}}$ to $\dot{\mathbf{X}}_{3N}$ can be done via the following transformation matrices :

$$\dot{\mathbf{X}} = \tilde{\mathbf{P}}\dot{\mathbf{X}}_{3N} \quad \text{and} \quad \dot{\mathbf{X}}_{3N} = \tilde{\mathbf{Q}}\dot{\mathbf{X}}$$

with

$$\tilde{\mathbf{P}} = \left(\begin{array}{cccc|cccc|ccccc} 1 & 0 & \dots & 0 & 0 & & \dots & 0 & & & 0_{2,N} & & \\ 0 & & \dots & 0 & 1 & 0 & \dots & 0 & & & & & \\ \hline & & & & & & & & 1 & 0 & \dots & \dots & 0 \\ & & & & & & & & -1 & 1 & 0 & \dots & 0 \\ & & 0_N & & & & 0_N & & 0 & -1 & 1 & \ddots & \vdots \\ & & & & & & & & \vdots & \ddots & \ddots & \ddots & \vdots \\ & & & & & & & & 0 & \dots & 0 & -1 & 1 \end{array}\right)$$

and

$$\tilde{\mathbf{Q}} = \left(\begin{array}{cc|cccc} 1 & 0 & & & & \\ \vdots & \vdots & & \tilde{Q}_1 & & \\ 1 & 0 & & & & \\ \hline 0 & 1 & & & & \\ \vdots & \vdots & & \tilde{Q}_2 & & \\ 0 & 1 & & & & \\ \hline & & 1 & 0 & \dots & 0 \\ & & 1 & 1 & \ddots & \vdots \\ & 0_{N,2} & \vdots & & \ddots & 0 \\ & & 1 & \dots & & 1 \end{array}\right), \tag{7.23}$$

where $\tilde{Q}_1$ and $\tilde{Q}_2$ are $N \times N$ matrices whose elements are given by the general formula

$$\begin{aligned} q_1^{i,j} &= -\Delta s \sum_{k=j}^{i-1} \sin\left(\sum_{m=1}^{k} \alpha_m\right) \\ q_2^{i,j} &= \Delta s \sum_{k=j}^{i-1} \cos\left(\sum_{m=1}^{k} \alpha_m\right), \end{aligned}$$

with $q_1^{i,j} = q_2^{i,j} = 0$ if $i \geq j$. The tildes recall that the nondimensionalisation has not yet been performed.

7.7.2 Matricial form of the ODE system

Using the explicit expressions of the different contributions (7.11), (7.14) and (7.15), and after nondimensionalising, we can rewrite the system (7.8)-(7.10) under matricial form:

$$\mathrm{Sp}^4 \mathbf{A}\mathbf{Q}\dot{\mathbf{X}} = \mathbf{B}. \tag{7.24}$$

where the terms are defined as follows:

— The matrix $\mathbf{A}$ is a $(N+2)\times 3N$ matrix whose coefficients are given, for all i in $\{1, \dots N\}$

and j in $\{i, \dots, N\}$, by

$$
\begin{aligned}
&a_{1,i} = -\cos^2\theta_i - \gamma \sin^2\theta_i;\\
&a_{2,i} = (\gamma - 1)\cos\theta_i \sin\theta_i;\\
&a_{1,N+i} = (\gamma - 1)\cos\theta_i \sin\theta_i;\\
&a_{2,N+i} = -\gamma\cos^2\theta_i - \sin^2\theta_i;\\
&a_{1,2N+i} = \tfrac{1}{2}\sin\theta_i;\\
&a_{2,2N+i} = -\tfrac{1}{2}\cos\theta_i;\\
&a_{i+2,j} = v(\mathbf{x}_i, \mathbf{x}_j)\, M_1(\theta_j);\\
&a_{i+2,N+j} = v(\mathbf{x}_i, \mathbf{x}_j)\, M_2(\theta_j);\\
&a_{i+2,2N+j} = v(\mathbf{x}_i, \mathbf{x}_j)\, M_3(\theta_j);
\end{aligned}
$$

where

$$
v(\mathbf{x}_i, \mathbf{x}_j) = \begin{pmatrix} 1 & \frac{x_j - x_i}{\Delta s} & \frac{y_j - y_i}{\Delta s} \end{pmatrix}
$$

and M_1, M_2, M_3 are the columns of the matrix (7.16). If $j < i$, then $a_{i+2,j} = a_{i+2,N+j} = a_{i+2,2N+j} = 0$.

— $\mathbf{Q}$ is the nondimensionalized version of the transformation matrix (7.23). It is defined by replacing $\tilde{Q}_1$ and $\tilde{Q}_2$ with $Q_1 = \tilde{Q}_1/\Delta s$ and $Q_2 = \tilde{Q}_2/\Delta s$ in the expression of $\tilde{\mathbf{Q}}$.

— $\mathbf{B}$ is a column vector of size $N + 2$, given by

$$
\mathbf{B} = \begin{pmatrix} 0 & 0 & 0 & \alpha_2 & \dots & \alpha_N \end{pmatrix}^T.
$$

7.7.3 Buckling instability system

The resolution of the buckling problem requires to introduce two unknown contact forces $\mathbf{P_0}$ and $\mathbf{P}_N$ (see section 7.5.1). It yields four more scalar unknowns: P_{0x}, P_{0y}, P_{Nx}, P_{Ny}. We add four equations to the system (7.17) by embedding the buckling kinematic constraints $\dot{\mathbf{x}}_0 = (k/2, 0)$ and $\dot{\mathbf{x}}_N = (-k/2, 0)$, where k is positive. We get a new system of $(N + 6)$ scalar equations that can be expressed in matricial form:

$$
\mathbf{A}_b \dot{\mathbf{X}}_b = \mathbf{B}_b, \tag{7.25}
$$

where

$$
\mathbf{X}_b = \left(\begin{array}{c} \mathbf{X} \\ \hline P_{0x} \\ P_{0y} \\ P_{Nx} \\ P_{Ny} \end{array}\right), \quad \mathbf{B}_b = \left(\begin{array}{c} \mathbf{B} \\ \hline -k/2 \\ 0 \\ k/2 \\ 0 \end{array}\right), \quad \mathbf{A}_b = \left(\begin{array}{c|c} \mathrm{Sp}^4\mathbf{AQ} & \mathbf{a}^T \\ \hline \mathbf{a} & \mathbf{0} \end{array}\right), \tag{7.26}
$$

$$
\mathbf{a} = \begin{pmatrix} 1 & 0 & 0 & \dots & \dots & 0 \\ 0 & 1 & 0 & \dots & \dots & 0 \\ 1 & 0 & -\sum_{k=1}^{N} \sin\theta_k & -\sum_{k=2}^{N} \sin\theta_k & \dots & -\sin\theta_N \\ 0 & 1 & \sum_{k=1}^{N} \cos\theta_k & \sum_{k=2}^{N} \cos\theta_k & \dots & cos\theta_N \end{pmatrix}, \tag{7.27}
$$

and matrices $\mathbf{A}$, $\mathbf{B}$ and $\mathbf{Q}$ are defined as in Appendix 7.7.2.

7.7.4 Magnetic swimmer

The matricial system describing a magnetically driven filament with the coarse-graining approach reads

$$\mathrm{Sp}^4\mathbf{A}\mathbf{Q}\dot{\mathbf{X}} = \mathbf{B} + \frac{1}{\kappa}\mathbf{C}^m. \tag{7.28}$$

It is simply obtained by adding to the system (7.17), the magnetic effect vector $\mathbf{C}^m = \begin{pmatrix} c_1 & \dots & c_{N+2} \end{pmatrix}^T$, with $c_1^m = c_2^m = 0$ and $\forall i \in \{1, \dots, N\}$,

$$c_{i+2}^m = \sum_{k=i}^{N} \mu_k (H_y(t)\cos\theta_k - H_x(t)\theta_k),$$

$H_x(t)$ and $H_y(t)$ being the components of the magnetic field along the x- and y-axis.

7.7.5 Cross-linked filament bundle

The system (7.22) describing a filament bundle with sliding resistance takes the following matricial form:

$$\mathrm{Sp}^4\mathbf{A}\mathbf{Q}\dot{\mathbf{X}} = \mathbf{B} + \frac{\kappa^s}{\kappa}\mathbf{C}^s, \tag{7.29}$$

with $\mathbf{C}^s = \begin{pmatrix} c_1 & \dots & c_{N+2} \end{pmatrix}^T$, with $c_1^s = c_2^s = 0$ and $\forall j \in \{1, \dots, N\}$,

$$c_{j+2}^s = \Delta s \sum_{i=j}^{N} \theta_i - \theta_1.$$

In the case of two interacting filaments, S and S', the new coupled dimensionless system of $(2N+4)$ equations reads

$$\mathrm{Sp}^4 \left(\begin{array}{c|c} (\mathbf{AQ})_S & 0 \\ \hline 0 & (\mathbf{AQ})_{S'} \end{array} \right) \begin{pmatrix} \mathbf{X}_S \\ \mathbf{X}_{S'} \end{pmatrix} = \begin{pmatrix} \mathbf{B}_S \\ \mathbf{B}_{S'} \end{pmatrix} + \begin{pmatrix} \mathbf{C} \\ \mathbf{C}' \end{pmatrix}. \tag{7.30}$$

In the above equation, $\mathbf{A}$, $\mathbf{B}$, $\mathbf{Q}$ and $\mathbf{X}$ are defined as previously, referring to S or S' depending on the index. The interaction vectors $\mathbf{C}$ and $\mathbf{C}'$ are defined as follows:

$$\begin{aligned} \begin{pmatrix} c_1 \\ c_2 \end{pmatrix} &= \tfrac{1}{\kappa}\textstyle\sum_{j=1}^{N} \mathbf{F}_j^{\mathrm{int}}; \\ \begin{pmatrix} c_1' \\ c_2' \end{pmatrix} &= -\tfrac{1}{\kappa}\textstyle\sum_{j=1}^{N} \mathbf{F}_j^{\mathrm{int}}; \\ \forall i \in \{1, \dots N\}, \quad c_{i+2} &= \tfrac{1}{\kappa}\textstyle\sum_{j=i}^{N} \mathbf{F}_j^{\mathrm{int}} \times (\mathbf{x}_j - \mathbf{x}_i), \\ c_{i+2}' &= -\tfrac{1}{\kappa}\textstyle\sum_{j=i}^{N} \mathbf{F}_j^{\mathrm{int}} \times (\mathbf{x}_j' - \mathbf{x}_i'). \end{aligned} \tag{7.31}$$

The above system describes a bundle with free endpoints. However, in the case studied in section 7.30, both filaments have a fixed proximal end, and the filament S is actuated at its proximal end (prescribed angle θ_1). We embed these boundary conditions in the system by replacing its first three lines by the constraint equations $\dot{x}_1 = 0$, $\dot{y}_1 = 0$, $\dot{\theta}_1 = a\cos t$, and its $N+3$-th and $N+4$-th equations (i.e., the first two equations for the second filament) by

the constraint equations $\dot{x}_1' = 0$ and $\dot{y}_1' = 0$.

Chapter 8

The hydrodynamic Euler-elastica

This chapter features an article in preparation, written in collaboration with Laetitia Giraldi and Hermes Gadêlha.

8.1 Introduction

The shape of an elastic filament submitted to external forces is, at steady-state, governed by the well-known Euler-elastica boundary value problem which admits exact solutions in terms of elliptic functions [Eul44]. In this limit, contact forces balance exactly the the imposed load, and the shape is defined by the torque balance [FTC17, LL86, TG09, Ant05].

Semi-flexible filaments are found everywhere in nature and often subject to high compressive forces or shear flows [TS04, LCS+18, BS01, HMMJG+19], that makes them buckle : DNA strands [FMC13, MN12], polymer chains [DPF85, GMP00], complex cytoskeletal microtubules [SCdP+06] and actin filaments, cilia and flagella [VS12, GGSKB10] used by micro-organisms such as sperm cells [GG19] and bacteria to propel in fluids. The Euler-elastica has been used as basis to study numerous problems associated to elasticity of filaments and buckling [LMQC12, BT09], such as the effect of counterbend forces for a filament bundle in [Gad18], or a model of morphoelastic filament in [GG06].

The transient dynamics of a filament buckling in a viscous fluid however depends to the distribution of both contact forces and torques that evolves in time, and the Euler elastica model thus does not take them into account. The time competition and interaction between the decay of high Fourier modes, the hydrodynamic drag and the displacement of the endpoints towards each other leads to specific phenomena that need ad hoc modelisation.

In this paper, we investigate the effect on hydrodynamics on the force-induced buckling problem. We display a range of thorough numerical observations that we believe are novel and of great interest for the understanding of the buckling phenomenon in a dynamical setting.

We study the importance of clamping one endpoint in the dynamical framework, and draw a comparison with the Euler elastica solutions. We then focus on the symmetric pinned case, and observe the decay of high Fourier modes of the curvature at short timescale. We model the decay of these unstable modes with an exponential law.

While the dynamic evolution for a buckling filament has been largely studied at a short timescale [WROG98, CDK17, LJT+16, GHBV05], one of the original aspects of our work lies in the fact that the simulation is carried out long enough for the endpoints of the filament to

get very close and eventually cross each other, as in the static Euler elastica (see [Gad18]). This feature, coupled with the dynamical aspect, allows to numerically observe the emergence of three different final shapes, in a timescale that we can interpret as a post-transient phase where all the high unstable Fourier modes have decayed. The three observed final shapes dominate at different buckling speed regimes, and coexist for some critical values of the parameters. In the regions where several shapes coexist, one can observe bifurcations that suggest a very chaotic behaviour, surprising even for this constrained and unstable problem.

An efficient numerical framework is crucial in order to cover the complexity and versatility of the buckling problem. In this paper, we adapt the coarse-grained model introduced in [MGG18], adding equations to the system to determine the unknown contact forces at the filament endpoints. Our description encompasses a large array of boundary conditions, from hinged to clamped ends and allows to prescribe either the velocity of the filament endpoints or the force applied to it. We hope that this detailed framework, along with the available Matlab code, can be of practical use for other buckling studies, in completion of our previous work [MGG18].

8.2 Brief description of the model

8.2.1 Numerical elastohydrodynamic coarse-grained framework

Consider a planar elastic filament with length L, bending stiffness E_b, and hydrodynamic drag parameters $\eta_{\parallel}$ and $\eta_{\perp}$, surrounded by a fluid of low Reynolds number. We use the coarse-graining formulation introduced in [MGG18], which approximates the filament with N rod-like elements of length $\Delta s = L/N$. This allows to geometrically describe it with $(N+2)$ state parameters: the position of the proximal end (x_1, y_1), its orientation θ with respect to the reference axis, and the angles between consecutive elements, namely $\alpha_2 \dots \alpha_N$.

The filament is submitted to hydrodynamic friction, which is modelled using the Resistive Force Theory, in which the force density is related to point velocity *via* an anisotropic operator, see [GH55] for more details. It also experiences internal elastic moments at the elements junctions, given by $\mathbf{m}_i = \frac{E_b}{\Delta s}\alpha_i \mathbf{e}_z$.

8.2.2 Boundary conditions

The situation we focus on is when the filament is aligned on a straight line and both ends of the filament are pushed towards each other at given speeds. This gives us the following kinematic constraints on the endpoints (x_1, y_1) and (x_{N+1}, y_{N+1}):

$$\begin{array}{ll} \dot{y}_1(t) = 0, & \dot{y}_{N+1}(t) = 0, \\ \dot{x}_1(t) = (1-a)V_p, & \dot{x}_N(t) = -(1+a)V_p, \end{array} \tag{8.1}$$

where V_p is the "buckling speed" and $a \in [0,1]$ is the asymmetry parameter. The case $a = 0$ represents the symmetric situation: both ends move towards each other at the same speed. On the contrary, when $a = 1$, the proximal end is pinned and only the distal end is moving. Let us highlight the fact that the symmetric and asymmetric situations are indistinguishable in the static case. On the contrary, in the dynamic case, pushing the endpoints at different speeds induces an asymmetric hydrodynamic drag that influences the way the filament shape evolves. We discuss the importance of this asymmetry parameter later on.

The initial condition is given by $(x_1(0), y_1(0)) = (0, 0)$ and a small random parameter for each angle, chosen according to a Gaussian distribution with mean 0 and variance 10^{-5}. This numerically models the infinitesimal bias that triggers buckling.

In order to study the influence on clamping extremity on the filament, we add an elastic moment $\mathbf{m}_c$ at its proximal end, proportional to the orientation θ of the first element:

$$\mathbf{m}_c = C\theta \mathbf{e}_z.$$

When the clamping parameter C is very large, the filament proximal extremity stays tangent to the horizontal axis at all times.

Unknown contact forces $\mathbf{F}_0$ and $\mathbf{F}_N$ are required at both endpoints to ensure that the prescribed boundary conditions (8.1) are respected. These unknown forces are embedded in the equations system following [MGG18] and computed along with the time evolution of the filament. Writing the balance of forces and torques over N subsystems, as detailed in [MGG18], and adding the four buckling constraints 8.1 allows to obtain a system of $N + 6$ scalar ordinary differential equations (ODEs). Solving this system gives access to the shape of the filament at all times as well as the unknown contact forces $\mathbf{F}_0$ and $\mathbf{F}_N$.

Finally, we rescale the equations with respect to length scale L and time scale $\eta_\parallel L^4/E_b$ – that takes into account the flexibility of the filament against the viscosity of the surrounding fluid. The dimensionless buckling number then reads

$$\mathrm{Bu} = \frac{\eta_\parallel L^3 V_p}{E_b}.$$

The buckling number Bu characterises the strength of the dynamical effects. Very small values of Bu approximately describe the Euler elastica case, while high buckling number will give rise to new behaviours as characteristic relaxation time becomes large against buckling time.

8.2.3 Discussion on parameter values

The value of the buckling number Bu varies on a wide range. Indeed, very different behaviours will be observed between floppy filaments such as flagella or long polymer chains and rigid filaments such as short microtubules. The typical length of biological filaments lie between 1-2 (for short microtubules [KHT95]) and 200-250 μm (for rodent sperm cells [CW85, GGS+11, RKHHJ07]). The hydrodynamic drag coefficient $\eta_\parallel$ varies between 10^{-2} for low viscous media and 1 Pa.s for high viscous media [OGC17, IGG+18]. The buckling stiffness E_b ranges from 1.10^{-23} (for microtubule protein [KHT95, SMSM04]) to 2.10^{-21} N.m^{-2} (for bull sperm [OGC17]). Assuming the pushing speed V_p can reasonably go from 1 to 100% of the filament length per second, the dimensionless buckling number Bu theoretically ranges from 10^{-2} to 10^5. Two sets of parameters are gathered in Table 8.1, giving examples of existing cases that match this numerical range.

The rest of the paper is dedicated to the results obtained through the numerical simulations. The equations are integrated using MATLAB. Unless otherwise stated, in all the simulations, $N = 30$ and the final time is chosen equal to 0.9/Bu (which means that the cumulated distance traveled by both ends of the filament at the end of the simulation equals $1.8\,L$).

Parameter	Human sperm [GGS+11] high viscosity	Short microtubule [KHT95] low viscosity
L (μm)	55	6
$\eta_{\parallel}$ (Pa.s)	0.14	5×10^{-3}
E_b (N.m^2)	1.2×10^{-21}	1×10^{-23}
V_p (μm.s^{-1})	5	2
Bu	126	0.21

Table 8.1 – Typical values of the parameters

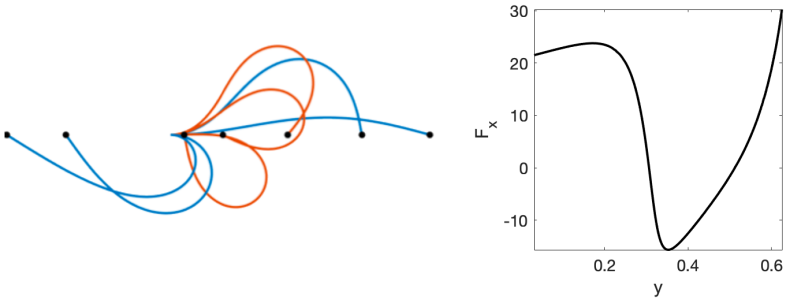

Figure 8.1 – Solution of static Euler-elastica in the clamped case, with evolution of the tangential force F_x with respect to displacement. [Gad18]

8.3 Role of clamped extremity

8.3.1 Tangential force profile

We briefly recapitulate the Euler-elastica solution for an inextensible and unshearable, slender elastic body, referred as elastica, that resists bending deformations via Euler–Bernoulli moments. Bending deformation causes the region under tension to exert a bending moment on the region under compression, along the cross section of an elastica, which is linearly related with curvature [Eul44], $M = E\theta s$, for a given elastic bending stiffness E. When the elastica is under the action of external, and opposing, forces at the end points, with magnitude Q, the bending moment density is simply balanced by external load,

$$E\theta ss + Q \sin\theta = 0.$$

This describes geometrically exact deformations of an Euler elastica, given specific conditions at the end points. [FTC17, LL86, TG09, Ant05] The solution for a clamped-extremity filament can thus be computed and is displayed on Figure 8.1 (taken from [Gad18]).

However, this solution is only valid in the static case. If the buckling occurs dynamically, i.e. the endpoints are pushed towards each other from the straight position, the filament adopts a strongly different behaviour. This is visible on Figure 8.2, where the variation in the force F_x (the tangential component of $\mathbf{F}_0$) along time at the proximal end is displayed for different values of Bu and clamping parameters C.

On this figure, on can observe that the filament usually "flips" shortly after the endpoints

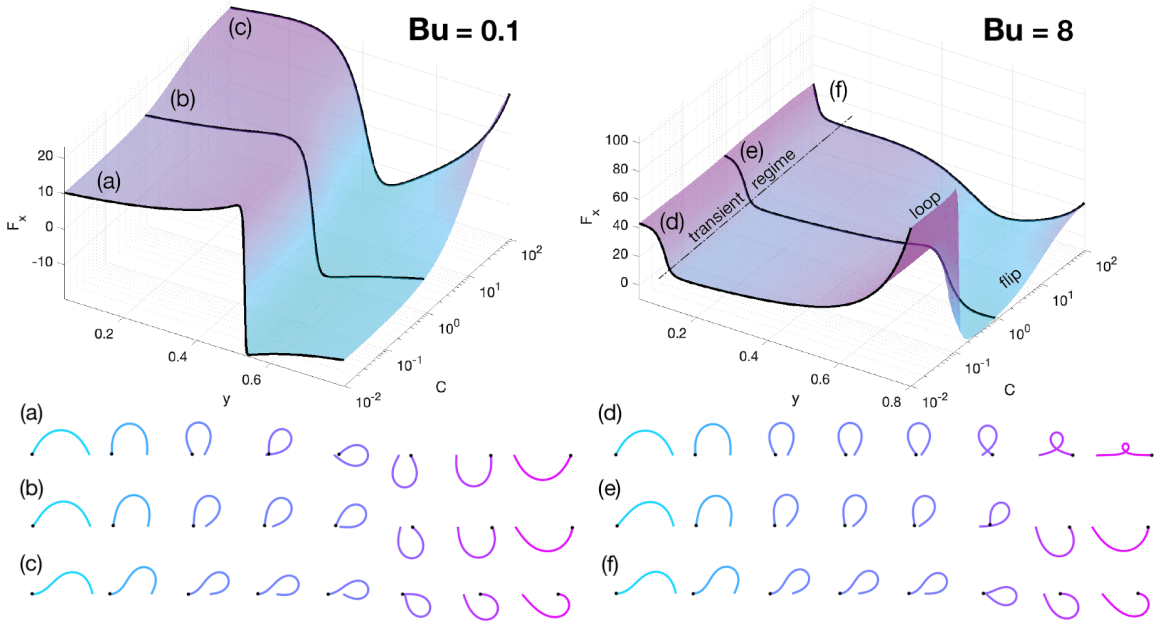

Figure 8.2 – Influence of the clamping of one end of the filament, for two different values of Bu. The surface plots display the algebraic intensity of the tangential force F_x applied to perform the required displacement at the non-clamped extremity, represented with respect to the displacement y and the clamping intensity C (on log scale). Three force plots on each graph have been highlighted with a thick black stroke. They allow to see the evolution of F_x for fixed values of clamping: $C = 10^{-2}$ ((a) and (d)), $C = 1$ ((b) and (e)) and $C = 100$ ((c) and (f)). The evolution of the filament shape (snapshots at selected instants, light blue for initial time to pink for final time) for force plots (a) to (f) is represented at the bottom of the figure. The point where F_x is calculated is symbolized by a black dot on each filament representation.

cross each other. When the filament flips, F_x changes sign on the surface plot. The less clamped is the left extremity, the quicklier the flip occurs. Note that the force curve (c) has the same aspect as the one from the static case seen in Figure 8.1, which matches what we could expect since a low Bu number represents quasistatic case. On the right surface plot, the buckling number Bu is higher, so a new behaviour appears in the pinned case: the filament does not flip anymore and a persistent loops appears. As clamping increases, asymmetry is induced, bringing back the filament flip. We investigate later on the role of symmetry in the filament buckling behaviour.

One can also observe a short peak in F_x at the beginning (on the top of the dashed line on the surface plot), corresponding to the transient regime where the unstable modes have not vanished yet (they are not visible on the bottom plots for they vanish quickly.) This transient phase will be studied further later on in Section 8.5.

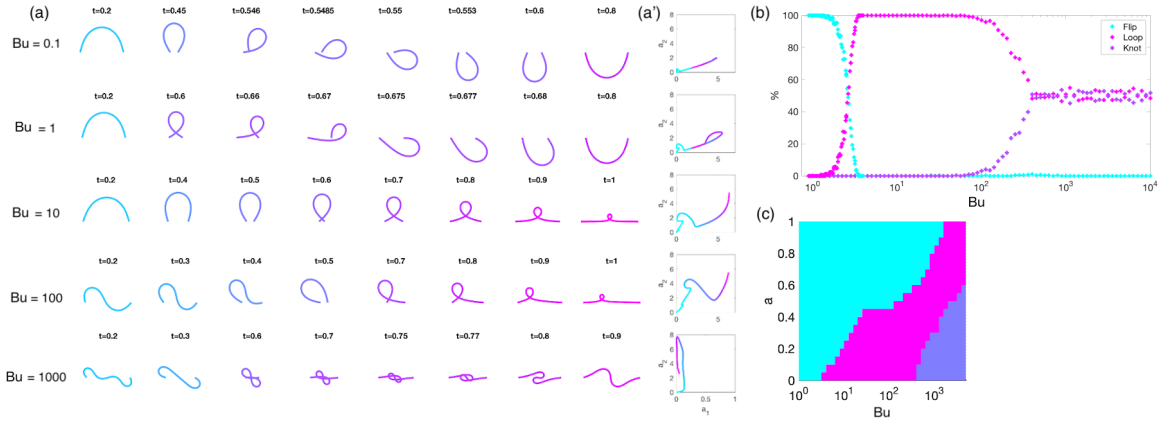

Figure 8.3 – The shape of the filament is plotted at different times and for different values of Bu on plots (a). One can see the flipping that occurs at low speed, the appearance of a loop at the end for medium-range Bu and the knot shape appearing at high Bu. Column (a') displays each of the five trajectories in (a) in the "Fourier plane". The amplitude of the first and second spatial Fourier mode of the filament curvature are plotted respectively on the x and y axis on each graph. The colored line indicates the time evolution: light blue at initial time to pink at the end of the simulation. On graphs (b) and (c) are displayed the predominance of each shape depending on buckling number Bu and asymmetry parameter a. For every value of Bu and a, 500 simulations were ran and the shape at final time was classified in one of the three categories through Fourier analysis: flip shape, loop shape and knot shape. Graph (b) shows the frequency of appearance of these shapes with respect to Bu, for $a = 0$. Graph (c) shows the regions where the flipping, loop and (equiprobably) knot/loop appear, with respect to Bu and a, respectively in blue, pink and purple.

8.4 Emerging shapes at long timescale

We now focus on the symmetric case $a = 0$, i.e. when both endpoints are pinned and move towards each other at the same speed. The randomness of the initial condition induces a range of outcomes, even for a constant value of Bu. These outcomes fall in three main categories that are visible in Fig. 8.3-(a), and that qualitatively correspond to three speed regimes. For relatively low Bu, a loop appears as the endpoints cross over each other, but this loop shape is unstable: the filament quickly flips to retrieve an arch shape. However, as Bu increases, the loop shape stabilises and remains until the end, as the filament does not have "enough time" to flip anymore. A third case appears for high values of Bu, where one can observe the unstable second mode dominating the shape of the filament. In this case, the filament shape resembles the shape of a knot.

In order to identify and classify the shapes, we calculate the spatial discrete Fourier transform of the filament curvature vector (i.e. the vector $(\alpha_2, \dots, \alpha_N)$). Observing the evolution of the curvature in this Fourier space allows to distinguish the three different shapes – see Figure 8.3-(a'). The first two graphs on this column display a "back turn" and overlapping that indicates that the filament flips. The profile of the third and fourth graphs indicate a final loop shape. The last graph shows a dramatic change of behaviour at high Bu for the knot shape, including the quasi-disappearance of the first mode — note the change of scale on the x-axis. In particular, the amplitude a_1 of the first mode is significantly different at the end of the simulation for the three shapes.

We measured the frequency of appearance of each shape over 500 simulations for Bu ranging from 10^{-1} to 10^4. Fig. 8.3-(b) displays the results, showing the shapes predominance as Bu increases.

Note that that two final shapes may coexist for some values of Bu. The coexistence between the flip and loop shape occurs for a narrow range of buckling numbers, roughly between Bu = 1.5 and Bu = 2.5. For Bu < 1.5, the filament always flips; for Bu > 2.5, it always loops, until Bu reaches approximately 3.10^3. From this value, the filament may take a knot shape and the loop and knot shape end up being equiprobable for very high Bu. Further investigation in Section 8.6 shows that the final shape for these ranges of buckling number where two shapes coexist is highly unpredictable, despite the model being deterministic and the initial conditions being extremely close to each other.

8.4.1 Role of symmetry

To further understand the role of symmetry in the filament buckling behaviour, we introduced the asymmetry parameter a (see Eq. (8.1)) that divides the push exerted on both ends between the two endpoints of the filament. If $a > 0$, one end is pushed faster than the other.

Along with the buckling number Bu, the asymmetry parameter a plays a strong role in the appearance of the three outcomes. The regions of predominance of the three shapes with respect to Bu and a is displayed on Fig. 8.3-(c). When $a > 0$, the induced asymmetry creates a hydrodynamic drag that shifts the emerging shapes left or right. Note, on Fig. 8.3-(c), how the buckling number range for which the loop shape predominates shifts towards high values of Bu as a increases. The purple region at the bottom right of the plot indicates the parameter sets for which the loop and knot shapes are equiprobable. Similarly, as a increases, the unstable knot shape only starts appearing for higher Bu, and even disappears

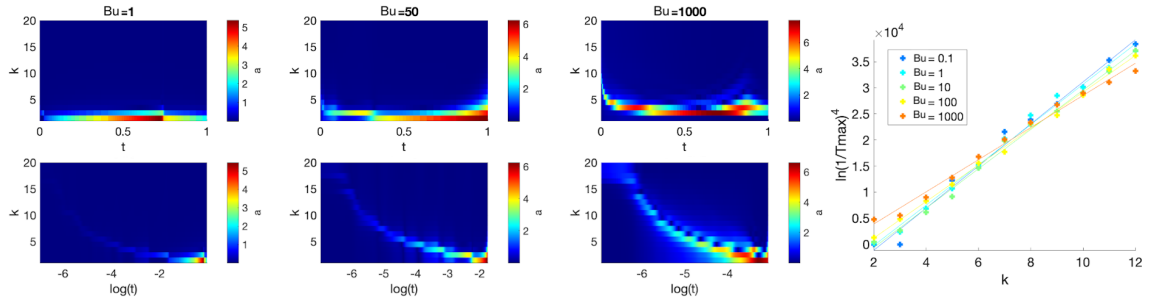

Figure 8.4 – Evolution of Fourier modes for different speed regimes. The surface plots display the amplitude of the first twenty Fourier modes amplitude (a_k , $k = 1 \dots 20$) on the y-axis with respect to time on the x-axis, from dark blue to red for highest amplitudes. The timescale is linear on the first row of plots and logarithmic on the second row.

for high values of a.

8.5 Decay of Fourier modes at short timescale

At the beginning of the buckling simulations, one observes that several waves (see for instance the bottom left filament on Figure 8.3) appear and quickly disappear. This phenomenon is characteristic of buckling instability and correspond with high order Fourier modes of the filament curvature.

In order to study the decay of these high Fourier modes, we plotted the amplitude of the first 20 Fourier modes of the filament curvature with respect to time on Figure 8.4. The plots on the first row shows that the first two (or three for high Bu) modes are dominant for most of the simulation. The highest modes ($k \geqslant 4$) vanish very fast, so their maximal amplitude can only be seen on the bottom row where timescale is logarithmic. The important role of the third mode for high speed is visible on the last column (Bu = 1000).

The bottom row of plots on Figure 8.4 allows to observe the successive appearance and decay of each mode. Every mode appears, reaches a maximum at a time $T^k_{\max}$, then quickly decays for $k \geqslant 4$. We numerically determined that the maximum amplitude time $T^k_{\max}$ follows a law of the form

$$T^k_{\max} = T_0 \exp(-\alpha k^{1/4}),$$

with α roughly independent of Bu.

8.6 Visualisation on the Fourier modes space

The predominant role of first, second and third Fourier modes confirms that the representation of the trajectories in a "Fourier plane" like on Figure 8.3, or in a "Fourier space" where we add the amplitude of the third mode, is relevant for visualising and analysing their behaviour. Figure 8.5 displays the evolution of these Fourier modes for different values of Bu.

Graphs (a) and (b) allow to observe what happens for values of Bu for which the flip and loop shapes coexist (roughly $1.5 < \mathrm{Bu} < 2.5$). One can see that all the trajectories follow a

common path before bifurcating either towards the flip or towards the loop shape. Note that the bifurcation towards the flip occurs later and more rarely for Bu = 2.1 than for Bu = 1.6, indicating that the loop shape is more predominant. The fact that the trajectories follow an common path make the final outcome highly unpredictable.

On graph (c) is plotted the evolution of first and second Fourier mode amplitudes when Bu = 200. For this value, all the trajectories end up as loop shapes. However, one can see that they follow various paths before reaching this shape, indicating complex dynamical behaviour. Graph (e) highlights the role of the third Fourier mode in the evolution of these trajectories.

Finally, graph (d) shows the emergence of knots at very high buckling number. Recall that for this range of Bu, the filament ends up equiprobably as a loop and as a knot. The knots trajectories are seen on the left hand-side of graph (d) and are characterised by a very attenuated first mode. Graph (f) shows how these knot trajectories evolve in a complex pattern in the y-z plane. Let us also highlight the fact that the two families of trajectories (loops and knots) at this speed range get separated at a very early time, which suggests that the higher mode, despite fast decay, could play an important role in the prediction of the final outcome.

We believe that the phenomena unveiled by these numerical observations are very intriguing and require analytical investigation, that however is beyond the scope of this study and left to future research.

8.7 Perspectives

In this paper, we conducted an exploratory numerical study of the dynamical elastic buckling of a microfilament. The long-time analysis shows that the dynamic effects lead to fascinating phenomena. We achieved this study thanks to the model presented in [MGG18]. Most importantly, we found that the filament takes three different shapes depending on the ratio between characteristic times of relaxation and buckling. For some of these ratios, two different shapes coexist despite very low discrepancy between initial conditions.

We investigated the role played by the Fourier modes of the curvature along the filament and found that after a rapid decay of high-order modes, only the first two or three modes seem to determine its behaviour.

We intend to realise a theoretical analysis of the equations of motion, in order to further understand the phenomena highlighted in the simulations. As a future perspective, it would also be interesting to explore buckling of micro-filaments in three dimensions.

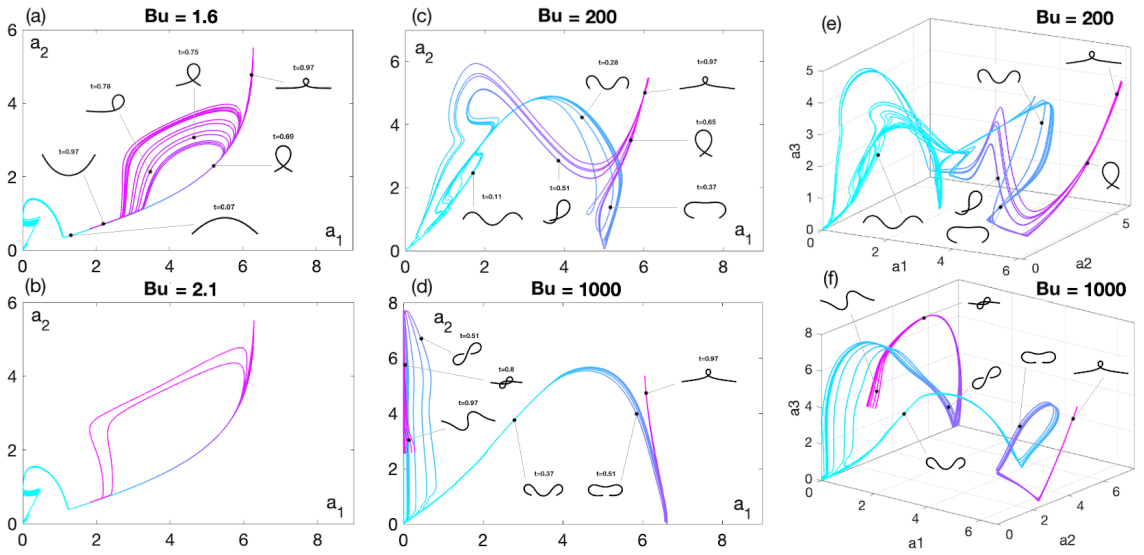

Figure 8.5 – Bifurcation and instability phenomena at different buckling regimes. For each graph (a) to (f), twenty buckling trajectories are plotted. Graphs (a) to (d) display a_1 and a_2, the amplitude of respectively the first and second Fourier modes, on resp. the x- and y-axis. Graphs (e) and (f) also display a_3, the amplitude of the third mode on the z-axis. The trajectories are plotted as a colored line going from light blue at the beginning of the simulation (note that the trajectories always start from the origin, as the initial shape is a straight line with all Fourier modes equal to zero) to pink at the end. The shape of the filament at a few selected instants has additionnally been represented on each graph. The corresponding times have been normalized so that the final time is always equal to 1. Graphs (a) and (b) display trajectories at the buckling number range for which the flip and loop shape coexist. The four leftmost graphs illustrate the behaviour of the filaments for higher values of Bu.

Appendix A

Details of calculations for the magnetic swimmers

A.1 Expression of matrices A_2 and A_3

The matrix A_2, of size 4×4, appearing in equation (2.56) is given by

$$
\begin{aligned}
a_{11} &= -2\eta_{\|}\ell\cos\alpha, & a_{21} &= \ell(\eta_{\perp}+\eta_{\|})\sin\alpha,\\
a_{12} &= -\ell(\eta_{\|}+\eta_{\perp})\sin\alpha, & a_{22} &= -2\eta_{\perp}\ell\cos\alpha,\\
a_{13} &= \tfrac{1}{2}\eta_{\|}\ell^2\sin\alpha, & a_{23} &= \tfrac{1}{2}\eta_{\perp}\ell^2(1+\cos\alpha),\\
a_{14} &= 0, & a_{24} &= \tfrac{1}{2}\eta_{\perp}\ell^2,\\
a_{31} &= -\tfrac{1}{2}\eta_{\perp}\ell^2\sin\alpha, & a_{41} &= 0,\\
a_{32} &= \tfrac{1}{2}\eta_{\perp}\ell^2(\cos\alpha-1), & a_{42} &= -\tfrac{1}{2}\eta_{\perp}\ell^2,\\
a_{33} &= \tfrac{1}{4}\eta_{\perp}\ell^3(-\cos\alpha+1), & a_{43} &= -\tfrac{1}{12}\eta_{\perp}\ell^3,\\
a_{34} &= -\tfrac{1}{3}\eta_{\perp}\ell^3, & a_{44} &= 0.
\end{aligned}
$$

The matrix A_3 appears in equation (2.57) and is also noted $M(\alpha_1,\alpha_2)$ in Chapter 6, equation (6.2). A_3 is of size 5×5 and its entries read

$$
\begin{aligned}
a_{11} &= \ell(\eta_{\perp}+2\eta_{\|})\sin(\alpha_1)\sin(\alpha_2) - 3l\eta_{\|}\cos(\alpha_1)\cos(\alpha_2),\\
a_{12} &= -\ell((\eta_{\perp}+2\eta_{\|})\cos(\alpha_2)\sin(\alpha_1) + (2\eta_{\perp}+\eta_{\|})\cos(\alpha_1)\sin(\alpha_2)),\\
a_{13} &= -\tfrac{1}{2}\ell^2((\eta_{\perp}+4\eta_{\|})\cos(\alpha_2)\sin(\alpha_1) + (\eta_{\perp}+2\eta_{\|}+(3\eta_{\perp}+2\eta_{\|})\cos(\alpha_1))\sin(\alpha_2)),\\
a_{14} &= -\tfrac{1}{2}\ell^2(\eta_{\perp}+2\eta_{\|})\sin(\alpha_2),\\
a_{15} &= 0,\\
a_{21} &= \ell(2\eta_{\perp}+\eta_{\|})\cos(\alpha_2)\sin(\alpha_1) + l(\eta_{\perp}+2\eta_{\|})\cos(\alpha_1)\sin(\alpha_2),\\
a_{22} &= \ell(2\eta_{\perp}+\eta_{\|})\sin(\alpha_1)\sin(\alpha_2) - 3l\eta_{\perp}\cos(\alpha_1)\cos(\alpha_2),\\
a_{23} &= -\tfrac{1}{2}\ell^2((5\cos(\alpha_1)+3)\cos(\alpha_2)\eta_{\perp} + \eta_{\perp} - (3\eta_{\perp}+2\eta_{\|})\sin(\alpha_1)\sin(\alpha_2)),\\
a_{24} &= -\tfrac{1}{2}\ell^2\eta_{\perp}(3\cos(\alpha_2)+1),\\
a_{25} &= -\tfrac{1}{2}\left(\ell^2\eta_{\perp}\right),
\end{aligned}
$$

$$
\begin{aligned}
a_{31} = \;& \tfrac{1}{2}\ell^2((2\eta_\perp+\eta_\parallel)\sin(\alpha_1)+(\eta_\perp-\eta_\parallel)\sin(2\alpha_1)+\eta_\perp\sin(\alpha_1+\alpha_2)\\
& +(\eta_\perp-\eta_\parallel)(\sin(2(\alpha_1+\alpha_2))+\sin(\alpha_1+2\alpha_2))),\\
a_{32} = \;& -\tfrac{1}{2}\ell^2(\cos(\alpha_1+\alpha_2)\eta_\perp+\cos(2(\alpha_1+\alpha_2))\eta_\perp+3\eta_\perp+2\eta_\parallel\\
& +(2\eta_\perp+\eta_\parallel)\cos(\alpha_1)+(\eta_\perp-\eta_\parallel)\cos(2\alpha_1)\\
& -\eta_\parallel\cos(2(\alpha_1+\alpha_2))+(\eta_\perp-\eta_\parallel)\cos(\alpha_1+2\alpha_2)),\\
a_{33} = \;& -\tfrac{1}{2}\ell^3(2\cos(\alpha_2)\eta_\perp+\cos(2\alpha_2)\eta_\perp+2\cos(\alpha_1+\alpha_2)\eta_\perp\\
& +\cos(2(\alpha_1+\alpha_2))\eta_\perp+5\eta_\perp+3\eta_\parallel+2(2\eta_\perp+\eta_\parallel)\cos(\alpha_1)\\
& +(\eta_\perp-\eta_\parallel)\cos(2\alpha_1)-\eta_\parallel\cos(2\alpha_2)-\eta_\parallel\cos(2(\alpha_1+\alpha_2))\\
& +2(\eta_\perp-\eta_\parallel)\cos(\alpha_1+2\alpha_2)),\\
a_{34} = \;& -\tfrac{1}{6}\ell^3(7\eta_\perp+3\eta_\parallel+3((2\eta_\perp+\eta_\parallel)\cos(\alpha_1)+2\eta_\perp\cos(\alpha_2)+\eta_\perp\cos(2\alpha_2)\\
& -\eta_\parallel\cos(2\alpha_2)+\eta_\perp\cos(\alpha_1+\alpha_2)+(\eta_\perp-\eta_\parallel)\cos(\alpha_1+2\alpha_2))),\\
a_{35} = \;& -\tfrac{1}{6}\ell^3\eta_\perp(3\cos(\alpha_2)+3\cos(\alpha_1+\alpha_2)+2),
\end{aligned}
$$

$$
\begin{aligned}
a_{41} = \;& \tfrac{1}{2}\ell^2((2\eta_\perp+\eta_\parallel)\sin(\alpha_1)+\eta_\perp\sin(\alpha_1+\alpha_2)+(\eta_\perp-\eta_\parallel)\sin(\alpha_1+2\alpha_2)),\\
a_{42} = \;& -\tfrac{1}{2}\ell^2((2\eta_\perp+\eta_\parallel)\cos(\alpha_1)+\eta_\perp\cos(\alpha_1+\alpha_2)+(\eta_\perp-\eta_\parallel)\cos(\alpha_1+2\alpha_2)),\\
a_{43} = \;& -\tfrac{1}{6}\ell^3(7\eta_\perp+3\eta_\parallel+3((2\eta_\perp+\eta_\parallel)\cos(\alpha_1)+2\eta_\perp\cos(\alpha_2)+\eta_\perp\cos(2\alpha_2)\\
& -\eta_\parallel\cos(2\alpha_2)+\eta_\perp\cos(\alpha_1+\alpha_2)+(\eta_\perp-\eta_\parallel)\cos(\alpha_1+2\alpha_2)))\\
a_{44} = \;& -\tfrac{1}{6}\ell^3(6\cos(\alpha_2)\eta_\perp+7\eta_\perp+3\eta_\parallel+3(\eta_\perp-\eta_\parallel)\cos(2\alpha_2)),\\
a_{45} = \;& -\tfrac{1}{6}\ell^3\eta_\perp(3\cos(\alpha_2)+2),
\end{aligned}
$$

$$
\begin{aligned}
a_{51} = \;& \tfrac{1}{2}\ell^2\eta_\perp\sin(\alpha_1+\alpha_2),\\
a_{52} = \;& -\tfrac{1}{2}\ell^2\eta_\perp\cos(\alpha_1+\alpha_2),\\
a_{53} = \;& -\tfrac{1}{6}\ell^3\eta_\perp(3\cos(\alpha_2)+3\cos(\alpha_1+\alpha_2)+2),\\
a_{54} = \;& -\tfrac{1}{6}\ell^3\eta_\perp(3\cos(\alpha_2)+2),\\
a_{55} = \;& -\tfrac{1}{3}\ell^3\eta_\perp
\end{aligned}
$$

A.2 Determinants of matrices A_2 and A_3

.

In order to write equations (2.56) and (2.57) as control systems, one needs to make sure that A_2 and A_3 are invertible. Let $\gamma = \frac{\eta_\perp}{\eta_\parallel}$; we have $\gamma \geqslant 1$. The determinant of A_2 reads

$$
D_2(\alpha) = -\frac{1}{9}\eta_\parallel^4\gamma^2\ell^8\left(\gamma^2\cos^2\alpha+\left(1+\frac{1}{4}\gamma\right)^2\sin^2\alpha\right) \tag{A.1}
$$

so we immediately see that $D_2(\alpha) < 0$ for all α.

The determinant of A_3 reads

$$
\begin{aligned}
D_3(\alpha_1,\alpha_2) \;& = \tfrac{1}{1728}\eta_\perp^5\gamma^2\ell^{11}(-3(2\gamma^3+37\gamma+56\gamma^2+16)\\
& +(\gamma-4)(2\gamma^2-17\gamma-12)(\cos 2\alpha_1+\cos 2\alpha_2)\\
& +(\gamma-4)^2(2\gamma-3)\cos 2\alpha_1\cos 2\alpha_2\\
& +\gamma(\gamma-4)^2\sin 2\alpha_1\sin 2\alpha_2.
\end{aligned} \tag{A.2}
$$

The functions cos and sin take values in $[-1,1]$, therefore

$$
D_3(\alpha_1,\alpha_2) \leqslant \frac{1}{1728}\eta_\perp^5\gamma^2\ell^{11}d(\gamma)
$$

with

$$\begin{aligned} d(\gamma) &= -3(2\gamma^3+37\gamma+56\gamma^2+16) \\ &+|\gamma-4|\cdot|2\gamma^2-17\gamma-12| \\ &+(\gamma-4)^2|2\gamma-3| \\ &+\gamma(\gamma-4)^2. \end{aligned}$$

Hence we need to study $d(\gamma)$ as a function of γ on $[1,+\infty)$. According to the sign of the expressions inside the absolute values, we compute

$$d(\gamma)=\begin{cases} -3\gamma^3-150\gamma^2-96\gamma-96 & \text{on} \quad [1,\frac{3}{2}), \\ \gamma^3-188\gamma^2+16\gamma & \text{on} \quad [\frac{3}{2},4]\cup[\frac{17+\sqrt{385}}{4},+\infty), \\ -7\gamma^3-88\gamma^2-208\gamma-192 & \text{on} \quad [4,\frac{17+\sqrt{385}}{4}]. \end{cases}$$

These third-degree polynoms are negative on the interval $[1,2(47+21\sqrt{5}))$ (this interval includes the interval $[1,180]$ which is more than enough to encompass the physical cases). For $\gamma \geqslant 2(47+21\sqrt{5})$, we check that $D(\alpha_1,\alpha_2)$ reaches a global maximum at $(0,0)$, whose value is given by

$$D(0,0)=-\frac{5}{48}\eta_\perp^5\gamma_4\ell^{11}<0.$$

A.3 Proof of Proposition 2.62 (section 2.4)

Proposition A.1. *For the N-link swimmer, $[\mathbf{F}_2,[\mathbf{F}_0,\mathbf{F}_2]](0)$ and $[\mathbf{F}_2,[\mathbf{F}_1,\mathbf{F}_2]](0)$ are colinear.*

Proof. Let $n=N+2$. The system for the N-link swimmer reads

$$A_N(\alpha)\dot{\mathbf{z}}_N = B_0 + H_\parallel B_1 - H_\perp B_2. \tag{A.3}$$

with

$$B_0=\begin{pmatrix} b_0^1 \\ \vdots \\ b_0^n \end{pmatrix}=\begin{pmatrix} 0 \\ 0 \\ 0 \\ -\kappa\alpha_2 \\ \vdots \\ -\kappa\alpha_N \end{pmatrix}, \tag{A.4}$$

$$B_1=\begin{pmatrix} b_1^1 \\ \vdots \\ b_1^n \end{pmatrix}=\begin{pmatrix} 0 \\ 0 \\ \sum_{k=2}^N M_k \sin\left(\sum_{l=2}^k \alpha_l\right) \\ \sum_{k=2}^N M_k \sin\left(\sum_{l=2}^k \alpha_l\right) \\ \vdots \\ M_N \sin\left(\sum_{l=2}^N \alpha_l\right) \end{pmatrix}, B_2=\begin{pmatrix} b_2^1 \\ \vdots \\ b_2^n \end{pmatrix}=\begin{pmatrix} 0 \\ 0 \\ M_1+\sum_{k=2}^N M_k \cos\left(\sum_{l=2}^k \alpha_l\right) \\ \sum_{k=2}^N M_k \cos\left(\sum_{l=2}^k \alpha_l\right) \\ \vdots \\ M_N \sin\left(\sum_{l=2}^N \alpha_l\right) \end{pmatrix} \tag{A.5}$$

The inverse of A_N is noted

$$A_N^{-1} = \left(\begin{array}{c|c|c|c} \mathbf{\Lambda}_1 & \mathbf{\Lambda}_2 & \dots & \mathbf{\Lambda}_n \end{array} \right) = \begin{pmatrix} \lambda_1^1 & \lambda_2^1 & \dots & \lambda_n^1 \\ \lambda_1^2 & \lambda_2^2 & \dots & \lambda_n^2 \\ \vdots & \vdots & \ddots & \vdots \\ \lambda_1^n & \lambda_2^n & \dots & \lambda_n^n \end{pmatrix}.$$

All the entries λ_m^i of A_N^{-1} are functions of $\alpha = (\alpha_1, \alpha_2, \dots, \alpha_N)$. Moreover, one has

$$\forall m \in [3,n], \forall k \in [1,N], \forall i \in [2,n], \partial_{\alpha_k} \lambda_m^i(0) = 0. \tag{A.6}$$

Multiplying (A.3) by A_N^{-1}, we get

$$\dot{\mathbf{z}}_N = \mathbf{F}_0 + H_{\parallel}(t)\mathbf{F}_1 + H_{\perp}(t)\mathbf{F}_2. \tag{A.7}$$

with

$$\mathbf{F}_p = \sum_{m=3}^{n} b_r^m \mathbf{\Lambda}_m$$

for $r = 0, 1, 2$.

For a function $f : \mathbb{R}^n \to \mathbb{R}$, we denote by $\nabla^T f$ the row vector

$$\nabla^T f = \begin{pmatrix} \partial_{x_1} f & \partial_{x_2} f & \dots & \partial_{x_n} f \end{pmatrix}.$$

and $\mathbf{\Lambda}'$ designates the Jacobian matrix of $\mathbf{\Lambda}$.

Let us compute the first bracket of interest:

$$\begin{aligned}
[\mathbf{F}_2, [\mathbf{F}_1, \mathbf{F}_2]] &= \left[\sum_{q=3}^{n} b_2^q \mathbf{\Lambda}_q, \left[\sum_{m=3}^{n} b_1^m \mathbf{\Lambda}_m, \sum_{p=3}^{n} b_2^p \mathbf{\Lambda}_p \right] \right] \\
&= \sum_{m=3}^{n} \sum_{p=3}^{n} \sum_{q=3}^{n} \left[b_2^q \mathbf{\Lambda}_q, [b_1^m \mathbf{\Lambda}_m, b_2^p \mathbf{\Lambda}_p] \right] \\
&= \sum_{m=3}^{n} \sum_{p=3}^{n} \sum_{q=3}^{n} \left[b_2^q \mathbf{\Lambda}_q, b_1^m \mathbf{\Lambda}_p \nabla^T b_2^p \mathbf{\Lambda}_m - b_2^p \mathbf{\Lambda}_m \nabla^T b_1^m \mathbf{\Lambda}_p + b_1^m b_2^p [\mathbf{\Lambda}_m, \mathbf{\Lambda}_p] \right] \\
&= \sum_{m=3}^{n} \sum_{p=3}^{n} \sum_{q=3}^{n} (b_1^m b_2^p [\mathbf{\Lambda}_m, \mathbf{\Lambda}_p]' b_2^q \mathbf{\Lambda}_q + [\mathbf{\Lambda}_m, \mathbf{\Lambda}_p] \nabla^T (b_1^m b_2^p) b_2^q \mathbf{\Lambda}_q \\
&\qquad + b_1^m (\mathbf{\Lambda}_p \nabla^T b_2^p \mathbf{\Lambda}_m)' b_2^q \mathbf{\Lambda}_q + \mathbf{\Lambda}_p \nabla^T b_2^p \mathbf{\Lambda}_m \nabla^T b_1^m b_2^q \mathbf{\Lambda}_q \\
&\qquad - b_2^p (\mathbf{\Lambda}_m \nabla^T b_1^m \mathbf{\Lambda}_p)' b_2^q \mathbf{\Lambda}_q - \mathbf{\Lambda}_m \nabla^T b_1^m \mathbf{\Lambda}_p \nabla^T b_2^p b_2^q \mathbf{\Lambda}_q \\
&\qquad - b_2^q \mathbf{\Lambda}_q' b_1^m \mathbf{\Lambda}_p \nabla^T b_2^p \mathbf{\Lambda}_m - \mathbf{\Lambda}_q \nabla^T b_2^q b_1^m \mathbf{\Lambda}_p \nabla^T b_2^p \mathbf{\Lambda}_m \\
&\qquad + b_2^q \mathbf{\Lambda}_q' b_2^p \mathbf{\Lambda}_m \nabla^T b_1^m \mathbf{\Lambda}_p + \mathbf{\Lambda}_q \nabla^T b_2^q b_2^p \mathbf{\Lambda}_m \nabla^T b_1^m \mathbf{\Lambda}_p \\
&\qquad - b_2^q \mathbf{\Lambda}_q' b_2^p b_1^m b_2^p [\mathbf{\Lambda}_m, \mathbf{\Lambda}_p] - \mathbf{\Lambda}_q \nabla^T b_2^q b_1^m b_2^p [\mathbf{\Lambda}_m, \mathbf{\Lambda}_p]).
\end{aligned}$$

Next, notice that

$$\forall m \in [3,n], b_1^m(0) = 0 \quad \text{and} \quad \nabla^T b_2^m(0) = 0. \tag{A.8}$$

Hence, evaluating the bracket at 0 and gathering the scalar factors in each term into functions

φ_1, φ_2, φ_3 yields

$$\begin{aligned}[\mathbf{F}_2,[\mathbf{F}_1,\mathbf{F}_2]](0) &= \sum_{m=3}^{n}\sum_{p=3}^{n}\sum_{q=3}^{n}([\mathbf{\Lambda}_m,\mathbf{\Lambda}_p]\nabla^T(b_1^m b_2^p)b_2^q\mathbf{\Lambda}_q)(0)\\ &\qquad - (b_2^p(\mathbf{\Lambda}_m\nabla^T b_1^m\mathbf{\Lambda}_p)'b_2^q\mathbf{\Lambda}_q)(0) + (b_2^q\mathbf{\Lambda}_q' b_2^p\mathbf{\Lambda}_m\nabla^T b_1^m\mathbf{\Lambda}_p)(0).\\ &= \sum_{m=3}^{n}\sum_{p=3}^{n}\sum_{q=3}^{n}\varphi_1(0)[\mathbf{\Lambda}_m,\mathbf{\Lambda}_p](0) + \varphi_2(0)(\mathbf{\Lambda}_m'\mathbf{\Lambda}_q)(0) + \varphi_3(0)(\mathbf{\Lambda}_q'\mathbf{\Lambda}_m)(0).\end{aligned}$$

Finally, we know thanks to (A.6) that for all $m \in \{3,\dots,n\}$, only the first line of $\mathbf{\Lambda}_m'$ is nonzero. We conclude that only the first component of $[\mathbf{F}_2,[\mathbf{F}_1,\mathbf{F}_2]](0)$ is nonzero.

The same calculations hold for $[\mathbf{F}_2,[\mathbf{F}_0,\mathbf{F}_2]](0)$, so $[\mathbf{F}_2,[\mathbf{F}_1,\mathbf{F}_2]](0)$ and $[\mathbf{F}_2,[\mathbf{F}_0,\mathbf{F}_2]](0)$ are colinear.

□

Bibliography

[ADGZ13] F. Alouges, A. DeSimone, L. Giraldi, and M. Zoppello. Self-propulsion of slender micro-swimmers by curvature control: N-link swimmers. *International Journal of Non-Linear Mechanics*, 56:132–141, 2013.

[ADGZ15] F. Alouges, A. DeSimone, L. Giraldi, and M. Zoppello. Can Magnetic Multilayers Propel Artificial Microswimmers Mimicking Sperm Cells? *Soft Robotics*, 2(3):117–128, 2015.

[ADGZ17] F. Alouges, A. Desimone, L. Giraldi, and M. Zoppello. Purcell magneto-elastic swimmer controlled by an external magnetic field. *IFAC-PapersOnLine*, 50(1):4120–4125, 2017.

[ADH+13] F. Alouges, A. DeSimone, L. Heltai, A. Lefebvre-Lepot, and B. Merlet. Optimally swimming stokesian robots. *Discrete and Continuous Dynamical Systems - Series B*, 18(5):1189–1215, 2013.

[ADL08] F. Alouges, A. DeSimone, and A. Lefebvre. Optimal strokes for low Reynolds number swimmers : an example. *Journal of Nonlinear Science*, 18:277–302, 2008.

[AFPRG19] Y. E. Alaoui-Faris, J.-B. Pomet, S. Régnier, and L. Giraldi. Optimal Actuation of Flagellar Magnetic Micro-Swimmers. *arXiv preprint arXiv:1911.02805*, 2019.

[AG93a] A. A. Agrachev and R. V. Gamkrelidze. Local controllability and semigroups of diffeomorphisms. *Acta Applicandae Mathematica*, 32(1):1–57, 1993.

[AG93b] A. A. Agrachev and R. V. Gamkrelidze. Local controllability for families of diffeomorphisms. *Systems & control letters*, 20(1):67–76, 1993.

[Agr99] A. A. Agrachev. Is it possible to recognize local controllability in a finite number of differentiations? In *Open problems in mathematical systems and control theory*, comm. Control Engin. Ser., pages 15–18. Springer, London, 1999.

[AKBDGB09a] F. Ammar-Khodja, A. Benabdallah, C. Dupaix, and M. González Burgos. A generalization of the Kalman rank condition for time-dependent coupled linear parabolic systems. *Differential Equations & Applications*, 1(3):427–457, 2009.

[AKBDGB09b] F. Ammar-Khodja, A. Benabdallah, C. Dupaix, and M. González-Burgos. A Kalman rank condition for the localized distributed controllability of a class of linear parabolic systems. *Journal of Evolution Equations*, 9(2):267–291, 2009.

[Alb02] B. Alberts. *Molecular Biology of the Cell*. Garland Science, New York, 2002.

[Ant05] S. Antman. *Nonlinear Problems of Elasticity*, volume 107 of *Applied Mathematical Sciences*. Springer, 2005.

[ARW95] U. M. Ascher, S. J. Ruuth, and B. T. R. Wetton. Implicit-explicit methods for time-dependent partial differential equations. *SIAM Journal on Numerical Analysis*, pages 797–823, 1995.

[BDE+95] L. Bourdieu, T. Duke, M. B. Elowitz, D. A. Winkelmann, S. Leibler, and A. Libchaber. Spiral Defects in Motility Assays: A Measure of Motor Protein Force. *Phys. Rev. Lett.*, 75:176–179, 1995.

[BKJH+11] S. Balasubramanian, D. Kagan, C.-M. Jack Hu, S. Campuzano, M. J. Lobo-Castañon, N. Lim, D. Y. Kang, M. Zimmerman, L. Zhang, and J. Wang. Micromachine-enabled capture and isolation of cancer cells in complex media. *Angewandte Chemie International Edition*, 50(18):4161–4164, 2011.

[BM18] K. Beauchard and F. Marbach. Quadratic obstructions to small-time local controllability for scalar-input systems. *Journal of Differential Equations*, 264(5):3704–3774, 2018.

[BMK+06] C. P. Brangwynne, F. C. MacKintosh, S. Kumar, N. A. Geisse, J. Talbot, L. Mahadevan, K. K. Parker, D. E. Ingber, and D. A. Weitz. Microtubules can bear enhanced compressive loads in living cells because of lateral reinforcement. *J Cell Biol*, 173(5):733–741, June 2006.

[BP94] A. Berman and R. J. Plemmons. *Nonnegative matrices in the mathematical sciences*. SIAM, 1994.

[Bro72] C. J. Brokaw. Flagellar Movement: A Sliding Filament Model. *Science*, 178(4060):455–462, November 1972.

[Bro14] C. J. Brokaw. Computer simulation of flagellar movement X: doublet pair splitting and bend propagation modeled using stochastic dynein kinetics. *Cytoskeleton*, 71(4):273–284, 2014.

[BS01] L. E. Becker and M. J. Shelley. Instability of elastic filaments in shear flow yields first-normal-stress differences. *Physical Review Letters*, 87(19):198301, 2001.

[BT09] J. Blundell and E. Terentjev. Buckling of semiflexible filaments under compression. *Soft Matter*, 5(20):4015–4020, 2009.

[BW77] C. Brennen and H. Winet. Fluid mechanics of propulsion by cilia and flagella. *Annual Review of Fluid Mechanics*, 9(1):339–398, 1977.

[CBFB06] M. M. Claessens, M. Bathe, E. Frey, and A. R. Bausch. Actin-binding proteins sensitively mediate F-actin bundle stiffness. *Nature materials*, 5(9):748–753, 2006.

[CDK17] J. Chopin, M. Dasgupta, and A. Kudrolli. Dynamic wrinkling and strengthening of an elastic filament in a viscous fluid. *Physical review letters*, 119(8):088001, 2017.

[CG17] R. Coy and H. Gadêlha. The counterbend dynamics of cross-linked filament bundles and flagella. *Journal of The Royal Society Interface*, 14(130):20170065, May 2017.

[CGM14] T. Chambrion, L. Giraldi, and A. Munnier. Optimal strokes for driftless swimmers: A general geometric approach. *hal-00969259*, 2014.

[Che57] K.-T. Chen. Integration of paths, geometric invariants and a generalized Baker-Hausdorff formula. *Annals of Mathematics*, pages 163–178, 1957.

[Cho39] W.-L. Chow. Über Systeme von linearen partiellen Differentialgleichungen erster Ordnung. *Math. Ann*, 117:98–105, 1939.

[CHS+17] X.-Z. Chen, M. Hoop, N. Shamsudhin, T. Huang, B. Özkale, Q. Li, E. Siringil, F. Mushtaq, L. Di Tizio, B. J. Nelson, et al. Hybrid magnetoelectric nanowires for nanorobotic applications: fabrication, magnetoelectric coupling, and magnetically assisted in vitro targeted drug delivery. *Advanced Materials*, 29(8):1605458, 2017.

[CJP99] S. Camalet, F. Jülicher, and J. Prost. Self-Organized Beating and Swimming of Internally Driven Filaments. *Phys. Rev. Lett.*, 82:1590, 1999.

[CLPL05] M. Cosentino Lagomarsino, I. Pagonabarraga, and C. P. Lowe. Hydrodynamic Induced Deformation and Orientation of a Microscopic Elastic Filament. *Physical Review Letters*, 94(14):148104, April 2005.

[Cor07] J.-M. Coron. *Control and nonlinearity*, volume 136 of *Mathematical Surveys and Monographs*. AMS, Providence, RI, 2007.

[CSRB08] M. M. A. E. Claessens, C. Semmrich, L. Ramos, and A. R. Bausch. Helical twist controls the thickness of F-actin bundles. *Proceedings of the National Academy of Sciences*, 105(26):8819–8822, 2008.

[CW85] J. Cummins and P. Woodall. On mammalian sperm dimensions. *Reproduction*, 75(1):153–175, 1985.

[DBR+05] R. Dreyfus, J. Baudry, M. L. Roper, M. Fermigier, H. A. Stone, and J. Bibette. Microscopic artificial swimmers. *Nature*, 437(7060):862, 2005.

[DCP15] B. Delmotte, E. Climent, and F. Plouraboué. A general formulation of Bead Models applied to flexible fibers and active filaments at low Reynolds number. *Journal of Computational Physics*, 286:14–37, April 2015.

[DPF85] S. J. DeTeresa, R. S. Porter, and R. J. Farris. A model for the compressive buckling of extended chain polymers. *Journal of materials science*, 20(5):1645–1659, 1985.

[Dup15] M. Duprez. *Contrôlabilité de quelques systèmes gouvernés par des équations paraboliques*. PhD thesis, Université de Franche-Comté, 2015.

[Eul44] L. Euler. *Methodus inveniendi lineas curvas maximi minimive proprietate gaudentes*. apud Marcum-Michaelem Bousquet, 1744.

[FCZ00] E. Fernández-Cara and E. Zuazua. Null and approximate controllability for weakly blowing up semilinear heat equations. In *Annales de l'IHP Analyse non linéaire*, volume 17, pages 583–616, 2000.

[FI96] A. V. Fursikov and O. Y. Imanuvilov. *Controllability of evolution equations*. Number 34. Seoul National University, 1996.

[Fli75] M. Fliess. Séries de Volterra et séries formelles non commutatives. *Comptes Rendus Acad. Sciences Paris*, 280:965–967, 1975.

[Fli78] M. Fliess. Développements fonctionnels en indéterminées non commutatives des solutions d'équations différentielles non linéaires forcées. *CR Acad. Sci. Paris Sér. A–B*, 287:1133–1135, 1978.

[FMC13] A. P. Fields, E. A. Meyer, and A. E. Cohen. Euler buckling and nonlinear kinking of double-stranded DNA. *Nucleic acids research*, 41(21):9881–9890, 2013.

[FR71] H. O. Fattorini and D. L. Russell. Exact controllability theorems for linear parabolic equations in one space dimension. *Archive for Rational Mechanics and Analysis*, 43(4):272–292, 1971.

[FTC17] Y.-c. Fung, P. Tong, and X. Chen. *Classical and computational solid mechanics*, volume 2. World Scientific Publishing Company, 2017.

[FWP08] H. C. Fu, C. W. Wolgemuth, and T. R. Powers. Beating patterns of filaments in viscoelastic fluids. *Phys. Rev. E*, 78:041913–041925, 2008.

[Gad13] H. Gadêlha. On the optimal shape of magnetic swimmers. *Regular and Chaotic Dynamics*, 18(1-2):75–84, 2013.

[Gad18] H. Gadelha. The filament-bundle elastica. *IMA Journal of Applied Mathematics*, 83(4):634–654, 2018.

[GF09] A. Ghosh and P. Fischer. Controlled propulsion of artificial magnetic nanostructured propellers. *Nano letters*, 9(6):2243–2245, 2009.

[GG06] R. E. Goldstein and A. Goriely. Dynamic buckling of morphoelastic filaments. *Physical Review E*, 74(1):010901, 2006.

[GG19] H. Gadêlha and E. A. Gaffney. Flagellar ultrastructure suppresses buckling instabilities and enables mammalian sperm navigation in high-viscosity media. *Journal of The Royal Society Interface*, 16(152):20180668, 2019.

[GGG13] H. Gadêlha, E. A. Gaffney, and A. Goriely. The counterbend phenomenon in flagellar axonemes and cross-linked filament bundles. *Proceedings of the National Academy of Sciences*, July 2013.

[GGOS+13] V. Garcia-Gradilla, J. Orozco, S. Sattayasamitsathit, F. Soto, F. Kuralay, A. Pourazary, A. Katzenberg, W. Gao, Y. Shen, and J. Wang. Functionalized ultrasound-propelled magnetically guided nanomotors: Toward practical biomedical applications. *ACS nano*, 7(10):9232–9240, 2013.

[GGS+11] E. A. Gaffney, H. Gadelha, D. J. Smith, J. R. Blake, and J. C. Kirkman-Brown. Mammalian sperm motility: observation and theory. *Annual Review of Fluid Mechanics*, 43:501–528, 2011.

[GGSKB10] H. Gadêlha, E. A. Gaffney, D. J. Smith, and J. C. Kirkman-Brown. Nonlinear instability in flagellar dynamics: a novel modulation mechanism in sperm migration? *Journal of The Royal Society Interface*, page rsif20100136, May 2010.

[GH55] J. Gray and J. Hancock. The propulsion of sea-urchin spermatozoa. *J. Exp. Biol.*, 32(4):802–814, 1955.

[GHBV05] J. Gladden, N. Handzy, A. Belmonte, and E. Villermaux. Dynamic buckling and fragmentation in brittle rods. *Physical review letters*, 94(3):035503, 2005.

[GKP+12] W. Gao, D. Kagan, O. S. Pak, C. Clawson, S. Campuzano, E. Chuluun-Erdene, E. Shipton, E. E. Fullerton, L. Zhang, E. Lauga, et al. Cargo-towing fuel-free magnetic nanoswimmers for targeted drug delivery. *small*, 8(3):460–467, 2012.

[GL95] R. E. Goldstein and S. A. Langer. Nonlinear dynamics of stiff polymers. *Phys. Rev. Lett.*, 75:1094–1097, 1995.

[GLA05] R. Golestanian, T. B. Liverpool, and A. Ajdari. Propulsion of a molecular machine by asymmetric distribution of reaction products. *Physical review letters*, 94(22):220801, 2005.

[GLMP16] L. Giraldi, P. Lissy, C. Moreau, and J.-B. Pomet. Controllability of a bent 3-link magnetic microswimmer. *arXiv preprint arXiv:1611.00993*, 2016.

[GLMP18] L. Giraldi, P. Lissy, C. Moreau, and J.-B. Pomet. Addendum to "Local Controllability of the Two-Link Magneto-Elastic Microswimmer". *IEEE Transactions on Automatic Control*, 63:2303–2305, 2018.

[GLMP19] L. Giraldi, P. Lissy, C. Moreau, and J.-B. Pomet. A necessary condition for local controllability of a particular class of systems with two scalar controls. *in preparation*, 2019.

[GMP00] L. Golubovic, D. Moldovan, and A. Peredera. Flexible polymers and thin rods far from equilibrium: buckling dynamics. *Physical Review E*, 61(2):1703, 2000.

[GMZ13] L. Giraldi, P. Martinon, and M. Zoppello. Controllability and Optimal Strokes for N-link Micro-swimmer. *Proc. CDC*, 2013.

[GMZ15] L. Giraldi, P. Martinon, and M. Zoppello. Optimal design of the three-link Purcell swimmer. *Phys. Rev. E*, 91(023012), 2015.

[GO14] E. Gutman and Y. Or. Simple model of a planar undulating magnetic microswimmer. *Physical Review E*, 90(1):013012, 2014.

[GP17] L. Giraldi and J.-B. Pomet. Local controllability of the two-link magneto-elastic micro-swimmer. *IEEE Transactions on Automatic Control*, 62(5):2512–2518, 2017.

[GSM+10] W. Gao, S. Sattayasamitsathit, K. M. Manesh, D. Weihs, and J. Wang. Magnetically powered flexible metal nanowire motors. *J. Am. Chem. Soc.*, 132(41):14403–14405, 2010.

[HB78] M. Hines and J. J. Blum. Bend propagation in flagella. I. Derivation of equations of motion and their simulation. *Biophysical Journal*, 23(1):41–57, July 1978.

[HB79] M. Hines and J. J. Blum. Bend propagation in flagella. II. Incorporation of dynein cross-bridge kinetics into the equations of motion. *Biophysical Journal*, 25(3):421–441, March 1979.

[Her63] R. Hermann. On the accessibility problem in control theory. In *International Symposium on Nonlinear Differential Equations and Nonlinear Mechanics*, pages 325–332. Elsevier, 1963.

[Her76] H. Hermes. Local controllability and sufficient conditions in singular problems. *Journal of Differential Equations*, 20(1):213–232, 1976.

[Her78] H. Hermes. Lie algebras of vector fields and local approximation of attainable sets. *SIAM Journal on Control and Optimization*, 16(5):715–727, 1978.

[Her82] H. Hermes. On local controllability. *SIAM Journal on Control and Optimization*, 20(2):211–220, 1982.

[HKS98] T. Y. Hou, I. Klapper, and H. Si. Removing the Stiffness of Curvature in Computing 3-D Filaments. *Journal of Computational Physics*, 143(2):628–664, July 1998.

[HLS94] T. Y. Hou, J. S. Lowengrub, and M. J. Shelley. Removing the stiffness from interfacial flows with surface tension. *Journal of Computational Physics*, 114(2):312–338, October 1994.

[HMMJG+19] A. L. Hall-McNair, T. D. Montenegro-Johnson, H. Gadêlha, D. J. Smith, and M. T. Gallagher. Efficient implementation of elastohydrodynamics via integral operators. *Physical Review Fluids*, 4(11):113101, 2019.

[How01] J. Howard. *Mechanics of motor proteins and the cytoskeleton.* Sinauer Associates Sunderland, MA, 2001.

[HSF10] C. Heussinger, F. Schüller, and E. Frey. Statics and dynamics of the wormlike bundle model. *Phys. Rev. E*, 81(2):021904, Feb 2010.

[IGG+18] K. Ishimoto, H. Gadêlha, E. A. Gaffney, D. J. Smith, and J. Kirkman-Brown. Human sperm swimming in a high viscosity mucus analogue. *Journal of Theoretical Biology*, 446:1–10, June 2018.

[Isi95] A. Isidori. *Nonlinear control systems*. Communications and Control Engineering Series. Springer-Verlag, Berlin, 3rd edition, 1995.

[JB79] R. E. Johnson and C. J. Brokaw. Flagellar hydrodynamics. *Biophys. J.*, 25:113–127, 1979.

[Kaw86] M. Kawski. *Nilpotent Lie algebras of vectorfields and local controllability of nonlinear systems*. PhD thesis, University of Colorado, 1986.

[Kaw87] M. Kawski. A necessary condition for local controllability. In *Differential geometry: the interface between pure and applied mathematics*, volume 68 of *Contemp. Math.*, pages 143–155. AMS, Providence, RI, 1987.

[Kaw90] M. Kawski. High-order small-time local controllability. In *Nonlinear controllability and optimal control*, volume 133 of *Monogr. Textbooks Pure Appl. Math.*, pages 431–467. Dekker, New York, 1990.

[KG12] V. Kantsler and R. E. Goldstein. Fluctuations, Dynamics, and the Stretch-Coil Transition of Single Actin Filaments in Extensional Flows. *Physical Review Letters*, 108(3):038103, January 2012.

[KHN63] R. E. Kalman, Y.-C. Ho, and K. S. Narendra. Controllability of linear dynamical systems. *Contributions to Differential Equations*, 1:189–213, 1963.

[KHT95] M. Kurachi, M. Hoshi, and H. Tashiro. Buckling of a single microtubule by optical trapping forces: direct measurement of microtubule rigidity. *Cell motility and the cytoskeleton*, 30(3):221–228, 1995.

[Kla96] I. Klapper. Biological Applications of the Dynamics of Twisted Elastic Rods. *Journal of Computational Physics*, 125(2):325–337, May 1996.

[Kra98] M. Krastanov. A necessary condition for small-time local controllability. *Journal of Dynamical and Control Systems*, 4:425–456, 1998.

[LB20] K. Le Balc'h. Global null-controllability and nonnegative-controllability of slightly superlinear heat equations. *Journal de Mathématiques Pures et Appliquées*, 135:103–139, 2020.

[LCS+18] Y. Liu, B. Chakrabarti, D. Saintillan, A. Lindner, and O. Du Roure. Morphological transitions of elastic filaments in shear flow. *Proceedings of the National Academy of Sciences*, 115(38):9438–9443, 2018.

[LdÁG+17] J. Li, B. E.-F. de Ávila, W. Gao, L. Zhang, and J. Wang. Micro/nanorobots for biomedicine: Delivery, surgery, sensing, and detoxification. *Science Robotics*, 2(4), 2017.

[Lin94] C. B. Lindemann. A" geometric clutch" hypothesis to explain oscillations of the axoneme of cilia and flagella. *Journal of theoretical biology*, 168(2):175–189, 1994.

[LJT+16] R. Lagrange, F. L. Jiménez, D. Terwagne, M. Brojan, and P. M. Reis. From wrinkling to global buckling of a ring on a curved substrate. *Journal of the Mechanics and Physics of Solids*, 89:77–95, 2016.

[LL86] L. D. Landau and E. Lifshitz. Course of Theoretical Physics, Theory of Elasticity, vol. 7, 1986.

[LM67] E. B. Lee and L. Markus. *Foundations of optimal control theory.* John Wiley & Sons Inc., New York-London-Sydney, 1967.

[LM14] J. Lohéac and A. Munnier. Controllability of 3D low Reynolds number swimmers. *ESAIM Control Optim. Calc. Var.*, 20(1):236–268, 2014.

[LML05] C. B. Lindemann, L. J. Macauley, and K. A. Lesich. The counterbend phenomenon in dynein-disabled rat sperm flagella and what it reveals about the interdoublet elasticity. *Biophysical journal*, 89(2):1165–1174, 2005.

[LMQC12] M. Le Merrer, D. Quéré, and C. Clanet. Buckling of viscous filaments of a fluid under compression stresses. *Physical review letters*, 109(6):064502, 2012.

[Loh12] J. Lohéac. *Contrôle en temps optimal et nage à bas nombre de Reynolds.* PhD thesis, Université de Lorraine, 2012.

[Low03] C. P. Lowe. Dynamics of filaments: modelling the dynamics of driven microfilaments. *Philosophical Transactions of the Royal Society of London. Series B: Biological Sciences*, 358(1437):1543–1550, September 2003.

[LP09] E. Lauga and T. R. Powers. The hydrodynamics of swimming microorganisms. *Reports on Progress in Physics*, 72(9):096601, 2009.

[LR95] G. Lebeau and L. Robbiano. Contrôle exact de l'équation de la chaleur. *Communications in Partial Differential Equations*, 20(1-2):335–356, 1995.

[LRB+09] T. G. Leong, C. L. Randall, B. R. Benson, N. Bassik, G. M. Stern, and D. H. Gracias. Tetherless thermobiochemically actuated microgrippers. *Proceedings of the National Academy of Sciences*, 106(3):703–708, 2009.

[LST13] J. Lohéac, J.-F. Scheid, and M. Tucsnak. Controllability and time optimal control for low Reynolds numbers swimmers. *Acta Applicandae Mathematicae*, 123(1):175–200, 2013.

[LTZ17] J. Lohéac, E. Trélat, and E. Zuazua. Minimal controllability time for the heat equation under unilateral state or control constraints. *Mathematical Models and Methods in Applied Sciences*, 27(09):1587–1644, 2017.

[LTZ18] J. Lohéac, E. Trélat, and E. Zuazua. Minimal controllability time for finite-dimensional control systems under state constraints. *Automatica*, 96:380–392, 2018.

[MGG18] C. Moreau, L. Giraldi, and H. Gadêlha. The asymptotic coarse-graining formulation of slender-rods, bio-filaments and flagella. *Journal of the Royal Society Interface*, 15(144):20180235, 2018.

[MJGS15] T. D. Montenegro-Johnson, H. Gadêlha, and D. J. Smith. Spermatozoa scattering by a microchannel feature: an elastohydrodynamic model. *Royal Society Open Science*, 2(3):140475, March 2015.

[MMSC+15] V. Magdanz, M. Medina-Sánchez, Y. Chen, M. Guix, and O. G. Schmidt. How to improve spermbot performance. *Advanced Functional Materials*, 25(18):2763–2770, 2015.

[MN12] J. F. Marko and S. Neukirch. Competition between curls and plectonemes near the buckling transition of stretched supercoiled DNA. *Physical Review E*, 85(1):011908, 2012.

[Mor19] C. Moreau. Local controllability of a magnetized Purcell's swimmer. *IEEE Control Systems Letters*, 3(3):637–642, 2019.

[MTT07] J. Martín, T. Takahashi, and M. Tucsnak. A control theoretic approach to the swimming of microscopic organisms. *Quarterly of applied mathematics*, 65(3):405–424, 2007.

[Nag66] T. Nagano. Linear differential systems with singularities and an application to transitive Lie algebras. *Journal of the Mathematical Society of Japan*, 18(4):398–404, 1966.

[OGBMC14] D. Oriola, H. Gadêlha, C. Blanch-Mercader, and J. Casademunt. Subharmonic oscillations of collective molecular motors. *EPL (Europhysics Letters)*, 107(1):18002, 2014.

[OGC17] D. Oriola, H. Gadêlha, and J. Casademunt. Nonlinear amplitude dynamics in flagellar beating. *Open Science*, 4(3):160698, March 2017.

[OLC13] S. D. Olson, S. Lim, and R. Cortez. Modeling the dynamics of an elastic rod with intrinsic curvature and twist using a regularized Stokes formulation. *Journal of Computational Physics*, 238:169–187, April 2013.

[PBLL09] D. W. Pelle, C. J. Brokaw, K. A. Lesich, and C. B. Lindemann. Mechanical properties of the passive sea urchin sperm flagellum. *Cytoskeleton*, 66(9):721–735, 2009.

[PF18] S. Palagi and P. Fischer. Bioinspired microrobots. *Nature Reviews Materials*, 3:113–124, May 2018.

[Pie10] M. Pierre. Global existence in reaction-diffusion systems with control of mass: a survey. *Milan Journal of Mathematics*, 78(2):417–455, 2010.

[Pow10] T. R. Powers. Dynamics of filaments and membranes in a viscous fluid. *Reviews of Modern Physics*, 82(2):1607, 2010.

[PTD+16] F. Plouraboue, I. Thiam, B. Delmotte, E. Climent, P. Collaboration, et al. Identification of internal properties of fibers and micro-swimmers. In *APS Meeting Abstracts*, 2016.

[Pur77] E. M. Purcell. Life at low Reynolds number. *American journal of physics*, 45(1):3–11, 1977.

[PZ17] D. Pighin and E. Zuazua. Controllability under positivity constraints of semilinear heat equations. *arXiv preprint arXiv:1711.07678*, 2017.

[PZN13] K. E. Peyer, L. Zhang, and B. J. Nelson. Bio-inspired magnetic swimming microrobots for biomedical applications. *Nanoscale*, 5(4):1259–1272, 2013.

[RAMB15] D. S. Rodrigues, R. F. Ausas, F. Mut, and G. C. Buscaglia. A semi-implicit finite element method for viscous lipid membranes. *Journal of Computational Physics*, 298:565–584, October 2015.

[Ras38] P. K. Rashevski. About connecting two points of complete nonholonomic space by admissible curve. *Uch Zapiski Ped. Inst. Libknexta*, 2:83–94, 1938.

[RKHHJ07] I. H. Riedel-Kruse, A. Hilfinger, J. Howard, and F. Jülicher. How molecular motors shape the flagellar beat. *HFSP journal*, 1(3):192–208, 2007.

[SCD+12] T. Sanchez, D. T. N. Chen, S. J. DeCamp, M. Heymann, and Z. Dogic. Spontaneous motion in hierarchically assembled active matter. *Nature*, 491(7424):431–434, November 2012.

[SCdP+06] I. A. Schaap, C. Carrasco, P. J. de Pablo, F. C. MacKintosh, and C. F. Schmidt. Elastic response, buckling, and instability of microtubules under radial indentation. *Biophysical journal*, 91(4):1521–1531, 2006.

[SGS+16] P. Sartori, V. F. Geyer, A. Scholich, F. Jülicher, and J. Howard. Dynamic curvature regulation accounts for the symmetric and asymmetric beats of Chlamydomonas flagella. *eLife*, 5:e13258, May 2016.

[SK18] S. F. Schoeller and E. E. Keaveny. From flagellar undulations to collective motion: predicting the dynamics of sperm suspensions. *Journal of The Royal Society Interface*, 15(140):20170834, March 2018.

[SMBU+09] A. A. Solovev, Y. Mei, E. Bermúdez Ureña, G. Huang, and O. G. Schmidt. Catalytic microtubular jet engines self-propelled by accumulated gas bubbles. *Small*, 5(14):1688–1692, 2009.

[SMSM04] J. H. Shin, L. Mahadevan, P. So, and P. Matsudaira. Bending stiffness of a crystalline actin bundle. *Journal of molecular biology*, 337(2):255–261, 2004.

[Son13] E. D. Sontag. *Mathematical control theory: deterministic finite dimensional systems*, volume 6. Springer Science & Business Media, 2013.

[SR97] L. F. Shampine and M. W. Reichelt. The Matlab ODE suite. *SIAM Journal on Scientific Computing*, 18(1):1–22, 1997.

[Ste84] G. Stefani. Local properties of nonlinear control systems. In *Int. School Bierutowice*, sept 1984.

[Ste86] G. Stefani. On the local controllability of a scalar-input control system. *Theory and Applications of Nonlinear Control Systems, Proc. of MTNS*, 84:167–179, 1986.

[Sus73] H. J. Sussmann. Orbits of families of vector fields and integrability of distributions. *Transactions of the American Mathematical Society*, 180:171–188, 1973.

[Sus83] H. J. Sussmann. Lie brackets and local controllability: a sufficient condition for scalar-input systems. *SIAM Journal on Control and Optimization*, 21(5):686–713, 1983.

[Sus85] H. J. Sussmann. Lie brackets and real analyticity in control theory. *Banach Center Publications*, 14(1):515–542, 1985.

[Sus87] H. J. Sussmann. A general theorem on local controllability. *SIAM Journal on Control and Optimization*, 25(1):158–194, 1987.

[SW89] A. Shapere and F. Wilczek. Efficiencies of self-propulsion at low Reynolds number. *J. Fluid Mech.*, 1989.

[SZ11] M. J. Shelley and J. Zhang. Flapping and bending bodies interacting with fluid flows. *Annual Review of Fluid Mechanics*, 43:449–465, 2011.

[TG09] S. P. Timoshenko and J. M. Gere. *Theory of elastic stability*. Courier Corporation, 2009.

[TH07] D. Tam and A. E. Hosoi. Optimal Strokes Patterns for Purcell's Three Link Swimmer. *Physical Review Letters*, 2007.

[Tre90] A. Tret'yak. Necessary conditions for optimality of odd order in a time-optimality problem for systems that are linear with respect to control. *Mat. Sb*, 181(5):625–641, 1990.

[TS04] A. K. Tornberg and M. J. Shelley. Simulating the dynamics and interactions of flexible fibers in Stokes flows. *J. Comput. Phys.*, 196:8–40, 2004.

[VS12] R. Vogel and H. Stark. Motor-driven bacterial flagella and buckling instabilities. *The European Physical Journal E*, 35(2):15, 2012.

[Wan13] J. Wang. *Nanomachines: fundamentals and applications*. John Wiley & Sons, 2013.

[WG98] C. H. Wiggins and R. E. Goldstein. Flexive and Propulsive Dynamics of Elastica at Low Reynolds Number. *Phys. Rev. Lett.*, 80:3879, 1998.

[WGD+18] O. Wiezel, L. Giraldi, A. DeSimone, Y. Or, and F. Alouges. Energy-optimal small-amplitude strokes for multi-link microswimmers: Purcell's loops and Taylor's waves reconciled. *arXiv preprint arXiv:1801.04687*, 2018.

[WIG19] B. J. Walker, K. Ishimoto, and E. A. Gaffney. A new basis for filament simulation in three dimensions. *arXiv preprint arXiv:1907.04823*, 2019.

[WIGG19] B. J. Walker, K. Ishimoto, H. Gadêlha, and E. A. Gaffney. Filament mechanics in a half-space via regularised Stokeslet segments. *Journal of Fluid Mechanics*, 879:808–833, 2019.

[WLdÁ+15] Z. Wu, J. Li, B. E.-F. de Ávila, T. Li, W. Gao, Q. He, L. Zhang, and J. Wang. Water-Powered Cell-Mimicking Janus Micromotor. *Advanced Functional Materials*, 25(48):7497–7501, 2015.

[WROG98] C. H. Wiggins, D. Riveline, A. Ott, and R. E. Goldstein. Trapping and wiggling: elastohydrodynamics of driven microfilaments. *Biophysical Journal*, 74(2):1043–1060, 1998.

[WS74] F. D. Warner and P. Satir. The structural basis of ciliary bend formation: radial spoke positional changes accompanying microtubule sliding. *The Journal of cell biology*, 63(1):35, 1974.

[XWO+16] G. Xu, K. S. Wilson, R. J. Okamoto, J.-Y. Shao, S. K. Dutcher, and P. V. Bayly. Flexural rigidity and shear stiffness of flagella estimated from induced bends and counterbends. *Biophysical Journal*, 110(12):2759–2768, 2016.

[YLH06] T. S. Yu, , E. Lauga, and A. E. Hosoi. Experimental investigations of elastic tail propulsion at low Reynolds number. *Phys. Fluids*, 18:0917011–0917014, 2006.

[You09] Y.-N. Young. Hydrodynamic interactions between two semiflexible inextensible filaments in Stokes flow. *Physical Review E*, 79(4):046317, April 2009.